Order Number 8916640

Large amplitude ship motions and capsizing in severe sea conditions

de Kat, Jean Otto, Ph.D.

University of California, Berkeley, 1988

U·M·I
300 N. Zeeb Rd.
Ann Arbor, MI 48106

Large Amplitude Ship Motions and Capsizing in Severe Sea Conditions

By

Jean Otto de Kat
B.Eng. (University of New South Wales, Sydney) 1979
M.S. (University of California) 1981

DISSERTATION

Submitted in partial satisfaction of the requirements for the degree of

DOCTOR OF PHILOSOPHY

in

ENGINEERING

NAVAL ARCHITECTURE AND OFFSHORE ENGINEERING

in the

GRADUATE DIVISION

OF THE

UNIVERSITY OF CALIFORNIA, BERKELEY

Approved: J. R. Paulling July 20, 1988
Chair Date

William A. Webster

Frederick S. Sherman

LARGE AMPLITUDE SHIP MOTIONS AND CAPSIZING IN SEVERE SEA CONDITIONS

Jean Otto de Kat

ABSTRACT

A numerical model has been developed to determine the large amplitude motions of a vessel subjected to severe wave conditions, including those that may lead to capsizing. The aim was to numerically identify different modes of capsizing, and to study relevant mechanisms and conditions. The theory is based on a combination of potential and viscous flow approaches in the time domain, where large displacements, the instantaneous free surface and memory effects are considered.

Reasonable agreement was found between predicted motions and experimental results for a variety of wave conditions. A number of capsizes, observed experimentally, were simulated successfully using the numerical model.

An investigation has been carried out to determine the sensitivity of the roll response to changes in the force components. The Froude-Krylov forces were found to be always of importance, irrespective of the wave conditions. Generally, the relative importance of the various components depends strongly on the ship and wave conditions.

Special attention has been paid to random following seas, which tend to have an important effect on capsizing. Wave statistics have been obtained for an observer in a random following seaway, represented by the superposition of a finite number of wave components. It was found that the mean square wave elevation observed at a fixed point, and from a reference point moving at an angle with the waves, can be different, suggesting that care must be taken when conducting simulations.

In random following seas, any point on the ship may be subjected to a quasi regular excitation, while the motion behavior is affected simultaneously by the spatial and temporal characteristics of the seaway. Also, for a short term simulation of an extreme event, it is shown that the random following sea may be replaced by an equivalent wave system, consisting of only two components. Several modes of capsizing in following to beam seas have been identified by simulation: low cycle resonance, loss of transverse static stability, broaching and resonant excitation. An analysis has been made of the behavior of the roll moment components associated with these capsize modes.

J R Paulling
July 20, 1988

Acknowledgements

In the following few paragraphs I would like to express my sincere gratitude to the institutions that have made it financially possible for me to start and complete my work as a doctoral student.

This work is a result of research sponsored in part by NOAA, National Sea Grant College Program, Department of Commerce, under grant number NA85AA-D-SG140, project number 78544-22570, through the California Sea Grant College Program. The U.S. Government is authorized to reproduce and distribute for governmental purposes.

IBM 3090 mainframe usage and workstation facilities were for a large part provided through the U.C. Berkeley DACE Grant from IBM. The mainframe computer was crucial in developing the code and performing the multitude of time simulations that were part of this dissertation.

The initial part of this work was funded by the Office of Naval Research, which in 1984 provided one of the incentives for me to leave Norway and start my Ph.D. studies. Welcome tuition waivers were frequently added to my joyful life in Berkeley, as well as a departmental Fellowship, for which I must thank the faculty and staff of the Department of Naval Architecture and Offshore Engineering.

To be really serious about my personal thanks, I could cover the whole of our globe and beyond. I will start with Dr. Farrokh Mistree, who was the first person trying to convince me to continue my graduate studies in Berkeley, and who, *I* am glad to say, was successful in doing so. During my Master's and Ph.D. degree studies I was fortunate to have Professor J. Randolph Paulling as advisor. I enjoyed very much working for him, as a doctoral student and research assistant, always being exposed to new (and some old!) ideas and often enough left alone to do some things my own way, and also as a crew member sailing from Kauai to San Francisco. Both from the personal and professional points of view, one benefits by being exposed to the sea for a prolonged period of time, at least when the vessel from which the observations are made is reliable. I

benefitted also in many ways from my association with Professor William C. Webster, whom I would like to thank for his continued support as well as comments and criticisms. Professor Frederick S. Sherman from the Mechanical Engineering department was kind enough to be my "outside" committee member, and I am grateful for his lively interest in my dissertation during the past few years. The other members of the Naval Architecture faculty have contributed in one way or another to the completion of this work, too, including Professors Alaa E. Mansour and Ronald W. Yeung. In particular, I enjoyed the hydrodynamic teachings of, and my personal relationship with Professor John V. Wehausen. Thanks are also due to Lydia Briedis and Leslie Service for making student life even more agreeable.

A significant part of my studies has been influenced (mostly in a positive manner) by a number of colleagues, be it through technical discussions or other social events; these honorable persons are Ananthakrishnan P., Rabi De, Mark Grosenbaugh, Stephen Hodges, Colin Moore, Frank Robert, Erik Tiemroth and Kirsi Tikka, among others.

Naturally, the bulk of my gratitude goes to my family, who have had to endure some hardship during my studies. To Catharina, especially, I am most grateful for her unwavering support and efforts, and also for keeping her sanity throughout my studies; furthermore, I must thank Annelien for providing so much joy during the last few chapters of my dissertation.

TABLE OF CONTENTS

CHAPTER 1

Introduction

Seakeeping has provided seafarers, platform operators and researchers with a multitude of challenging problems, to which, seemingly, an even larger array of solutions has been proposed in the various fields. With the advent of computers, theoretical models and numerical simulations have been becoming increasingly important (and fashionable), so that nowadays the designer of an ocean going "structure", be it a ship or platform, has to choose between quite a large number of numerical tools for his calculations. Regardless of the type of structure that is being designed, one of the designer's tasks is to ensure the safety and seaworthiness of the structure, a prime consideration being the safety against capsizing. Despite recent advances in ship hydrodynamics, the possibility and actual process of capsizing are still difficult to predict with a good measure of confidence, and in fact relatively little attention has been paid to the mechanism of capsizing.

The main objective of this work is to develop a model which represents realistically the motions of a steered vessel in severe, random seas. The motions are those of a rigid body having six degrees of freedom, and are not necessarily small. An important part is the investigation of factors leading to a capsize, as well as the simulation thereof. Most of the theory is applicable also to platform motions, bearing in mind that mooring effects are not accounted for. Use is made of previously obtained experimental results to validate the present approach. Special attention is paid to the ship motion behavior and wave statistics in quartering to following sea conditions, since those conditions may affect ship motions most severely.

The approach taken in this work is to solve the equations of motion in the time domain, where linear and nonlinear force contributions are considered. The advantage of time domain simulations is that, for a given set of conditions, the response for large displacements, or even up to the

point of capsize, can readily be determined, the only limitation being the validity of the theory employed. The obvious drawback of the method is that the response is obtained for a unique set of conditions, which makes it difficult to make any general conclusions as to the response behavior, unless one performs a large number of simulations from which statistics can be extracted with a reasonable degree of confidence. Other methods dealing with the estimation of large angles of motion and capsizing are based on deterministic linear theory, statistics coupled with linear spectral analysis, or on some kind of nonlinear statistical approach. Of these alternative methods it seems that the nonlinear statistical approach is most appropriate, when one is interested in obtaining statistics concerning large roll angles, for example. As opposed to the linear approach, a nonlinear statistical method should make it possible to account for certain nonlinearities, be it in an approximate manner, that may significantly influence the overall behavior of a vessel in a severe seaway. Nevertheless, the statistical approach is typically based on nonlinear vibration theory, which permits the prediction of motion instabilities, but is not necessarily relevant when considering the actual occurrence of a capsize. That is, roll motion instabilities do not have to result in the capsizing of a vessel. It is not the aim of the author to defend or justify the use of the time domain method in light of the various alternative procedures, nor to discuss their facets in any detail, so in the following literature overview only experimental and theoretical work, thought to be relevant with respect to time domain simulations of vessel motions in a severe sea state, are treated.

Overview of Relevant Experimental Work

Seaworthiness may be described as the ability of a structure to withstand waves and wind in a safe manner, whilst exhibiting comfortable motion characteristics. For a ship the maneuverability characteristics are also of importance. Experimental and theoretical research in the field of seakeeping and stability behavior started the last century, one of the most notable early works being on ship rolling due to waves by Froude (1872), who laid the theoretical foundations for predicting roll motions. Extensive capsize experiments have been carried out on the San Francisco Bay to

investigate the large motion behavior, specifically the occurrence of capsizing, of ships in severe following and quartering seas. Tests were performed with free running models of typical cargo ships, and also in the towing tank with restrained models (for following sea conditions only). Results of the experiments on the Bay are given by Haddara *et al.* (1972), Kastner (1973), Chou *et al.* (1974), and Oakley, Paulling and Wood (1974). A numerical model was developed in the course of the above work, and reasonable results were obtained for the predicted motions in following waves up to the point of capsize, when compared with some of the model tank tests involving the same conditions. However, the correlation between measured and predicted results was in general not very good. Parts of that simulation model have been used in the present work. The final report of the towing tank experiments and numerical simulator has been presented by Fallon *et al.* (1980). The ship models tested in the towing tank were allowed three degrees of freedom: heave, roll and pitch. The numerical model had been developed specifically for the calculation of large motions in following sea conditions, and for low encounter frequencies of encounter. Pérez y Pérez (1974) investigated the time domain simulation of a steered ship in random seas, taking into account roll, sway and yaw, and his results showed quite good agreement with some of the San Francisco Bay experiments.

Capsizing of the models tested on the San Francisco Bay was found to occur during following or quartering sea conditions, and less often for beam seas. The models were tested in ballast and full load condition, for a variety of metacentric heights and Froude numbers. Three different modes of capsizing were observed for following or quartering sea conditions: 1) low cycle resonance, also referred to as autoparametric excitation, which can be shown to be due to the time dependence of the roll restoring moment in waves; 2) pure loss of static stability (mostly in following seas), where the ship remains for a significant time stationary at a large heel angle while the waves pass by; and 3) broaching due to successive waves followed by a large amount of heeling. The models in full load condition, and with a low metacentric height, were found to be most susceptible to capsizing, where the low freeboard was also thought to be contributing to the catastrophic behavior.

Other capsize experiments have mostly concentrated on the behavior of small vessels (e.g. fishing trawlers) in beam seas. The capsizing of fishing vessels, caused by shifting cargo and shipping green water, has been investigated experimentally by Kawashima *et al.* (1978) for severe beam and quartering seas. Experimental observations of the capsizing of fishing trawlers subjected to breaking beam seas have been reported by Dahle and Kjærland (1979) and Morrall (1979). The capsizing of small vessels in following and quartering seas has been studied experimentally by Takaishi (1982) and Yamakoshi *et al.* (1982). Capsizing in regular beam seas was studied by Wright and Marshfield (1979), who compared experimental results, for a vessel having different amounts of freeboard, with those from a simple mathematical model describing the roll behavior.

The capsizing of medium size cargo ships (100 to 200 m in length) has been investigated extensively by Blume and Hattendorf (1984). Model experiments were carried out in severe random seas, which were unidirectional, with four different models at different drafts. According to the authors, capsizing in beam seas was not of relevance for the vessels considered, and head sea conditions resulted in capsizing only at, or close to, zero ship speed. Following sea conditions (where the waves come in at an angle of 0° to 30° from astern) were found to be the most conducive to capsizing, and therefore were used in the majority of the experiments. Based on the analysis of built ships, the authors introduce a form factor, depending on the beam, draft, depth, *KG* and fulness, expressed by the block and waterplane area coefficients. This form factor would be large for ships being sufficiently safe against capsizing, and small for unsafe ships. Stability criteria are proposed by formulating the criteria in terms of the righting arm curve properties and the form factor. It is also suggested that the risk of capsizing decreases for slower ship speeds ($Fn < 0.15$).

Large angle roll motions, the origin of which was reportedly attributed to parametric excitation, have been experienced occasionally by full size container ships and offshore transportation vessels. Especially vessels

exhibiting a large variation in waterplane area (and hence in righting moment) with draft, may be prone to parametric resonance, which has also been observed in model experiments with Ro-Ro ships, see Sjöholm and Kjellberg (1984). It is not certain whether ships have been lost due to this phenomenon, but it is suspected that it has contributed to a number of vessel losses. Large roll angles, attributed to the loss of static stability in following sea conditions, have been reported by containership operators, among others. This behavior can be of concern when the ship speed is close to the wave speed. The loss of transverse stability can also lead to capsizing in beam seas. Broaching is dangerous especially for small high-speed vessels, but it occurs much less frequently in the case of larger ships. Two types of broaching may be observed: (1) the ship speed is approximately equal to the wave speed, so that the ship becomes directionally unstable as it is carried along by the wave (the amplitude of which does not have to be very large), or (2), the ship can lose rudder control at relatively slow speed in steep seas, where the vessel is brought off course due to successive large waves coming from astern.

The importance of surge, and hence of the relative position of the ship, in waves does not apply only to broaching but also to other motion behavior and stability. For example, the static righting arm of a heeled ship in large following waves undergoes a significant and periodic variation as the wave crest moves along the ship. This has been illustrated by, for example, Grim (1952), Kerwin (1955) and Paulling (1961). This phenomenon can lead to parametric excitation due to a Mathieu-type instability. Paulling and Rosenberg (1959) showed, using the Mathieu equation, that unstable motions may result from nonlinear coupling between heave, pitch and roll. Thus, it seems desirable to be able to predict the correct position of the ship with respect to the waves, if one wants to carry out realistic simulations of the motion behavior in the time domain.

Since it may be of importance as regards large roll motions or capsizing, experimental (and related theoretical) investigations concerning broaching are considered in the following. Davidson (1948) studied the directional stability and broaching behavior of ships in following seas. Du

Cane and Goodrich (1962) investigated in detail the occurrence and mechanism of broaching. With their experiments they indicated the importance of surge with respect to broaching behavior in following seas. Conolly (1972) discussed the various factors that might contribute to broaching, and stated that at that time there was a clear lack of theoretical tools for studying this problem in a reliable fashion; unfortunately, this is still the case. Grim (1951) studied the stability and roll motions of a ship in regular following sea conditions (theoretically and experimentally), and formulated nonlinear equations for the surge motions in irregular following seas (1963). Grim (1983) investigated the influence of wave groups on the surge motions of a ship with forward speed. As regards broaching, the importance of the position of the ship with respect to the wave crest is also suggested in the work by Wahab and Swaan (1964) and by Renilson (1982). Motora, Fujino and Fuwa (1982) confirmed that, based on experimental observations and some numerical computations, under certain wave conditions and ship speeds, broaching occurs due to the large wave-induced yaw moment exceeding the course keeping moment, which is exerted by the rudder. Although it appears that through experiments a significant amount of knowledge has been gathered as regards broaching, not much attention seems to have been devoted to studying broaching in combination with capsizing.

Theoretical Approaches for Simulating Large Amplitude Motions

Next a number of numerical models are reviewed that deal with the prediction of nonlinear motions of floating structures, so as to place the model presented by the author in chronological context. These nonlinear models have been developed over the past ten years or so, and only highlights of the various theoretical aspects are discussed.

As was mentioned above, the time domain model described by Oakley, Paulling and Wood (1974), and also by Fallon *et al.* (1980), was developed specifically for a slender ship in following sea conditions. The low encounter frequencies made it possible to estimate the diffraction forces using the "relative motion principle", which allows the diffraction forces

acting on a section of a slender body, to be expressed in terms of the added mass and damping coefficients, multiplied by a mean water particle acceleration or velocity. As a result, the combined radiation and diffraction forces would depend on the relative velocity and acceleration between the hull and the fluid. For long waves this is a reasonable assumption, and diffraction effects tend to be relatively small in any case under these conditions. The Froude-Krylov forces were evaluated over the complete wetted portion of the hull at each time instant, whereby it was assumed that the wave profile along the the ship was that of the undisturbed incoming wave. The added mass and damping coefficients were considered time independent, except that at each time instant the coefficients were scaled by the time-dependent cross-section area, which is not justifiable theoretically. The Frank Close Fit method, see Frank (1967), was used to obtain the sectional hydrodynamic coefficients. No assumptions were made concerning small angles of rotation, so large roll motions could be handled numerically, up to the point of capsize. Some aspects of this time domain model have been employed in the present work, as will be discussed in subsequent chapters.

Salvesen (1978) developed a second-order theory for calculating the heave and pitch motions of a ship in the frequency domain. The assumption is made that the ship is slender and/or that the frequency of motion is low, and also that the wave amplitude is small. After evaluating the first order motions, the second order exciting forces were determined for a number of cross-sectional shapes. The results indicated that these forces were of significance mostly for V-shaped bow sections. In a time domain simulation procedure one could quite easily add these second order forces to the first order ones.

At Det norske Veritas a numerical model was derived to compute the motions and loads of a slender ship with forward speed in large, regular head seas. The theory and results of this time domain model have been described by Børresen and Hambro (1978), and by Børresen and Tellsgård (1979). One of the features that is different from the models discussed above, is that the sectional added mass and damping coefficients are determined at each time step for the instantaneous sectional draft, with

the cross section being considered in the upright position. Although this may seem to be a practical way of dealing with the time dependence of the hydrodynamic forces, theoretically it is not correct as the theory is based on small periodic motions about the mean position. As a result, it is not possible to say whether such an approach will result in better motion predictions. The diffraction forces were estimated by applying the relative motion principle, and forces due to bow flare and slamming were included. Effects of water on deck were estimated in a very simplified fashion as an added inertia force.

Chapman (1979) solved the transient motion of two-dimensional bodies in waves by using source distributions over the static wetted surface. The free surface boundary conditions are linearized, and the body boundary conditions are satisfied exactly, thereby permitting "large" motions. Green's theorem is applied to obtain the source distribution, from which the pressures can be calculated. In conjunction with the above work, Chapman (1980) extended the theory to the three-dimensional case for bodies of arbitrary shape having forward speed. Here arbitrary motions can be handled, but the assumption is made that the motions are sufficiently small, so as to linearize the boundary conditions. The ship hull is represented by a set of quadrilateral surface panels.

A single degree of freedom model has been developed by Wright and Marshfield (1980) to study the roll behavior in beam seas. Perturbation theory was used to derive the equation of motion, where damping and the hydrostatic restoring moment were considered nonlinear. Stability theory was applied to identify regions of unstable roll behavior.

Parametric roll excitation in the time domain has been investigated by Blocki (1980), who studied the heave, roll and sway behavior of vessels in regular and random waves; surge, sway and yaw motions were considered to be unimportant with respect to Mathieu instabilities. Based on the results for regular waves, an attempt was made to derive a probability distribution of capsizing in random waves.

The theory of the transient response of two-dimensional cylinders in calm water was studied by Yeung (1982). By applying unsteady Green functions, and using Volterra's method, he obtained integral equations for the velocity potential. The numerical evaluation of the memory effect integrals is discussed in detail. He showed that the heave response of a lightly damped cylinder, as predicted alternatively using constant coefficients at the natural frequency, is practically the same as that predicted by the formal time domain method. Predictions were found to compare well with experimental results.

Motions in large, regular waves were studied experimentally by Yamamoto *et al.* (1982), and a numerical model was developed to compare the theoretical results with those from the experiments. Linear theory was used to compute the forces, and the calculation of the diffraction forces was based on the relative motion principle, which has been applied to a slender ship with forward speed. The added mass and damping coefficients were determined for the instantaneous position of the ship, and bow-flare slamming forces were taken into account in a simplified manner.

A time domain method for calculating the forces on two-dimensional submerged and surface piercing bodies has been presented by Vinje, Maogang and Brevig (1983). In their method the free surface conditions are satisfied exactly in an inner domain, and matched to an outer domain where a linear solution is assumed. The nonlinear potential theory allows for the occurrence of breaking waves, by means of the Euler/Lagrangian method. The problem is formulated as an initial value problem, and the motion of the free surface is represented by discrete, marked particles. Calculations were performed for a submerged cylinder situated close to the free surface. Results were found to agree fairly well with results from linear theory, but the method as such is not practical yet for three-dimensional ship hulls. The Euler-Lagrangian method was applied in two dimensions by Greenhow *et al.* (1982), to study the capsizing of a wave energy device in breaking waves. The basis of the above approach can be found in Vinje and Brevig (1981).

Lin, Newman and Yue (1984) present a nonlinear theory for the forces acting on a three-dimensional, axisymmetric body. The computational domain is considered nonlinear, and is matched to an outer domain governed by linear theory. The method was applied to the case of a nonlinear impulsive wave maker, and in a preliminary fashion to the heave motion of a circular cylinder. Although promising, the method as such cannot be applied (similarly to the previous method) to arbitrary three-dimensional bodies, and it is computationally intensive.

A higher order theory for ship motions is described by Papanikolaou (1984). The theory is based on a perturbation scheme where all terms up to second order are retained consistently. The forces on the body are determined in the frequency domain by integration of the pressure, which is given by the velocity potential (also calculated up to second order). The velocity potential is obtained by solving for the distribution of sources over the wetted surface of the cylinder or hull, by means of integral equations. Hydrostatic effects are treated linearly in this theory. It is suggested that second order effects may be of importance when studying capsizing. Second order perturbation theory has been applied by Papanikolaou and Zaraphonitis (1987) in the development of a time domain simulation model; the model is applicable for regular beam seas of small amplitude, and considers only the roll mode of motion, with some correction for changes in hydrostatic forces due to heave.

A consistent linear theory in the time domain is given by Liapis and Beck (1985) for a vessel with forward speed in calm water. The theory is applicable to bodies of arbitrary shape, undergoing forced motions that can be arbitrary but of small amplitude. The hydrodynamic forces are determined by integration of the pressure over the mean wetted surface. The pressure is given in terms of the velocity potential for an impulsive source, involving convolution integrals of the impulse response function and the motion. A set of integral equations must be solved to obtain the velocity potential due to an impulsive velocity. A similar time domain method has been presented by Beck and Liapis (1987) for computing the three-dimensional radiation problem for an arbitrarily shaped body.

Brook (1986) has presented comparisons between simulation predictions and experimental results for vessels in irregular seas. The simulation model is based on modified linear seakeeping theory, where coupled yaw, sway and roll are taken into account and nonlinearities in the roll equation are included. Nonlinearities in roll comprise the exact evaluation of the hydrostatic restoring moment and "quadratic" damping due to viscous effects. Also the frequency dependence of the potential roll added mass and damping were considered by means of convolution integrals. Some sensitivity analyses were carried out to determine the influence of certain force contributions on the roll response. It is suggested that the magnitude of the nonlinear roll coefficients has a significant influence on roll, while the frequency dependence of added mass and damping is not always of importance, depending on the type of vessel.

A second order theory for a ship with forward speed in regular waves is presented by Ohkusu (1986). Following sea conditions, and thereby low encounter frequencies, are assumed so that the Froude-Krylov forces would tend to dominate. It was found that the higher order disturbance effects of the incoming waves could be of significance locally, but were small compared with the total exciting forces. It is suggested that the phase relationship between the wave and the exciting force is improved by including the higher order terms.

Fujino and Yoon (1986) apply an extended version of strip theory to the problem of large motions in regular waves. All degrees of freedom, except for surge, are considered, and the responses are solved in the time domain. The added mass and damping forces are determined at each time step, by evaluating the coefficients for the exact instantaneous position using Frank's method. The diffraction forces are determined using the relative motion principle. Certain quadratic terms involving the incoming wave potential are considered in the expression for the pressure. It is suggested that for wave height to length ratios of up to 1/20, the nonlinear theory does not give any better results for ship motions than linear theory, for practical purposes that is. Nonlinearities in the shear forces and bending moments seemed to be more pronounced for

increasing wave heights. Of course, for wave height ratios larger than 1/20 nonlinearities in the rigid body motions may become much more significant.

A time domain method based on strip theory has been presented by Elsimillawy and Miller (1986). In the model surge is omitted from the calculations, the added mass and damping coefficients are determined at the instantaneous position for each section using Frank's method, and the diffraction forces are calculated by integrating the radiation potentials, as given by Salvesen, Tuck and Faltinsen (1970). The variation of the righting moment during the passage of a wave is discussed.

Kröger (1986) describes a model for simulating the roll motions of a ship in the time domain. All six degrees of freedom are considered, where the yaw, sway and roll motions are decoupled from the heave, pitch and surge motions; heave, sway, yaw and pitch are considered to be linear, while the roll and surge motions are taken to be nonlinear. Nonlinearities in the roll restoring moment are taken into account as well as viscous damping effects. The frequency dependence of added mass and damping in the time domain is not treated. Roll responses are given as a function of various parameters, such as wave heading angle, metacentric height, and encounter frequencies. The conditions for capsizing in irregular waves are studied, where in the simulations use is made of an equivalent wave to approximate the actual time dependence of the wetted surface. Kröger's model has been used by Söding (1987) to investigate critical ranges of wave conditions that may lead to capsizing. Simulations were carried out for a certain cargo ship, subjected to severe following to quartering seas; critical wave heights were estimated for the various conditions.

The nonlinear roll behavior of barges in beam seas has been studied in the time domain by Robinson and Stoddart (1987). A one degree of freedom model is presented for the roll motion, where the hydrodynamic coefficients are assumed to be constant; nonlinearities are represented by quadratic damping due to viscous effects, and by the hydrostatic restoring moment. The quadratic damping coefficient is based on the force

prediction using a discrete vortex method. The hydrostatic restoring moment is adjusted for the wave slope, by taking the relative angle between the barge and sea surface into account. This is a reasonable approach for waves having a length which is long compared with the beam, and has been investigated by, for example, Blagoveshchensky (1962) and Visineau (1979).

A time domain model to study the broaching behavior of patrol craft has been presented by Rutgersson and Ottosson (1987). In this model surge, sway, roll and yaw were considered in regular and random wave conditions, and theoretical parameters were combined empirically with measured force results of free-running models in regular waves to form the total mathematical description of the process. Certain nonlinearities, such as damping due to viscous effects and drift forces, were taken into account.

Poincaré mapping and bifurcation theory have been applied by Virgin (1987) to the single degree of freedom roll model for a ship in regular beam waves, based on the model proposed by Wright and Marshfield (1980). Analysis yielded frequency and amplitude regions for which roll motion instabilities could be expected to occur.

An overview of a method to simulate the motions of ships in severe seas has been presented by Hooft (1988). Motions up to the point of capsizing in beam and following waves were studied, where wind was also taken in to consideration. The wave exciting forces were based on measured results in waves for different model speeds, and simulation results were obtained for a variety of ship speeds, wind and wave conditions.

The behavior of semisubmersible platforms has been investigated quite extensively, and in recent times thorough studies, both experimental and theoretical, have been performed concerning damaged semisubmersibles in large waves. In connection with this, the comprehensive "MOPS" project (Mobile Offshore Platform Stability) carried out in Norway deserves attention; one of the final reports on the experimental results and recommendations has been presented by Dahle (1984), and some of

the numerical modelling concerning the motions of a semisubmersible, having a list angle in regular waves, has been described by Huang, Hoff and Næss (1982), and by Næss and Hoff (1984). Matsuura, Ikegami and Seto (1987) developed a similar time domain procedure, where the motions of a semisubmersible in extreme conditions were considered in order to study adverse effects such as flooding, heavy list or mooring line rupture. Both of the aforementioned time domain methods for semisubmersibles are largely based on the work by Paulling (1977). Although the present work is concerned with the motions of a freely floating body, several aspects of the theory and numerical model should be applicable to moored structures as well.

Problem Statement and Solution Procedure

As a synthesis of the above theoretical models, there still appears to be a need for a theoretical model that is capable of conjunctively treating all six degrees of freedom of a steered vessel sailing in a severe random sea, where the wave-induced vessel motions can attain large values. Furthermore, due to the lack of the appropriate tools, very little theoretical work has been performed with the aim of studying the mechanisms of capsizing in waves. Thus, an attempt is made to contribute some new material to our sparse knowledge of capsizing in waves.

The theory and related computer program developed in the present work are basically an extension of those from the approach described by Oakley, Paulling and Wood (1974) and Fallon *et al.* (1980). Improvements and additions to the theory have been made such that the theory is not restricted to astern seas and low encounter frequencies. Also, more viscous effects have been incorporated. There is a need to investigate certain issues pertaining to simulations in the time domain, which up to now have not received much attention; this applies especially to the behavior in wave groups for following, or quartering, sea conditions. In the course of this work it was found that the statistics of the observed random seaway, for following sea conditions, can be different from those commonly accepted. Also, it was deemed useful to investigate the relative importance of the various exciting force contributions. This is done using

two approaches: (1) the sensitivity of the roll response to variations in the force components is considered for several conditions, so as to obtain information regarding their relative significance; (2) the time series of the moment components are plotted along with the motion records.

An overview is given next of the contents of this dissertation, which is an attempt to deal with the problem of large ship motions, up to the point of capsizing, in a realistic and rational manner. An investigation is made of factors that are relevant to the prediction of capsizing. Some of the basic assumptions that are made in the present work comprise the following: the waves can be random but are assumed unidirectional, the vessel is freely floating and may have forward speed, cargo and stowed goods are assumed to remain stationary under all conditions. The last assumption especially, is one that is easily overlooked when considering severe motions from the theoretical point of view, while in fact shifting cargo or ballast may be one of the leading causes for a ship to exhibit undesirable motion behavior in severe conditions, or even to capsize, see e.g. Saunders (1965) and Kawashima *et al.* (1978). It would be a difficult task to incorporate nonstationary cargo effects in a motion program, but might be worthy of future consideration. Although of possible importance, breaking waves and water-on-deck effects have not been considered.

In Chapter 2 the theory of computing the motions in large waves is described. This chapter deals mainly with the description of the various exciting forces and sea surface. The approach has been to separate the potential flow problem from the viscous flow problem, making it possible to estimate separately potential and viscous flow effects, and subsequently superimpose them. The potential forces are based on an extension of linear theory, where some integrations are performed over the instantaneous free surface, large angles instead of small angles are used, and first-order memory effects are considered. Viscous forces are modelled empirically as regards the roll damping moment, drag forces in the surge, sway and yaw directions, and sway-roll coupling. Force contributions are assumed to be due to waves, maneuvering, rudder and possibly wind. It is assumed that the free surface conditions can be linearized, so that linear wave theory can be used to compute relevant

wave kinematics up to the free surface; linear theory has been shown to yield reasonable results for deep water conditions, even for waves of finite height. The motion behavior in unidirectional random waves only is determined, since it was thought that wave directionality can be quite easily implemented in the numerical model, if so desired, at a later stage. Presumably most of the important motion characteristics can be deduced from the results in unidirectional seas. Some new results for wave statistics pertaining to the simulation of random following seas are also presented in Chapter 2; these results are relevant with respect to the simulation of ship motions in following or quartering sea conditions.

Aspects of the implementation of the theory in the computational algorithm are given in Chapter 3. The numerical model has been verified by means of comparisons with experimental results in waves of small and large amplitude, as is discussed in Chapter 4. The sensitivity of the roll response is investigated in Chapter 5, where the changes in roll related to systematic changes in the various force components are considered for beam and following sea conditions. These results provide some new information on the relative importance of the various fluid force components that affect large amplitude roll motions. Based on some of the theoretical results obtained in Chapter 2, simulations of random following seas have been performed, as well as some computations of motions in following sea conditions, the results of which are presented in Chapter 6. Also, an outline has beer given in Chapter 6 of a method for representing a random seaway by an equivalent wave system, which consists of only two components and which may be useful to simulate e.g. capsizing. In Chapter 7 a number of different capsize modes are identified numerically, followed by an attempt to determine critical ranges of speed and heading conditions for which capsizing of a given vessel may be expected to occur.

CHAPTER 2

Theory of Ship Motions in Large Waves

The objective is to formulate a model capable of treating in a realistic manner the motions of an ocean going vessel caused by severe waves. Wind may be considered in a rather simplified fashion. Since it should be possible, with the aid of this model, to investigate potentially dangerous situations that may lead to capsizing, the model cannot be restricted to handling only, for example, small amplitude wave conditions. That is, the model should be able to handle storm generated wave conditions also.

At the onset of this work a number of basic assumptions have been made: wave breaking does not occur, impact loads due to slamming are not considered, and effects of water on deck are neglected. In order to deal with these phenomena the reader is referred to the following references. The theory and model for simulating the effects of water on deck in two and three dimensions have been treated by Dillingham (1981, 1986). Breaking waves and capsizing of small vessels have been studied experimentally by, for example, Dahle and Kjærland (1979), Morrall (1979), and Allievi *et al.* (1986). An empirical procedure has been presented by Blume (1987) to estimate the roll moment impulse due to a breaking wave. Another assumption made in this study, is that the ship or platform motion problem is applied to deep water conditions only, where the water depth is sufficiently large, so that the waves are not affected by the bottom. The vessel is considered as freely floating, that is, mooring forces are not taken into account, and it is assumed that the center of gravity remains stationary within the vessel at all times. Effects due to currents are not considered.

In order to predict the seakeeping behavior of a vessel, it is necessary to determine the fluid pressure acting on the structure. Pressures can be calculated fairly accurately for a ship in small waves, however, most theories break down when the wave height becomes relatively large. Forward speed effects of a ship present additional problems. It is assumed that inviscid fluid effects may be treated independently of viscous

effects, which is obviously an approach of convenience and theoretically not correct since there may be strong interactions, see for example the discussion by Odabasi (1981). It has been found that in many marine applications this is usually not a disastrous assumption, as viscous effects often are confined to relatively thin boundary layers.

Therefore, the treatment of fluid forces has been split into two main sections: free surface effects due to vessel motion and wave excitation forces are treated in Chapter 2.1, where the fluid is considered inviscid and the flow field irrotational, so that potential flow theory is valid. The theory should be applicable to both low and high frequency waves coming from any direction with respect to the vessel. Chapter 2.2 deals with viscous effects associated with, for example, friction and vortex shedding, especially with respect to roll. Chapter 2.3 is concerned with other external forces, such as rudder and wind-induced forces, which are treated only briefly. Chapter 2.4 deals with the theory of wave kinematics for both regular and irregular waves. In this work special attention is paid to the motion behavior and statistical properties in wave groups in random, following seas. The above theoretical model forms the basis of simulating the vessel motions in severe sea conditions, which may be critical with respect to capsizing. In order to proceed, we give an overview of the coordinate system convention and of the general equations of motion that are to be solved.

Coordinate System Convention

Several coordinate systems are necessary for expressing the forces and moments acting on a vessel, and for solving the equations of motion. The earth-fixed, or inertial, system is defined by Oxyz, where the y-axis points vertically upwards. The local system O*x*y*z* is fixed in the body with the origin O* being located at the center of gravity of the structure, and where x* points forward (towards the bow), y* points upward at right angles to O*x*z*, and z* points in the starboard direction at right angles to O*x*y*. All coordinate systems are considered to be right-handed, so that e.g. pitch is bow up, and yaw is the bow towards port. The vessel may have forward speed, U, and the system $O^e x^e y^e z^e$ translates in the Oxz

plane with the vessel at its mean speed, where x^e points in the mean forward direction of the vessel, i.e., along the x-axis, and y^e points vertically upwards. A schematic overview of the various coordinate systems is shown in Figure 2.1.

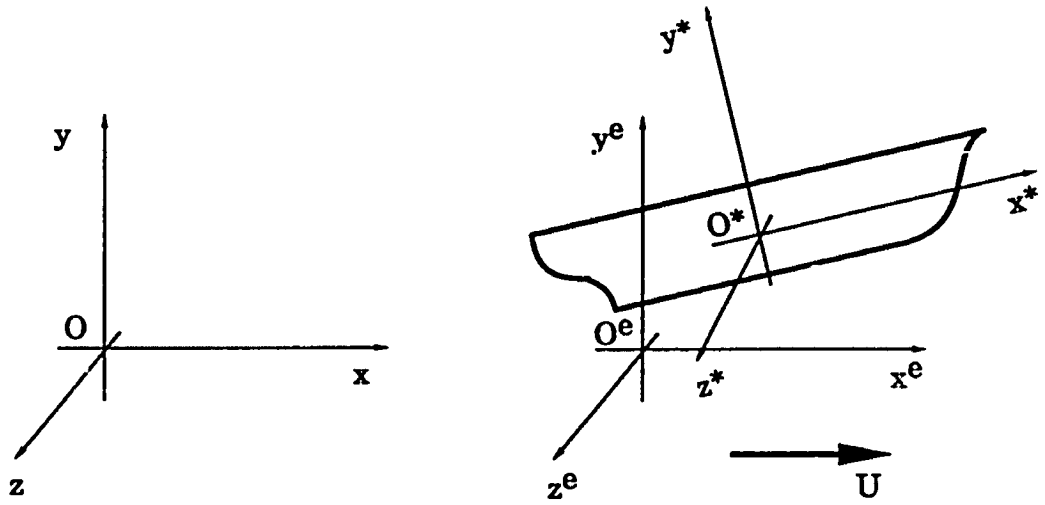

Figure 2.1. Coordinate System Representation

Equations of Motion

The approach for solving the motions of a structure subjected to various external forces is to consider the equations of motions in the time domain. Both linear and nonlinear components are to be incorporated in their full (or approximate) form. If there is no interaction among certain force components, this method allows one to easily add or remove those components in the equations of motion. In order to apply Newton's second law the body is assumed rigid, and all six degrees of freedom are to be taken into account conjunctively.

The system of equations of motion is described by Newton's second law, stating the conservation of linear momentum:

$$\frac{d}{dt} m \mathbf{v} = \mathbf{k},$$

and the conservation of angular momentum:

$$\frac{d}{dt} \mathbf{I} \omega = \mathbf{q},$$

where m is the mass of the vessel, **k** represents the external force vector, which has a hydrodynamic component due to the motion of the structure and due to the wave-induced forces acting on the hull, as well as other external force components, such as rudder or wind forces, and **v** is the velocity vector. Similarly, **I** is the inertia matrix, ω is the angular velocity vector, and **q** is the moment vector. In this work, the conservation of linear momentum equations will be solved in the fixed reference system, while the conservation of angular momentum will be expressed in the local, body-fixed system. To obtain the forces in the earth-fixed reference system, the various force components are first calculated in the the structure-fixed O*x*y*z* system. These components are added so as to yield the total forces on the right hand side of the equations of motion, and the total force vector can be resolved into the Oxyz system by a straightforward coordinate transformation, using the transformation matrix **T**, as is discussed further on in this chapter. An overview of possible ways of evaluating the equations of motion in time domain simulations has been given by Hooft (1986).

The position of the vessel can be expressed in terms of the location of the center of gravity in the fixed system Oxyz, and by the angles of rotation (given about the local axes of O*x*y*z*). In order to solve for these quantities, first the position of the mass center in the fixed system is defined by the vector **x**(t):

$$x(t) = \begin{bmatrix} x_1 \\ y_1 \\ z_1 \end{bmatrix},$$

and the velocity of the mass center is its time derivative:

$$v(t) = \frac{d}{dt} x(t) = \dot{x} .$$

Here and further throughout this work, a dotted quantity denotes differentiation with respect to time. The rotation of the ship coordinate system is uniquely defined by the following order of rotations, characterized by the Euler angles : first rotate by the yaw angle ϕ, followed by the pitch angle ψ, and finally by the roll angle θ. The Euler angles are represented by the vector χ:

$$\chi = \begin{bmatrix} \theta \\ \phi \\ \psi \end{bmatrix} .$$

In order to express a vector in the system O*x*y*z* in terms of the Oxyz system, use must be made of transformation matrices associated with these angles; these are given in Appendix A. The angular velocities about the vessel coordinate axes given by ω can be related to the time derivatives of the Euler angles, $\dot{\chi}$, as follows :

$$B\,\dot{\chi} = \omega ,$$

where the matrix **B** is also a function of the Euler angles, and is defined in Appendix A. It is noted that with large motion simulations the Euler angles must be retained, so that the various transformation matrices are time dependent.

The moments and products of inertia in **I** are constants in the moving and rotating O*x*y*z* system, and the rate of change of angular momentum in that coordinate system is given by

$$\frac{d}{dt}\mathbf{I}\omega = \mathbf{I}\frac{d}{dt}\omega + \omega \times \mathbf{I}\omega .$$

The inertia matrix contains the conventional moments and products of inertia of the vessel:

$$\mathbf{I} = \begin{bmatrix} I_{xx} & -I_{xy} & -I_{xz} \\ -I_{xy} & I_{yy} & -I_{yz} \\ -I_{xz} & -I_{yz} & I_{zz} \end{bmatrix} .$$

The heart of the problem of calculating the motions lies in the computation of the hydrodynamic forces, which appear on the right hand side of the equations of motion. This problem is compounded by the required ability of the model to treat random waves that are "large", i.e., for which the maximum amplitude is of the order of, say, the draft of the structure. An overview is shown in Table 2.1 of the various potential and viscous force components that may occur in the equations of motion, together with some relevant background information. Since in this work the emphasis is placed on wave-induced motions, wind forces have been included only in a simplified fashion, i.e., constant velocity and profile; if desired at a later stage, it would be relatively easy to model the velocity and profile as time-dependent quantities. A brief discussion is given of the assumptions involved with the determination of the various force components. Next a summary is presented of the nonlinearities that occur in the equations of motion. Details about the determination of the force components and other related phenomena are treated in the following sections of this chapter. Certain aspects of the numerical procedures for solving the equations of motion are discussed in Chapter 3.

Force Components	Comments
- Froude-Krylov	due to wave induced pressures
.static	(evaluated over instantaneous wetted
.dynamic	surface)
- Radiation	first order memory effects
- Diffraction	linear transfer functions
- Viscous	
.roll damping	linear and quadratic (relative motion)
.sway-roll coupling	quadratic drag (vessel motion)
.maneuvering	nonlinear (calm water)
.sway, roll and yaw	quadratic drag (waves)
- Resistance	total calm water resistance (relative motion)
- Propulsion	constant RPM, variable thrust
- Rudder	lifting line (instantaneous velocity)
- Wind	time-independent profile and velocity

Table 2.1. Summary of Force Components in Equations of Motion

Assumptions in the Determination of the Force Components

Next an overview is given of the assumptions involved with the determination of the various force components listed in Table 2.1. Linear theory is used for determining the potential flow forces, where the velocity potential is decomposed into several components, comprising a potential associated with the incoming wave system, a radiation and diffraction potential. It is assumed that the Froude-Krylov forces, associated with the pressure of the incoming wave system, are critical, so that they must be evaluated in an accurate fashion. The wave pressure is evaluated over the exact wetted surface, and it is assumed that linear wave theory is applicable above the mean water level for predicting the pressure. It has been shown that, even for large amplitude waves, linear theory predicts the kinematic and dynamic wave properties quite well. From the sensitivity analysis in Chapter 5, it appears that the Froude-Krylov forces are always of importance, that is, for all wave conditions considered in the analyis.

The determination of the radiation forces is based on potential theory applied in the time domain. The theory is valid for arbitrary, small motions, and approximations are made to take into account large angles of rotation. The radiation forces are expressed in terms of memory effect integrals, which depend on first order kernel functions. The kernel functions are based on the Fourier transform of the frequency-dependent added mass and damping coefficients. The vessel is assumed to be slender, so that strip theory can be used to estimate the hydrodynamic coefficients. Memory effects associated with surge motions can be incorporated by means of externally obtained kernel functions for surge. The radiation forces are evaluated with respect to a nonrotating coordinate system that moves with the vessel at its mean speed, and it is assumed that the kernel functions are independent of the direction of motion of the vessel. That is, the kernel functions are assumed time independent, and therefore need to be evaluated only once before determining the ship response. From the simulations it was found that the radiation forces yielded better motion results by assuming the vessel to be in the upright position at each time instant.

It is assumed that linear strip theory can be used to determine also the diffraction forces, where the vessel is considered in its upright position, and approximations are made to deal with large angles of motion. Furthermore, it is assumed that the wave motion has been going on for a sufficiently long time for transient effects to disappear, so that the time-dependent diffraction forces can be expressed in terms of a frequency-dependent transfer function and the instantaneous wave elevation at the center of gravity. The forces are determined with respect to the translating, nonrotating reference system.

Viscous effects are assumed to be independent of potential flow effects, so that the various viscous flow forces can be added directly to the potential flow forces. All viscous effects are treated separately and in an empirical, approximate manner. Rather than attempt to deal with the viscous forces in an exact fashion, the intention was to incorporate all possibly relevant contributions more or less rationally. The distinction is made between the

following effects: roll damping, coupling between sway and roll, maneuvering, and wave-induced drag. The roll damping moment is considered as the sum of a linear and quadratic term, where the damping coefficients are assumed to be time independent. Although the damping coefficients depend on the roll amplitude and frequency, in this work they are based *a priori* on the natural roll frequency and an amplitude that can be expected to occur for the conditions considered. It is assumed that the method of component damping may be used, in which the total damping moment is assumed to consist of independent contributions: hull lift, friction, eddy shedding, and bilge keel. The empirical data are valid for rolling in calm water with forward speed. However, if the waves in a direction transverse to the vessel are sufficiently long, it is assumed that the roll damping moment depends on the relative rotational velocity between hull and fluid; only the undisturbed incoming wave system is considered, i.e., diffraction and wave radiation effects are assumed negligible.

It is assumed that coupling between sway and roll due to viscous effects can be modelled by a quadratic drag term. This results in a roll moment caused by the vessel's sway velocity, and a sway force caused by the roll motion. The empirical coefficients are based on the motions in calm water, and the coupling coefficients are assumed to be independent of the wave conditions and time.

Maneuvering theory in calm water is assumed to be valid when used in conjunction with the prediction of motions in waves. Maneuvering forces are assumed to be associated with cross-flow effects, where the sway force and yaw moment are considered to depend on the sway and yaw velocities of the vessel. A nonlinear empirical model is used, and the empirical coefficients are assumed to be time independent.

For waves that are sufficiently long in a direction transverse to the vessel, it is assumed that a wave-induced drag force acts in the sway direction. This drag force causes a sway force, a roll and yaw moment. It is assumed that the drag force can be modelled by a quadratic drag term,

which depends on the mean velocity of the wave transverse to the hull and a drag coefficient. The drag coefficient is considered constant.

The ship resistance is based on the total resistance in calm water for constant forward speed. It is assumed that the resistance coefficients are independent of the wave conditions and time. It is assumed that the RPM of the propeller is time independent, so that the propeller thrust can be estimated for any forward speed.

The forces acting on the rudder are assumed to depend on the instantaneous, relative flow velocity, evaluated at the center of the rudder. Lift and drag forces are modelled by expressions that are based on data for foils in steady flow conditions, and it is assumed that the lift and drag coefficients are independent of time and fluid flow conditions.

Nonlinearities in the Equations of Motion

The equations of motion are treated as exactly as possible within the limitations of the theory, the result being that the motions are nonlinear. That is, the vessel motion is related in a nonlinear fashion to the wave amplitude, for example. Nonlinearities arise from a variety of sources, and are summarized in different categories:

1. *Rigid-body dynamics with large angles* -- large angles are retained in the equations of motion, resulting in the nonlinear dependence on angular velocities due to the cross product $\omega \times I\omega$ in the conservation of angular momentum;

2. *Transformation matrices with large angles* -- the transformation matrices **T** and **B** contain products of sines and cosines of the Euler angles, so that applying those matrices to the force and rotational velocity vectors, respectively, causes a nonlinear dependence of those forces and rotational velocities (expressed in the earth-fixed system, for example) on the angles of rotation;

3. *Fluid flow effects* -- the forces acting on the structure can be nonlinear with respect to several parameters: the angles of rotation, linear and angular displacements and velocities of the vessel, wave amplitude, and wave particle velocities. The various forces can be characterized as follows.

   3.a. The Froude-Krylov forces are integrated over the exact wetted surface due to the incoming wave system, which may result in a nonlinear dependence on the wave amplitude and on the linear and angular displacements of the vessel.

   3.b. The viscous roll damping forces depend in a nonlinear manner on the vessel's roll velocity, the rotational velocity of the wave surface, and the vessel's sway velocity.

   3.c. Viscous maneuvering forces and moments (w.r.t. sway and yaw) depend in a nonlinear manner on the vessel's sway and yaw velocities.

   3.d. Viscous wave-induced drag forces and moments (w.r.t. sway, roll and yaw) depend in a nonlinear manner on the wave particle velocities transverse to the vessel.

   3.e. The total ship resistance may depend in a nonlinear fashion on the forward velocity of the vessel and wave particle velocity in the surge direction.

   3.f. Rudder forces (lift and drag) depend in a nonlinear fashion on the incoming flow velocity, which itself depends on the components of the ship velocity and wave particle velocity.

2.1. Potential Flow Effects

The total hydrodynamic pressure force is evaluated using potential theory. Viscous effects are usually associated with relatively thin boundary layers, and this is used as a justification to separate the viscous force computations from the potential flow calculations. The computation of the viscous forces is treated separately in Chapter 2.2. The general potential flow problem is considered first, followed by a detailed treatment of subproblems, such as the computation of the Froude-Krylov, radiation and diffraction forces, as well as the description of the wave kinematics. Linear theory is used, and certain approximations are made to account for large amplitude random waves and large motions.

Hydrodynamic Forces in Regular Waves

The forces acting on the vessel are considered to be due to the waves and the motion of the vessel itself. The usual assumptions are made: the fluid is inviscid, and the flow field irrotational, so that a velocity potential Φ exists. As a consequence of irrotationality there must be zero vorticity, i.e.,

$$\nabla \times \mathbf{v} = 0 \ ,$$

where $\mathbf{v}$ is the fluid velocity vector, and ∇ is the gradient operator:

$$\nabla = \left(\frac{\partial}{\partial x}, \frac{\partial}{\partial y}, \frac{\partial}{\partial z}\right) \ .$$

Also, the fluid is assumed to be incompressible, so that the conservation of mass equation, or the continuity equation, is given by:

$$\frac{\partial u}{\partial x} + \frac{\partial v}{\partial y} + \frac{\partial w}{\partial z} = \nabla \cdot \mathbf{v} = 0 \ ,$$

which can also be written as

$$u_x + v_y + w_z = 0 \ .$$

Introducing the definition of the velocity potential, $\Phi(x,y,z;t)$ must satisfy the Laplace equation throughout the entire fluid domain:

$$\Phi_{xx} + \Phi_{yy} + \Phi_{zz} = \nabla^2\Phi = 0 \ .$$

As a result of the irrotational flow assumption and neglecting surface tension, the dynamic boundary condition on the free surface, $y = \eta(x,z;t)$, can be expressed by Euler's Integral:

$$\frac{p}{\rho} + \frac{1}{2}|\nabla\Phi|^2 + \frac{\partial\Phi}{\partial t} + gy = 0 \text{ at } y = \eta \ .$$

The kinematic boundary condition applied to a solid boundary is given by

$$\mathbf{v}.\mathbf{n} = \mathbf{V}.\mathbf{n} \ ,$$

where **V** is the velocity vector of the body, and **n** is the normal vector (taken to be pointing out of the fluid always). For a depth large enough to be considered infinite, the kinematic condition on the sea floor is in the absence of current:

$$\lim_{y \to -\infty} \nabla\Phi = 0 \ .$$

The kinematic boundary condition on the free surface is given by

$$\Phi_y(x,\eta,z;t) = \eta_t(x,z;t) + \Phi_x\eta_x + \Phi_z\eta_z \ .$$

Linearizing the kinematic and dynamic boundary conditions at the free surface, results in the following combined free surface condition, which must be applied to the reference state of the fluid, y = 0:

$$\Phi_{tt}(x,0,z;t) + g\Phi_y = 0 \ .$$

With the presence of a floating vessel in the fluid, the kinematic boundary condition must be applied at the hull:

$$\mathbf{v}.\mathbf{n} = \mathbf{V}.\mathbf{n} \ ,$$

and the dynamic boundary condition on the hull is expressed by Newton's equations of motion, consisting of the conservation of linear and angular momentum combined:

$$\mathbf{M}\frac{d^2\mathbf{x}}{dt^2} = \mathbf{f}(t) \ ,$$

where **M** is the generalized mass matrix of the vessel, **x** is the translation and rotation vector, and **f** is the vector containing the force and moment components acting on the vessel.

Using the linear theory approach, the total velocity potential can be considered to be composed of the linear superposition of several potentials:

$$\Phi(x,y,z;t) = \Phi_I + \Phi_S \ ,$$

where Φ_I is the velocity potential of the undisturbed incident waves, and Φ_S is the potential due to presence of the vessel and its disturbance in the waves. Then Φ_S can be assumed to comprise the following potentials:

$$\Phi_S(x,y,z;t) = \Phi_U + \Phi_R + \Phi_D \ ,$$

where Φ_U = potential due to forward speed (in calm water)
Φ_R = potential due to wave radiation (forward speed in calm water)
Φ_D = potential due to wave diffraction (zero forward speed) .

A detailed discussion about the force contributions due to the individual potentials is given in subsequent chapters. According to Euler's Integral the total pressure in the fluid can be written as

$$p = -\rho g y - \rho\frac{\partial \Phi}{\partial t} - \frac{1}{2}\rho|\nabla\Phi^2| \ ,$$

which, in order to be consistent with the decomposition of the velocity potential Φ_S, becomes

$$p = -\rho g y - \rho\frac{\partial \Phi}{\partial t} \ .$$

The total hydrodynamic force and moment vectors can be obtained theoretically by integrating the pressure in the fluid over the exact wetted surface. Thus, if the normal is defined as pointing out of the fluid, the total force (in generalized notation) is given by

$$\mathbf{f}(t) = \iint_S p\,\mathbf{n}\,ds \ ,$$

where S is the instantaneous wetted surface. The normal $\mathbf{n}$ is the general normal vector in the local coordinate system O*x*y*z*, i.e., its first three components $\mathbf{n}_{1,2,3}$ contain the conventional unit normal components, and the last three components are cross-products: $\mathbf{n}_{4,5,6} = \mathbf{r}^* \times \mathbf{n}_{1,2,3}$. Here $\mathbf{r}^*$ represents the position vector to a point on the hull from the center of gravity. Thus, the (6x1) force vector $\mathbf{f}$ contains both force and moment

components, and is therefore referred to as a *generalized* force vector; for example, f_1 denotes the surge force and f_6 denotes the pitch moment.

The general approach taken here is to consider nonlinear motions in waves for which linear theory is assumed to be applicable, where the water depth is sufficiently large to be considered infinite. Displacements and angles can be large, and wave-induced pressures are integrated over the instantaneous wetted surface. In subsequent analyses it was found that the Froude-Krylov forces (associated with the pressure of the incoming wave system) were significant for all conditions, indicating the importance of modelling those forces correctly.

The velocity potential of the incoming wave system, Φ_I, satisfies the linearized free surface conditions and its general form is given by

$$\Phi_I(x,y,z;t) = \varphi_I(x,y,z)\cdot e^{i\sigma t} ,$$

where φ_I is the time-independent part of the potential, the expression for which is given in Chapter 2.4, and σ is the wave frequency. Φ_I is of order α (or $O(\alpha)$), where α is the wave steepness parameter given by the wave amplitude to wave length ratio :

$$\alpha = A_w / \lambda .$$

In the determination of Φ_S it is assumed that the structure is slender. The slenderness parameter is given by the ratio of beam (or draft) to length :

$$\varepsilon = B/L ,$$

so if $L = O(1)$, the beam and draft are of order ε, i.e., $B = O(\varepsilon)$ and $d = O(\varepsilon)$.

In the following sections all of the relevant force components comprising the total force are treated separately. For each case details are given about the particular theory and inherent assumptions. The potential flow force components consist of the following: static and dynamic Froude-Krylov forces (due to the pressure in the wave system), radiation forces (due to forced motion in calm water) and diffraction forces. The Froude-Krylov forces are evaluated over the instantaneous wetted surface, and the forces associated with Φ_R and Φ_D are computed for the equilibrium position of the vessel, in accordance with linear theory. The effects due to the forward motion potential, Φ_U, are approximated by considering the calm water resistance separately.

2.1.1. Froude-Krylov Forces

The Froude-Krylov force is, according to classical linear theory, the force associated with the pressure in the undisturbed incoming wave, where the pressure is integrated over the mean wetted surface of the vessel. In this work the wave pressure is evaluated up to the instantaneous water level, so that the Froude-Krylov force is obtained by integrating the pressures over the instantaneous wetted surface; therefore, this approach can be considered to be accurate within the framework of the present work.

The wave pressure is considered to be of the order of the wave slope, i.e., the quadratic term in the pressure,

$$\frac{1}{2}|\nabla\Phi_I|^2 ,$$

is neglected. The force associated with this quadratic term is important when one is concerned about slow drift motions of moored structures, or added resistance in waves, however, for the wave induced motions of a ship it is assumed to be negligible. The justification for neglecting this force contribution is that its amplitude is typically very small compared

with the total force (see e.g. Papanikolaou (1984)), and exhibits itself dynamically in terms having frequencies that are the sum or difference of the wave component frequencies. The sum frequencies are relatively high and can be neglected for a typical vessel, while the low frequency components are not likely to excite any of the modes of a freely floating ship. Nevertheless, care should be taken when, for example, the natural roll frequency is very low, under which condition roll resonance could occur due to slowly varying forces of higher order. Thus, the wave pressure is given by

$$p = -\rho g y - \rho \frac{\partial \Phi_I}{\partial t} = p_S + p_D \ ,$$

where p_S and p_D are the "static" and "dynamic" pressure, respectively, where both parts are time dependent. The force associated with p_S is the static Froude-Krylov force, and can also be considered as the usual vertical hydrostatic force. The vector comprising the static force and moment components is given by

$$f_{FK,S}(t) = -\rho g \iint_S y \, \mathbf{n} \, ds \ ,$$

where S is the wetted surface (which varies with time), and $\mathbf{n}$ is the generalized six-component outward normal as defined above. Changes in hydrostatic forces occur because of body displacements or changes in wave elevation, and detailed expressions of the forces and moments are given in Appendix B for any position of the vessel.

At each time instant, the vessel's position must be evaluated exactly, as well as the position of the wave surface along the hull. Having this information, it is possible to determine the total hydrostatic force and moment components by integration around each section. It should be noted that in these evaluations the wave surface is based on the undisturbed, incoming wave system. Thus, changes to the incoming waves caused by waves generated by the hull at mean forward speed, the

motions and body-wave interactions (diffraction), are neglected. At least for relatively low ship speeds and low frequencies of encounter, this should be a reasonable assumption. Thus, what are called the hydrostatic or static Froude-Krylov forces in this work, are not the exact hydrostatic forces since these would depend on the actual free surface. It has been shown that large changes can occur in the righting moment when a wave passes by a heeled ship, see e.g. Paulling (1961) or Elsimillawy and Miller (1986). For this reason the static restoring force component should not be treated by means of a time-independent coefficient. A study on the changes in righting arm values due to diffraction effects has been presented by Barrie (1986). It was found that for a trawler diffraction did change the stability of the vessel, but to a relatively small extent, where the overall transverse stability was somewhat larger with diffraction effects accounted for (under the conditions considered, of course).

Gravitational effects can be accounted for as follows. The static Froude-Krylov force component, acting in the y-direction of the earth-fixed system, can be balanced with the gravitational force, so as to obtain the change in the static force compared with the equilibrium position. If the mass of the vessel is given by m, then

$$m = \rho.V \ ,$$

where V is the displaced volume in calm water. The resulting static balance in the static vertical force is given by subtraction of the weight from the vertical component of the static Froude-Krylov force, $f^2_{FK,S}$:

$$f^*_{FK,S}(t) = f^2_{FK,S}(t) - mg = f^2_{FK,S}(t) - \rho g V \ .$$

It should be borne in mind that what hereafter is called the static Froude-Krylov force for heave, is in fact the change in vertical static force with respect to the still water equilibrium condition.

The dynamic Froude-Krylov force vector associated with the pressure p_D in the wave field is

$$f_{FK,d}(t) = -\rho \iint_S \frac{\partial \Phi_I}{\partial t} n \, ds \ ,$$

detailed expressions of which are also given in Appendix B.

The conventional Froude-Krylov forces would be obtained by evaluating the surface integral over the mean wetted surface S_0, in the mean equilibrium position up to the mean water level. Then these forces would be of order α. Salvesen (1978) derived second order expressions for the wave forces acting on a slender body in a second order Stokes wave train in the frequency domain. He applied asymptotic expansions to the velocity potentials, and also to the motion ξ of the structure :

$$\xi(t) = \xi^{(1)} + \xi^{(2)} + \ldots = \zeta^{(1)} e^{i\sigma t} + \zeta^{(2)} e^{i2\sigma t} + \ldots \ ,$$

where σ is the frequency, and ζ is the amplitude of order α. By integration over the total wetted surface and considering all forces up to second order, he obtained expressions for second order heave forces acting on two-dimensional sections.

In the present work no assumption is made as regards the form of the motion and the integration is to be carried out over the exact wetted surface at each time instant, so what are called herein the dynamic Froude-Krylov forces are in fact the "exact" forces associated with the $\partial\Phi_I/\partial t$ term of the incident waves, although one may question the validity of evaluating the velocity potential Φ_I above the mean water level (see Chapter 2.4 for a more detailed discussion). This method was applied in the numerical model described by Oakley, Paulling and Wood (1974), and Fallon *et al.* (1980). When integrating over the wetted length of the vessel, the only assumption made is that the wetted volume must be continuous. That is, the stern and bow can be totally emerged, but the case of an emerged midship section with immersed sections forward and aft is not allowed.

Froude-Krylov Surge Forces

It is of interest to note that in following or quartering seas the Froude-Krylov force, acting in the surge direction, can be of significant amplitude. As is shown in Appendix B, the surge force is given by integration of the pressure gradient $-\partial p/\partial x$ over the wetted volume. For following sea conditions, this pressure gradient will have the same sign along the length of the vessel when positioned between crest and trough, provided that the wave length is equal to or larger than the ship length. The maximum force will occur for a vessel positioned one quarter wave length on either side of the wave trough; the sign of the force would be positive for the leading edge position , and negative for the trailing edge position, as a consequence of which the resulting ship speed may undergo noticeable variations during the passage of a long wave. The larger the wave length to ship length ratio, as well as wave amplitude, the larger the exciting force will be. Grim (1963) has illustrated the importance of the Froude-Krylov forces in his study on ship motions in following seas; he showed that the speed of a vessel, travelling slower than the predominant wave speed, can be increased significantly for a certain amount of time. Such a speed increase could have an important bearing on the possibility of broaching. The Froude-Krylov surge forces have also been examined by Eda (1972b), who modelled the coupled surge, yaw and sway motions of a ship in waves, so as to study the directional stability behavior in following seas.

A consequence of integrating the fluid pressures over the instantaneous wetted surface is that the resulting force can have a nonzero mean value, so that a steady drift force may be present among the exciting forces. In Appendix B it is shown that the drift force, due to a regular wave acting on a heaving cylinder of small diameter, differs from zero when the heave motion is out of phase with the wave motion. The drift force is zero for a stationary cylinder, or when the cylinder heaves in phase with the wave. The Froude-Krylov drift force increases with increasing wave amplitude.

2.1.2. Radiation Forces

Linear theory is applied in the time domain to deal with the hydrodynamic forces caused by the forced, possibly random motions of the structure and by subsequent free surface disturbances. First, the zero forward speed case with small motions about the equilibrium condition is considered, followed by the forward speed case. Use is made of the two-dimensional hydrodynamic coefficients obtained in the frequency domain, from which the three-dimensional hydrodynamic coefficients are estimated for a thin ship by methods of strip theory. The three-dimensional coefficients can be transformed, so as to express the time-dependent forces acting on the vessel by means of kernel functions and memory effect integrals. Linear theory is applied to the forward motion case, combined with small motions relative to the moving reference frame. In the third section a treatment is given of the possible combination of the linear theory with large motions, and of its inclusion in the equations of motion.

2.1.2.A. Zero Forward Speed

In this section the problem considered is that of a structure undergoing small motions about the equilibrium position at the free surface in calm water. Pressure fluctuations are caused by the radiated waves, and the fluid forces acting on the body can be calculated when the radiation potential Φ_R is known. First, an overview is given of the boundary value problem from which Φ_R can be determined for small harmonic motions. The use of linear theory allows the total velocity potential to be decomposed into several contributions, as has been discussed in Chapter 2.1:

$$\Phi = \Phi_R + \Phi_D + \Phi_I + \Phi_U \ ,$$

where Φ_R has to satisfy the Laplace equation

$$\nabla^2\Phi_R = 0 \ ,$$

and also the linearized free surface boundary condition at the mean water level:

$$\Phi_{R_{tt}}(x,0,z;t) + g\Phi_{R_y}(x,0,z;t) = 0.$$

For small harmonic motions, and forward speed, the Kirchhoff decomposition can be applied, so as to obtain time-independent parts of the radiation potential for the various modes of motion:

$$\Phi_R(x,y,z;t) = \sum_{i=1}^{6} u_i^{(0)}(t) \cdot \varphi_R^{(i)}(x,y,z) \ ,$$

where the compact notation is used for the time-dependent coefficients $u^{(0)}_i$. Embedded in these are the translational velocities (i = 1,2,3), and terms involving the rotational velocities (i = 4,5,6). The kinematic boundary conditions are applied to the mean wetted surface of the body, S_0:

$$\frac{\partial\varphi_R^{(i)}}{\partial n}\Big|_{S_0} = n_i \ .$$

Also, for infinite water depth:

$$\frac{\partial\varphi_R^{(i)}}{\partial n} = 0 \text{ as } y \to -\infty \ .$$

In the above n refers to the unit normal, which is directed out of the fluid. The potential Φ_R must satisfy the radiation condition, which for a three-dimensional body is given by

$$\lim_{R \to \infty} \sqrt{R} \cdot \left[\frac{\partial \varphi_R^{(i)}}{\partial R} - ik\varphi_R^{(i)} \right] = 0,$$

where $k = \sigma^2/g$ (= wave number).

Theoretical aspects of the motion of a ship with mean zero forward speed have been investigated extensively by Wehausen (1967, 1971). Employing linear potential theory and Cummins' decomposition (see Cummins (1962)), he derived expressions for the hydrodynamic forces and equations of motion in the time domain, as an initial value problem, and showed how these could be related to the problem of harmonic excitation in the frequency domain.

Let us first consider the forced motion of a floating body (it could be a cylinder or a ship) as an initial value problem, starting at time $t = 0$. The hydrodynamic force acting on the body at time t is determined by the conditions at $t = 0$ and by certain hydrodynamic properties of the body, expressed in terms of a kernel function $L(\tau)$, which is similar to the impulse response function concept used by Cummins (1962). This kernel function is integrated from $t = 0$ to the present time t, i.e., over the "past", so that the fluid's past history, or "memory effects", contribute to the forces acting on the body at the present time t. This can be visualized by waves radiating away from the moving body but still influencing the pressure on the body, see Newman (1966, 1977), for example. Thus it seems that the frequency-dependent added mass and damping forces exhibit themselves in the time domain by means of fluid memory effects.

These memory effects have been considered for some time in aerodynamic theory, where the time-dependent lift on a wing in an unsteady flow field is influenced by the past history of the velocity in the unsteady wake. In the field of naval architecture it is only a fairly recent phenomenon that one is starting to take memory effects into account in time simulations. Haskind (1946) alluded to the use of convolution integrals in the equations of motion, and Golovato (1959) suggested experimentally that memory effects exist. Tick (1959) pointed out the equivalence between the equations

of motion with constant coefficients in the frequency domain and the equations in the time domain with convolution integrals. Cummins (1962) presented the theory of arbitrary, small ship motions in the time domain, by considering the response as a continuous series of small impulsive displacements, so that use can be made of impulse response functions to describe the time-dependent fluid forces. Ogilvie (1964) derived expressions for the time-dependent velocity potentials for a ship having forward speed, and he gives the relationship between the frequency domain and time domain problem. The work by Wehausen (1967, 1971) in this respect has been mentioned already. Cummins' theory was also used as a basis by Van Oortmerssen (1976), who derived expressions for the time-dependent velocity potential and applied it to the time domain analysis of a moored vessel. Guo (1978) developed a time domain theory for ship maneuvering in calm water; he applied a boundary integral method using Green's functions, and considered all forces up to second order, thereby obtaining second order memory effect integrals. Yeung (1982) considered the transient motions of two-dimensional cylinders in calm water, and showed, using time-dependent Green's functions, that the transient response of a circular cylinder, predicted by employing constant coefficients in the equations of motion, compared quite well with the more exact theoretical solution. This suggests that it may not be necessary to evaluate memory effect integrals (for transient motion conditions) for structures that do not create appreciable free surface disturbances. It is noted, however, that in irregular wave conditions it does not seem valid to use constant coefficients. Liapis and Beck (1985) derived the equations for a ship with forward speed and undergoing small motions (in calm water), using the integral equation approach and time-dependent Green's functions to determine the velocity potentials. Beck and Liapis (1987) presented a time domain method for transient motions in calm water at zero forward speed.

Since the treatment of the radiation problem in this work is based largely on the linear, three-dimensional theory developed by Wehausen (1967, 1971), only some of the relevant results are discussed below and the reader is referred to these references for more details on the derivations. Using

the concept of impulse response functions and Cummins' decomposition Wehausen (1967) showed that the forced motion potential (radiation potential) Φ_R for the linearized problem could be expressed as a Volterra integral equation:

$$\Phi_R(P;t) = \int_0^t \ddot{x}_i(t)\, \phi_i(P;t-\tau)\, d\tau \ , \quad i = 1,...,6 \ ,$$

where $\ddot{x}_i$ is the acceleration in the i^{th} direction, and where $\phi_i(P;\tau)$ is the velocity potential at point P, associated with the impulse velocity at time τ. The following expression is obtained for the generalized force component f_i acting on the body in the i^{th} direction subjected to transient excitation x_j in the j^{th} direction, assuming that we are dealing with a linear system :

$$f_i(t) = -\left\{A_{ij}\ddot{x}_j(t) + \int_0^t \ddot{x}_j(t)\, L_{ij}(t-\tau)\, d\tau\right\}, \quad i,j = 1,...,6 \ ,$$

and the associated integro-differential equations of motion are then the following :

$$(M_{ij} + A_{ij})\,\ddot{x}_j + C_{ij}\,x_j + \int_0^t L_{ij}(t-\tau)\,\ddot{x}_j(\tau)\, d\tau = f_{0,i}(t) + f_{w,i}(t) \ , \quad i,j = 1,...,6 \ ,$$

where M_{ij} is the structural mass, A_{ij} is an added mass coefficient, which can be taken as the infinite frequency added mass, and C_{ij} represents the hydrostatic restoring force coefficient (hereafter in this chapter the hydrostatic force component will be considered as being part of the force $f_{w,i}(t)$; for a treatment of the hydrostatic force see Chapter 2.1.1). $f_{0,i}(t)$ is the force associated with the initial conditions at t = 0. If the transient motion is caused by a transient wave (for which the Fourier transform exists) $f_{w,i}(t)$ in the right hand side of the equations of motions is non-zero and represents the wave exciting force, comprising the force due to the incident waves and diffracted waves. The kernel function $L_{ij}(t-\tau)$ in the

memory effect integral may be considered as the force acting on the body in the i-direction at time t due to an impulse velocity in the j-direction at time lag τ. Because of the linearization of the problem, only first order memory effect integrals are taken into account, which can be considered as keeping only the first term of an infinite series of such integrals. The general application of Volterra series to the ship motion problem, and subsequent linearization to conform with linear ship motion theory, has been discussed by Bishop, Burcher and Price (1973).

In the above notation, and throughout this work, repeated indices imply summation, generalized motion vectors consist of displacements (i = 1,2,3) and rotations (i = 4,5,6), and, similarly, generalized forces consist of forces and moments.

Forced Harmonic Motion

It is useful to determine the forces for sinusoidal excitation, especially because then one can make a direct comparison with frequency domain predictions. Suppose x_j represents forced harmonic motion starting at t = 0:

$$x_j(t) = x_A \cos\sigma t + x_B \sin\sigma t \ ,$$

Then it follows that

$$\int_0^t \ddot{x}_j(\tau)\, L_{ij}(t-\tau)\, d\tau = \ddot{x}_j(t) \int_0^t L_{ij}(\tau) \cos\sigma\tau d\tau + \sigma \dot{x}_j(t) \int_0^t L_{ij}(\tau) \sin\sigma\tau \, d\tau \ ,$$

and the hydrodynamic force becomes

$$f_i(t) = -\{A_{ij} + \int_0^t L_{ij}(\tau)\cos\sigma\tau d\tau\}\,\dot{x}_j(t) - \sigma\{\int_0^t L_{ij}(\tau)\sin\sigma\tau d\tau\}\,\dot{x}_j(t) \quad .$$

As $t \to \infty$ transient effects should disappear and the motion should become purely harmonic. Then the hydrodynamic force comprises the usual added mass and damping forces:

$$f_i(t) = -A_{ij}(\sigma)\,\ddot{x}_j(t) - B_{ij}(\sigma)\,\dot{x}_j(t) \quad ,$$

and the equations of motion are the conventional ones with constant, frequency-dependent added mass and damping coefficients $A_{ij}(\sigma)$ and $B_{ij}(\sigma)$:

$$\{M_{ij} + A_{ij}(\sigma)\}\,\ddot{x}_j(t) + B_{ij}(\sigma)\,\dot{x}_j(t) + C_{ij}(\sigma)\,x_j(t) = 0 \quad .$$

From the above the following relationships can be derived, relating the frequency dependent coefficients and the kernel functions (also referred to as the Kramer-Kronig relations):

$$A_{ij}(\sigma) = A_{ij} + \int_0^t L_{ij}(\tau)\cos\sigma\tau d\tau \quad ,$$

$$B_{ij}(\sigma) = \sigma\int_0^t L_{ij}(\tau)\sin\sigma\tau d\tau \quad .$$

Conversely, the kernel functions $L_{ij}(\tau)$ can also be determined as a function of A_{ij} or B_{ij}:

$$L_{ij}(t) = \frac{2}{\pi}\int_0^\infty \{A_{ij}(\sigma) - A_{ij}\}\cos\sigma t\, d\sigma = \frac{2}{\pi}\int_0^\infty \frac{B_{ij}(\sigma)}{\sigma}\sin\sigma t\, d\sigma \quad .$$

It may be of relevance to consider motions that have been going on for a long time, and that are not influenced by the initial conditions. It can be shown that if the excitation started at $t = -\infty$, the expressions for the equations of motion are the same as above, but with the lower limit of integration of the memory effect integral being $-\infty$, and the force components $f_{0,i}(t)$ resulting from the initial conditions being zero. With the same definitions for A_{ij} and L_{ij} the following expressions are obtained:

$$f_i(t) = -\{A_{ij}\ddot{x}_j(t) + \int_{-\infty}^{t} \ddot{x}_j(\tau)\, L_{ij}(t-\tau)\, d\tau\}$$

$$= -\{A_{ij}\ddot{x}_j(t) + \int_{0}^{\infty} \ddot{x}_j(t-\tau)\, L_{ij}(\tau)\, d\tau\} \ ,$$

and the associated equations of motion are the following :

$$\{M_{ij} + A_{ij}\}\ddot{x}_j(t) + \int_{0}^{\infty} L_{ij}(t)\ddot{x}_j(t-\tau)\, d\tau = f_{w,i}(t) \ .$$

The above equations of motion are applicable both to the problem of excitation due to transient waves and excitation due to irregular waves, see Wehausen (1971). The unsteady motion of a body in waves is also treated by Adachi and Ohmatsu (1980), who solve for the time-dependent velocity potential and suggest some numerical solution procedures using asymptotic expansions for large time. Results from their unsteady motion experiments compare favorably with the theory, some of which are similar to results obtained by Yeung (1982).

For computational convenience it was decided that memory effect integrals based on the velocity components $\dot{x}_i(t)$, rather than integrals based on accelerations $\ddot{x}_i(t)$, were preferable. Liapis and Beck (1985) and Van Oortmerssen (1976), for example, apply velocity based memory effect

integrals to the linear ship motion problem. Liapis and Beck (1985) obtain the following forced motion potential Φ_R:

$$\Phi_R(P;t) = \int_0^t \dot{x}_j(\tau)\, \phi_i(P;t-\tau)\, d\tau \ , \quad i = 1,...,6 \ .$$

Using velocity-based convolution integrals, the equations of motion can be expressed as follows (where the hydrostatic force term again is included in the exciting force $f_{w,i}(t)$):

$$\{M_{ij} + A_{ij}\}\, \ddot{x}_j(t) + \int_0^\infty L_{ij}(\tau)\, \dot{x}_j(t-\tau)\, d\tau + B_{ij}\, \dot{x}_j(t) = f_{w,i}(t) \ .$$

When we consider, as was done above, the case where $x_j(t)$ represents forced harmonic motion, the following relationships are found between the frequency-dependent coefficients and the kernel functions:

$$A_{ij}(\sigma) = A_{ij} - \frac{1}{\sigma} \int_0^\infty L_{ij}(\tau) \sin\sigma\tau\, d\tau \ ,$$

$$B_{ij}(\sigma) = B_{ij} + \int_0^\infty L_{ij}(\tau) \cos\sigma\tau\, d\tau \ .$$

The coefficients A_{ij} and B_{ij} can be found from the above relationships for any frequency σ. It is sometimes convenient to evaluate these coefficients by letting the frequency σ go to infinity, so that use can be made of the Riemann-Lebesgue theorem (which states that the integrals become zero for $\sigma \rightarrow \infty$):

$$A_{ij} = A_{ij}(\infty) \ ,$$

$$B_{ij} = B_{ij}(\infty) = 0 \ .$$

A convenient way to obtain the kernel functions $L_{ij}(\tau)$ is to take the cosine transform of the damping coefficients:

$$L_{ij}(\tau) = \frac{2}{\pi} \int_0^\infty B_{ij}(\sigma) \cos\sigma\tau \, d\tau \ .$$

It is noted that the kernels $L_{ij}(\tau)$ depend solely on the geometry of the ship and time lag, i.e., they are independent of the excitation and do not depend on actual time. Then the equations of motion can be written as

$$\{M_{ij} + A_{ij}(\infty)\} \ddot{x}_j(t) + \int_0^\infty L_{ij}(\tau) \dot{x}_j(t-\tau) \, d\tau = f_{w,i}(t) \ .$$

It is emphasized that the above theory is, strictly speaking, valid only for small arbitrary motions.

2.1.2.B. Non-Zero Forward Speed

The next problem to be addressed is that of a vessel undergoing small motions about a mean position, which is steadily moving forward in calm water. Liapis and Beck (1985) developed theoretical expressions for bodies of arbitrary shape having forward speed. By means of Green's functions they obtained integral equations that could be solved numerically using a panel method. Ankudinov (1983) studied the steering of a ship in waves in the time domain, and evaluated the equations of motion by a system of higher order differential equations, derived from series expansions of the added mass and damping coefficients obtained by strip theory. McCreight (1986) also considered the maneuvering of a ship in waves, and used polynomial filters to obtain series expansions for the added mass and

damping coefficients, so as to avoid the disadvantages of the exact evaluation of the memory effect integrals. The added mass and damping coefficients were obtained using linear strip theory.

For this investigation the theory discussed in section 2.1.2.A is applied to a ship for which the beam and draft are small compared with the length. For a slender vessel the frequency dependent, three-dimensional added mass and damping coefficients can be estimated using the strip theory described by Salvesen, Tuck and Faltinsen (1970), where the two-dimensional coefficients for each station are integrated along the length of the ship while accounting for only the kinematic effects of forward speed (see Yeung and Kim (1981) for a complete treatment of forward speed effects). The hydrodynamic coefficients are then obtained for coupled heave and pitch, and coupled sway, roll and yaw. Frank's method is used to evaluate the two-dimensional coefficients for each station, see Frank (1967), and Bedel and Lee (1971). The above strip theory is valid for a relatively high frequency of encounter. For low encounter frequencies reasonable results have been obtained also, but this is due to the dominating effects of the hydrostatic and dynamic Froude-Krylov forces at those frequencies.

If linear ship theory is used to obtain the three-dimensional hydrodynamic coefficients in the frequency domain, and if the kernel functions are based on these coefficients, then the radiation forces in the time domain are subject to the same limitations of the theory. Thus, the forces expressed in terms of memory effect integrals are equivalent to those obtained by the Salvesen, Tuck and Faltinsen method in the frequency domain, so that the equations of motion containing the above kernel functions $L_{ij}(\tau)$ are subject to the same constraints, such as high encounter frequency and thin ship aspects.

Applying the method by Salvesen, Tuck and Faltinsen, and this is the case for other strip methods too, results in the decoupling of the coupled heave and pitch motions from the coupled roll, sway and yaw motions for the forced motion problem. Surge cannot be considered with that method as surge forces are of higher order than $O(\alpha)$. Added mass and damping

coefficients could be obtained for a thin ship, by means of a full three-dimensional source/sink method. These coefficients then could be used to generate kernel functions for the forced surge motion. This aspect of the force computations will be addressed in Chapter 3. Wu (1985) has presented a hybrid method for calculating the hydrodynamic forces acting on a ship, by applying a strip method to the parallel midbody, and a full three-dimensional analysis to the bow and stern regions.

The kernel functions obtained from the frequency dependent damping coefficients as mentioned above, contain all memory effects and depend on geometry, forward speed and time lag. Since the evaluation of the hydrodynamic coefficients, and hence of the kernel functions, is carried out with respect to a moving reference system (here: $O^e x^e y^e z^e$), the memory effect integrals depend on the relative velocity, $v_{j,rel}$ in relation to that system rather than the earth-fixed system Oxyz. The $O^e x^e y^e z^e$ system translates with the vessel along the x-axis, so that the relationship between relative absolute velocities is given by

$$v_{rel,1} = \dot{x}_1 - \dot{x}_{O^e}$$
$$v_{rel,j} = \dot{x}_j \ .$$

Defining the local acceleration in the j^{th} direction by $a_{rel,j}$, the radiation force and moment components are the following:

$$f_{rad,i}(t) = - A_{ij}(\infty)\, a_{rel,j} - \int_0^\infty L_{ij}(\tau)\, v_{rel,j}(t-\tau)\, d\tau \ , \quad i,j = 1,\ldots,6 \ ,$$

where

$$L_{ij}(\tau) = \frac{2}{\pi} \int_0^\infty B_{ij}(\sigma) \cos\sigma\tau \, d\tau \ .$$

Since the above expressions are applicable to random but small motions, it was not necessary to consider any force or motion quantities in the local O*x*y*z* coordinate system. The transformation between the local and fixed coordinate systems can be taken into account for large angles of motion in an approximate manner, and this is treated in the following section.

2.1.2.C. Forward Speed, and Large Angle Approximation

An attempt is made to incorporate the linear radiation forces realistically in a large motion model, despite the inherent contradiction in terms. As obtained from above, the components of the generalized radiation force are given by

$$f_i(t) = - A_{ij} a_{rel,j} - \int_0^\infty L_{ij}(\tau).v_{rel,j}(t-\tau)\, d\tau \quad , \quad i,j = 1,...,6 \ ,$$

where $a_{rel,j}$ is the local, relative acceleration of the center of gravity in the j-direction, and $v_{rel,j}$ is the relative velocity with respect to the steadily translating coordinate system. Since the angles were assumed small, the accelerations and forces in the local system O*x*y*z* would be the same when expressed in the fixed system Oxyz. Now we would like to account for the rotation and translation of the structure in a more precise fashion. It is assumed that the added mass coefficients $A_{ij}(\infty)$ and kernel functions $L_{ij}(\tau)$ are constants, i.e., time independent, in the direction of motion of the vessel. Since the determination of the radiation forces is based on linear theory, the kernels are of first order and have to be evaluated only once, i.e., they can be determined numerically before the start of the time simulations, or by experiment. As was stated previously, the translational equations of motion are to be solved in the Oxyz system, while the rotational motions are to be solved in the O*x*y*z* system. All velocities and accelerations treated below apply to the center of gravity of the vessel.

Two methods are discussed for estimating the radiation forces and moments when the vessel has undergone large angles of rotation. The first method, (i), is a simple approach that follows closely the principles of linear theory, where no distinction is made between the actual position of the vessel and the equilibrium system. With the second method, (ii), the various forces and moments are resolved from the local coordinate system of the vessel to its equilibrium system, by means of time-dependent transformation matrices. In both methods the translating system $O^ex^ey^ez^e$ is considered as the reference equilibrium system in which the forces are calculated; this is in accordance with the strip theory approach by Salvesen, Tuck and Faltinsen (1970). During the time simulations, the actual forces must be expressed in the earth-fixed reference system, and the moments in the structure-fixed system. At each time step, the radiation forces are determined first in the equilibrium system $O^ex^ey^ez^e$ (with either method), resolved into the local system $O^*x^*y^*z^*$ and added to the other force components, and finally the total forces (and moments) are transformed back to the absolute system Oxyz, before solving the equations of motion. It was found that for large angles of rotation the first method gave better results (compared with experiments) than the second one, while for small angles the differences were negligible. It is clear that neither method is theoretically correct, nor can one be better defended than the other.

The two approaches to deal with the computation of the resulting hydrodynamic forces are expressed in more detail as follows:

(i) After the linear and angular accelerations in $O^ex^ey^ez^e$ have been determined, assume the vessel to be positioned in the upright position when calculating the radiation forces and moments in $O^ex^ey^ez^e$. The moments in the local system $O^*x^*y^*z^*$ are assumed to be equal to the moments in $O^ex^ey^ez^e$.

(ii) After the linear and angular accelerations in $O^ex^ey^ez^e$ have been determined, resolve the velocities and accelerations along the ship-fixed coordinate system $O^*x^*y^*z^*$, where the large angles are retained in the transformation. These velocity and acceleration components are used to

calculate the radiation forces and moments acting in the $O^e x^e y^e z^e$ system. Finally, the forces and moments are resolved back into the local system $O^*x^*y^*z^*$ by applying the time-dependent transformation matrix **T**.

Consider a two-dimensional section, heeled by the roll angle θ, being subjected to a harmonic motion, $x^e_2(t)$, along the vertical $O^e y^e$ axis, as shown in Figure 2.2. Using method (i), the total added mass force, for example, would always have the magnitude $F^e_2 = A_{22} \cdot \ddot{x}^e_2(t)$ along the $O^e y^e$ axis, irrespective of the direction of acceleration, θ. A consequence of this approach is that unsymmetrical sections are assumed to create the same disturbance (and forces) as symmetrical sections.

One would expect the resultant hydrodynamic force not to be vertical due to the unsymmetrical shape; a more realistic approach may be to use method (ii), where the magnitude of the vertical component along $O^e y^e$ would be given by $F^e_2 = A_{22} \cdot \ddot{x}^e_2(t) \cdot \cos\theta$, and the horizontal component by $F^e_1 = A_{33} \cdot \ddot{x}^e_2(t) \cdot \sin\theta$. Thus, in the second approach the acceleration (or velocity) in the $O^e x^e y^e z^e$ system is first resolved along the $O^*x^*y^*z^*$ axes, the components of which are used to determine the forces in the $O^e x^e y^e z^e$ system. In this example, the acceleration **a** is decomposed into $\mathbf{a} \cdot \cos\theta$ along the O^*y^* axis and into $\mathbf{a} \cdot \sin\theta$ along the O^*z^* axis; subsequently, the resulting added mass forces are expressed along the $O^e y^e$ and $O^e z^e$ axes, respectively. For a three-dimensional body, yaw and pitch angles would have to be considered also, and cross-coupling effects would depend on the various angles of rotation.

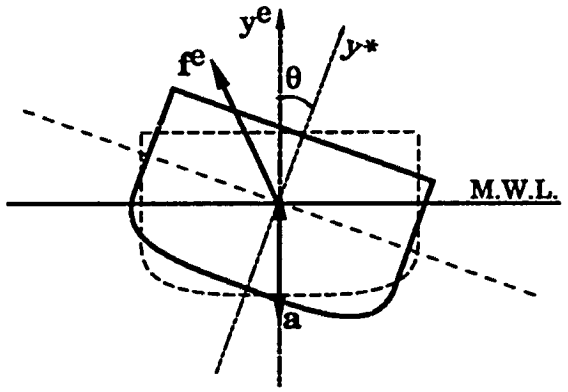

Figure 2.2. Hydrodynamic Force Acting on a Section Due to Acceleration a

The following definitions are introduced: let **v** denote a velocity vector, and let **a** denote an acceleration vector; $\mathbf{v}^e$ is the velocity vector of the center of gravity (i.e., of O*) of the vessel relative to the steadily translating $O^e x^e y^e z^e$ system, and $\mathbf{a}^e$ is the absolute acceleration vector of O* in that system. Since the vessel, and hence the O*x*y*z* system, is rotating, it is necessary to define the relative acceleration of O* (with respect to O^e) by the vector $\mathbf{a}^e_{rel}$. The absolute velocity of the $O^e x^e y^e z^e$ system in Oxyz is given by $\mathbf{v}_{O^e}$, which, for a vessel moving steadily forward along the x-axis at speed U, would be

$$\mathbf{v}_{O^e} = \begin{bmatrix} U \\ 0 \\ 0 \end{bmatrix} .$$

It is assumed that this velocity vector varies slowly with time and can be considered constant, so that its derivative is negligible, i.e.,

$$a_{O^e} = 0 .$$

To obtain the actual hydrodynamic forces or moments acting on the vessel in its rotated position, the forces are transformed from the upright position to the local position. For these transformations use is made of the coordinate transformation matrix **T**, which depends on the angles of rotation, or Euler angles, and on the order in which they are applied: ϕ (yaw), ψ (pitch) and θ (roll), and is therefore time dependent. It is given by

$$\mathbf{T} = \begin{bmatrix} \cos\phi\cos\psi & -\cos\phi\sin\psi\cos\theta+\sin\phi\sin\theta & \cos\phi\sin\psi\sin\theta+\sin\phi\cos\theta \\ \sin\psi & \cos\psi\cos\theta & -\cos\phi\sin\theta \\ -\sin\phi\cos\psi & \sin\phi\sin\psi\cos\theta+\cos\phi\sin\theta & -\sin\phi\sin\psi\sin\theta+\cos\phi\cos\theta \end{bmatrix} .$$

The matrix **T** has the property that its inverse is equal to its transpose, and the derivation of **T** is given in Appendix A. For consistency, the hydrodynamic forces are resolved into the ship-fixed coordinate system; this will be advantageous when considering the total forces acting on the vessel along its own coordinate system. However, since the linear equations of motion are solved in the earth-fixed system Oxyz, the total force components (including the hydrodynamic forces) acting on the vessel have to be transformed from O*x*y*z* to Oxyz, resulting in the same components of the hydrodynamic force as were obtained in terms of the $O^ex^ey^ez^e$ system, originally. The rotational velocities and accelerations about the local O*x*y*z* axes are resolved into the $O^ex^ey^ez^e$ system. The transformation matrix **B** is used to transform the local angular velocity vector ω^*, also referred to as ω:

$$\omega^e = \mathbf{B}^{-1}\omega^* = \mathbf{B}^{-1}\omega .$$

It is noted that when using method (i): $\omega^e = \omega$.

The inverse of **B** is given by

$$\mathbf{B}^{-1} = \begin{bmatrix} 1 & -\cos\theta\tan\psi & \sin\theta\tan\psi \\ 0 & \cos\theta/\cos\psi & -\sin\theta/\cos\psi \\ 0 & \sin\theta & \cos\theta \end{bmatrix}$$

and details about the derivation of **B** can be found also in Appendix A.

The radiation forces and moments in the system $O^e x^e y^e z^e$ are based on the "transformed equilibrium velocities" (and accelerations), which are defined as

$$\mathbf{v}^{e*} \text{ and } \mathbf{a}^{e*} ,$$

and which are different for methods (i) and (ii). If the above vectors contain both linear and rotational velocities or accelerations, the radiation force and moment components would then be given in generalized notation:

$$f_i^e(t) = -A_{ij}a_j^{e*} - \int_0^\infty L_{ij}(\tau).v_j^{e*}(t-\tau)\,d\tau \quad , \quad i,j = 1,\ldots,6 \; .$$

The transformed velocities for calculating the forces in the $O^e x^e y^e z^e$ system are defined as follows:

$$\mathbf{v}^{e*} = \begin{bmatrix} \mathbf{v}^e \\ \boldsymbol{\omega} \end{bmatrix} \quad \text{for method (i)} ,$$

and

$$v^{e*} = \begin{bmatrix} T^{-1}v^{e} \\ \\ B^{-1}\omega \end{bmatrix} \text{ for method (ii) .}$$

Similarly, the transformed acceleration vector is defined as

$$a^{e*} = \begin{bmatrix} a^{e}_{rel} \\ \\ \dot{\omega} \end{bmatrix} \quad \text{for method (i) ,}$$

and

$$a^{e*} = \begin{bmatrix} T^{-1}a^{e}_{rel} \\ \\ T\,\dot{\omega} \end{bmatrix} \text{ for method (ii) .}$$

The actual force components acting on the vessel in the instantaneous, rotated position are obtained by applying the inverse transformation matrix, T^{-1}, to the forces in $O^{e}x^{e}y^{e}z^{e}$. If approach (i) is used, the moments in $O^{*}x^{*}y^{*}z^{*}$ are considered to be the same as the ones in $O^{e}x^{e}y^{e}z^{e}$; if approach (ii) is used, the inverse transformation matrix is applied also to the moment components in the generalized radiation force vector $f^{e}(t)$:

$$f^*(t) = \begin{bmatrix} T^{-1}\begin{bmatrix} f_1^e \\ f_2^e \\ f_3^e \end{bmatrix} \\ \begin{bmatrix} f_4^e \\ f_5^e \\ f_6^e \end{bmatrix} \end{bmatrix} \quad \text{for method (i)},$$

and

$$f^*(t) = \begin{bmatrix} T^{-1}\begin{bmatrix} f_1^e \\ f_2^e \\ f_3^e \end{bmatrix} \\ T^{-1}\begin{bmatrix} f_4^e \\ f_5^e \\ f_6^e \end{bmatrix} \end{bmatrix} \quad \text{for method (ii)}.$$

It is necessary to express the velocities and accelerations in terms of the absolute quantities, since in the motion simulations the translational modes of motion are considered in the earth-fixed system Oxyz. The relationship between the absolute (linear) velocity of the vessel, **v**, and the relative velocity $\mathbf{v}^e$ is

$$\mathbf{v}^e = \mathbf{v} - \mathbf{v}_{O^e} .$$

When the vessel is rotating as well as translating, the relative translational accelerations in $O^e x^e y^e z^e$, denoted by $\mathbf{a}^e_{rel}$, depend on the absolute acceleration of O^* and also on the cross-product of the rotational and translational velocities, which gives rise to Coriolis forces. Here the hydrodynamic forces are considered with respect to $O^e x^e y^e z^e$, so that the relevant accelerations and velocities are taken with respect to O^e. The vector with relative accelerations is given by

$$\mathbf{a}^e_{rel} = \mathbf{a}^e - \boldsymbol{\omega}^e \times \mathbf{v}^e .$$

If the absolute acceleration vector of O^* in the Oxyz system is given by $\mathbf{a}$, the acceleration vector $\mathbf{a}^e$ is equal to $\mathbf{a}$, as the $O^e x^e y^e z^e$ system is translating steadily ($\mathbf{a}_{Oe} = 0$) and not rotating. Hence

$$\mathbf{a}^e = \mathbf{a} ,$$

and

$$\mathbf{a}^e_{rel} = \mathbf{a} - \boldsymbol{\omega}^e \times \mathbf{v}^e .$$

The cross-product terms must be taken into account when calculating the hydrodynamic forces in a nonrotating reference frame. The acceleration vector $\mathbf{a}^{e*}$ can then be described in terms of the kinematic quantities obtained during the simulation process.

An effort was made to determine the effects of using approach (i) and compared them with response results from approach (ii). Simulations, performed for beam and following sea conditions, indicated that for small wave amplitudes the two approaches yielded very small differences in response, as would be expected since the angles of rotation are always

small under those conditions; for a variety of wave frequencies the roll amplitudes were consistently somewhat larger using approach (ii). In waves with large amplitudes, however, the response behavior depended rather significantly on the method used. These differences exhibited themselves in two ways: the roll response was often more severely overpredicted with (ii) than was the case with (i), when compared with experimental results. Also it was found that, when using approach (ii), the roll response sensitivity to changes in the radiation forces was always significantly higher than for approach (i). Based on these observations it was decided to use approach (i), which is also more consistent with linear theory, in subsequent simulations.

2.1.3. Diffraction Forces

The diffraction force can be estimated by considering the vessel fixed in its mean position and the waves impinging upon it, whereby the associated boundary value problem must be solved in terms of the diffraction potential. The general boundary value problem applicable to small wave amplitudes, in accordance with linear theory, is briefly stated in the next section. Then some approximations are made to apply the linear theory to a vessel undergoing large motions, which can be done in a manner similar to the one used in the preceding chapter.

2.1.3.A. Small Angles of Motion

The diffraction problem is solved using linear theory as was discussed in Chapter 2.1. As a consequence of linearization, the total velocity potential associated with the diffraction problem can be split up into three velocity potential components for a vessel with forward speed:

$$\Phi = \Phi_I + \Phi_D + \Phi_U \ ,$$

where from the diffraction point of view the vessel is considered stationary. The diffraction potential has to satisfy the Laplace equation

$$\nabla^2\Phi_D = 0$$

throughout the fluid. The free surface boundary condition applies:

$$\Phi_{D_{tt}}(x,0,z;t) + g\Phi_{D_y} = 0.$$

For harmonic excitation due to small amplitude waves the diffraction potential can be expressed in terms of a time-independent part, φ_D:

$$\Phi_D(x,y,z;t) = \mathrm{Re}\{\varphi_D e^{-i\sigma t}\} \ ,$$

where

$$\varphi_D = \varphi_{D1} + i\varphi_{D2} \ ,$$

The kinematic boundary condition on the body, i.e., on the mean wetted surface S_0, is given by

$$\frac{\partial\Phi_D}{\partial n} = -\frac{\partial\Phi_I}{\partial n} \ ,$$

where n is, as usual, the normal directed out of the fluid. The other kinematic condition is for infinite depth:

$$\nabla\Phi_D = 0 \text{ as } y \to -\infty \ .$$

The radiation condition determines the behavior far away from the structure, and if φ_D is the diffraction potential for a three-dimensional body, then it must satisfy

$$\lim_{R\to\infty} \sqrt{R} \cdot \left[\frac{\partial \varphi_D}{\partial R} - ik\varphi_D\right] = 0 \ ,$$

$$R = \sqrt{x^2 + z^2} \ .$$

A consequence of the radiation condition is that the diffracted waves are outgoing, and

$$\varphi_D = O(\sqrt{R}) \text{ as } R \to \infty \ .$$

The following approach is used to deal with the diffraction problem in the time domain. We first restrict the development to small wave steepness and small angles of motion. Then, the linear diffraction forces acting on a thin ship are determined as a function of the wave frequency by means of the procedure outlined as in Salvesen, Tuck and Faltinsen (1970). Here, use is made of the Haskind relations in order to express the diffraction forces in terms of the incoming wave and radiation potentials for heave, sway and roll of a two-dimensional section. One needs to integrate the radiation potentials (obtained using Frank's method) distributed around each section to determine the sectional diffraction force. The three-dimensional diffraction forces are then estimated using the thin ship approach with forward speed. This is a very cursory description of the procedure involved, but all necessary details can be found in the reference by Salvesen, Tuck and Faltinsen.

The diffraction forces may be considered as the forces induced on the ship by waves of unit amplitude. This allows one to obtain a frequency domain transfer function $H^D_i(\sigma)$ for the diffraction forces and moments:

$$H^D_i(\sigma) = \frac{F^D_i(\sigma)}{A_w(\sigma)} \ , \quad i = 1,...,6 \ ,$$

where $F^D_i(\sigma)$ is the generalized (complex) diffraction force for frequency σ, and $A_w(\sigma)$ is the corresponding wave amplitude.

In order to find the diffraction force in the time domain, having the correct phase, we take the Fourier transform of $F^D_i(\sigma)$ and apply the convolution theorem :

$$f^D_i(t) = \mathcal{F}^+\{F^D_i(\sigma)\} = \frac{1}{2\pi}\int_{-\infty}^{\infty} F^D_i(\sigma)\, e^{i\sigma t}\, d\sigma$$

$$= \frac{1}{2\pi}\int_{-\infty}^{\infty} H^D_i(\sigma)\, A_w(\sigma)\, e^{i\sigma t}\, d\sigma \ .$$

$$\Rightarrow \quad f^D_i(t) = \mathcal{F}^+\{H^D_i(\sigma).A_w(\sigma)\}$$

$$= \int_0^t W_i(t-\tau)\,\eta(\tau)\, d\tau = \int_0^t W_i(\tau)\,\eta(t-\tau)\, d\tau \ ,$$

where

$$W_i(t) = \mathcal{F}^+\{H^D_i(\sigma)\} \ ,$$

$$\mathcal{F}^+\{y\} = \frac{1}{2\pi}\int_{-\infty}^{\infty} y.e^{i\sigma t}\, d\sigma \ ,$$

and $\eta(t)$ is the instantaneous wave elevation.

Employing the above approach implies that memory effects due to diffraction exist in the time domain, and the approach would be valid for impulsive waves impinging upon the body, for example. In this work it is assumed that the wave motion has been going on for a long enough time for transients to die out, and the wave process is assumed to be stationary.

Considering the foregoing, the time-dependent linear diffraction force can be expressed in terms of the transfer function for regular wave conditions:

$$f_i^D(t) = \int_{-\infty}^{t} W_i(t-\tau)\,\eta(\tau)\,d\tau = A_w(\sigma)\,H_i^D(\sigma)\,e^{i\sigma t} ,$$

where the phase information is contained in the complex transfer function $H^D{}_i(\sigma)$, and where $\eta(t)$ represents the instantaneous wave elevation (taken at the center of gravity of the ship). The above relationship can be proved as follows.

$$f_i^D(t) = \int_{-\infty}^{t} W_i(t-\tau)\,\eta(\tau)\,d\tau = \int_{0}^{\infty} W_i(\tau)\,\eta(t-\tau)\,d\tau$$

$$= \int_0^\infty \frac{1}{2\pi} \int_{-\infty}^{\infty} H_i^D(\sigma')\,e^{i\sigma' t} d\sigma' \,.\, A_w(\sigma)\,e^{i\sigma(t-\tau)}\,d\tau$$

$$= A_w(\sigma)\,e^{i\sigma t} \,.\, \frac{1}{2\pi} \int_0^\infty \int_{-\infty}^{\infty} H_i^D(\sigma)\,e^{i(\sigma'-\sigma)\tau}\,d\sigma'\,d\tau$$

$$= A_w(\sigma)\,e^{i\sigma t} \,.\, \frac{1}{2\pi} \int_{-\infty}^0 \int_{0}^{\infty} H_i^D(\sigma)\,e^{i(\sigma'-\sigma)\tau}\,d\tau\,d\sigma'$$

$$\Rightarrow \quad f_i^D(t) = A_w(\omega)\,e^{i\sigma t} \int_{-\infty}^{\infty} H_i^D(\sigma')\,\delta(\sigma'-\sigma)\,d\sigma' = A_w(\sigma)\,H_i^D(\sigma)\,e^{i\sigma t} \,.$$

In the above, use is made of the Dirac delta function, $\delta(x)$.

For long-crested random seas the linear diffraction force can be determined by summing the contributions from the various wave components. For a given sea spectrum, $S_{\eta\eta}$, the irregular sea surface can be modeled as the summation of a discrete number, N, of random

components (see Chapter 2.4 for a description of the sea surface and wave kinematics):

$$\eta(x,z;t) = \sum_{n=1}^{N} \eta_n(x,z;t) \ ,$$

where $\eta_n(x,z;t) = A_n \, e^{i(k_{x,n} \cdot x + k_{z,n} \cdot z - \sigma_n t + \varepsilon_{w,n})}$

A_n = amplitude of n^{th} wave component

$k_{x,n} = k_n \cos\delta$

$k_{z,n} = -k_n \sin\delta$

$k_n = \sigma_n^2 / g$ = wave number

σ_n = circular frequency of n^{th} wave component

δ = direction of wave travel

$\varepsilon_{w,n}$ = phase of n^{th} wave component

Then the linear diffraction force associated with the above random wave climate is given by

$$f_i^D(t) = \mathrm{Re} \sum_{n=1}^{N} H_i^D(\sigma_n) \, . \, \eta_n(x,z;t) \ .$$

The diffraction transfer function can be obtained for a number of headings. If the relative heading angle β is defined as the difference between the wave direction and yaw angle, as shown in Figure A.2 of Appendix A, the corresponding transfer function is $H^D{}_i(\sigma,\beta)$. To compute the time-dependent diffraction force for varying heading angles, it will be necessary to assume that the change in heading occurs at a slower time scale than the oscillatory motions; for a typical seagoing ship this is nearly always the case. Then, the linear diffraction force and moment components due to unidirectional random waves are

$$f_i^D(t) = \mathrm{Re} \sum_{n=1}^{N} H_i^D(\sigma_n,\beta(t)) \, . \, \eta_n(x,z;t) \ , \quad i = 1,\ldots,6 \ .$$

These components are given in the moving reference frame $O^e x^e y^e z^e$. The wave elevation of the wave components are taken at a reference point on the vessel about which the moments are computed, which is the center of gravity of the vessel.

2.1.3.B. Large Angle Approximation

The determination of the diffraction forces in the case of large vessel motions, due to large amplitude waves, may also be based on a modification of linear theory. Taking a similar approach as in Chapter 2.1.2 for the radiation forces, the force components given in the $O^e x^e y^e z^e$ system may be considered as dependent on the instantaneous angles of rotation, while it is assumed that the vessel's center of gravity is located at O^e, thereby neglecting the linear displacements due to surge, heave and sway. This time dependence is effected through the transformation matrix **T**, which has been derived in Appendix A.

Defining the computed diffraction force components, $f^D{}_i(t)$, as in the previous section, the force vector in the $O^e x^e y^e z^e$ system is then given by

$$f^{D^e}_{1,2,3}(t) = \begin{bmatrix} f^D_1 \\ f^D_2 \\ f^D_3 \end{bmatrix},$$

and the diffraction moment vector is

$$f^{D^e}_{4,5,6}(t) = \begin{bmatrix} f^D_4 \\ f^D_5 \\ f^D_6 \end{bmatrix}.$$

If the approach (i) is used as in Chapter 2.1.2, the diffraction forces are transformed into the local O*x*y*z* system, while the moments in O*x*y*z* are assumed to be the same as the moments computed above, so that the generalized force vector in the local system would be given by

$$f^{D^*}(t) = \begin{bmatrix} T^{-1} f^{D^e}_{1,2,3}(t) \\ f^{D^e}_{4,5,6}(t) \end{bmatrix}.$$

If the approach (ii) is used, the inverse of the transformation matrix T is applied to both the forces and moments in $O^e x^e y^e z^e$, in which case the resulting vector in generalized notation is given by:

$$f^{D^*}(t) = \begin{bmatrix} T^{-1} f^{D^e}_{1,2,3}(t) \\ T^{-1} f^{D^e}_{4,5,6}(t) \end{bmatrix}.$$

For reasons stated at the end of Chapter 2.1.2, it was decided to use approach (i) to estimate the radiation force and moment components. In order to be consistent with the computation of the wave radiation forces, the diffraction moments were also estimated using approach (i) in subsequent analyses.

2.2 Viscous Fluid Effects

Viscous effects exhibit themselves in the formation of boundary layers and flow separation. Although boundary layers may have a significant influence on resistance or propeller performance, their influence on the wave-induced motions of a vessel is usually sufficiently small to be neglected, except possibly for roll. Flow separation and related eddy shedding, on the other hand, may contribute significantly to the total drag forces for different modes of motion. Viscous effects provide an important source for damping as regards the roll behavior of a vessel, where vortex shedding, for example around bilge keels, tends to be dominant. Roll damping due to wave radiation, i.e., the so-called potential damping, may also be of significance, however, this part is incorporated in the potential flow calculations discussed in Chapter 2.1.2. Considerable drag forces will occur when a vessel undergoes steady sway motion, possibly combined with yawing, due to flow separation. These drag forces are hereafter referred to as the "maneuvering forces".

If the general hydrodynamic problem, where viscosity is included, must be solved, it would be necessary to deal with the complete Navier-Stokes equations. To do this consistently is a formidable task, and only recently have methods emerged for treating these equations correctly in two dimensions. However, for a freely floating body in arbitrary waves this has not yet been accomplished, and to attempt to do so lies beyond the scope of this work. So far, the methods developed are useful for treating the two-dimensional rolling problem in beam waves. Promising applications of discrete vortex methods to ship motions have been performed by a number of researchers, such as Graham (1980), Faltinsen and Sortland (1987), and Downie, Bearman and Graham (1988), for example. The discrete vortex method has the advantage that one can superpose analytically the potential, irrotational flow effects upon the flow effects due to introduced vorticity. The method is, however, very computationally intensive. It would be more efficient to use a theoretically correct approach to compute viscosity related forces, but at present the theory is not suitable for application to a three-dimensional body of arbitrary shape at the free surface. Forward speed effects complicate the

theoretical solution. As a consequence of all of the above, the present work will rely upon empirical methods to treat viscous effects.

A common approach to predict roll damping is to make use of empirical data, mostly obtained from experiments with either models or full size vessels rolling in calm water. An overview of roll damping data for an extensive number of vessels, as well as roll damping devices, is given by Barr and Ankudinov (1977). In Japan a large amount of effort has been devoted to analyzing the roll damping behavior of ships, see Himeno (1981), for example. At present, one can make use of purely empirical methods to predict roll damping, where regression analysis is applied to experimental roll data, or one can apply a semiempirical approach based on a combination of theory and measurements. Unfortunately, there are very few reliable methods available to predict roll damping in calm water, and even those suffer from quite large discrepancies at times. There are no such methods that deal with rolling in waves, the result being that calm water damping data are applied to wave conditions, using the wave-induced roll frequency and roll amplitude.

In order to deal with the roll damping forces in the present work, use is made of the concept of component damping, where the total roll damping moment is split up into components due to boundary layer drag, hull lift, eddy shedding, and bilge keel contributions. Semiempirical methods are applied to determine each component separately, and subsequently all components are added together. Obviously, there is no real physical justification for separating these damping contributions, since the choice of e.g. linear and quadratic components is rather arbitrary, and all of the effects are closely intertwined. In light of the present lack of rational methods to predict viscous roll damping forces, the model considered below must be used with caution. Also, there is unfortunately no realistic model available at present, which deals with maneuvering forces in a seaway. Therefore, it is assumed that conventional maneuverability theory, applicable in principle only for calm water conditions, can be used for a steered vessel in waves. All of these (semi)empirical models dealing with viscous effects make it difficult to defend this work from a purely theoretical point of view. Nevertheless, even if the viscous forces are not

modelled quite correctly, it will be possible at least to gain some understanding concerning the relative importance of the various force contributions.

2.2.1 Roll Damping

The nature of viscous forces is such that to incorporate them into the ship motion problem, one must overcome several major stumbling blocks. As a first approach to determine the viscous roll damping moment, it is assumed that the total moment (per section) can be split into a number of separate components, each of which can be estimated independently of the others. A procedure to determine some of these components has been given by Schmitke (1978). A significant amount of work on component damping has been developed in Japan, and has been reviewed by Himeno (1981). Viscous roll damping can be attributed to the following mechanisms:

- frictional damping associated with flat plate drag;
- lift damping (for a vessel with forward speed) due to circulation around the hull and resulting lifting effect;
- eddy damping due to pressure variations associated with vortex shedding;
- bilge keel damping due to additional pressures in the presence of bilge keels.

Himeno (1981) gives a practical method for calculating the various damping components, largely based on theoretical considerations combined with curve fitting to empirical data from model experiments in calm water, where forward speed is taken into account. Whereas Himeno linearized all damping forces so as to obtain "equivalent" damping coefficients, in the present work the linear and nonlinear (quadratic) terms are retained, but otherwise the same method is adhered to. The form of the roll damping moment is then

$$f_{rd,4}(t) = B_{44,L}.\dot{\theta} + B_{44,Q}.|\dot{\theta}|.\dot{\theta} \ ,$$

or, if the viscous roll moment is considered as being added to the right hand side of the equations of motion, this would be:

$$f_{rd,4}(t) = - B_{44,L}.\dot{\theta} - B_{44,Q}.|\dot{\theta}|.\dot{\theta} \ ,$$

where $\dot{\theta}$ is the angular roll velocity of the vessel. $B_{44,L}$ is the linear damping coefficient, assumed to be composed of the frictional damping coefficient $B_{F,lam}$ in case of laminar flow, and also due to the lift damping coefficient B_L . The lift damping moment is in fact linearly dependent on the rotational velocity and forward speed of the vessel. $B_{44,Q}$ is the quadratic damping coefficient associated with the eddy and bilge keel damping, B_E and B_K, respectively, as well as frictional damping due to turbulent boundary layers, $B_{F,turb}$. An outline of the calculation of $B_{44,L}$ and $B_{44,Q}$ is given below, and the reader is referred to Himeno (1981) for further details.

The damping coefficients are determined as follows. The linear damping is given by

$$B_{44,L} = B_{F,lam} + B_L \ ,$$

where $B_{F,lam}$ and B_L can be easily estimated for the vessel in its entirety. The quadratic damping coefficient is given by

$$B_{44,Q} = B_{F,turb} + B_E + B_K \ ,$$

where B_E is the coefficient associated with flow separation around the bow, stern and bilge radius, i.e., due to eddy shedding, and B_K is an additional damping coefficient in the presence of bilge keels, and is assumed to be decomposed into a normal drag force component and a hull pressure component. Since it is assumed that the viscous effects are two-

dimensional, the damping coefficients B_E and B_K can be estimated for each discrete section of the vessel, from which the total damping coefficients can be determined by straightforward integration along the length of the hull.

For most practical purposes, damping due to skin friction is relatively insignificant, so $B_{44,L}$ tends to become more significant at higher ship speeds, since lift damping is linearly proportional to speed. The other damping components depend also on speed, and corrections to account for speed effects are given by Himeno (1981); linear damping has been found to be more sensitive to speed than quadratic damping. Also, it has been observed that apart from skin friction, scale effects usually do not play an important role in determining roll damping coefficients, so that the formulas based on model experiments should yield results that are not significantly different from the full scale values.

Despite the simplicity of this model, there are a number of difficulties associated with predicting the roll damping moment, aside from the inherent physical assumptions concerning the mechanisms involved. The coefficients representing eddy shedding effects depend not only on ship geometry and forward speed, but also on the roll frequency and amplitude, which obviously are unknown before any motion simulations have been performed. One can circumvent this difficulty by using an iterative procedure, and adjust the coefficients until convergence is reached. For long simulations this would be a very tedious and time consuming procedure. Another method commonly used is to determine the damping coefficients for the "natural" roll frequency, and use those for other frequencies of motion as well, so that the damping is estimated at least reasonably well for the resonance condition, assuming the roll amplitude is known. The problem is even more complex for random motions, where use must be made of some kind of average amplitude. Another drawback of the model is that wave interaction with vessel motion is neglected; this is discussed below in more detail.

Relative Motion in Waves

The calculation of the roll damping moment resulting from viscous fluid effects is based on a fairly simple model, which neglects the effects of the water particle kinematics. For example, vortex shedding is governed by the local water particle motion at the hull, i.e., by the motion between the hull and the surrounding fluid, so that the above model might result in an incorrect estimate of the roll moment for a vessel in, say, beam or quartering seas. The quadratic damping component has been found to be of importance in a number of studies. For example, Haddara (1970) found the motion response and directional stability of a ship to be most sensitive to changes in the nonlinear roll damping coefficient. Brook (1986) reported that the accuracy of the calculated roll response of a ship was affected most significantly by uncertainties in the roll damping. Although the effect of the relative fluid motion on the roll response of a forward moving vessel is not well established, it would be more appropriate to incorporate wave effects in the damping moment expressions.

Due to its theoretical premises, the lift damping moment should not be based on the relative roll velocity. The roll response tends to be sensitive to changes in the eddy and bilge keel damping terms, since eddy shedding effects are generally more significant than hull friction. The eddy shedding forces may be modelled more realistically by taking into account the relative motion between the hull and the fluid particles. In the following an attempt is made to formulate expressions for the relative roll motion and the resulting damping moment, using the same empirical approach as above. Here the relative velocity is based on the roll velocity of the vessel and an average roll velocity of the wave particles for relatively long waves.

The empirical damping coefficient $B_{44,Q}$, according to the method by Himeno (1981), has two main components: one due to eddy shedding around the hull, B_E, and an additional one due to the presence of a bilge keel, B_K, if applicable. The frictional contribution, $B_{F,turb}$, resulting from turbulent boundary layers is typically very small compared with the other

components. The above method allows one to determine the damping coefficients for each station separately. Without making any distinctions between B_E and B_K, the total quadratic damping coefficient can be estimated by the integration of the local eddy and bilge keel damping coefficients along the wetted portion of the hull (to which the friction component for turbulent flow should be added):

$$B_{44,Q} = \int_0^L b_2(x)dx ,$$

where the integration is carried out for the equilibrium position of the vessel, and $b_2(x)$ is the local quadratic damping coefficient. For a vessel consisting of a finite number of strips the integral sign can be replaced by a summation sign:

$$B_{44,Q} = \sum_{m=1}^{M} b_2(x_m).\Delta x_m ,$$

where Δx_m is the section length for station m and M is the total number of stations.

If the vessel is rolling in a monochromatic wave, the length of which is long compared with the beam of the vessel, the relative motion argument can be used to base the damping moment on the rotational velocity difference between hull and fluid. As a first approach, the average rotational wave particle velocity for each station is averaged over the length of the vessel, so that the nonlinear damping moment is estimated by

$$f_4(t) = - B_{44,Q} \cdot |\dot{\theta}-\dot{\alpha}| \cdot (\dot{\theta}-\dot{\alpha}) ,$$

where α is the wave slope averaged over the length of the ship, and $\dot{\alpha}$ its time derivative, i.e., the average rotational wave particle velocity. It

might be more appropriate to base the calculations on the integration of the local damping coefficient and local wave particle velocity along the length of the ship. The method reported by Himeno (1981) has been developed for the rolling of vessels in calm water. If the incoming wave is long compared with the beam, the relative velocity concept can be considered valid, as the wave will appear as a flat rotating surface to the vessel. Also, the wave's rotational velocity is typically of the same order of magnitude as the roll velocity of the vessel.

Here, it is assumed that the contribution of the radiated and diffracted waves is negligible, so that the expressions for the water particle kinematics are based on those for the undisturbed incoming wave system. For a long wave, the rotational velocity at a point can be determined by taking the time derivative of the wave slope, or the isobar (line of equal pressure) at that point. Using this approach, the rotational wave velocity for a long-crested wave travelling in the x-direction is given by

$$\frac{\partial \alpha(x,y;t)}{\partial t} = \frac{\partial}{\partial t}\frac{dy}{dx}_{(p=const.)} .$$

For a harmonic wave the description of the isobar at a mean depth y_p is according to linear theory

$$Y_p(x;t) = y_p + A_w e^{ky_p} \cos(kx-\sigma t) ,$$

and for a wave travelling in the Oxz-plane with frequency σ (see Appendix A) the equation for the isobar is given by

$$Y_p(x,z;t) = y_p + A_w e^{ky_p} \cos(k_x x+k_z z-\sigma t+\varepsilon) .$$

It is seen that the isobars follow the wave surface contour, η, and that for a long wave ($k << 1$) the slope of an isobar is equal to the wave slope. The above expression is given in the earth-fixed coordinate system, and can be

rewritten in terms of the local, structure-fixed system, by means of the methods discussed in Appendix A. This transformation of coordinates is necessary, since the forces and moments in the time simulation process are evaluated first in the local coordinate system. Then the rotational wave particle velocity can be expressed as

$$\dot{\alpha} = \frac{\partial}{\partial t}\frac{\partial Y_p}{\partial z^*} = \dot{\alpha}\,(x^*,y^*,z^*;t) \ .$$

The total average wave particle velocity is obtained by averaging the local velocities (averaged over the cross section) over the length of the vessel:

$$\dot{\alpha} = \frac{1}{L}\int_{x_A}^{x_F} \dot{\alpha}_m(x^*,y^*,z^*;t)\,dx^* \ ,$$

where $\dot{\alpha}_m$ is the average wave particle velocity at station m, L is the total length of the vessel, and x_A and x_F are the x*-coordinates of the most aft and forward points on the hull, respectively. The average sectional velocity $\dot{\alpha}_m$ is estimated by evaluating the rotational water particle velocity at the center line of the ship, $z^* = 0$, and at the mean water level $y = 0$. Since the waves are considered long with respect to the beam, the rotational wave velocity will be almost uniform across the submerged section of the vessel. For the wave to have any effect, the wave length transverse to the vessel must be of a certain minimum length compared with the beam, where one to two times the beam is an acceptable minimum. If, for example, the shortest effective wave length is set to twice the beam, then

$$\dot{\alpha} = 0 \quad \text{if} \quad (k_x \sin\phi + k_z \cos\phi) > \frac{2\pi}{2.B} \ ,$$

where B is the beam, ϕ is the yaw angle, and k_x and k_z are the wave numbers as defined in Chapter 2.4.1.

Random Waves

Long-crested random waves are considered as the superposition of many component waves with given amplitude and random phase, as is discussed in Chapter 2.4. To determine the damping moment, the same procedure is used as above. In accordance with the superposition assumption, the total rotational wave velocity, $\dot{\alpha}_m$, at a certain ship section is assumed to be given by the summation of the various wave component contributions:

$$\dot{\alpha}_m(x^*,y^*,z^*;t) = \sum_{n=1}^{N} \dot{\alpha}_{m,n}(x^*,y^*,z^*;t) \ ,$$

where $\dot{\alpha}_{m,n}$ is the rotational wave particle velocity of the n^{th} wave component (averaged over the cross section) at station m, and N is the number of wave components comprising the irregular sea surface. Then

$$\dot{\alpha} = \frac{1}{L} \int_{x_A}^{x_F} \dot{\alpha}_m(x^*,y^*,z^*;t)\, dx^* \ ,$$

and the roll damping moment is estimated by

$$f_4(t) = - B_{44,Q} \cdot |\dot{\theta}-\dot{\alpha}| \cdot (\dot{\theta}-\dot{\alpha}) \ .$$

When the length of a wave component, in a direction transverse to the ship, is less one or two times the beam, its contribution, $\dot{\alpha}_{m,n}$, can be assumed negligible.

2.2.2. Coupling Between Roll and Sway Motions

Rolling of a two-dimensional section will result not only in a damping moment acting on the section, but also in a viscous sway force, and

conversely, drag forces resulting from oscillatory sway motion will induce a roll moment. An obvious example is the case of the rolling of a vessel with bilge keels, where there would be a moment due to the normal forces acting on both bilge keels. Taking the components of those forces in the local y* direction would yield a net sway force. The effect of roll on sway in this sense is presumably quite small, but the coupling of sway into roll may be significant. Large sway motions would result in large drag forces, which in turn might affect the viscous roll damping moment noticeably. Whether this coupling would increase or decrease the damping moment would depend on the phasing between the roll and sway motion.

Extending the method of component roll damping discussed in the previous chapter, a formulation is given by Ikeda, Ishikawa and Tanaka (1980) for estimating viscous sway-roll coupling in calm water. Coupling is assumed to be due to the quadratic forces associated with eddy shedding and bilge keels. The sway force due to roll is given by

$$f_3(t) = - B_{34,Q} \cdot |\dot{\theta}| \cdot \dot{\theta} \quad ,$$

where the quadratic coupling coefficient is composed of two contributions:

$$B_{34,Q} = B_{34,E} + B_{34,K} \quad .$$

Similar to the approach described by Himeno (1981), $B_{34,E}$ and $B_{34,K}$ are the roll-into-sway coupling coefficients due to eddy shedding and bilge keels, respectively, the expressions of which are directly related to those of B_E and B_K as given by Himeno. The roll moment due to sway is given by

$$f_4(t) = - B_{43,Q} \cdot |\dot{x}_3| \cdot \dot{x}_3 \quad ,$$

where

$$B_{43,Q} = B_{43,E} + B_{43,K} ,$$

and $\dot{x}_3$ is the sway velocity. Details of the expressions for the coupling coefficients can be found in the reference by Ikeda *et al.*(1980), and will not be repeated here. Based on simulations in small and large amplitude waves, the above sway-into-roll coupling is computed using the sway velocity only, since it was found that the difference between hull sway and water particle velocities was typically quite significant, especially for large wave amplitudes. That is, the usage of relative fluid velocities could lead to misleading results.

In summary, the total viscous roll damping moment associated with the oscillatory roll and sway velocities is given by

$$f_{rd,4}(t) = - B_{44,L}.\dot{\theta} - B_{44,Q}.|\dot{\theta}-\dot{\alpha}|.(\dot{\theta}-\dot{\alpha}) - B_{43,Q}.|\dot{x}_3|.\dot{x}_3 ,$$

and the roll-induced sway force is based on the relative roll velocity:

$$f_{rd,3}(t) = - B_{34,Q}.|\dot{\theta}-\dot{\alpha}|.(\dot{\theta}-\dot{\alpha}) .$$

2.2.3. Maneuvering Forces in Calm Water

One of the objectives of this work is to consider the behavior of a *steered* vessel in waves. This implies that the classical maneuvering behavior must be taken into account. Traditionally, the investigation of the wave-induced motions and ship maneuvering has been conducted along separate paths, with the result that there is presently no consistent theory which accounts for the combined effects of maneuvering in a seaway. The steering and broaching behavior of a vessel in a severe following seaway were studied experimentally by Davidson (1948), who also developed a simple mathematical model describing the various forces acting on the vessel. One of the first treatments of ship maneuvering in waves was

presented by Rydill (1959), who combined linear maneuverability theory with linear motion theory in small amplitude waves. Wahab and Swaan (1964) studied the directional stability of a vessel in following waves for zero-encounter frequency and different positions with respect to the wave crest, and the stability and motions of a steered vessel in following waves were studied by Eda (1972a, 1972b) for various ship speeds. Renilson and Driscoll (1982), and Renilson (1982), have presented a method where the classical maneuverability derivatives are considered frequency dependent, rather than being constant. The frequency-dependent derivatives were based on measurements in waves and on linear motion theory. Although this is a possibly realistic approach, it is fundamentally not correct to use the same theory for waves and for calm water conditions, and it would be rather cumbersome to obtain data for a variety of ship types, wave and operating conditions. Considering the lack of appropriate maneuverability theory, the approach taken in the present work has been to simply combine nonlinear theory, for determining the viscous forces due to steady sway and yaw motion of a steered vessel in calm water, with potential theory for wave-induced effects.

The use of calm water maneuvering theory with constant coefficients (in the time domain) results in the neglect of memory effects associated with viscous flow phenomena. More exact formulations in the time domain have been presented by e.g. Frank *et al.* (1976) and Wehausen (1978), by whom linear theory was applied, and Guo (1978), who has presented a time domain approach that accounts for both linear and quadratic effects due to maneuvering in calm water. Nonlinearities associated with maneuvering calculations in the time domain were taken into account in an approximate manner by Ankudinov (1983).

Viscous drag can be significant during the swaying and yawing of a ship, necessitating an attempt to account for these viscous effects in a ship motion model. The classical maneuvering equations include both potential and viscous flow effects. The potential part of the theory has already been treated in Chapter 2.1, so that only viscous effects need to be dealt with in this section. Most of the development of maneuvering theory has been applied to the lateral motions of a ship in calm water. The

conventional way of treating these motions consists of Taylor series expansions of the various hydrodynamic forces, with the assumption that the motions are small. Often only the linear terms in the expansion are retained, resulting in a simple model, but one that has been found useful even for relatively large motions.

As a first approximation to the modelling of viscous effects, linear theory can be used. The "maneuvering" sway force and yaw moment due to small sway and yaw velocities in calm water (on the right hand side of the equations of motion) would be then the following:

$$f_{m,3}(t) = - Z_v \cdot \dot{x}_3(t) - Z_\phi \cdot \dot{\phi}(t) \ ,$$

$$f_{m,5}(t) = - N_v \cdot \dot{x}_3(t) - N_\phi \cdot \dot{\phi}(t) \ .$$

The sway and yaw velocities are given by $\dot{x}_3$ and $\dot{\phi}$, respectively, and Z_v, Z_ϕ, N_v and N_ϕ are the conventional maneuverability derivatives. An overview of linear and nonlinear maneuvering theory in calm water is found in Comstock (1967), in which also values of the derivatives for a Mariner type hull are given. The nonlinear theory used in the present work is based on a semi-empirical method presented by Inoue *et al.* (1981a, 1981b). Based on model data, this method allows one to estimate the linear and nonlinear derivatives as a function of basic ship characteristics such as overall dimensions and block coefficient. The expressions for the maneuvering forces associated with viscous effects are given below, where the reader is referred to the original references for the necessary details.

Using the symbol convention given by Inoue *et al.*, the yaw velocity is expressed as $r = \dot{\phi}$, and the sway velocity by $v = \dot{x}_3$, or in nondimensional form:

$$r' = \frac{r.L}{U} \text{ , and } \beta = -\sin\frac{v}{U} .$$

Here L is the length of the vessel, and U is the forward speed. Taking into account the sign convention used in the present work, the sway force associated with viscous maneuvering effects is given by

$$f_{m,3} = \frac{1}{2}\rho L d U^2 . \left\{ Z'_{\beta}\beta - Z'_{r}r' + Z'_{\beta\beta}|\beta|\beta + Z'_{\beta r}\beta|r'| - Z'_{rr}|r'|r' \right\} ,$$

and the maneuvering yaw moment is

$$f_{m,5} = \frac{1}{2}\rho L^2 d U^2 . \left\{ -N'_{\beta}\beta - N'_{r}r' + N'_{rr}|r'|r' + (N'_{\beta\beta r}\beta - N'_{rr\beta}r').\beta r' \right\} .$$

It is assumed that the instantaneous sway and yaw velocities can be used in the above expressions. Closely linked to maneuvering is the effect of the rudder, as well as the autopilot which controls the rudder. These topics are discussed in Chapter 2.3.2.

2.2.4. Wave-Induced Drag Forces

In the foregoing chapters viscous effects have been treated empirically in relation to rolling, based on relative rotational velocities and the sway velocity of the vessel, and maneuvering in calm water. It is clear that drag forces transverse to a vessel will be caused by oblique or beam seas. These forces may be significant in severe sea conditions, and as yet their importance has not been investigated sufficiently. Lacking an adequate mathematical model to represent these forces, a simple method is used to estimate the drag forces in the sway direction (resulting also in a roll and yaw moment) associated with the wave particle velocities. The main objective is to obtain information on the sensitivity of the roll response to changes in these viscous forces, i.e., to establish the relative importance of these forces.

It is assumed that the viscous drag force acting on a section of a vessel is given as follows:

$$f_{w,3x}(x^*;t) = \frac{1}{2}\rho C_D A |\dot{u}_3|.\dot{u}_3 ,$$

where C_D is a drag coefficient, $\dot{u}_3$ is the wave particle velocity transverse to the section, and A is the projected area of the section:

$$A = y_s.dx_s ,$$

where y_s is the maximum distance (along the y*-axis) between the bottom of the section and the waterline, and dx_s is the width of the section.

The velocity $\dot{u}_3$ is the mean water particle velocity (due to the incoming wave, where radiation and diffraction effects are assumed negligible) transverse to the ship along the z*-axis at a given station, evaluated at an average depth and on the center line of the vessel:

$$\dot{u}_3(x^*;t) = \left.\frac{\partial \Phi_I}{\partial z^*}\right|_{x=x^*,\, y^*=\bar{y},\, z^*=0} ,$$

where $\bar{y}$ is the average depth. Similar to the computation of the average rotational water particle velocity, the mean sway velocity is determined only for waves exceeding a certain minimum length, e.g. twice the beam, transversely to the ship.

The selection of the drag coefficient is obviously difficult, as it would depend on the Reynolds number, Keulegan-Carpenter number and section shape, among others. It suffices for the purposes of this investigation to assume C_D to be constant along the ship length, and to be chosen rather arbitrarily. Analysis of sway experiments of cylindrical

ship-shape sections, see e.g. Graham (1979) and Tanaka (1980), has indicated that the range of drag coefficients is approximately

$$1 < C_D < 3 .$$

The total sway force and yaw moment may be estimated by integration of the sectional drag forces over the wetted length of the vessel:

$$f_{w,3}(t) = \int_L f_{w,3x}(x^*;t)\, dx^* ,$$

$$f_{w,5}(t) = -\int_L f_{w,3x}(x^*;t) \cdot x^*\, dx^* .$$

The roll moment caused by the sway drag force acting on a section can be estimated by multiplying the drag force by an appropriate moment arm, y_r (which has a positive value):

$$f_{w,4x}(x^*;t) = -f_{w,3x}(x^*;t).y_r .$$

The total induced roll moment can then be determined by integration over the wetted length.

It is noted that the above forces are based solely on the water particle velocities, while in fact they would depend on the *relative* sway motion. However, the total sway force and yaw moment due to the motion of the vessel itself have been accounted for by the maneuvering forces, as discussed in the Chapter 2.2.3, so that it would not be appropriate to consider the vessel motion twice when evaluating these viscous forces. The coupling between sway and roll, due to sway motion of the vessel, has already been accounted for using the empirical approach outlined in Chapter 2.2.2.

2.3. Other Force Contributions

To complete the treatment of the forces acting on the steered vessel, the following contributions are considered:

1. Total resistance and propeller thrust;
2. Autopilot model and rudder forces;
3. Wind forces.

These items are discussed in some detail in the sections below.

2.3.1. Propulsion and Resistance Characteristics

The resistance referred to in this chapter is the calm water resistance to which the vessel is subjected when moving at a steady speed. This resistance may be considered to be due to viscous and wave making effects. The wave making part can be regarded as the force associated with the velocity potential Φ_U, which is one of the components of the total potential Φ_S as was discussed in Chapter 2.1. The calm water resistance curve can be fairly easily constructed for the full-scale ship. By estimating the resistance for a discrete number of forward speeds, a polynomial such as a quadratic, say, can be used to approximate the actual resistance curve.

Consider the case where the resistance would be given by a quadratic polynomial:

$$f_{res}(t) = A_1.U + A_2.|U|.U \ ,$$

where U is the forward speed. Although it should be assumed that U is steady, in reality it will be time dependent. Typically the speed variations about the mean velocity are quite small and slowly varying, so that it is more realistic to consider the ship speed as a function of time, U(t). This leads to a time-dependent calm water resistance, $f_{res}(t)$. It is noted that added mass effects are accounted for by the evaluation of the wave

radiaiton forces, as has been discussed in Chapter 2.1.2. In waves that are long compared with the length of the ship along its longitudinal axis, one can incorporate the wave particle velocity by considering the relative velocity between ship and wave in the surge direction. Especially in long following seas the wave-induced velocities may affect the resistance. In analogy with the computation of the wave velocity in the transverse direction (see Chapter 2.2.1), the average wave velocity in the surge direction of the vessel is taken into account, if the wave length along the x*-axis is of the order of the ship length. The average velocity is then estimated by

$$\dot{u}_1 = \frac{1}{L} \int_{x_A}^{x_F} \frac{\partial \Phi_I}{\partial x^*} dx^* \ ,$$

which is evaluated at the center line of the vessel ($z^* = 0$), and at an average depth of $y^* = -d/2$. The resistance force, acting on the vessel in the longitudinal direction and added to the right hand side of the equations of motion, is estimated as follows for the quadratic polynomial model:

$$f_{res}(t) = - A_1 \cdot (U - \dot{u}_1) - A_2 \cdot |U - \dot{u}_1| \cdot (U - \dot{u}_1) \ .$$

The propeller characteristics can also be approximated quite easily. The basic assumption made is that the rotational speed of the propeller, n, does not vary with time. Knowing the number of blades, diameter, etc., use can be made of the so-called K_T curves to estimate the thrust produced by the propeller for different speeds of advance, expressed by the advance ratio, J. For example, use can be made of the Troost B-Series, which present nondimensional thrust as curves of K_T versus J. A schematic representation of K_T curves for constant values of P/D (pitch-to-diameter ratio) is shown in Figure 2.3.

K_T and J are given by the following nondimensional expressions:

$$K_T = \frac{T}{\rho n^2 D^4} \quad \text{and} \quad J = \frac{V.n}{D} ,$$

where T is the propeller thrust, ρ is the density of water, D is the propeller diameter, n is the number of propeller revolutions per second, and V is the velocity of advance. This simple method will at least model the effect of thrust increase with decreasing ship speed, and conversely, thrust decrease with increasing speed. Again, it is assumed that the forward speed changes slowly.

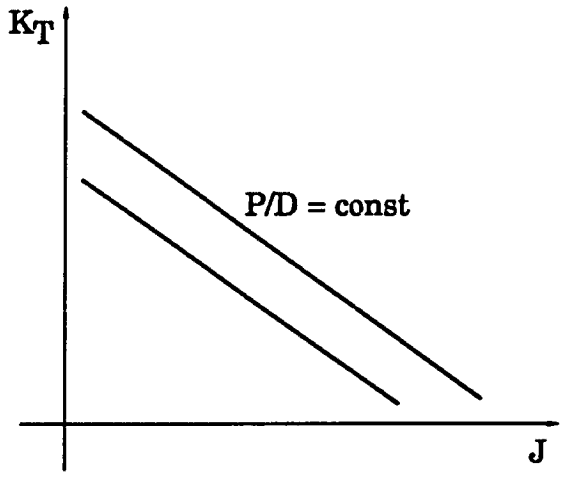

Figure 2.3. Typical K_T Curves

2.3.2. Rudder and Autopilot

For a steered vessel it is important to model the rudder and autopilot characteristics correctly. The lift exerted by the rudder will cause a yaw moment, a sway force, and also a roll moment, all of which should be taken into account. Rudder lift depends on the rudder geometry (cross-sectional shape, area, aspect ratio), incoming flow velocity and angle of attack. There are a variety of methods available to estimate lift forces, and

most models are based on the following formula, where the lift force is given by

$$f_{rud,L} = \text{Constant} \times \rho A V^2 f(\alpha) .$$

A is the area of the rudder, V is the water particle velocity past the rudder, and α is the angle of attack between rudder and incoming flow. The velocity V is the total flow velocity experienced by the rudder, and depends on the forward speed of the vessel and propeller race. For a rudder behind a propeller the velocity is significantly increased, and is typically

$$V = 1.3 \times \text{ship speed.}$$

The velocity increase depends on the vessel type, and for highly loaded propellers, as is the case for tanker vessels, the velocity may be increased by a factor 2 or more. In this work V is considered as the vectorial sum of the forward speed, wake, propeller-induced velocity increase, the average wave particle velocity, as well as the ship motion induced velocity due to e.g. yaw and roll. These velocity components are determined at a point situated in the middle (between top and bottom, or, if the rudder is partially emerged, between the free surface and bottom) of the rudder, which should be close to the center of pressure.

Rawson and Tupper (1984) recommend the following formulae for estimating the lift and drag coefficient for a typical rudder:

$$C_L = \frac{F_L}{\frac{1}{2}\rho A V^2} = \frac{a_0 \cdot a_e}{\cos\Omega \cdot \sqrt{\frac{a_e^2}{\cos^4\Omega} + 4} + \frac{57.3\, a_0}{\pi}} \times \alpha + \frac{C_{Dc}}{a_e} \cdot \left(\frac{\alpha}{57.3}\right)^2 ,$$

where a_e = aspect ratio = $(\text{span})^2/A$,

a_0 = section lift curve slope at $\alpha = 0$

= 0.9 ($2\pi/57.3$) per degree for NACA 0015 section,

C_{Dc} = cross-flow drag coefficient,

= 0.80 for square tips and taper ratio 0.45,

Ω = sweep angle.

The drag force $f_{rud,D}$ can be estimated from the drag coefficient:

$$C_D = \frac{f_{rud,D}}{\frac{1}{2}\rho A V^2} = C_{d0} + \frac{C_L^2}{0.9\pi a_e},$$

where C_{d0} = minimum section drag coefficient

= 0.0065 for NACA 0015.

Some comments can be made as regards the usage of the above formulae. The drag force of the rudder is usually quite small compared with the resistance of the ship, for example, and therefore is relatively insignificant. The formulae are based on steady flow and angles of attack that are less than the stall angle. Rudder stall angles lie in the range from 30 to 45 degrees, beyond which the lift and drag forces may be estimated using flat plate theory. Since the lift coefficient, C_L, is theoretically based on steady flow conditions, inclusion of the wave particle velocities in the incoming flow field will result in a time-dependent lift coefficient, which will lead to a more qualitative than quantitative estimate of the lift force. However, for relatively low frequencies of encounter and wave lengths that are long compared with the rudder chord length, the usage of the steady flow approach is justified. Also the span of the rudder will be time dependent when, for example, the rudder is partially emerged due to pitching in severe seas. Obviously, the rudder force should be zero when the rudder is totally emerged. Using the above empirical method gives an estimate of the lift and drag forces acting on the rudder. These forces can be resolved along the vessel's axes to yield the forces in the local surge, sway, roll, yaw and pitch directions.

The rudder angle is controlled in the numerical simulations by an autopilot, the parameters of which are based on the autopilot used for the San Francisco Bay experiments; a comprehensive description of the autopilot has been given by Haddara *et al.* (1972) and Chou *et al.* (1974). The same autopilot system was used in the computations by Pérez y Pérez (1974). The desired rudder angle is taken to be linearly proportional to the yaw angle and yaw rate:

$$\delta_r = \delta_1 + \delta_2 = a_1\phi + a_2\dot{\phi} \qquad |\phi| \geq \phi_0$$

$$\delta_r = 0 \qquad |\phi| < \phi_0 ,$$

where δ_r = rudder angle
δ_1 = yaw proportional rudder response
δ_2 = yaw rate proportional rudder response
ϕ = yaw angle
$\dot{\phi}$ = yaw velocity
ϕ_0 = dead band
a_1, a_2 are constant coefficients.

The yaw angle is positive when the bow of the vessel turns to port, and the rudder angle is positive when the rudder turns to port, since it would result in a positive yaw moment. The purpose of the dead band is to avoid excessive rudder motions, particularly in severe seas; generally $\phi_0 = 0$ for calm seas, and $\phi_0 > 0$ for rough seas. In the report by Haddara *et al.* (1972) typical autopilot values are given for a cargo vessel:

ϕ_0	0.75° to 4°
a_1	1 to 4 (deg/deg)
a_2	4 to 20 (deg.sec/deg)
a_2 / a_1	4 to 5 (sec)
$\dot{\delta}_r$	2.3 (deg/sec).

$\dot{\delta}_r$ is the helm response rate which is needed in calculating the actual change in rudder angle. In the simulations, the required rudder angle is calculated and compared with the previous value at each time instant; rudder correction is taken if necessary The rudder force components and induced roll, yaw and pitch moments are determined for the new values of rudder angle and incoming flow velocities.

2.3.3. Wind Effects

A beam wind can exert a significant roll moment on a vessel, and may have detrimental effects when combined, for example, with severe seas. It is not one of the principal objectives of this work to fully investigate wind effects. Nevertheless, a simple wind force model is included, so that wind effetcs can be investigated in a very approximate way. One of the main assumptions is that the wind is steady and has a constant profile. The wind excitation force, transverse to the ship, can then be estimated by using an empirical drag coefficient, C_{Dw}, in the following relationship:

$$f_w = \frac{1}{2}\rho_a A V_w^2 C_{Dw} ,$$

where ρ_a is the density of air, A is the projected cross-sectional area of the structure, and V_w is the mean wind velocity.

The above formulation will give only a very approximate estimate of the wind-induced forces, especially since time-dependent effects are not accounted for. For example, in practice the wind speed is very time dependent and may represented by a spectrum, the profile varies with height above mean water level as well as wind speed, and wind-induced pressures are characterized by a certain spatial correlation function.

2.4. Description of the Sea Surface

The wave theory used throughout this work assumes infinite water depth (i.e., the depth is large enough for the waves not to be influenced by the bottom), the fluid is assumed inviscid and incompressible, and the flow irrotational. Surface tension is neglected, as it is of significance only for waves of very short wave length. In this chapter the wave kinematics are treated as follows: first, harmonic waves of small amplitude are considered, where classical linear theory is applied, and this is subsequently extended to large amplitude conditions in Chapter 2.4.2. In Chapter 2.4.3 random waves and wave grouping are discussed, and special attention is given to the appearance of wave groups in reference frames moving with the waves, as would be applicable to ships with forward speed. Expressions are obtained for the observed mean square value of the wave elevation process for fixed and moving reference frames. Based on the findings in Chapter 2.4.3, an investigation has been made in Chapter 2.4.4 of the statistical aspects of the encountered mean square value in following seas, and of the apparent wave energy in Chapter 2.4.5.

2.4.1. Harmonic Waves of Small Amplitude

The following free surface profile is assumed:

$$\eta(x,z;t) = A\cos(k_x x + k_z z - \sigma t + \varepsilon) \ ,$$

where
- A = wave amplitude
- σ = circular wave frequency
- ε = phase of wave (0° denotes wave crest at C.G. of vessel)
- $k_x = k\cos\delta$
- $k_z = -k\sin\delta$
- $k = \sigma^2/g$ = wave number.

The wave direction, δ, is defined as in Figure A.2 in Appendix A, from which it is seen that a zero degree direction implies following sea conditions.

The velocity potential of the incoming wave must satisfy the Laplace equation,

$$\nabla^2\Phi_I(x,y,z;t) = 0 ,$$

throughout the fluid domain. Assuming small amplitude wave conditions apply, i.e., kA << 1, the boundary conditions can be linearized, so that Φ_I must satisfy the following combined kinematic and dynamic free surface boundary condition at the mean water level, y = 0:

$$\Phi_{tt}(x,0,z;t) + g\Phi_y = 0 ,$$

which for a harmonic wave can be written in terms of the time-independent part, φ_I, of the potential Φ_I:

$$\varphi_I(x,0,z) - \frac{g}{\sigma^2}\varphi_I = 0 ,$$

where

$$\Phi_I(x,y,z;t) = \varphi_I(x,y,z)\, e^{i\sigma t} .$$

The kinematic boundary condition at the bottom (or "infinite" depth) can be stated as follows:

$$\lim_{y \to -\infty} \nabla\Phi_I(x,y,z;t) = 0 .$$

The velocity potential satisfying the above conditions is given by

$$\Phi_I(x,y,z;t) = \frac{A\,g}{\sigma}\,.\,e^{ky}.\,\sin(k_x x+k_z z-\sigma t+\varepsilon)\ ,\quad -\infty < y \le 0\ ,$$

which can also be expressed in complex notation as

$$\Phi_I(x,y,z;t) = \mathrm{Re}\ -i\frac{A\,g}{\sigma}e^{ky}\,e^{i(k_x x+k_z z-\sigma t+\varepsilon)}\ .$$

2.4.2. Harmonic Waves of Large Amplitude

Despite the apparent theoretical limitations, linear wave theory applied to large amplitude waves in deep water has been found to yield quite adequate results as regards wave profile, water particle kinematics and pressure. Oceanographical research, see e.g. Wiegel (1964), has suggested that linear theory can be extended above the mean water level; Sobey *et al.* (1987) have shown that wave profiles and crest velocities predicted by extended linear theory compare favorably with predictions from several higher order theories, at least for deep water conditions. Linear theory does give incorrect results for shallow water waves, particularly when the wave height is large. It has been suggested that linear theory severely overpredicts the crest velocities of large deep water waves, as was done by, for example, Gudmestad and Connor (1986).

In this work it is assumed that linear wave theory can be extended up to the actual free surface level, so that the velocity potential can be written as

$$\Phi_I(x,y,z;t) = \frac{A\,g}{\sigma}\,.\,e^{ky}.\,\sin(k_x x+k_z z-\sigma t+\varepsilon)\ ,\quad -\infty < y \le \eta\ ,$$

where η is the free surface elevation defined as above. Chakrabarti (1971) has suggested that applying linear wave theory to particle kinematics in the crest results in a pressure discontinuity at the mean water level. However, in his view of extending linear theory, the pressure above the mean water level is purely hydrostatic, as the dynamic term is not

considered valid in the crest ($y \geq 0$). In order to justify using the extended linear theory for severe wave conditions, it is shown below that the pressure at the free surface is constant to lowest order. Another consequence of this approach is that there is no pressure discontinuity at the mean water level.

Neglecting higher order terms, according to extended linear theory the wave pressure can be expressed by

$$p(x,y,z;t) = -\rho g y - \rho \frac{\partial \Phi_I}{\partial t} , \quad -\infty < y \leq \eta ,$$

which results in

$$p(x,y,z;t) = -\rho g y + \rho A g e^{ky} \cos(k_x x + k_z z - \sigma t + \varepsilon) .$$

In accordance with linear theory, the wave amplitude is small compared with the wave length, i.e., $kA << 1$, so that in the neighborhood of the mean water level, $y = 0$, the exponential term can be expanded about $ky = 0$:

$$e^{ky} = 1 + ky + \frac{(ky)^2}{2!} + \frac{(ky)^3}{3!} + \ldots$$

$$\cong 1 .$$

Even in severe wave conditions where wave breaking does not occur, the wave amplitude is relatively small compared with the wave length, since a typical amplitude to length ratio would be 1:10. Thus, up to lowest order, the pressure close to the mean water level is given by

$$p(x,y,z;t) = -\rho g y + \rho g \eta(x,z;t) .$$

Hence, at the free surface $y = \eta$ the pressure is zero to lowest order for all wave conditions, suggesting that under the appropriate conditions linear theory is not inconsistent for waves of finite amplitude. By inspection it is seen that the pressure derivative $\partial p/\partial y$ does not have a discontinuity at $y = 0$.

2.4.3. Random Waves and Wave Groups

The objective of this chapter is to investigate the modelling and behavior of random waves, observed from a stationary and moving reference point. Statistical analyses of waves in deep water have shown that the distribution of the wave elevation typically is Gaussian or close to it, and that the peaks and troughs have approximately the Rayleigh distribution. In order to represent the surface of a unidirectional random sea, it is assumed that the wave surface can be considered as being composed of an infinite number of component waves having different frequencies and infinitesimal amplitudes. Also, the phase lags ε_n are assumed to be uniformly distributed over the interval $(-\pi,\pi)$. If the phases of the individual components are uniformly distributed, the distribution of the wave elevation would be Gaussian as a result of the linear superposition model. According to the superposition model, the time-dependent wave elevation observed at a stationary reference point, is given by

$$\eta(x,z;t) = \sum_{n=1}^{\infty} A_n \cos(k_{x,n}x+k_{z,n}z-\sigma_n t+\varepsilon_n) ,$$

where the subscript n refers to the properties of the n^{th} wave component. This representation has been found to be adequate for modelling deep water wave conditions observed at a fixed point, and has been used by Longuet-Higgins (1984), among others, to study the statistical properties of surface waves.

When creating random wave records for time simulation purposes, a number of simplifications have to be made. If one starts from a standard formula for the spectral representation of the sea surface, $S_{\eta\eta}(\sigma)$, a high-

frequency cut-off point must be chosen, for example. The one-sided spectral density can be defined as follows:

$$S_{\eta\eta}(\sigma) = \frac{1}{2\pi} \int_0^\infty R(\tau) \cos\sigma\tau \, d\tau \ ,$$

$$R(\tau) = \int_0^\infty S_{\eta\eta}(\sigma) \cos\sigma\tau \, d\sigma \ .$$

The function $R(\tau)$ is the autocorrelation function, and τ is the time lag; by definition of the one-sided spectrum, negative wave frequencies are not considered in the above relationships. Estimated spectra of wave elevations, say, are usually based on smoothed periodograms related to the Fourier transformation of the wave record; for more details on the estimation of spectra and related statistical aspects, see e.g. Brillinger (1981).

If one is interested in the overall behavior of the wave group envelope, it may suffice to consider only the wave components in the range from approximately $0.5\sigma_p$ to $1.5\sigma_p$, where σ_p is the peak frequency of the spectrum, as has been proposed by Longuet-Higgins (1984). The final choice is obviously also a function of the dynamic properties of the vessel of interest; if, for example, one is interested in the seakeeping behavior of a small boat, it will be necessary to choose the cut-off frequency such that it lies in the same range as the natural pitch frequency, say. Conversely, the cut-off frequency need not be high for a relatively large vessel.

Another necessary simplification in the time simulation of waves is that the total number of wave components will be finite. The representation of the sea surface having a finite number of N components is given by

$$\eta(x,z;t) = \sum_{n=1}^{N} A_n \cos(k_{x,n}x + k_{z,n}z - \sigma_n t + \varepsilon_n) \ .$$

In order to generate wave records that have the same spectral properties as the original spectrum, the amplitudes of the wave components can be determined as follows:

$$A_n = \sqrt{2S_{\eta\eta}(\sigma_n)\,\Delta\sigma_n} \quad ,$$

where $S_{\eta\eta}(\sigma_n)$ is the spectral density associated with the n^{th} wave component, and $\Delta\sigma_n$ is the corresponding frequency interval. It is argued by Tucker, Challenor and Carter (1984) that the above representation may affect the statistical properties of the sea surface, and particularly the wave group properties; a statistically more correct way of representation would supposedly be obtained by randomly choosing the finite set of component amplitudes out of a Rayleigh distribution, and the phases out of a uniform distribution. In this case the n^{th} amplitude should be chosen out of a Rayleigh distribution having a standard deviation equal to

$$s_n = \sqrt{2S_{\eta\eta}(\sigma_n)\,\Delta\sigma_n} \quad .$$

This may be valid for the case where one wants to generate a large number of random wave records which are ergodic, but it seems that e.g. wave group properties still would depend on the number of frequencies employed. One way to minimize the problem of wave group properties is to use randomly varying phases, or frequency intervals of varying width (by using equal amplitudes for all the components, for example). In this work the amplitudes are determined deterministically, and constant frequency intervals are used. However, in the simulation of random waves the frequency spacing is considered random by assuming that the frequency of each component is uniformly distributed over the corresponding frequency interval $\Delta\sigma_n$.

If the number of wave components are sufficiently high, the statistics of the modelled wave process are the same for the deterministic and random amplitude methods. This can be proved by applying the Central Limit Theorem. It was found by Elgar, Guza and Seymour (1985) that N = 2100

was large enough for the random phase method (with deterministic amplitudes) to model a Gaussian process realistically.

It is assumed that the wave-induced pressure, as well as other flow properties such as velocity and acceleration, in a random wave system can be determined according to the linear superposition principle, whereby the total velocity potential of the wave system consists of the summation of the individual velocity potentials:

$$\Phi_I(x,y,z;t) = \sum_{n=1}^{N} \Phi_{I,n} = \sum_{n=1}^{N} \frac{Ag}{\sigma_n} e^{ky} \sin(k_{x,n}x + k_z z - \sigma_n t + \varepsilon_n) \ ,$$

so that the pressure at any point in the fluid can be estimated by

$$p(x,y,z;t) = -\rho g y - \rho \sum_{n=1}^{N} \frac{\partial \Phi_{I,n}}{\partial t} \ , \quad -\infty < y \leq \eta \ .$$

When calculating the forces acting on a vessel in random waves, the above pressure would be the one used to determine the Froude-Krylov forces by integration over the instantaneous wetted surface.

Wave Groups in Stationary and Moving Reference Frames

Next the phenomenon of wave grouping is considered due to the presence of two or more wave components in a seaway. Wave groups were found to be of importance in the study of model capsizing in the San Francisco Bay, as has been reported by Oakley, Paulling and Wood (1974), and Chou *et al.* (1974). It was observed that wave groups enhanced the parametric excitation of a ship in a following sea, for example, by providing a nearly harmonically varying excitation over a prolonged period of time. In the case of a short wave group there often was not sufficient time for resonant motions to build up to a serious level. While in reality wave groups in following seas may not necessarily be the most important contributor to

capsizing, it is a fact that often under following or quartering sea conditions undesirable roll motions are observed on board ships of various types. It is also well known that under storm conditions it is not advisable to maintain a course in following seas. Wave groups were observed to increase the likelihood of broaching during the San Francisco Bay experiments, where the ship would be put off course by one big wave, and yawed even further by a consecutive large wave, before the vessel had time respond to the rudder. Grim (1963, 1983) showed that a ship could be accelerated in a following wave group to a certain critical speed, at which point broaching would be more likely to occur.

Moored offshore platforms can be very sensitive to wave grouping, especially when the group frequency lies close to the natural surge or sway frequency of the structure, as a result of which significant slow drift excursions may occur. This aspect will not be further discussed, as the slow drift behavior is not considered of importance in an investigation of large motions or capsizing of freely floating vessels. The main concern for ships seems to lie in the possibility of some kind of dynamic excitation due to wave groups, where the group length, wave frequency and the envelope amplitude are the critical parameters. The occurrence of groups with waves of extreme height, including waves which may be breaking, has been studied by Su (1986), where "extreme wave groups" were considered to be possibly due to wave instabilities and current. In the present work these groups are not considered, since their occurrence is relatively rare and wave breaking cannot yet be incorporated properly into the prediction of ship motions. Chou (1977) has presented a method to determine the likelihood of occurrence of groups having certain characteristics such as length, number of waves and group amplitude. Longuet-Higgins (1984) has derived expressions for estimating the statistical properties of group length and amplitude. In the following some characteristics of wave groups are studied for the case of a stationary and moving reference frame. The latter gives an indication of the waves and their groupiness as encountered by a vessel with forward speed. Specifically, following and quartering sea conditions are studied, where the reference frame moves with respect to the waves at an angle less than 90°.

Two-Component Wave System

Let us first consider a wave system consisting of two components. This is the most elementary way of studying wave grouping, and results in the well-known beating phenomenon. For convenience, the waves are assumed to be moving along the positive x-axis, i.e., $k_z = 0$. Then the wave elevation is given by

$$\eta(x;t) = A_1 \cos(k_1 x - \sigma_1 t + \varepsilon_1) + A_2 \cos(k_2 x - \sigma_2 t + \varepsilon_2) ,$$

where $k_1 = \sigma_1^2/g$
$k_2 = \sigma_2^2/g.$

The wave elevation can be written in terms of a slowly-varying modulation with a carrier wave having frequency σ_1, as given by Newman (1977):

$$\eta(x;t) = A_1 e^{-i(k_1 x - \sigma_1 t + \varepsilon_1)} \cdot \left\{ 1 + \frac{A_2}{A_1} \cdot e^{-i(\delta k . x - \delta\sigma . t + \delta\varepsilon)} \right\} ,$$

where real parts are implied and

$$\delta k = k_2 - k_1$$
$$\delta\sigma = \sigma_2 - \sigma_1$$
$$\delta\varepsilon = \varepsilon_2 - \varepsilon_1 .$$

The group (or wave envelope) frequency, as would be observed at a stationary point, is given by $\sigma_{g,0} = \delta\sigma$, and the group length is equal to $2\pi/\delta k$. It is assumed that $\delta\sigma$ is positive. The above equation shows that these group properties are not affected by the phases of the wave components. The group speed of the two component wave system, in the fixed reference frame, is given by

$$C_g = \frac{\delta\sigma}{\delta k} ,$$

and in the limit this becomes

$$C_g = \frac{d\sigma}{dk} .$$

If the two components have almost the same frequency, i.e., $\sigma_2 \rightarrow \sigma_1$, then the group velocity is equal to half the phase speed of the waves, C_p, (here based on the frequency $\sigma = \sigma_1$):

$$C_g = \frac{g}{2\sigma_1} = \frac{1}{2} . C_p .$$

The mean square value of the process, obtained at a fixed point (x = 0, say), is a useful measure of the global statistical behavior of the seaway, and is directly proportional to the mean energy present in the waves as observed at the fixed point. The definition of the mean square value is the following:

$$\eta_{M.S.} = \lim_{T \rightarrow \infty} \frac{1}{T} \int_0^T \eta^2(t)\, dt ,$$

which for the two-component wave system is equal to

$$\eta_{M.S.} = \frac{1}{2} A_1^2 + \frac{1}{2} A_2^2 .$$

It is of considerable interest to study the waves as they would appear to a moving vessel, especially in following sea conditions. This aspect seemingly has not received much attention, although the importance of the collapse of the encounter spectrum in following seas and increase in

observed number of waves in groups, was stressed by Chou *et al.* (1974), among others. A discussion on the encounter spectrum for different ship headings and speeds has been presented by Webster and Trudell (1981). An important consequence of forward speed in the wave direction, is that under certain conditions the wave excitation experienced by the vessel seems to become more regular, i.e., for a given time period the envelope of the wave process appears to have a more constant amplitude than would be observed over the same amount of time by a stationary observer. This is shown below both analytically and by simulation for the two-component wave system.

If the moving reference frame, $O^e x^e y^e z^e$, has a speed U, the position of a point in that frame becomes time dependent, and is given by

$$x = x^e + U.t \ ,$$

and if the wave elevation is considered at the origin of $O^e x^e y^e z^e$, the relationship is

$$x = U.t \ .$$

This expression for x can be substituted into the wave elevation expression so as to obtain a description of the wave surface as it would appear to an observer positioned at O^e:

$$\eta(x;t) = A_1 \cos(k_1 U.t - \sigma_1 t + \varepsilon_1) + A_2 \cos(k_2 U.t - \sigma_2 t + \varepsilon_2) \ .$$

Let the forward speed be expressed as being proportional to the phase speed of the first component, C_{p1}:

$$U = b.C_{p1} = b.\frac{g}{\sigma_1} \ ,$$

where b is a constant. Then the observed wave elevation can be written as

$$\eta(t) = A_1\cos\{(b-1)\sigma_1 t + \varepsilon_2\} + A_2\cos\{(b\sigma_2^2/\sigma_1 - \sigma_2)t + \varepsilon_2\} ,$$

so that

$$\eta(t) = A_1 e^{i\{(b-1)\sigma_1 t - \varepsilon_1\}} \cdot \left\{1 + \frac{A_2}{A_1} e^{i\{b\sigma_2^2/\sigma_1 - \sigma_2 - (b-1)\sigma_1\}t - i\delta\varepsilon}\right\} .$$

In analogy with the wave group behavior observed from a stationary vantage point, the wave groups, as they would appear to an observer located at the moving origin O^e, are varying with a frequency $\sigma_{g,U}$ given by

$$\sigma_{g,U} = b\sigma_2^2/\sigma_1 - \sigma_2 - (b-1)\sigma_1 .$$

This frequency can be expressed in terms of the group frequency $\sigma_{g,0} = \delta\sigma$:

$$\sigma_{g,U} = b\{\delta\sigma^2/\sigma_1 + 2\delta\sigma + \sigma_1\} - \delta\sigma - \sigma_1 - b\sigma_1 + \sigma_1$$

$$= b\{\delta\sigma^2/\sigma_1 + 2\delta\sigma\} - \delta\sigma .$$

Next a short investigation is made to determine for what speeds, from the moving reference point of view, the observed groups are more slowly varying compared with the groups observed at a fixed point. The criterion that can be used for this purpose is the wave group frequency, as the lower the frequency $\sigma_{g,U}$ is, the longer it takes for the group to pass the moving reference point. Thus, it is desirable to know for what conditions the following holds:

$$|\sigma_{g,U}| \leq \delta\sigma .$$

Case (i): $\sigma_{g,U} = 0$.

The apparent wave group frequency $\sigma_{g,U}$ is zero if the constant b is equal to

$$b = \frac{1}{\delta\sigma/\sigma_1 + 2} \; .$$

Hence, if the speed of the moving reference point is equal to

$$U = \frac{1}{\delta\sigma/\sigma_1 + 2} \cdot \frac{g}{\sigma_1} \; ,$$

the observer at that point would always see the same waves pass by, i.e., there would be no apparent change in amplitude or frequency. In the limit where $\delta\sigma$ approaches zero, the speed constant would be given by

$$b = \lim_{\delta\sigma \to 0} \frac{1}{\delta\sigma/\sigma_1 + 2} = \frac{1}{2} \; ,$$

which results in the speed of the moving reference point being equal to the half the phase speed:

$$U = \frac{1}{2} C_p = C_g \; .$$

Thus, when an observer travels at the group speed, there will be no change in apparent wave amplitude and frequency of encounter, and the waves will overtake the observer in a regular fashion. This is not a new result, however, it has some interesting implications which are discussed further on in this section.

Case (ii): $\sigma_{g,U} < \delta\sigma$.

For the apparent group frequency to be smaller than the one observed at a fixed point, the following result applies:

$$b\{\delta\sigma^2/\sigma_1 + 2\delta\sigma\} < 2\delta\sigma$$

$$\Rightarrow \quad b < \frac{2}{\delta\sigma/\sigma_1 + 2} \ .$$

Case (iii): $\sigma_{g,U} > -\delta\sigma$.

This requirement leads to

$$b\{\delta\sigma^2/\sigma_1 + 2\delta\sigma\} > 0$$

$$\Rightarrow \quad b > 0 \ .$$

In summary, the wave group (or envelope) frequency observed from a reference frame moving with the waves can be smaller than would be observed otherwise, so that under those conditions the excitation remains harmonic over a longer period of time. The apparent wave group frequency is smaller than $\delta\sigma$ for a wave system having two components, when the speed of the moving frame lies in the range

$$0 < U < 2.C_g \ ,$$

and the apparent group frequency is zero when the forward speed is equal to the group speed:

$$U = C_g = \frac{\delta\sigma}{\delta k} \ .$$

Although the above observations are valid only for a simple composite wave system, it does indicate that prolonged harmonic excitation may occur when a ship travels with the waves at their group speed. This could result in undesirable roll motions, for example, through parametric excitation. Obviously, the excitation experienced by the vessel would depend largely on the position with respect to the wave envelope. If the ship travels at group speed, but is located at the point of minimum amplitude of the envelope, it will never be exposed to waves of any significant amplitude. Conversely, if the ship travels with the crest of the wave envelope, it will be subjected to harmonic wave excitation where the amplitude of the waves may be large. The mean square value of the waves as observed by the moving vessel can be easily calculated, and is discussed next in some more detail.

If the encounter frequencies with the individual wave components are defined as follows:

$$\sigma_1^e = k_1 U - \sigma_1 \ , \qquad \sigma_2^e = k_2 U - \sigma_2 \ ,$$

and if zero phase angles are assumed for the moment being (random phase angles will be considered later), the wave elevation observed from the moving reference point is given by

$$\eta(t) = A_1 \cos(\sigma_1^e.t) + A_2.\cos(\sigma_2^e.t) \ ,$$

so that

$$\eta^2(t) = A_1^2.\cos^2(\sigma_1^e.t) + A_2^2.\cos^2(\sigma_2^e.t) + 2A_1A_2.\cos(\sigma_1^e.t).\cos(\sigma_2^e.t) \ .$$

The mean square value of the observed process, evaluated over an infinitely long period, is given by

$$\eta_{M.S.} = \lim_{T\to\infty} \frac{1}{T}\int_{0_T}^{T} \eta^2(t)\,dt$$

$$= \lim_{T\to\infty} \frac{1}{T}\int_{0}^{} \{A_1^2\cos^2\sigma_1^e t + A_2^2\cos^2\sigma_2^e t + 2A_1A_2\cos\sigma_1^e t.\cos\sigma_2^e t\}\,dt \ .$$

Evaluation of the first two terms gives the mean square value of the process as would be obtained from a fixed reference point:

$$\frac{1}{2}A_1^2 + \frac{1}{2}A_2^2 \ .$$

The contribution from the third term depends on the value of the encounter frequencies: the third term is given by

$$= A_1A_2 \text{ if } \sigma_1^e = \sigma_2^e$$
$$\text{or } \sigma_1^e = -\sigma_2^e$$

$$= 0 \text{ otherwise.}$$

Hence, if the two encounter frequencies have the same magnitude, the mean square value of the observed process is that of a regular wave system with an amplitude equal to that of the wave envelope, i.e.,

$$\text{if } \sigma_1^e = \sigma_2^e,\ U = \frac{\sigma_1 - \sigma_2}{k_1 - k_2} = C_g, \text{ and } \eta_{M.S.} = \frac{1}{2}(A_1+A_2)^2 \ .$$

The velocity, U, for which the encounter frequency with both wave components is the same, is the group velocity pertaining to those components. It is noted that if the encounter frequencies are of the same magnitude but of opposite sign, the following relationship is obtained for the velocity and mean square value:

$$\text{if } \sigma_1^e = -\sigma_2^e,\ U = \frac{\sigma_1 + \sigma_2}{k_1 + k_2}\ ,\ \text{and}\ \eta_{M.S.} = \frac{1}{2}(A_1 + A_2)^2\ .$$

The discussion above suggests that when an observer travels with the group speed along the crest of the wave envelope, he will be subjected to a higher amount of wave energy than if it were stationary, as

$$\frac{1}{2}(A_1 + A_2)^2 > \frac{1}{2}A_1^2 + \frac{1}{2}A_2^2 \text{ always.}$$

On the other hand, when an observer travels with the trough of the wave group, he will be subjected to a smaller than average amount of wave energy. One may question whether the same applies for a vessel travelling in random following seas.

Let us now consider a two-component wave system having random phase angles, where an observer travels at an angle β relative to the waves. Then the observed wave elevation is

$$\eta(t) = A_1.\cos(\sigma_1^e.t + \varepsilon_1) + A_2.\cos(\sigma_2^e.t + \varepsilon_2)\ ,$$

where the encounter frequencies with the individual components are defined as

$$\sigma_1^e = k_1.U.\cos\beta - \sigma_1$$

$$\sigma_2^e = k_2.U.\cos\beta - \sigma_2\ .$$

At least for the moment being the above definition for encounter frequency is used, whereas the conventional expression would have *opposite* signs. This is done simply for convenience so as to avoid minus signs in the relevant expressions. The velocity U is considered to be positive always,

and the relative heading is taken such that quartering or following wave conditions exist, i.e.,

$$-90° < \beta < 90° \ .$$

It is noted that for head or bow sea conditions there is a one-to-one mapping between the wave component frequencies and encounter frequencies, so that under those conditions the mean square value of the observed process, for example, would always be equal to that of the wave process observed at a fixed point. It seems that for following sea conditions this may not necessarily be the case, which warrants further investigation.

The square of the observed wave process defined above is

$$\eta^2(t) = A_1^2.\cos^2(\sigma_1^e t + \varepsilon_1) + A_2^2.\cos^2(\sigma_2^e t + \varepsilon_2) + 2A_1A_2.\cos(\sigma_1^e t+\varepsilon_1).\cos(\sigma_2^e t+\varepsilon_2) \ ,$$

where the last term can be written as

$$\begin{aligned} 2A_1A_2.\{&\cos\sigma_1^e t.\cos\sigma_2^e t.\cos\varepsilon_1.\cos\varepsilon_2 + \sin\sigma_1^e.\sin\sigma_2^e t.\sin\varepsilon_1.\sin\varepsilon_2 \\ &- \sin\sigma_1^e t.\cos\sigma_2^e t.\sin\varepsilon_1.\cos\varepsilon_2 - \cos\sigma_1^e t.\sin\sigma_2^e t.\cos\varepsilon_1.\sin\varepsilon_2\} \ . \end{aligned}$$

The mean square value of this process has the following contribution from the first two terms:

$$\frac{1}{2}A_1^2 + \frac{1}{2}A_2^2 \ ,$$

while the contribution from the last term clearly depends on the phase angles. The following four integrals result from the expression for the mean square value of the last term, where the limit $T \to \infty$ is taken:

$$\frac{1}{T}\int_0^T \cos\sigma_1^e t.\cos\sigma_2^e t.\cos\varepsilon_1.\cos\varepsilon_2 dt = \frac{1}{2}\cos\varepsilon_1.\cos\varepsilon_2 \text{ if } |\sigma_1^e| = |\sigma_2^e|$$
$$= 0 \qquad \text{otherwise .}$$

$$\frac{1}{T}\int_0^T \sin\sigma_1^e t.\sin\sigma_2^e t.\sin\varepsilon_1.\sin\varepsilon_2 dt = \frac{1}{2}\sin\varepsilon_1.\sin\varepsilon_2 \quad \text{if } \sigma_1^e = \sigma_2^e$$
$$= -\frac{1}{2}\sin\varepsilon_1.\sin\varepsilon_2 \quad \text{if } \sigma_1^e = -\sigma_2^e$$
$$= 0 \qquad \text{otherwise}$$

$$\int_0^\infty \sin\sigma_1^e t.\cos\sigma_2^e t.\sin\varepsilon_1.\cos\varepsilon_2 dt = 0 \ .$$

$$\int_0^\infty \cos\sigma_1^e t.\sin\sigma_2^e t.\cos\varepsilon_1.\sin\varepsilon_2 dt = 0 \ .$$

Thus, the mean square value of the observed process is given by

$$\eta_{M.S.} = \frac{1}{2}A_1^2 + \frac{1}{2}A_2^2 + A_1A_2.\cos(\varepsilon_1 - \varepsilon_2) \text{ if } \sigma_1^e = \sigma_2^e$$
$$= \frac{1}{2}A_1^2 + \frac{1}{2}A_2^2 + A_1A_2.\cos(\varepsilon_1 + \varepsilon_2) \text{ if } \sigma_1^e = -\sigma_2^e$$
$$= \frac{1}{2}A_1^2 + \frac{1}{2}A_2^2 \qquad \text{otherwise.}$$

From these expressions it is seen that, for example, for the case where the two encounter frequencies are the same in sign and magnitude,

$$\eta_{M.S.} > \frac{1}{2}A_1^2 + \frac{1}{2}A_2^2 \quad \text{if } \cos(\varepsilon_1 - \varepsilon_2) > 0 ,$$
$$\text{i.e., if } |\varepsilon_1 - \varepsilon_2| < \pi/2 \ ,$$

and

$$\eta_{M.S.} < \frac{1}{2}A_1^2 + \frac{1}{2}A_2^2 \quad \text{if } \cos(\varepsilon_1 - \varepsilon_2) < 0 \ .$$

In the following circumstances the observed mean square value would be significantly smaller than what would be observed at a fixed point (provided the component amplitudes are of the same order of magnitude):

$$\eta_{M.S.} = \frac{1}{2}(A_1 - A_2)^2 \quad \text{if} \quad \sigma_1^e = \sigma_2^e \quad \text{and} \quad |\varepsilon_1 - \varepsilon_2| = \pi \ .$$

Thus, for any given simulation, the mean square value encountered when travelling at the group speed can be significantly different from the mean square value at a fixed point. By inspection of the expression for the encountered mean square value it is seen that, if many simulations are performed with random phase angles, the *average* encountered mean square value of the ensemble will be equal to the value observed at a fixed point.

Random Unidirectional Wave System

Certain aspects pertaining to the two-component wave system can be used to study properties of a random sea. Unidirectionality is assumed, and also the commonly used assumption is made that the phase angles are randomly distributed, but otherwise independent of time. The wave elevation for the random sea having a certain number of components, N (where in the limit $N \to \infty$), is given by

$$\eta(t) = \sum_{i=1}^{N} A_i.\cos(k_i x - \sigma_i t + \varepsilon_i) \ ,$$

so that the wave elevation observed from a point moving at an angle with the waves, at speed U, is

$$\eta(t) = \sum_{i=1}^{N} A_i.\cos(\sigma_i^e.t + \varepsilon_i) \ ,$$

where the encounter frequency with an individual wave component is again defined as previously:

$$\sigma_i^e = k_i.U.\cos\beta - \sigma_i \ .$$

Then

$$\eta^2(t) = \sum_{i=1}^{N} A_i^2.\cos^2(\sigma_i^e t + \varepsilon_i) + 2\sum_{j=1}^{N-1} \left\{ \sum_{k>j}^{N} A_j A_k.\cos(\sigma_j^e t + \varepsilon_j).\cos(\sigma_k^e t + \varepsilon_k) \right\} \ .$$

In analogy with the two-component wave system, the mean square value of the above process associated with the first series is given by

$$\sum_{i=1}^{N} \frac{1}{2} A_i^2 \ ,$$

and the mean square value of one of the cross-product terms in the second series (where $k > j$ and the limit $T \to \infty$ is applied) is

$$\frac{1}{T}\int_0^T 2\, A_j A_k.\cos(\sigma_j^e t + \varepsilon_j).\cos(\sigma_k^e t + \varepsilon_k)dt = A_j A_k.\cos(\varepsilon_j - \varepsilon_k) \quad \text{if} \quad \sigma_j^e = \sigma_k^e$$
$$= A_j A_k.\cos(\varepsilon_j + \varepsilon_k) \quad \text{if} \quad \sigma_j^e = -\sigma_k^e$$
$$= 0 \quad \text{otherwise.}$$

It is noted that for a given encounter frequency (positive or negative) in a random following seaway, there are always three individual component waves that lead to the same absolute value of the encounter frequency, see e.g. Webster and Trudell (1981). Also in a random sea, for a given forward speed, there will be an infinite number of combinations of encounter frequencies, for which there would be a nonzero value of A_jA_k. However, the combinations of wave components that will possibly contribute to a nonzero mean square value do not occupy the whole frequency domain (ranging from zero to infinite frequency), i.e., there is

only a *finite* frequency range where the requirements for possible contributions to the mean square value can be satisfied. This is discussed next in somewhat more detail.

Let us consider the case of following seas where an observer travels with the waves, at an angle β, and at constant speed U. In Figure 2.4 a schematic representation of the sea spectrum is given, as well as the curve with the corresponding encounter frequencies σ^e. Three areas are denoted:

A -- range where the longer waves overtake the observer;
B -- range where the shorter waves overtake the observer;
C -- range where the short waves are overtaken by the observer.

Certain combinations of wave components belonging to these different regions would yield equal encounter frequencies with the different components, resulting in a (possibly) nonzero contribution to the overall mean square value of the observed wave process.

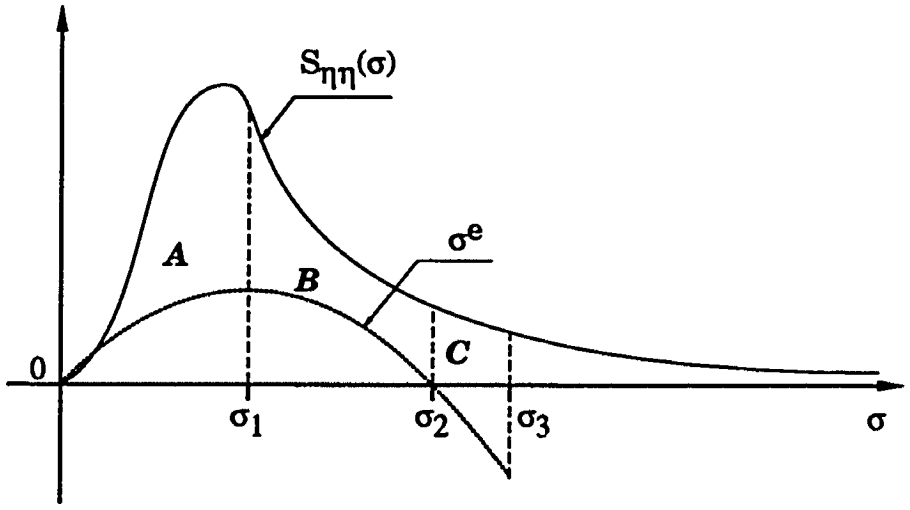

Figure 2.4. Schematic Description of the Sea Spectrum (Observed from a Fixed Point) and Encounter Frequency Curve for a Given Vessel Speed U. The frequency domain comprising A, B and C is the range for which there are equal encounter frequencies with different wave components.

In this case the curve denoting the enccunter frequencies is given by the conventional definition:

$$\sigma^e = \sigma - k.U.\cos\beta = \sigma - \frac{\sigma^2}{g}.U.\cos\beta \ ,$$

which yields the same magnitude of encounter frequency with a given wave component as the definition used previously, but of opposite sign. The wave with frequency $\sigma = \sigma_1$, separating the region ***A*** from ***B*** , is the one whose group speed, which is equal to half its phase speed ($= g/2\sigma$), corresponds to the velocity $U\cdot\cos\beta$ of the observer. This wave component also results in the maximum encounter frequency, σ^e_{max}, that can be obtained with any component in the range from $\sigma = 0$ to $\sigma = \sigma_3$. The frequency $\sigma = \sigma_2$, separating the region ***B*** from ***C*** , is the one for which the encounter frequency is zero. The frequency $\sigma = \sigma_3$ marks the upper limit of the region ***C***, beyond which equal encounter frequencies (in absolute value) with components from ***A*** and ***B*** cannot be obtained. The following summary of wave frequencies and corresponding encounter frequencies is easily shown:

σ	σ^e
$\sigma_0 = 0$	0
$\sigma_1 = g/(2U\cdot\cos\beta)$	$\sigma^e_{max} = g/(4U\cdot\cos\beta)$
$\sigma_2 = g/(U\cdot\cos\beta)$	0
$\sigma_3 = (1+\sqrt{2})\cdot g/(2U\cdot\cos\beta)$	$-g/(4U\cdot\cos\beta)$.

The subscripts j, k and m of the encounter frequencies are defined such that the corresponding wave components belong to the regions ***A***, ***B*** and ***C***, respectively. The following relationships must be satisfied for the encounter frequencies:

$$\sigma_j^e = \sigma_k^e$$
$$\sigma_j^e = -\sigma_m^e$$
$$\sigma_k^e = -\sigma_m^e \ .$$

For clarity, be it noted that the encounter frequencies $\sigma_j{}^e$ and $\sigma_k{}^e$ are due to both a long and a shorter wave component overtaking the observer, respectively. These two components can be said to form a "component wave group" travelling in the same direction as the observer (or at an angle with him), and typically will carry most of the energy. The encounter frequency with the opposite sign, $\sigma_m{}^e$, is due to the observer overtaking a short (slow) wave, which usually has associated with it a smaller amount of energy than the two previous components.

Now let us assume that there are M wave components in both regions A and B, located symmetrically about $\sigma = \sigma_1$, so that there are M pairs of components for which the encounter frequencies are equal in sign and magnitude. If all the wave frequencies are equidistant, there *cannot* be M wave components in the region C for which the encounter frequencies are equal in magnitude and opposite in sign. This is due to the σ^e curve exhibiting different behavior in C than in A or B. If one wants to create M wave components in C also that satisfy the above encounter frequency requirements, it is necessary to first choose a finite number of values for the encounter frequency, σ^e, from which subsequently the corresponding values of the wave frequencies pertaining to the regions A, B and C can be determined quite easily. This will result in unequal and smaller frequency intervals in C. If the wave frequencies are obtained in this way, there will be 3M pairs of frequencies for which the encounter frequencies are equal. In the case for which the discrete wave frequencies of A and B are not distributed symmetrically around σ_1, there will be no contribution from those components to the mean square value of the observed process.

If the wave frequencies are chosen based on the given encounter frequencies, which would result in equal encounter frequencies for the regions A, B and C , and assuming that there are N wave components in

total in the seaway, the expression for the mean square value of the encountered seaway would given by

$$\eta^{e}_{M.S.} = \frac{1}{2}\sum_{i=1}^{N} A_i^2 + \sum_{j=1}^{M} \sum_{k=2M-j+1} A_j A_k \cos(\varepsilon_j - \varepsilon_k)$$
$$+ \sum_{j=1}^{M} \sum_{m=2M+j} A_j A_m \cos(\varepsilon_j + \varepsilon_m)$$
$$+ \sum_{k=M+1}^{2M} \sum_{m=M+k} A_k A_m \cos(\varepsilon_k + \varepsilon_m) \ .$$

For the hypothetical and unrealistic case with all 3M phase angles being zero, the mean square value of the observed wave process would be significantly higher than the value obtained at a fixed point, as all the combination products A_jA_k would contribute to the overall mean square value in a positive manner. For a purely random sea, where the phase angles are randomly distributed, it is obvious that there will be additive and subtractive contributions (with equal probability of occurrence), which depend on the magnitude and sign of the individual phase angles. This means that, for many simulations, the expected value of the encountered mean square wave elevation is exactly the same as the one obtained at a fixed point. However, for any given simulation, the mean square values observed at a fixed and moving reference point can be different.

Jefferys (1987) observed a somewhat similar consequence of the model for directional sea spectra, where a finite number of frequencies and directions are used to represent the random sea surface observed at a fixed point. He showed that, if there are several (finite) directions in a wave surface realization having exactly the same frequency and random phase, standing waves will be created, so that the mean square value at one point can be very different from the value observed at a different location; the difference will depend on the phasing of the individual components and has been shown to be experimentally reproducible. He

argues that in a truly random sea this cannot occur, because there would be an infinite number of frequencies and directions.

It is of relevance to ask oneself whether there is a certain speed, at a given relative heading, for which the observed mean square value is likely to be higher than the fixed point value, and if so, how much the increase in the observed value would be. Since travelling at the group speed in a two-component seaway may result in the largest possible harmonic excitation, it is of interest to consider the case where an observer travels at the "mean group speed" of a random, following seaway (assume $\beta = 0°$ for convenience). Supposing that the random sea is narrow banded, where the peak frequency is σ_p and the spectral density is given by the Bretschneider spectrum, for example, the mean group velocity, $C_{g,p}$, is defined as half the phase velocity of the wave component with the peak frequency, i.e.,

$$C_{g,p} = \frac{g}{2.\sigma_p} \quad .$$

In a random seaway that is narrow banded, it will not be possible to remain in one group for an indefinite period. However, if a ship travels at the mean group speed with the waves, it may be subjected to a more regular excitation and larger amplitude over a significant time interval than would be experienced otherwise. As is shown in the next section, it is equally likely that the vessel will be subjected to a smaller amplitude wave process for a given time period. For illustrational purposes, let us consider an idealized narrow banded, random seaway, where the spectral density is symmetrically distributed around the component with the peak frequency, σ_p, so that the peak frequency is the same as the median or mean frequency. The spectral density becomes zero at $\sigma_p \pm \Delta\sigma$, where

$$\Delta\sigma \leq \frac{g}{2U} \quad .$$

The phases are assumed to be randomly distributed over the interval $(0,2\pi)$. Also let us suppose that there are $N = 2M$ wave components in the system, where M is large. Then there are M wave components in the interval $\Delta\sigma$, located symmetrically on either side of the peak frequency. If an observer were to travel at the mean group speed, $C_{g,p}$, there would be M pairs of encounter frequencies for which

$$\sigma_j^e = \sigma_k^e ,$$

because the group speeds are the same (and equal to $C_{g,p}$) for the individual pairs of wave components located symmetrically around the peak frequency:

$$\frac{(\sigma_p - m\delta\sigma) - (\sigma_p + m\delta\sigma)}{k_{-m\delta\sigma} - k_{+m\delta\sigma}} = \frac{(\sigma_p - n\delta\sigma) - (\sigma_p + n\delta\sigma)}{k_{-n\delta\sigma} - k_{+n\delta\sigma}} , \quad 1 \le m,n \le M , \quad m \ne n .$$

Here $\delta\sigma$ is the frequency spacing of the individual components, and the various wave numbers are defined as follows:

$$k_{-m\delta\sigma} = \frac{(\sigma_p - m.\delta\sigma)^2}{g} , \quad k_{+m\delta\sigma} = \frac{(\sigma_p + m.\delta\sigma)^2}{g} .$$

Thus for the combination of the above M cases the mean square value of the observed wave process would be equal to

$$\eta^e_{M.S.} = \eta^0_{M.S.} + \sum_{j=1}^{M} \sum_{k=2M-j+1} A_j A_k \cos(\varepsilon_j - \varepsilon_k) ,$$

where $\eta^0_{M.S.}$ is the mean square value of the process observed from a fixed point, i.e.,

$$\eta^{0}_{M.S.} = \sum_{i=1}^{N} \frac{1}{2} A_i^2 \ .$$

Now consider a different speed of the observer moving with the waves:

$$U = b.C_{p,g} \ , \quad b \neq 1,$$

which corresponds to half the phase speed of the component with frequency σ_b, say. From the above it can be seen that there are fewer pairs of wave components with frequencies located symmetrically around σ_b than around σ_p, i.e., the number of components, J, for which (for $U \neq C_{g,p}$)

$$\sigma^e_j = \sigma^e_k \ ,$$

is smaller than M. Also the J pairs of wave components with equal encounter frequencies will yield sums of products involving smaller wave amplitudes in the expression for the encountered mean square value, when compared with the case for which $U = C_{p,g}$. Therefore, the variance of the encountered mean square value will be largest when the speed of the observer is equal to the group speed of the waves with the peak frequency in the spectrum, i.e.,

$$\text{Var}\, \eta^e_{M.S.}|_{U=C_{p,g}} > \text{Var}\, \eta^e_{M.S.}|_{U\neq C_{p,g}} \ .$$

The above conclusion has been verified by simulations where a large number of wave components were used, results of which are discussed in Chapter 6. Also, this may be of practical importance to ship operators, since it may be undesirable to move with a given seaway at its mean group speed. It would be quite easy to estimate the mean group speed of the seaway, so that certain precautions, such as a change in speed or heading, could be taken if necessary.

A few more general remarks are made concerning the general statistical properties. Since the phase angles are uniformly distributed over $(-\pi,\pi)$ and operated on by a cosine function, the distribution must be symmetric with mean zero, and the following should hold also:

$$P(\eta^{e}_{M.S.} < \eta^{0}_{M.S.}) = P(\eta^{e}_{M.S.} > \eta^{0}_{M.S.}) \ .$$

The probability

$$P(\eta^{e}_{M.S.} > \eta^{0}_{M.S.})$$

will depend on the joint distribution of the wave amplitudes and phase angles. If the amplitudes of all wave components were the same, this probability would be significantly smaller than for the case with a strongly peaked spectrum. In the next section probability theory is applied to study the statistical behavior of the mean square value pertaining to the encountered wave process for a two-component wave system.

Some of the above observations have been observed experimentally by Takaishi (1982). Random wave elevations in a model basin were measured at a fixed point as well as from a reference point moving with the waves, where the velocity was equal to the mean group speed, $C_{p,g}$. The observed waves at the moving point were found to be of larger than average height and of regular appearance over a prolonged period of time. It should be mentioned, however, that there is an equal likelihood of encountering a smaller than average wave height in random following seas.

2.4.4. Statistical Aspects of the Encountered Mean Square Value in Following Seas

In the previous section it has been shown that the mean square value of the wave process, encountered by an observer moving at an angle with the

waves, can be different from the value that would be obtained at any stationary point. It is of interest to study the probability characteristics associated with the encountered mean square value, $\eta^e_{M.S.}$. The additive or subtractive components contributing to the total mean square value consist typically of the product of wave component amplitudes multiplied with the cosine of their phase differences (or sums), viz.

$$A_jA_k\cos(\varepsilon_j-\varepsilon_k) \text{ or } A_jA_k\cos(\varepsilon_j+\varepsilon_k) .$$

Basic probability theory can be used to determine the cumulative distribution function and probability density function of these components. As was discussed in the previous section, the distribution of the amplitudes of the wave components can be considered either deterministically, or it can be assumed that they have the Rayleigh distribution. An investigation is made in the following as to the statistical properties of the cosine terms.

Distribution Properties of $\cos(\varepsilon_j-\varepsilon_k)$ and $\cos(\varepsilon_j+\varepsilon_k)$

In the random wave model the phases of the wave components are assumed to be independently uniformly distributed over the interval $[-\pi,\pi]$. The domain of both the phase differences and sums encompasses the interval $[-2\pi,2\pi]$, so that if the random variable Y is defined as

$$Y = \varepsilon_j - \varepsilon_k \text{ or } Y = \varepsilon_j + \varepsilon_k ,$$

its domain will be $[-2\pi,2\pi]$. The distribution properties of the phase differences and sums are the same, since their domains and marginal distribution functions are the same. Let $F_Y(Y)$ denote the cumulative distribution function (c.d.f.) of Y:

$$F_Y(y) = P(Y \le y) ,$$

and let $f_Y(y)$ denote the probability density function (p.d.f.) of Y, where

$$f_Y(y) = \frac{d}{dy} F_Y(y) \ .$$

It is easy to show that the p.d.f. of Y has the following properties:

$$f_Y(y) = \frac{2\pi - y}{4\pi^2} \qquad \text{if } 0 \le y \le 2\pi$$

$$= \frac{2\pi + y}{4\pi^2} \qquad \text{if } -2\pi \le y \le 0$$

$$= 0 \qquad \text{elsewhere.}$$

The behavior of $f_Y(y)$ is shown graphically in Figure 2.5. The c.d.f. of Y is obtained by integration:

$$F_Y(y) = \int_{-2\pi}^{y} f_Y(y)\, dy \ ,$$

which results in the following:

$$F_Y(y) = \frac{1}{8\pi^2} y^2 + \frac{1}{2\pi} y + \frac{1}{2} \qquad \text{if } -2\pi \le y \le 0$$

$$= \frac{-1}{8\pi^2} y^2 + \frac{1}{2\pi} y + \frac{1}{2} \qquad \text{if } 0 \le y \le 2\pi \ .$$

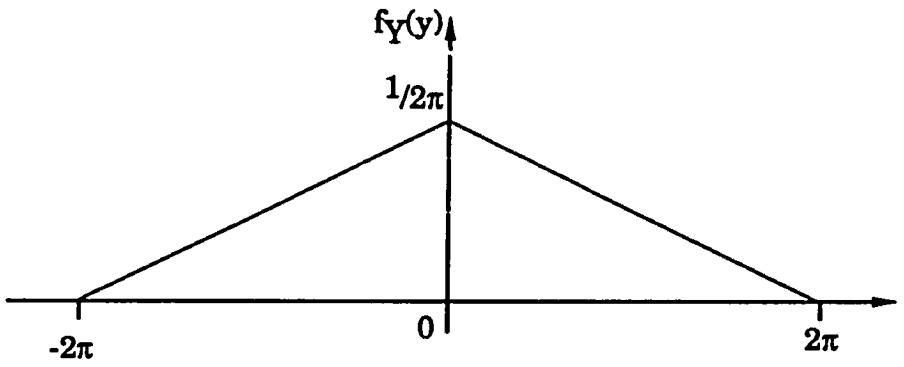

Figure 2.5. Probability Density Function of Random Variable Y

The random variable Z is defined as

$$Z = \cos(Y) \ ,$$

and the relationship between Y and Z is represented graphically in Figure 2.6. In order to find the distribution properties of Z, use can be made of Figure 2.5. It is clear that the properties are the same for positive and negative values of Y, i.e.,

$$\begin{aligned} F_Z(z) &= P(Z \le z) \qquad \text{for } -2\pi \le Y \le 2\pi \\ &= 2.P(Z \le z) \quad \text{for } 0 \le Y \le 2\pi \ , \end{aligned}$$

so that only one side, $Y \ge 0$ say, needs to be considered. From Figure 2.6 one can also see that $-1 \le Z \le 1$, and that for $Y \ge 0$ the behavior of Z is symmetrical about $Y = \pi$. Consequently, the probability $P(-1 \le Z \le z)$ can be conveniently expressed in terms of Y as follows. Let us define the quantity dy as being associated with the value z, and restrict dy to the range

$$0 \le dy \le \pi \ .$$

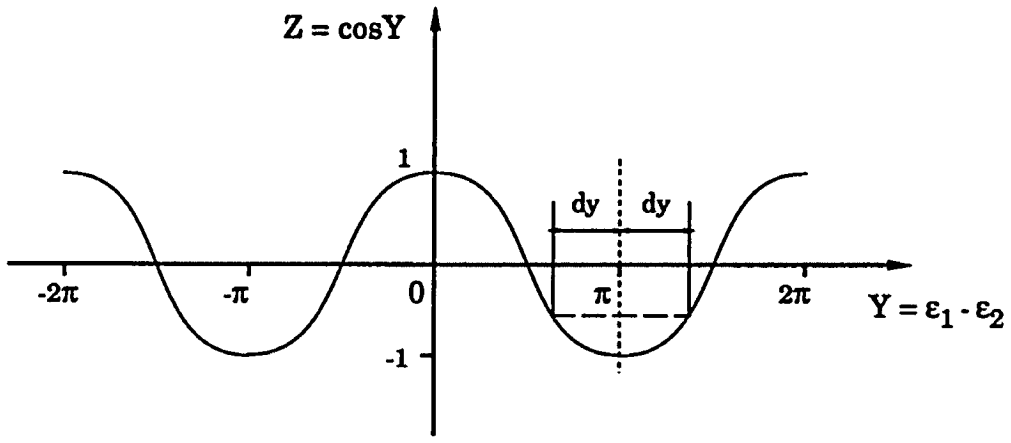

Figure 2.6. Characteristics of the Random Variables Y and Z

Then $Z = \cos Y = z$ has associated with it two values of Y: (1) $Y = \pi - dy$, and (2) $Y = \pi + dy$, i.e.,

$$\pi - dy = \cos^{-1} z \quad \text{and} \quad \pi + dy = \cos^{-1} z \ .$$

The probability $P(-1 \le Z \le z)$ is equivalent to

$$P(-1 \le Z \le z) = 2.P(\pi - dy \le Y \le \pi + dy), \quad 0 \le Y \le 2\pi \ .$$

To avoid the duality problem, the function *arccos* can be used, which is defined only over the interval $[0,\pi]$:

$$\arccos z: [-1,1] \rightarrow [0,\pi] \ .$$

Then dy can be expressed as

$$dy = \pi - \arccos z \ ,$$

and

$$\begin{aligned} P(-1 \le Z \le z) &= 2.P\{\pi - (\pi - \arccos z) \le Y \le \pi + \pi - \arccos z\} \\ &= 2.P(\arccos z \le Y \le 2\pi - \arccos z) \\ &= P(Z \le z) = F_Z(z) \ . \end{aligned}$$

The above can be evaluated by making use of the distribution of Y:

$$P(\arccos z \le Y \le 2\pi - \arccos z) = P(Y \le 2\pi - \arccos z) - P(Y \le \arccos z) \ ,$$

and

$$P(Y \le \arccos z) = \frac{1}{2} + \frac{1}{2\pi}\arccos z - \frac{1}{8\pi^2}\arccos^2 z \ ,$$

and similarly,

$$\begin{aligned} P(Y \le 2\pi - \arccos z) &= \frac{1}{2} + \frac{1}{2\pi}(2\pi - \arccos z) - \frac{1}{8\pi^2}(2\pi - \arccos z)^2 \\ &= 1 - \frac{1}{8\pi^2}\arccos^2 z \ . \end{aligned}$$

Hence

$$P(\arccos z \le Y \le 2\pi - \arccos z) = \frac{1}{2} - \frac{1}{2\pi}\arccos z \ ,$$

and the cumulative distribution function of Z is then given by

$$F_Z(z) = P(Z \le z) = 1 - \frac{1}{\pi}\arccos z \ .$$

The probability density function of Z can now also be derived:

$$f_Z(z) = \frac{d}{dz}\left(1 - \frac{1}{\pi}\arccos z\right) = \frac{1}{\pi\sqrt{1 - z^2}} \ .$$

Expectation and Variance of the Random Variable Z

The expectation can be calculated as follows:

$$E(Z) = \int_{-1}^{1} z\, f_Z(z)\, dz = \frac{-1}{\pi}\left[\sqrt{1 - z^2}\right]_{-1}^{1} = 0 \ .$$

The variance is given by

$$\text{Var } Z = E(Z^2) - \{E(Z)\}^2 = E(Z^2) = \int_{-1}^{1} z^2 f_Z(z)\, dz$$

$$= \frac{1}{\pi}\int_{-1}^{1} \frac{z^2}{\sqrt{1 - z^2}}\, dz = \frac{1}{\pi}\left[-\frac{z}{2}\sqrt{1 - z^2} + \frac{1}{2}\sin^{-1} z\right]_{-1}^{1} = \frac{1}{2} \ .$$

Thus, the expected value of Z is zero, and its variance is 1/2. This implies that, for the two-component wave system with random phase angles, the expected value of the encountered mean square wave elevation is given by

$$E(\eta^e_{M.S.}) = \eta^0_{M.S.} = \frac{1}{2}A_1^2 + \frac{1}{2}A_2^2 \ ,$$

and the variance of the encountered mean square value is equal to

$$\text{Var } \eta^e_{M.S.} = \frac{1}{2}A_1 \cdot A_2 \ .$$

The above expressions for the expected value and variance are valid for the case where the encounter frequencies with both wave components have the same absolute value, and where their phase angles are uniformly distributed.

It is not obvious that in the case of J pairs of wave components, for which the encounter frequencies are equal, the variance decreases linearly with increasing J, because the products $A_iA_j\cos(\varepsilon_i-\varepsilon j)$ are *not* independently and identically distributed, as would be required when applying the Central Limit Theorem. The terms are not identically distributed, because the wave energy in a random sea tends to be concentrated around a peak frequency. If the wave process were pure white noise, where the spectral density is constant, i.e.,

$$S_{\eta\eta}(\sigma_i) = S_{\eta\eta}(\sigma_j) \ , \ i \neq j \ ,$$

then the Central Limit Theorem would apply, and the variance of the mean square value would decrease proportionally with increasing J. Also, the variance would then vanish for $J \rightarrow \infty$.

In the case of a typical wave spectrum, where the energy is distributed unequally among the components, no proof is given here as to whether the Central Limit Theorem does or does not apply. In Chapter 6 it is shown by simulation that the variance of the mean square wave elevation, observed in random following seas, does in fact decrease as the number of wave components increase.

Implications

The foregoing treatise on observed wave statistics has several implications with respect to statistical analysis in the time and frequency domain. When studying wave excitation processes in (random) following or quartering sea conditions, by means of time domain simulations or model basin experiments, the mean square value of the observed wave elevations may be different from the value observed at a stationary point. The difference will depend to a large extent on the phasing and amplitudes of

the wave components, no matter how long simulations are carried out for. In particular, if the observer travels at the mean group speed, the differences in observed RMS wave elevation can be quite large when compared with the value obtained at a fixed location. The observer may then see a series of large amplitude waves for a prolonged period of time, but it is equally likely that he or she will see smaller than average waves during the same time period.

For frequency domain analysis the consequence is somewhat embarrassing: the encountered spectrum for following or quartering sea conditions becomes dependent on the phasing of the individual components for a given realization. What is implied here is that the usual transformation from fixed to moving coordinates in the spectral sense is not valid for following sea conditions, i.e.,

$$S_{\eta\eta}(\sigma)\,d\sigma \neq S^{e}_{\eta\eta}(\sigma^{e})\,d\sigma^{e} \quad \text{if} \quad |\beta| \leq \pi/2 \ .$$

This is probably more of academic interest, since it is unlikely that any serious errors result in practice from the usual, be it erroneous, transformation procedure.

2.4.5. Apparent Wave Energy in a Following Seaway

One major conclusion resulting from the foregoing is that the mean square value of the wave process, observed from a point moving at an angle *with* the waves, at any finite speed, will most likely be different from the value obtained at any stationary point in the same seaway. As a result of the conventional model of superposed wave components with random phase, the difference will depend on the phasing of the individual wave components with respect to the travelling observer, on the number of components used in a realization, and on the shape of the energy spectrum. Traditionally, the mean square value of a wave process is linked directly to the mean energy in the wave system. In the following section an attempt is made to determine the mean wave energy, as would

be encountered by an observer moving with the waves; according to the common notion of mean square wave elevation, there should also here be a proportional constant separating the mean square value from the mean wave energy. For convenience, it is assumed that the wave system moves along the x-axis, and that for the case of a moving observer the relative heading angle is zero. The results can be easily extended to the case for quartering seas, and the same conclusions would apply as for the $\beta = 0°$ case.

The energy in a wave system is characterized by the sum of the potential and kinetic energy, see e.g. Newman (1977) or Wiegel (1964). In a given volume $\mathcal{V}$ the total energy is given by the sum of the kinetic and potential energy:

$$E^* = E_{kin} + E_{pot} = \rho \iiint_{\mathcal{V}} \{\frac{1}{2} V^2 + gy\}\, dV \ .$$

By considering the potential energy about the mean still water level, the total energy density in a column extending vertically throughout the fluid domain, is

$$E = \rho \int_{-\infty}^{\eta} \frac{1}{2} V^2 dy + \int_{0}^{\eta} gy\, dy \ ,$$

where η is the instantaneous wave elevation with amplitude A, and V is the vectorial sum of the horizontal and vertical wave particle velocities:

$$V^2 = \left[\frac{\partial \Phi_I}{\partial x}\right]^2 + \left[\frac{\partial \Phi_I}{\partial y}\right]^2 \ .$$

Energy Observed at a Fixed Reference Point

For a single component wave system the time-dependent energy density, observed at a stationary point, can be shown to be

$$E(t) = \frac{1}{4}\rho g A^2 \cdot e^{2k\eta} + \frac{1}{2}\rho g \eta^2 \ ,$$

which for waves having a small slope, where kA << 1, can be expressed approximately as

$$E(t) = \frac{1}{4}\rho g A^2 + \frac{1}{2}\rho g \eta^2 \ .$$

The total mean energy density is obtained by averaging over one wave cycle:

$$\bar{E} = \frac{1}{T}\int_0^T E(t)\,dt = \frac{1}{2}\rho g A^2 ,$$

so that the contribution from the potential and kinetic energies is the same, and the mean energy density is linearly proportional to the mean square value:

$$\bar{E} = \rho g \cdot \eta^0_{M.S.} \ .$$

It is noted that the same result for the mean energy density is obtained by taking the limit $T \to \infty$:

$$\bar{E} = \lim_{T\to\infty} \frac{1}{T}\int_0^T E(t)\,dt = \frac{1}{2}\rho g A^2 \ .$$

For a two-component wave system the velocity potential is assumed to be given by the superposition of the individual potentials:

$$\Phi_I(x,y;t) = \sum_{i=1}^{2} \frac{A_i g}{\sigma_i} \cdot e^{k_i y} \cdot \sin(k_i x - \sigma_i t + \varepsilon_i) \ .$$

Using the above definitions of energy density, it is easy to show that the mean energy density in the composite wave system is given by

$$\bar{E} = \frac{1}{2}\rho g\{A_1^2 + A_2^2\} \ ,$$

so that also in this case

$$\bar{E} = \rho g \cdot \eta^0_{M.S.} \ .$$

Energy Encountered by a Moving Reference Point

An attempt is made to determine the energy density of a two-component wave system, as would be observed from a reference point that moves steadily along the x-axis at speed U. Oxy is the earth-fixed coordinate system, and the system $O^e x^e y^e$ translates steadily along the x-axis. The aim is to determine the energy present in the wave system, at any time instant and for any location through which the observer passes, and subsequently to take the time average to obtain the mean encountered energy. Therefore, the expressions for the kinetic energy in the waves do not depend on the relative velocity between the observer and the fluid, whereas the frequency at which the encountered energy varies is linked to the encounter frequencies associated with the individual wave components. That is, the magnitude of the water particle velocities is expressed in terms of the earth-fixed system Oxy for any given location in the fluid, while the frequency of the velocities depends on the encounter frequencies.

The velocity potential of the waves, as encountered by the observer, is expressed in the moving reference system through the following relationships:

$$x = U.t + x^e$$
$$y = y^e ,$$

so that

$$\Phi_I(x^e,y^e;t) = \sum_{i=1}^{2} \frac{A_i g}{\sigma_i} \cdot e^{k_i y} \cdot \sin\{k_i(U \cdot t + x^e) - \sigma_i t + \varepsilon_i\} .$$

In the above expression the contribution of the steady forward speed to the potential, $-U \cdot x^e$, has been omitted, since it does not contribute to the energy in the wave system, as has been discussed above. Defining the encounter frequencies with the individual wave components as

$$\sigma_i^e = k_i U - \sigma_i ,$$

the horizontal and vertical water particle velocities, expressed in the earth-fixed system Oxy and encountered by the moving observer (located at $x^e = 0$), are given by

$$u = \sum_{i=1}^{2} A_i \sigma_i e^{k_i y} .\cos(\sigma_i^e t + \varepsilon_i)$$
$$v = \sum_{i=1}^{2} A_i \sigma_i e^{k_i y} .\sin(\sigma_i^e t + \varepsilon_i) .$$

The encountered potential energy density is given by

$$E_{pot} = \int_0^{\eta} y\,dy = \frac{1}{2}\rho g\eta^2 =$$
$$= \frac{1}{2}\rho g\cdot\{A_1^2\cos^2(\sigma_1^e t+\varepsilon_1) + A_2^2\cos^2(\sigma_2^e t+\varepsilon_2) + 2A_1A_2\cos(\sigma_1^e t+\varepsilon_1)\cos(\sigma_2^e t+\varepsilon_2)\}\ ,$$

so that the mean potential energy can be determined in a manner analogous to the one used for computing the mean square value of the observed wave process:

$$\bar{E}_{pot} = \frac{1}{2}\rho g.\{\frac{1}{2}A_1^2 + \frac{1}{2}A_2^2\} \qquad \text{if } |\sigma_1^2| \neq |\sigma_2^e|$$
$$= \frac{1}{2}\rho g.\{\frac{1}{2}A_1^2 + \frac{1}{2}A_2^2 + A_1A_2\cos(\varepsilon_1 - \varepsilon_2)\} \text{ if } \sigma_1^e = \sigma_2^e$$
$$= \frac{1}{2}\rho g.\{\frac{1}{2}A_1^2 + \frac{1}{2}A_2^2 + A_1A_2\cos(\varepsilon_1 + \varepsilon_2)\} \text{ if } \sigma_1^e = -\sigma_2^e\ .$$

The encountered kinetic energy density is given by

$$E_{kin} = \frac{1}{2}\rho\int_{-\infty}^{\eta} V^2\,dy\ ,$$

where

$$V^2 = u^2 + v^2\ .$$

Defining

$$\alpha_1 = \sigma_1^e t + \varepsilon_1\ ,\quad \alpha_2 = \sigma_2^e t + \varepsilon_2\ ,$$

the following expression is obtained for the V^2 term:

$$V^2 = \sum_{i=1}^{2} A_i^2 \sigma_i^2 e^{k_i y} .\{\cos^2\alpha_i + \sin^2\alpha_i\}$$
$$+ 2A_1A_2\sigma_1\sigma_2 . e^{(k_1+k_2)y} .\{\cos\alpha_1\cos\alpha_2 + \sin\alpha_1\sin\alpha_2\} .$$

The last term in brackets yields the following results as a function of the encounter frequencies:

$$\begin{aligned} \cos\alpha_1\cos\alpha_2 + \sin\alpha_1\sin\alpha_2 &= \cos(\alpha_1 - \alpha_2) \\ &= \cos(\varepsilon_1 - \varepsilon_2) \qquad \text{if } \sigma_1^e = \sigma_2^e \\ &= \cos(2\sigma_1^e + \varepsilon_1 - \varepsilon_2) \qquad \text{if } \sigma_1^e = -\sigma_2^e \ . \end{aligned}$$

The mean kinetic energy density is expressed by the integral

$$\bar{E}_{kin} = \lim_{T\to\infty} \frac{1}{T}\int_0^T E_{kin}\, dt \ ,$$

which involves $\cos^2$ and $\sin^2$ terms. Time averaging of the kinetic energy density will obviously result in a zero additional contribution for the case where the encounter frequencies are equal in magnitude and opposite in sign.

As was done previously, it is assumed that the wave slope is small:

$$k_1A << 1 \text{ and } k_2A << 1 \ ,$$

so that (to the order of the amplitude squared) only the first term of the expansion of the exponentials needs to be considered, which is equal to unity. Then by defining the quantity

$$\dot{E}_0 = \frac{1}{2}\rho g.\{\frac{1}{2}A_1^2 + A_2^2\} \ ,$$

the encountered mean kinetic energy density is found to be the following:

$$\dot{E}_{kin} = \dot{E}_0 \qquad \text{if } \sigma_1^e \neq \sigma_2^e$$

$$= \dot{E}_0 + \rho g A_1 A_2 \frac{\sigma_1.\sigma_2}{(\sigma_1)^2 + (\sigma_2)^2} \cdot \cos(\varepsilon_1 - \varepsilon_2) \qquad \text{if } \sigma_1^e = \sigma_2^e$$

Hence, the total encountered mean energy density in the wave system is given by

$$\dot{E} = \rho g.\{\frac{1}{2}A_1^2 + \frac{1}{2}A_2^2\} \qquad \text{if } |\sigma_1^e| \neq |\sigma_2^e|$$

$$= \rho g.\{\frac{1}{2}A_1^2 + \frac{1}{2}A_2^2 + \frac{1}{2}A_1A_2\cos(\varepsilon_1 + \varepsilon_2)\} \qquad \text{if } \sigma_1^e = -\sigma_2^e$$

$$= \rho g.\{\frac{1}{2}A_1^2 + \frac{1}{2}A_2^2 + A_1A_2.(\frac{1}{2} + \frac{\sigma_1\sigma_2}{\sigma_1^2 + \sigma_2^2}).\cos(\varepsilon_1 - \varepsilon_2)\} \qquad \text{if } \sigma_1^e = \sigma_2^e \ .$$

In comparison, the encountered mean square wave elevation in the two-component wave system was found to be equal to

$$\eta^e_{M.S.} = \frac{1}{2}A_1^2 + \frac{1}{2}A_2^2 \qquad \text{if } |\sigma_1^e| \neq |\sigma_2^e|$$

$$= \frac{1}{2}A_1^2 + \frac{1}{2}A_2^2 + A_1A_2\cos(\varepsilon_1 + \varepsilon_2) \qquad \text{if } \sigma_1^e = -\sigma_2^e$$

$$= \frac{1}{2}A_1^2 + \frac{1}{2}A_2^2 + A_1A_2\cos(\varepsilon_1 - \varepsilon_2) \qquad \text{if } \sigma_1^e = \sigma_2^e.$$

<u>Summary</u>

The observations from this chapter and the previous one suggest the following, when an observer moves at an angle *with* a two-component wave system and the magnitude of the encounter frequencies is the same:

(1) the mean square value of the encountered wave elevation process can be different from the value observed at a stationary point; (2) the encountered mean energy density can be different from the mean energy density observed at a stationary point; (3) the mean square value of the encountered waves may not be directly proportional to the encountered wave energy. Also, when an observer moves at an angle *into* the wave system, the mean square wave elevation and mean energy density are the same as would be observed at a stationary point.

It is emphasized that the observations concerning encountered wave energy are treated as an aside to this work, since they are not considered to have an influence on the theory and numerical modelling of ship motions presented here. Nevertheless, the findings in this chapter seem to indicate that, in random following seas with a finite number of wave components, the observed wave system has certain energy characteristics that have not been addressed previously. These findings should be regarded merely as a first step in gaining some understanding of the observed wave properties associated with random following sea conditions, and might be worthy of further investigation.

CHAPTER 3

Aspects of the Time Domain Simulation Algorithm

In this chapter an overview is given of the implementation of the theory in the numerical model. Aspects pertaining to the algorithm comprise the equations of motion and the computation of the memory effect integrals. The computer program that reflects the present theory has been called *KAPSIZE*, the general functioning of which is shown by flowcharts in Appendix D.

3.1 Integration of the Equations of Motion

The motion behavior of the vessel is governed by the equations of motion, as described in Chapter 2. The position of the vessel's center of gravity is determined by the conservation of momentum equation and by kinematics. The conservation of linear momentum can be used to determine the linear accelerations, and the angular accelerations are obtained by the conservation of angular momentum, both of which are described below.

3.1.A. Conservation of linear momentum

The aim is to find the translational position vector, $\mathbf{x}$, of the center of gravity of the vessel at each time step. The position of the center of gravity is to be obtained in the earth-fixed reference system Oxyz, which can be achieved by integrating the velocity vector $\mathbf{v}$. The linear accelerations, i.e., the time derivatives of the velocities, are given in vector notation by the conservation of linear momentum:

$$\mathbf{a} = \frac{d}{dt}\mathbf{v} = \frac{1}{m}\mathbf{k} \ ,$$

where $\mathbf{v}$ is related to $\mathbf{x}$ by

$$\frac{d}{dt}\mathbf{x} = \mathbf{v} .$$

The vectors **v**, **x** and **k** are expressed in the system Oxyz, but for ease of computation the force vector **k** is based on the forces expressed in the ship-fixed coordinate system O*x*y*z*. The local force components are transformed into the inertial system Oxyz as follows:

$$\mathbf{k} = \mathbf{T}\,\mathbf{f}^{*}_{total} = \mathbf{T}\,\{\sum_{i=1}^{J}\mathbf{f}^{*}_{i}\} ,$$

where **T** is the transformation matrix discussed in Appendix A, $\mathbf{f}^{*}_{total}$ is the vector containing the total forces acting on the vessel for surge, heave and sway (in the O*x*y*z* system), $\mathbf{f}^{*}_{i}$ is the i^{th} force component, such as the diffraction force (but itself a vector), and J is the total number of force components. Each force component is a vector consisting of three forces acting in the x*, y* and z* direction, all of which are associated with the same physical phenomenon. Denoting the acceleration vector of the center of gravity by $\ddot{\mathbf{x}}$, the conservation of linear momentum equation can be written as

$$m\,\ddot{\mathbf{x}} = \mathbf{k} = \mathbf{T}\,\mathbf{f}^{*}_{total} .$$

It is convenient to separate those added mass terms that depend on linear acceleration, from the total forces on the right hand side of the above equation, so as to add the added mass to the structural mass terms. The added mass forces consist of inertia terms and cross-coupling terms, so that the total force vector can be written in terms of an added mass inertia component (given in the ship-fixed coordinate system, and with the correct sign convention) and a remainder term, $\mathbf{f}^{**}_{tot}$:

$$\mathbf{f}^{*}_{total} = \mathbf{f}^{**}_{tot} - \mathbf{T}^{-1}\,\mathbf{A}\,\mathbf{a}^{e*} ,$$

where the 6x1 vector $\mathbf{a}^{e*}$ contains the linear and rotational accelerations, and cross-product terms, as has been discussed in Chapter 2.1.2 Thus in the above notation $\mathbf{f}^{**}_{tot}$ is the total force vector given by the summation of all force components, except for the added mass terms. When considering the added mass forces, cross coupling has to be taken into account, such as e.g. pitch-induced heave or roll-induced sway forces, so that the upper half of the 6x6 added mass matrix A, say $\mathbf{A}^1$ (which would be a 3x6 matrix, and contains both added mass and hydrodynamic coupling coefficients), is of relevance here. Then the vector with the total force components is given by

$$\mathbf{f}^{*}_{total} = \mathbf{f}^{**}_{tot} - \mathbf{T}^{-1}\,\mathbf{A}^{1}\,\mathbf{a}^{e*} \ .$$

This force vector is expressed in terms of the equilibrium system by applying the transformation matrix T:

$$\mathbf{f}^{e} = \mathbf{T}\,\mathbf{f}^{*}_{total} = \mathbf{T}\,\mathbf{f}^{**}_{tot} - \mathbf{A}^{1}\mathbf{a}^{e*} \ .$$

All acceleration terms, including the rotational components, must be addressed due to cross coupling. Let hereafter the vector $\ddot{x}$ refer to the generalized (6x1) acceleration vector, of which the first three are the absolute linear accelerations, and the last three components are the rotational accelerations in the system O*x*y*z*; let $\ddot{x}_{(1,2,3)}$ represent the vector with the linear accelerations given in Oxyz (referred to as a in Chapter 2.1.2). The added mass force vector consists of components depending on linear and rotational accelerations, and on cross-product (Coriolis) terms. Using the relationships established in Chapter 2.1.2, the acceleration vector $\mathbf{a}^{e*}$ can be split up into a vector $\mathbf{a}^{e**}$, which contains only the linear and rotational accelerations, and into a vector with the cross-product terms. Then the conservation of linear momentum can be written as

$$m\ddot{x}_{(1,2,3)} + A^1 a^{c**} = T f_{tot}^{**} + A^1 T^{-1}(\omega^c \times v^c) ,$$

where

$$A^1 = \begin{bmatrix} A_{11} & A_{12} & \cdots & A_{16} \\ A_{21} & A_{22} & \cdots & A_{26} \\ A_{31} & A_{32} & \cdots & A_{36} \end{bmatrix} ,$$

and

$$a^{c**} = \begin{bmatrix} T^{-1}\ddot{x}_{(1,2,3)} \\ T\dot{\omega} \end{bmatrix} .$$

It is noted that the added mass coefficients associated with A^1, involve the infinite-frequency added mass coefficients (see Chapter 2.1.2). The two inertia terms on the left hand side of the equations of motion can be combined by adding zeroes to the structural mass terms, so that only one acceleration vector can be used. Defining the following mass matrix as

$$m^1 = \begin{bmatrix} m & 0 & 0 & 0 & 0 & 0 \\ 0 & m & 0 & 0 & 0 & 0 \\ 0 & 0 & m & 0 & 0 & 0 \end{bmatrix} ,$$

the structural mass terms can be combined with the added mass terms in the equations of conservation of linear momentum:

$$\{m^1 + A^{1*}\}\ddot{x} = T f_{tot}^{**} + A^1 T^{-1}(\omega^c \times v^c) ,$$

where

$$\ddot{\mathbf{x}} = \begin{bmatrix} \ddot{x} \\ \ddot{y} \\ \ddot{z} \\ \dot{\omega}_1 \\ \dot{\omega}_2 \\ \dot{\omega}_3 \end{bmatrix} ,$$

and where the 3x6 matrix $\mathbf{A}^{1*}$ represents $\mathbf{A}^1$, of which the left 3x3 half has been operated on by $\mathbf{T}^{-1}$, and the right half by $\mathbf{T}$.

The linear accelerations can be obtained at each time step by solving the above set of simultaneous equations, from which the velocity vector for the next time step can be estimated using Euler's method. Euler's integration method has been described in Appendix C. The corresponding linear displacements are obtained from the estimated velocity at the next time step as follows. If a time stepping interval of Δt is used, and if

x_i = displacement at time step i,
v_i = velocity at time step i,
v_{i+1} = velocity at next time step (i+1),

then the displacement at time step i+1 is estimated by

$$x_{i+1} = x_i + \Delta t \cdot (v_i + v_{i+1}) / 2 \quad .$$

The above procedure is used to estimate the displacements in the x, y and z directions.

3.1.B. Conservation of Angular Momentum

The conservation of angular momentum equations are expressed in the moving coordinate system O*x*y*z*, enabling one to deal with moments and products of inertia that are time independent:

$$\mathbf{I}\frac{d}{dt}\omega = \mathbf{q} - \omega \times \mathbf{I}\omega \ ,$$

where **q** is the vector containing the total moments acting on the vessel (expressed in the local coordinate system O*x*y*z*), given by the sum of the J moment components as in 3.1.A:

$$\mathbf{q} = \sum_{i=1}^{J} \mathbf{q}_i \ ,$$

I is the moment of inertia matrix, and ω is the vector containing the rotational velocities about the x*, y* and z* axes. The angles of rotation, or the Euler angles, which are represented by the vector χ, can be determined by integration from the vector ω by means of the transformation matrix **B** (see Appendix A):

$$\frac{d}{dt}\chi = \mathbf{B}^{-1}\omega \ .$$

As in section 3.1.A, the added mass moments of inertia can be combined with the structural moments of inertia, where in this case the lower half of the 6x6 added mass matrix is used, represented by $\mathbf{A}^2$. The matrix with the moments of inertia is given in an analogous fashion:

$$\mathbf{m}^2 = \begin{bmatrix} 0 & 0 & 0 & I_{xx} & -I_{xy} & -I_{xz} \\ 0 & 0 & 0 & -I_{xy} & I_{yy} & -I_{yz} \\ 0 & 0 & 0 & -I_{xz} & -I_{yz} & I_{zz} \end{bmatrix} .$$

Then the matrices $\mathbf{m}^2$ and $\mathbf{A}^2$ can be combined appropriately so as to have one inertia term on the left hand side of the equations of motion.

3.1.C. Generalized Equations of Motion

The equations expressing the conservation of linear and angular momentum can be combined to form a set of six coupled integro-differential equations. Summarizing, in vector notation the generalized equations of motion can be written as

$$\hat{\mathbf{M}}\,\ddot{\hat{\mathbf{x}}} = \hat{\mathbf{f}} ,$$

where the mass matrix contains structural and added mass terms, as well as moments of inertia, operated on by the transformation matrix T, so that the mass matrix is time dependent. The generalized force vector contains the total forces (including cross-product terms from the added mass forces) and moments, and the acceleration vector consists of the linear and angular accelerations; the linear accelerations are given in the earth-fixed system Oxyz, and the angular accelerations are given in the structure-fixed system O*x*y*z*. The linear displacements are described by

$$\frac{d}{dt}\mathbf{x} = \mathbf{v} ,$$

and the angular displacements by

$$\frac{d}{dt}\chi = B^{-1}\omega \ .$$

The set of equations of motion can be solved by a standard equation solver for simultaneous linear equations. The integration of the accelerations must be performed by a numerical time stepping procedure. As was mentioned above, for this purpose Euler's integration method is applied, which is a simple but reliable procedure (see Appendix C), provided a small enough step size is used. Also, this procedure should not be unstable, because the excitation can be considered harmonic. At each time step the right hand side of the equations of motion, i.e., the total force vector, is evaluated once for given position and velocity of the vessel, so that the accelerations can be determined for that time step. Then the linear velocities in the fixed coordinate system Oxyz can be estimated for the next time step, as well as the rotational velocities about the local axes. With this information the corresponding position of the center of gravity, and the angles of rotation of the structure, are determined for the next time step. A typical time interval employed in the numerical simulations was $\Delta t = 0.1$ s for beam sea conditions, and $\Delta t = 0.2$ s for following seas.

3.2 Evaluation of the Memory Effect Integrals

The linear wave radiation forces are expressed in terms of memory effect integrals, as has been discussed in Chapter 2.1.2. The kernel functions $L_{ij}(\tau)$ depend on the time lag τ and, in this case, on the three-dimensional damping coefficients $B_{ij}(\sigma)$:

$$L_{ij}(\tau) = \frac{2}{\pi} \int_0^\infty B_{ij}(\sigma) \cos\sigma\tau \, d\sigma \,, \quad i,j = 1,...,6 \,.$$

In the following a brief discussion is given as regards the computation of the three-dimensional damping coefficients, the kernel functions, and the numerical evaluation of the memory effect integrals.

3.2.A. Three-dimensional Coefficients

Since the theory presented here is applied to a vessel of thin shape, the three-dimensional damping and added mass coefficients can be estimated using the strip method by Salvesen, Tuck and Faltinsen (1970). With this method the two-dimensional coefficients are integrated along the length of the vessel, and some speed dependent terms are included in the expressions. The two-dimensional coefficients for each section are easily computed by means of the Frank Close Fit method, the details of which are given by Frank (1967) and by Bedel and Lee (1971).

Frank's method is used to compute the hydrodynamic coefficients for the vessel at its position of equilibrium in calm water. The coefficients are evaluated for a range of discrete frequencies: from $\sigma = \hat{0}$ to $\sigma = \sigma_F$, and also the coefficients at the infinite frequency are determined. A sufficiently small frequency interval, $\Delta\sigma$, must be chosen, so as to model the characteristics of the damping due to wave radiation accurately. The limiting frequency σ_F is the frequency beyond which it becomes numerically impractical to calculate the hydrodynamic coefficients.

The asymptotic behavior of the hydrodynamic coefficients presents a problem in the determination of the kernel functions. Damping approaches zero as the frequency goes towards infinity, but the exact decay behavior is not known. Although theoretically not appealing, it is necessary to assume some kind of decay curve, which is a linear or higher order polynomial. If the decay is considered linear, it is necessary to choose a suitable truncation frequency, σ_L, at which damping becomes zero. A reasonable method was applied by Van Oortmerssen (1976), who used polynomial decay curves for the various modes of motion, based on the asymptotic behavior of wave energy transfer for forced motion in calm water. These curves can be estimated for heave or roll, for example, but the behavior for coupled modes, such as sway-induced roll, cannot be determined in the same fashion, requiring some arbitrary decay curve approaching zero at a finite frequency σ_L. It should be noted that the error associated with cross-coupling terms should be small, since their influence on the total force is usually small. More details about the asymptotic behavior of hydrodynamic coefficients can also be found in the treatment by Greenhow (1986).

In this work both linear and nonlinear decay curves of the damping coefficients have been considered, and a comparison was made for a typical vessel. For the nonlinear decay behavior, the approach by Van Oortmerssen (1976) was used, and for the linear decay the limiting frequency σ_L was determined by extrapolating the damping curve linearly from the frequency σ_F. Simulations were performed to compare the roll damping decay in calm water for different vessels, using the two different formulations for the damping curves. It was found that for simulation purposes the accuracy of the results was hardly affected by the shape of the tail end of the damping curves. More details about the sensitivity of the response to changes in the memory effect integrals are discussed in Chapter 5. The various characteristics of a typical damping curve are shown in Figure 3.1; here three-dimensional coefficients have been plotted, but the graph could equally well apply to two-dimensional damping behavior.

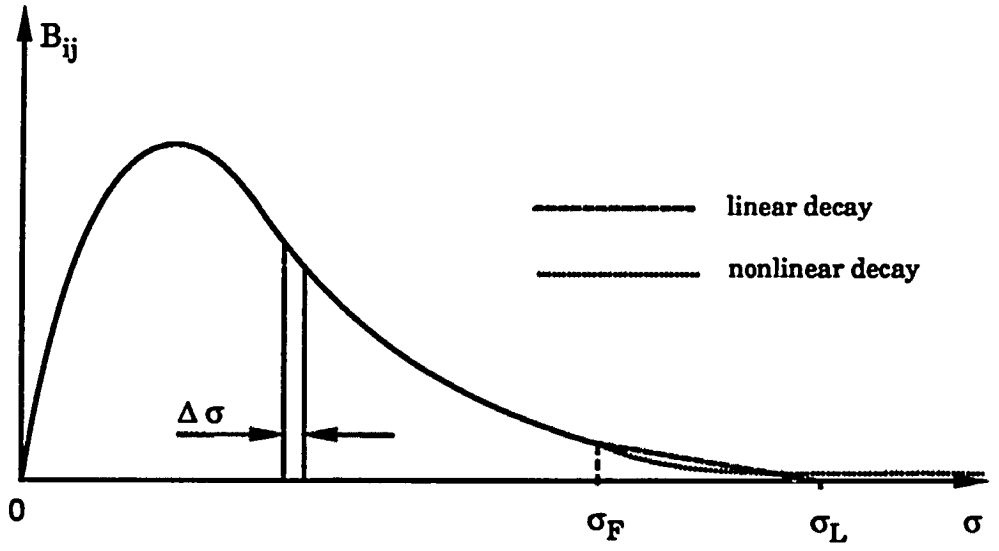

Figure 3.1. Typical Damping Curve Characteristics

The frequency σ_F is determined by a nondimensional cut-off limit applicable to typical ship shape sections. If the nondimensional frequency, σ^*, is defined as

$$\sigma^* = \sigma\sqrt{b/(2g)} \ ,$$

and b is the section width at the waterline, then the two-dimensional damping coefficients become relatively small for $\sigma^* \geq 2.5$ (see Vugts (1968), for example). In order to determine the frequency σ_F for three-dimensional bodies, the nondimensional frequency is based on the beam, B, of the ship, i.e., the width of the largest section:

$$\sigma^* = \sigma\sqrt{B/(2g)} \ .$$

Choosing the nondimensional cut-off frequency as:

$$\sigma_F^* = 2.5 \ ,$$

yields the following value of σ_F:

$$\sigma_F = 2.5\sqrt{2g/B} \ .$$

First the case with linear decay is considered. The upper limit, σ_L, at which damping vanishes, is determined by extrapolating linearly from the damping values at σ_F. This is done by performing a linear regression to the last four damping values up to the frequency σ_F, so that the slope of the curve at σ_F is known. With this information the value σ_L can be calculated easily. For the case with nonlinear high-frequency behavior, the approach by Van Oortmerssen (1976) can be followed, where the tail end of the damping curve is assumed to be given by

$$B(\sigma) = \frac{C}{\sigma^m} \ ,$$

where C is a constant which depends on σ_F, and m is an integer power, depending on the mode of motion, e.g. m = 3 for roll and m = 7 for heave (for which the limiting frequency is $\sigma_L \rightarrow \infty$).

3.2.B. Kernel Functions and Memory Effect Integrals

The kernel functions as discussed in Chapter 2.1.2 can be estimated numerically as follows :

$$L_{ij}(\tau) \approx \int_0^{\sigma_L} B_{ij}(\sigma) \cos\sigma\tau \, d\sigma \ ,$$

where σ_L is the limiting frequency as defined above. The kernel integrals are calculated by a summation of discrete integrals, assuming that the

coefficients $B_{ij}(\sigma)$ behave linearly between the discrete frequencies. The frequency interval $\Delta\sigma$ must be sufficiently small to properly account for the response characteristics. The integration method employed is that due to Filon, and detailed expressions of the method are given in Appendix C. For purposes of illustration, the kernel functions $L_{22}(\tau)$ and $L_{44}(\tau)$, for respectively the heave and roll modes, are shown in Figure 3.2 for a full scale American Challenger vessel (one of the types that was used for the San Francisco Bay experiments, and approximately the same as a Mariner vessel). Both kernels have been nondimensionalized by their maximum values for zero time lag, and it is seen that the roll kernel reaches a zero value after approximately 15 seconds, while this is close to 20 seconds for the heave kernel.

The time-dependent memory effect integrals associated with the linear radiation forces are of the form

$$M_i(t) = \sum_{j=1}^{6} \int_0^{\infty} L_{ij}(\tau)\, \dot{x}_j(t-\tau)\, d\tau \ , \qquad i = 1,\ldots,6 \ .$$

These integrals do not have to be integrated up to infinity since the kernel functions attain a practically constant value (zero, for e.g. heave or roll as can be seen from Figure 3.2) after a finite time lag τ_F. Typically τ_F is the value for which the ratio with the maximum kernel value is small:

$$\frac{|L_{ij}(\tau_F)|}{|L_{ij}(o)|} < r \ ,$$

where $r << 1$, e.g. $r = 0.01$.

The value τ_F is taken to be the same for all kernels $L_{ij}(\tau)$, and is based on the heave kernel; since heave is one of the most heavily damped modes of motion, the heave kernel has associated with it a relatively large value of τ_F. Thus, the above integrals can be estimated by truncated integrals, which are solved using trapezoidal integration:

$$M_i(t) \approx \sum_{j=1}^{6} \int_0^{\tau_F} L_{ij}(\tau)\, \dot{x}_j(t-\tau)\, d\tau \quad .$$

The values of the kernel functions are obtained using a time lag interval $\Delta\tau$, while the velocities (and displacements) are obtained successively with a time step Δt. If $\Delta\tau = \Delta t$, the memory effect integrals can be evaluated by assuming that both the kernels and velocities vary linearly during each time step. Then the total integral would be given by the discrete sum of N_τ integrals (for N_τ time lag intervals), each of which may be evaluated exactly on the premise that both components of the integrand behave linearly. If, say, $\Delta t = 2\Delta\tau$, an interpolation procedure can be used to obtain estimates of the velocities having a $\Delta\tau$ time lag interval, so that the same procedure can be used to evaluate the integrals M_i.

The main reason for integrating the equations of motion with the Euler method, is that with that method the memory effect integrals have to be evaluated only once at each time step, using the velocities $\dot{x}$ from time $t-\tau_F$ to the present time t. The discrete time lag interval employed was typically $\Delta\tau = 0.1$ s for beam sea conditions, and 0.2 s for following seas. It is not necessary to use the same interval for the whole integration process, as the kernel functions exhibit quite smooth behavior for relatively large time lags. For example, for $\tau = 0$ to $\tau = 8$ s the time integration interval should be small ($=\Delta\tau$), but for the remaining part of the integration, $\tau > 8$ s, one could use an interval of $2\Delta\tau$, or even larger.

Surge Motion

The kernel functions $L_{ij}(\tau)$ can be obtained numerically through Fourier transformation of the three-dimensional damping coefficients, as described above. Using strip theory, however, it is not possible to obtain the damping coefficients and kernels associated with surge. When considering the motions in severe folowing seas, for example, the surge motion may be significant and the added mass should be taken into

account, despite its value being small. There are other means to determine the three-dimensional damping coefficients for surge: by experiment or 3-D computer programs. For this work the three-dimensional added mass and damping coefficients are obtained for a particular vessel using a fully three-dimensional, linear approach. The damping values for the surge motion were used to obtain the kernel function $L_{11}(\tau)$, and it is assumed that hydrodynamic coupling between surge and the other modes of motion is negligible. From the kernel functions obtained by Van Oortmerssen (1976) it is seen that coupling between surge and heave was relatively significant for the vessel that was analyzed. The sensitivity of the the overall vessel motions to changes in the forces in the surge direction is discussed in Chapter 5.

Small surge motions about the mean position of the vessel are assumed, so that the surge velocity, $\dot{x}_1$ (given in the earth-fixed coordinate system Oxyz), does not deviate to a great extent from the forward speed U of the moving reference system. Neglecting hydrodynamic coupling effects involving surge, the memory effect integral for the surge mode is estimated by

$$M_1(t) = \int_0^\infty L_{11}(\tau) \cdot \{\dot{x}_1(t-\tau) - U\}\, d\tau \ .$$

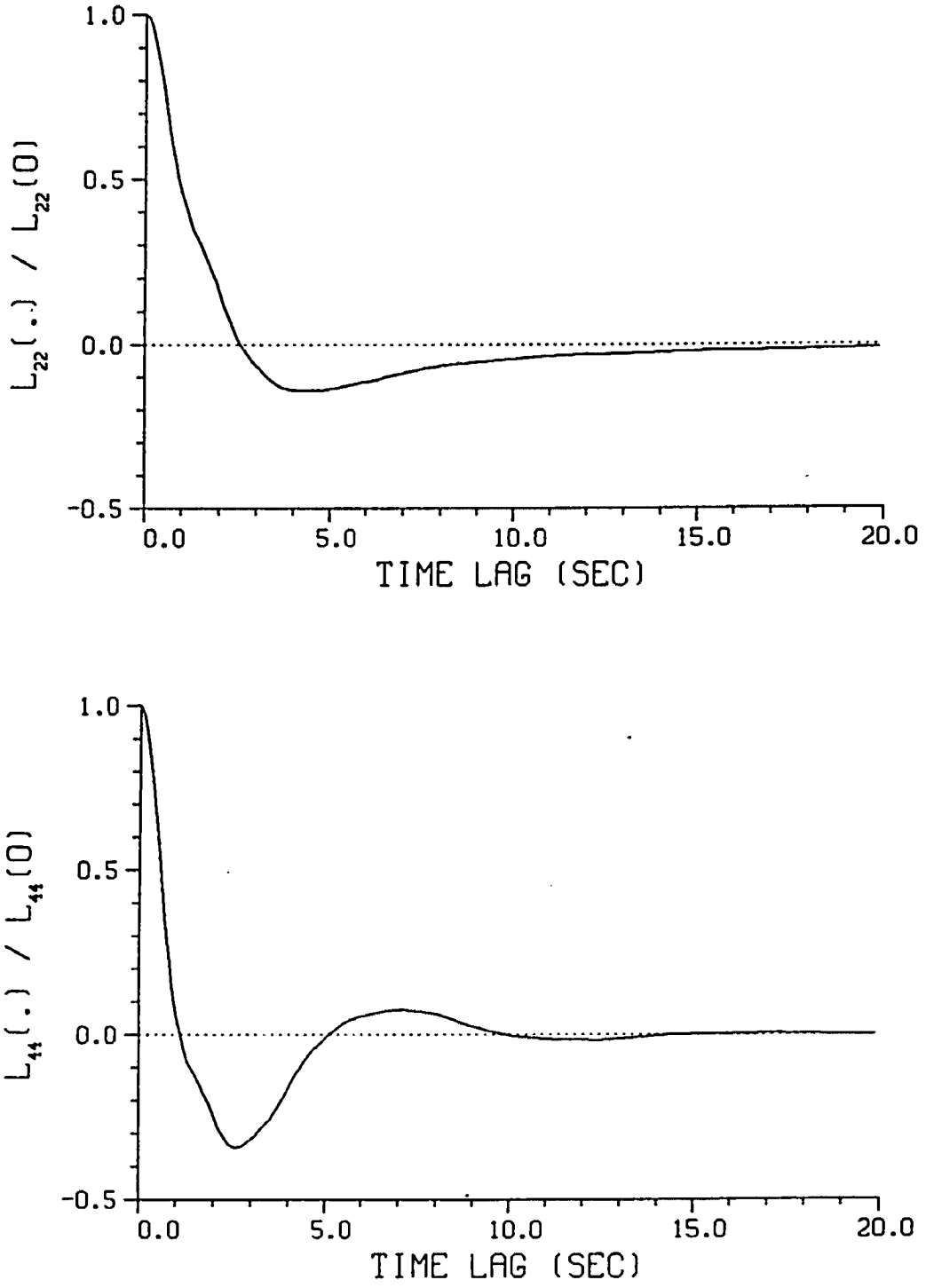

Figure 3.2. Normalized Kernel Functions for American Challenger Vessel

CHAPTER 4

Verification of Theory

A numerical model needs to be verified qualitatively and quantitatively before one can assess its usefulness. Since the model used in this work attempts to cover a wide variety of possible vessel conditions, such as steered with autopilot or unsteered, in head, beam or following seas, regular or random waves, etc., it is not practical to check each mode of motion for the various combinations of conditions. It is even more difficult, perhaps impossible, to determine the correct magnitude of the force components for all six degrees of freedom of motion. In order to verify a ship motion program, use can be made of experiments or similar numerical models that have been developed independently; the former approach is used to validate the present theory and algorithm.

Here, the simulated motions of a vessel are checked against experiments for which the wave conditions and vessel characteristics are known precisely. Use is made of experiments performed in small amplitude regular waves, as well as in relatively large regular and random waves. Also comparisons are made with roll decay experiments in calm water, so as to assess the correctness of the computed roll damping coefficients. The various comparisons are discussed below in detail. First, the rolling of a ship in calm water is investigated to compare the predicted roll damping with experimental values. In Chapter 4.2 comparisons are made for the motions in small, regular waves, and in Chapter 4.3 for motions in large amplitude waves (both regular and random).

4.1. Comparison with Roll Decay Experiments

Since rolling is a significant mode of motion, it is important to verify the prediction of the roll damping coefficients, the estimation of which is treated in Chapter 2.2.1. One practical way to investigate the correctness of the damping coefficients is to compare the predicted coefficients with the results obtained from roll decay experiments in calm water. If a vessel is heeled over at a given angle, and then released to oscillate freely,

the only forces contributing to the subsequent motion behavior are the hydrostatic, wave radiation and viscous forces. The hydrostatic force components can be checked easily by comparing the computed righting arm values for an inclined vessel with another method, such as e.g. the wall-sided formula. The wave radiation forces cannot be measured, but can be determined quite accurately using potential theory. If the period of roll oscillation is large, wave radiation damping becomes small compared with the total viscous damping. Then an estimate can be made as regards the viscous roll damping contribution by inspection of the roll decay rate.

Roll decay experiments were conducted with the models used for the ship motion experiments which were conducted on the San Francisco Bay and reported by, for example, Chou *et al.* (1974). For the verification of the algorithm presented here, use is made of roll decay results obtained for the American Challenger model, having a length of about 17 ft, and approximately 1/30 of full scale, in calm water and at zero forward speed (dated August 24, 1972). No bilge keels were present during the runs. Records were examined for four runs with identical conditions, except for different values of the vertical position of the center of gravity, KG. The initial heel angles were on the order of 20 degrees, and the roll period during the first cycles was noticeably shorter than the final decay period, which corresponded closely to the calculated natural roll period. The natural roll period of the model varied between 4 and 8 seconds (depending on KG), and the length of all runs was 300 seconds.

The experimental damping coefficients can be estimated by means of the measured log decrement, where it is noted that theoretically this approach is valid only for a constant roll period, i.e., small roll angles. The damping ratio is dependent on the roll decay rate as follows:

$$\xi = \frac{\zeta}{\zeta_0} \approx \frac{\delta_m}{2\pi m} ,$$

where ζ is the linear damping and ζ_0 is the critical damping coefficient. In this case ζ represents an "equivalent linear damping coefficient", since

the viscous roll damping is not purely linear. δ_m is the log decrement corresponding to m cycles, and is given by

$$\delta_m = \ln \left\{ \frac{x_n}{x_{n+m}} \right\} ,$$

where x_n is the roll amplitude after n cycles, and x_{n+m} is the roll amplitude after n+m cycles. The critical damping is according to linear vibration theory equal to

$$\zeta_0 = \frac{2\rho g V.GM}{\sigma_{n,4}} ,$$

where V is the displaced volume, GM is the transverse metacentric height, and $\sigma_{n,4}$ is the natural roll frequency. Here the natural frequency is estimated as follows:

$$\sigma_{n,4} \approx \sqrt{\frac{g.GM}{1.1\ \rho_{xx}^2}} \quad \text{rad/s} ,$$

and ρ_{xx} is the roll gyradius, which is multiplied by the factor 1.1 to account for added mass effects.

The damping ratio ξ was calculated for each of the four runs with different numbers of cycles, where m was varied between 10 and 20 full cycles per run. The results showed that ξ was not very dependent on m, nor on the KG value. The experimental damping ratio was found to be within the following range:

$$\xi = 0.011 \pm 0.001 .$$

Next an overview is given of the determination of the damping ratio obtained from the numerical model.

Predicted Roll Decay Coefficients

As has been discussed in Chapter 2.2.1, the viscous roll damping moment in calm water is estimated by

$$f_4(t) = B_{44,L}\cdot\dot{\theta} + B_{44,Q}\cdot|\dot{\theta}|\cdot\dot{\theta} \quad .$$

In order to compare the predicted damping values with the measured ones, it is necessary to express the linear and quadratic coefficients in terms of an equivalent linear damping coefficient:

$$f_{4,eq}(t) = B_{44,eq}\cdot\dot{\theta} \quad .$$

The method of equivalent linear damping implies that the work done during one cycle must be the same for both the nonlinear damping moment and the equivalent linear damping moment. Assuming the ship model to oscillate with pure sinusoidal motion, at frequency σ, and with amplitude θ_{max}, the equivalent damping coefficient can be estimated as

$$B_{44,eq} = B_{44,L} + \frac{8}{3\pi}\sigma\theta_{max}\cdot B_{44,Q} \quad .$$

In the prediction of the viscous damping coefficients it was assumed that the roll frequency was equal to the natural frequency, and that the roll amplitude could be taken as the mean of the decay amplitudes between 2 and 12 cycles after the start of the roll decay experiments, i.e.,

$$\theta_{max} = \frac{\theta_2 + \theta_{12}}{2} \quad .$$

The contribution from the wave radiation damping, which is considered linear, must be added to the equivalent damping coefficient, so as to take

all damping contributions into account. Examination of the various roll moment contributions in the simulated roll decay process, indicated that the damping due to the rudder was negligible compared with the other damping contributions. The total damping coefficient is then given by

$$B_{44,eq} = B_{44,L} + \frac{8}{3\pi}\sigma\theta_{max} \cdot B_{44,Q} + B_{wave} \cdot$$

The damping coefficient is made nondimensional by dividing by the critical damping ζ_0:

$$B^*_{44,eq} = \frac{B_{44,eq}}{\zeta_0} = B^*_{44,L} + B^*_{44,Q} + B^*_{wave} \cdot$$

Two roll decay runs with the American Challenger model were investigated, where the following GM values (model scale) were applicable:

(1) GM = 0.222 ft (ballast weight position #3);
(2) GM = 0.702 ft (ballast weight position #7).

The experiments were conducted with the model being in the heavy load condition, i.e., Δ_m = 1600 lbs, resulting in a natural roll period of 6.70 s for case (1), and 4.05 s for case (2). The measured decay amplitudes at 2 and 12 cycles after the start of case (1) were 13.7 and 6.7 degrees, respectively, and 13.3 and 6.5 degrees for case (2). The results of the roll damping predictions for the two cases are shown in Table 4.1.

Case	$B_{44,L}^*$	$B_{44,Q}^*$	B_{wave}^*	$B_{44,eq}^*$
(1)	0.0003	0.010	0.00005	0.0104
(2)	0.0002	0.008	0.0002	0.0084
Experimental (both cases)				0.011

Table 4.1. Predicted and Experimental Equivalent Linear Damping Coefficients

The damping ratios obtained from the experiments were equal to 0.011 both for case (1) and for case (2), based on the log decrement for n = 2 and m = 10. This suggests that the predicted equivalent damping for case (1) is within approximately 5% of the measured damping, while the damping for case (2) is underpredicted by about 25%. Considering the assumptions involved with the method of component damping, these results are quite good and suggest that roll damping can be predicted to at least the correct order of magnitude.

4.2. Comparison with Model Experiments in Small Regular Waves

Experiments conducted in small amplitude waves are useful to investigate the simulated motions, particularly because the results should lie close to predictions made by means of conventional linear theory. A large number of model experiments in regular waves have been performed at several research institutions. Time domain simulations can be carried out for the same conditions as the motion experiments, provided that there are sufficient data available concerning the relevant ship characteristics, such as radii of gyration, metacentric height, etc.

Some of the experimental data considered here were obtained by Gerritsma (1960) for different Series 60 models in head sea conditions. For the purposes of this investigation, simulations were performed with program *KAPSIZE* for a Series 60 vessel with 0.70 block coefficient, having a Froude number of Fn = 0.2, and subjected to waves of different lengths

and small amplitude. The parameters of interest are the heave and pitch amplitudes, as well as their phasing. In Figure 4.1 the computed and experimental heave and pitch amplitudes are plotted as a function of wave length in nondimensional form. The nondimensional heave and pitch amplitudes are defined, respectively, as

$$\frac{x_{2,0}}{A} \text{ and } \frac{\Psi}{\alpha} ,$$

$x_{2,0}$ being the heave amplitude, A the wave amplitude, ψ the pitch amplitude, and α the maximum wave slope ($=2\pi A/\lambda$). The wave lengths are nondimensionalized by the ship length:

$$\frac{\lambda}{L} .$$

It can be seen that the agreement between measured and predicted results is quite good, especially for the lower and higher frequencies. The largest discrepancies in heave and pitch occur at $\lambda/L = 1.25$. Although not plotted, it was found that both the phasing of heave with respect to the wave, and pitch with respect to heave, were in close correspondence with the measured values. Thus for these conditions the program *KAPSIZE*, with all theoretical features included, yields results similar to those that would be obtained from conventional linear theory.

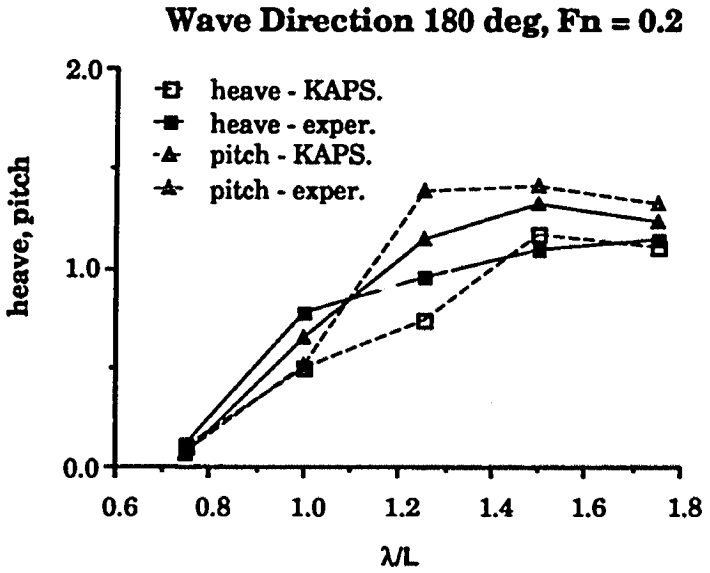

Figure 4.1. Heave and Pitch Amplitudes in Regular Head Seas for Series 60 Vessel. Comparison of simulation results with experimental results by Gerritsma (1960).

Vossers, Swaan and Rijken (1960) performed an extensive series of model tests with Series 60 hull forms, which were tested for a variety of headings and wave lengths. Some of their results were used in this work to compare the heave, pitch and roll motions of a Series 60 hull with 0.70 block coefficient and Fn = 0.1. The predicted and measured motion amplitudes are shown for 10, 50, 90 and 170 degrees wave heading (from following sea to head sea conditions) as a function of wave length in Figures 4.2a through 4.2d, respectively. The same nondimensionalization is used as above, i.e., the heave amplitudes are made nondimensional by the wave amplitude, and both roll and pitch are nondimensionalized by the maximum wave slope α. From these figures it can be seen that, in general, the predicted heave and pitch amplitudes are close to the measured results for all wave lengths and headings. The roll angles for the 10° and 170° heading cases are very small; the roll amplitudes for the 170° heading are in good agreement with the experimental results, while the agreement is fairly good for the 10° case. In the experiments it had been observed that the roll motion was larger for the 50° heading angle

than for the 90° case, for all wave lengths considered. The same behavior showed up from the simulation results, especially for the longer wave lengths. In the simulations the roll amplitude was underpredicted quite significantly for the longest wave length at 50° heading angle, and overpredicted for the 90° case with the exception of $\lambda/L = 1.5$, where the agreement between measured and predicted results is good.

In summary, heave and pitch predictions correspond well with measured results, for all headings and wave lengths considered; the same applies to the roll amplitudes for the 10° and 170° heading angles. The largest discrepancies occur for roll in beam seas for most wave lengths, which may be due to underprediction of the viscous damping coefficients used in the simulation, or (less likely) scale effects in the experiments.

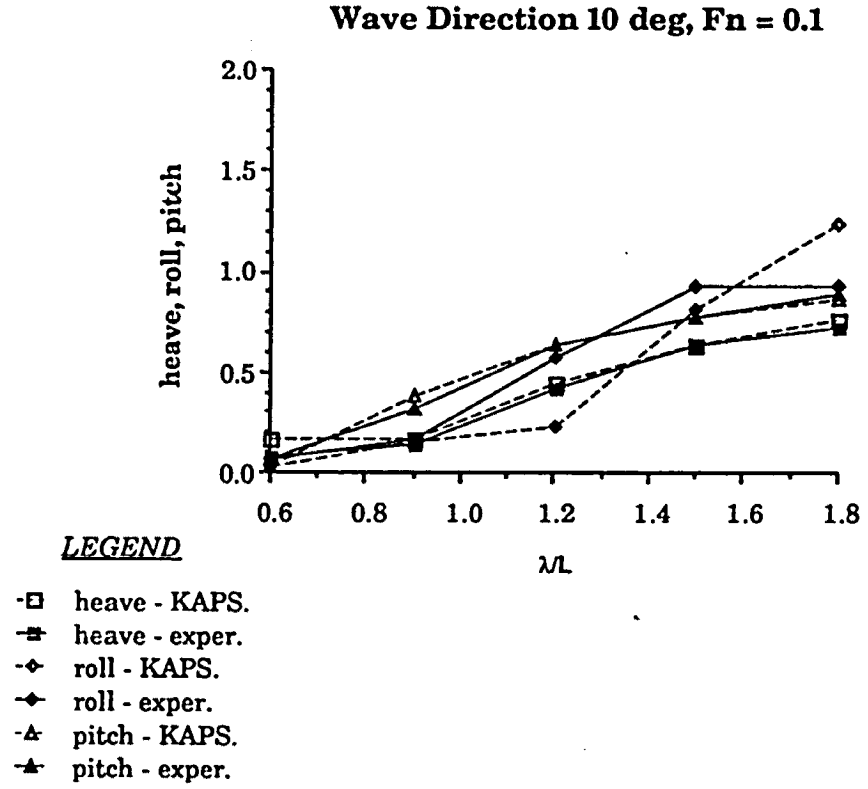

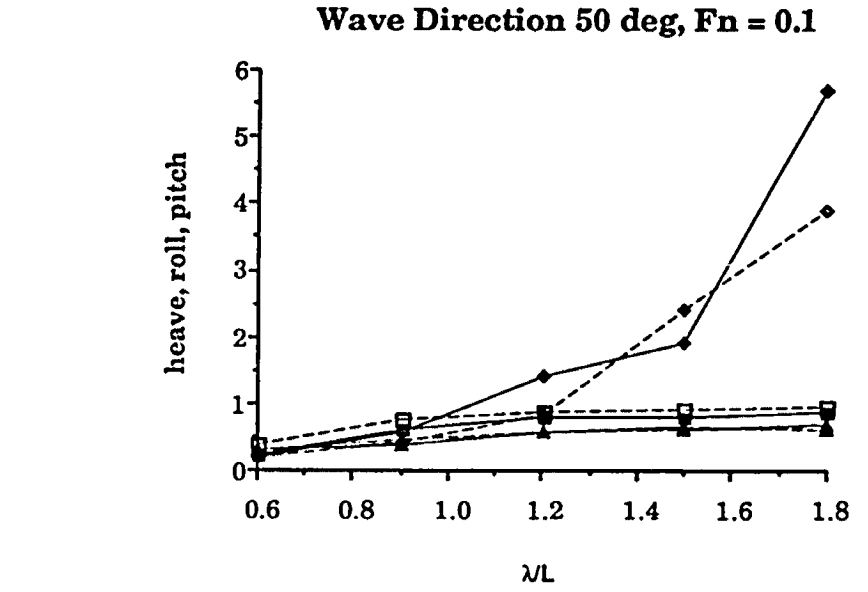

Figures 4.2a and 4.2b. Heave, Roll and Pitch Amplitudes of Series 60 Vessel in Regular Waves. Comparison of simulation results with experimental results by Vossers et al. (1960).

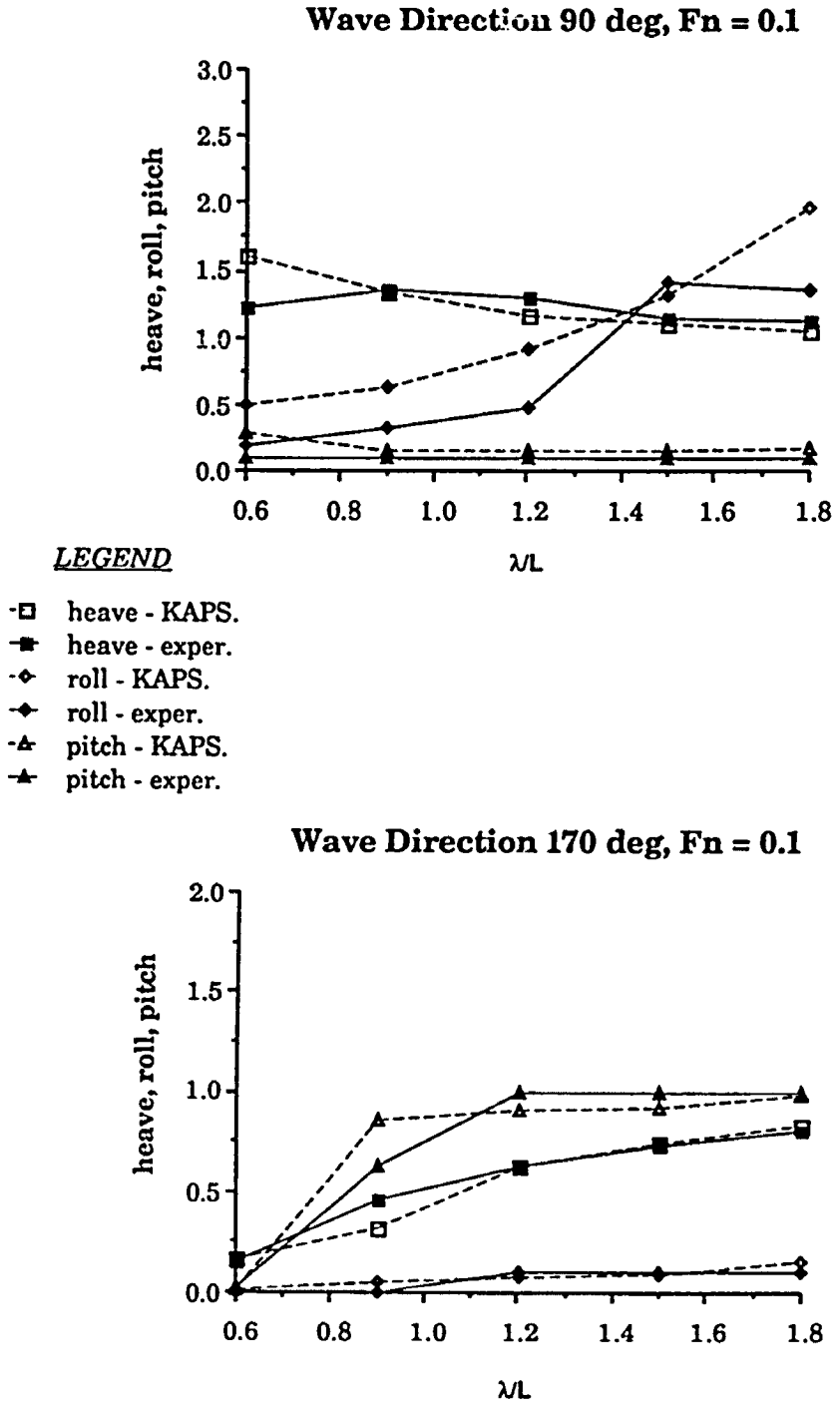

Figures 4.2c and 4.2d. Heave, Roll and Pitch Amplitudes of Series 60 Vessel in Regular Waves. Comparison of simulation results with experimental results by Vossers et al. (1960).

4.3. Comparison with Experiments in Severe Wave Conditions

The data obtained from the San Francisco Bay capsize experiments, and from the related towing tank experiments, lend themselves quite well for numerical duplication of the encountered wave climate. The laboratory experiments, especially, are useful for this purpose as most of the important parameters were recorded, such as wave elevation alongside the model, phase, roll angle and velocity, etc. The model experiments were conducted so as to approximately simulate conditions encountered during the Bay experiments by means of regular waves. The San Francisco Bay data have been presented in spectral form, so that any time domain simulation will be only one realization of an infinite number of possible realizations, due to e.g. unknown initial conditions of the vessel and unknown phase behavior of the waves.

4.3.1. Experiments in Regular Waves

Model experiments in the towing tank have been carried out to investigate the capsize behavior of various ship types in following seas, as has been reported by Fallon *et al.* (1980). These experiments were conducted in the wake of the San Francisco Bay experiments, which will be considered in more detail in the next section. Due to laboratory constraints only three modes of motion of the models were allowed: heave, roll and pitch. In this section results are compared for a Mariner model (which is very similar in overall characteristics to the American Challenger), and for a container ship model, a Sea Land 7, also referred to as SL-7. Numerical simulations were performed accordingly by imposing constant forward speed and allowing only three degrees of freedom. Full scale conditions were simulated, and the initial conditions used were those supplied with the experimental data. The viscous roll damping coefficients were estimated using the method discussed in Chapter 2.2.1. As can be seen from the following, most predictions using the present numerical model compare favorably well with the experimentally observed roll behavior up to the point of capsizing, while earlier predictions shown in Fallon *et al.* (1980) generally did not exhibit good correlation.

Results for the Mariner

Simulations were carried out for the case corresponding to Figure III-5 in Fallon *et al.* (1980), i.e., autoparametric resonance conditions (where the encounter frequency was equal to approximately twice the natural roll frequency) with the Mariner ship travelling at 7.3 knots in regular following seas of 17.5 feet amplitude and 10 seconds period. Experimentally this resulted in a capsize after about 80 seconds. Both the experimental and numerical results are shown in Figure 4.3, from which it is seen that the predicted behavior follows the experimental one quite closely. The predicted roll period is very close to the experimental value, and the predicted roll amplitudes before capsizing have the same order of magnitude as the experimental amplitudes.

Symbol Convention in Simulation Plots

In these and subsequent plots, *Eta* refers to the instantaneous wave elevation given at the center of gravity of the vessel (w.r.t. the mean water level), yaw and rudder angles are shown conjunctively, and *Vx* and *Vz* are the forward and sway velocity, respectively, along the axes of the ship coordinate system. For simulating the model tank conditions exactly, the following quantities were set equal to zero in the simulations: surge and sway displacements, and yaw and rudder angles. *Eta* is always denoted by a dashed line, and *Vz* is represented by a chain-dotted line. The experimental values for the roll angles are denoted by + symbols, which were obtained by digitizing the experimental roll records given in the report by Fallon *et al.* (1980).

It is noted that the old *CAPSIZE* simulator, used for the numerical simulations by Fallon *et al.* (1980), did not predict a capsize for the above case with the three degrees of freedom suppressed, while its prediction was quite close to the experimental values when all six degrees of freedom were taken into account and a high value of quadratic roll damping was used. Another run which resulted in a capsize is shown in Figure 4.4;

this case corresponds to the conditions as in Figure III-7 in Fallon *et al.* (1980), namely U = 7.8 knots, 10 s wave period and 12.8 feet amplitude. Also here the correspondence between experiment and prediction is quite good, and it is seen that in both an almost unstable condition is reached at around 40 seconds.

The simulated behavior in the two previous cases, and especially the latter one, was found to be quite sensitive to the initial conditions, such as initial heave position and velocity (for which no data were reported), and in the latter case the linear and quadratic damping roll coefficients had to be increased fivefold to avoid a premature capsize. It should be noted that when a simulation is started at time t = 0, there are initially no memory effects due to wave radiation effects, while this is not true for the experiments where memory effects would have been present at the time measurements started to be taken. Such discrepancies do have a bearing on the predicted behavior, although their effect is probably small because of the relatively short memory (which is around 15 to 20 seconds for heave and about 10 seconds for roll, for example).

Results for the SL-7

In Figure 4.5 results are shown for a run of the SL-7 model where no capsizing occurred, which corresponds to the case in Figure III-23 in Fallon *et al.* (1980). The predicted roll response has the same frequency as the measured one, and the amplitudes are of the same order, although the later cycles in the sequence show amplitudes that are somewhat underpredicted. Simulations were carried out for the case corresponding to Figure III-25 in Fallon *et al.* (1980), i.e., autoparametric resonance conditions with the SL-7 ship travelling at 9.8 knots in regular following seas of 15.9 feet amplitude and 13 seconds period. Experimentally this resulted in a capsize after about 125 seconds, and both the experimental and numerical results are shown in Figure 4.6, from which it is seen that the predicted behavior compares quite well with the experimental one, and capsizing is predicted to occur at the same time instant as in the experiments. However, the numerical roll amplitudes before capsizing are seen to vary with time, whereas they stayed approximately constant,

at ±35°, during the experiments. The predicted roll behavior was found to be very dependent on the initial heave displacement and velocity, whereas the roll characteristics were not very sensitive to changes in the viscous roll damping coefficients. It is also noted that the old *CAPSIZE* simulator, used for the numerical simulations by Fallon *et al.* (1980), did not predict a capsize for the above SL-7 case with the three degrees of freedom suppressed. A slow-speed capsize sequence is shown in Figure 4.7, which corresponds to Figure III-27 in Fallon *et al.* (1980); the ship speed is equal to 1.3 knots, and the wave has a period of 16 seconds and 15.4 feet amplitude. The predicted capsize occurs after 140 seconds with increasingly large roll angles, and the same behavior was observed experimentally.

Summarizing, the simulated roll motion behavior of the American Challenger and SL-7 vessels seems to correspond closely to the experimentally observed behavior; only heave, roll and pitch motions were allowed in following seas with large amplitude. It was found that for those conditions the motion behavior was generally quite sensitive to the initial heave position and velocity, and that capsizing would occur after a shorter period when roll damping was reduced.

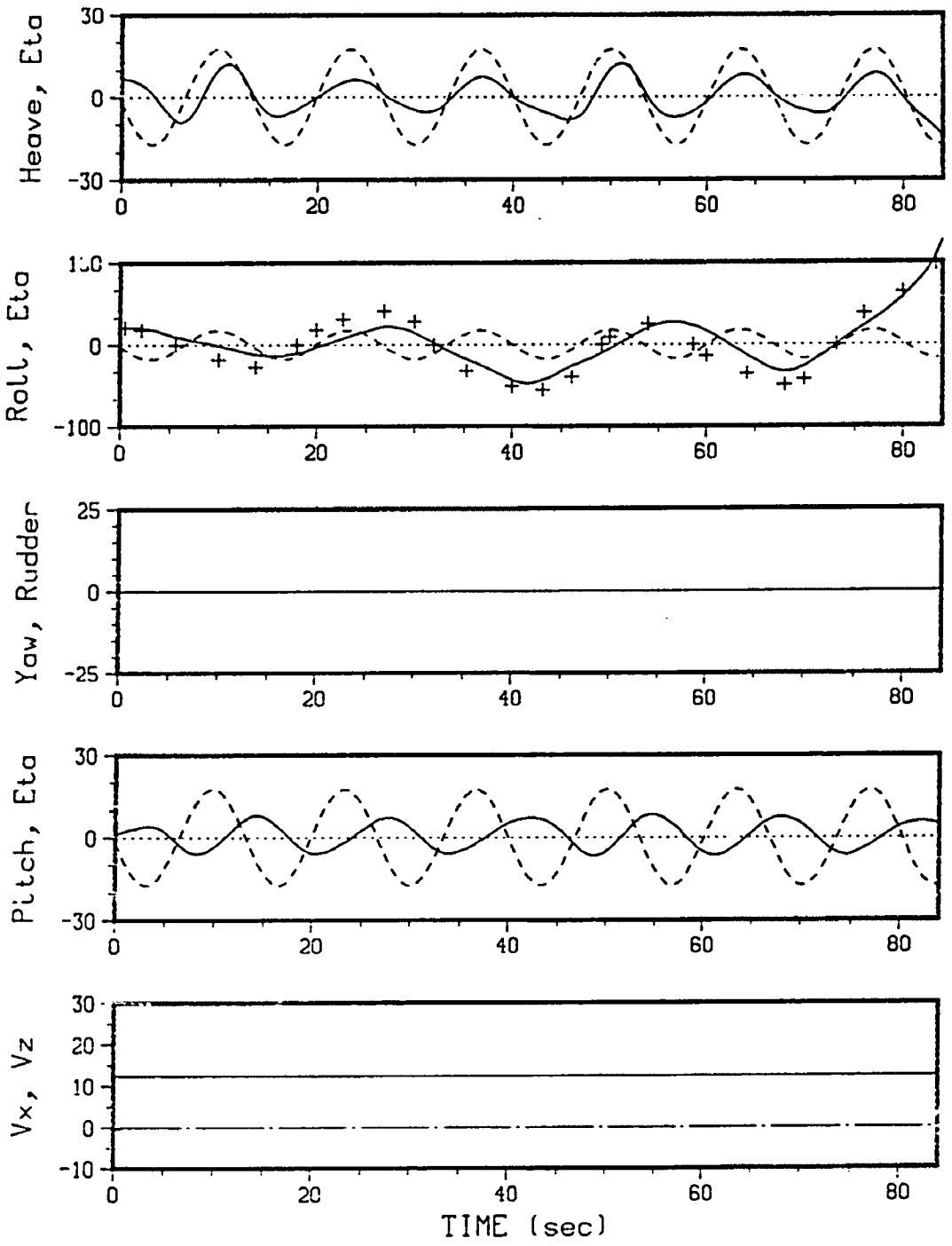

Figure 4.3. Capsize Simulation in Following Seas for Mariner Vessel. The + symbols refer to the digitized values of experimentally obtained roll angles, and the dashed lines refer to the wave elevation at the C.G. Displacements are in feet, angles in degrees, and velocities in ft/s.

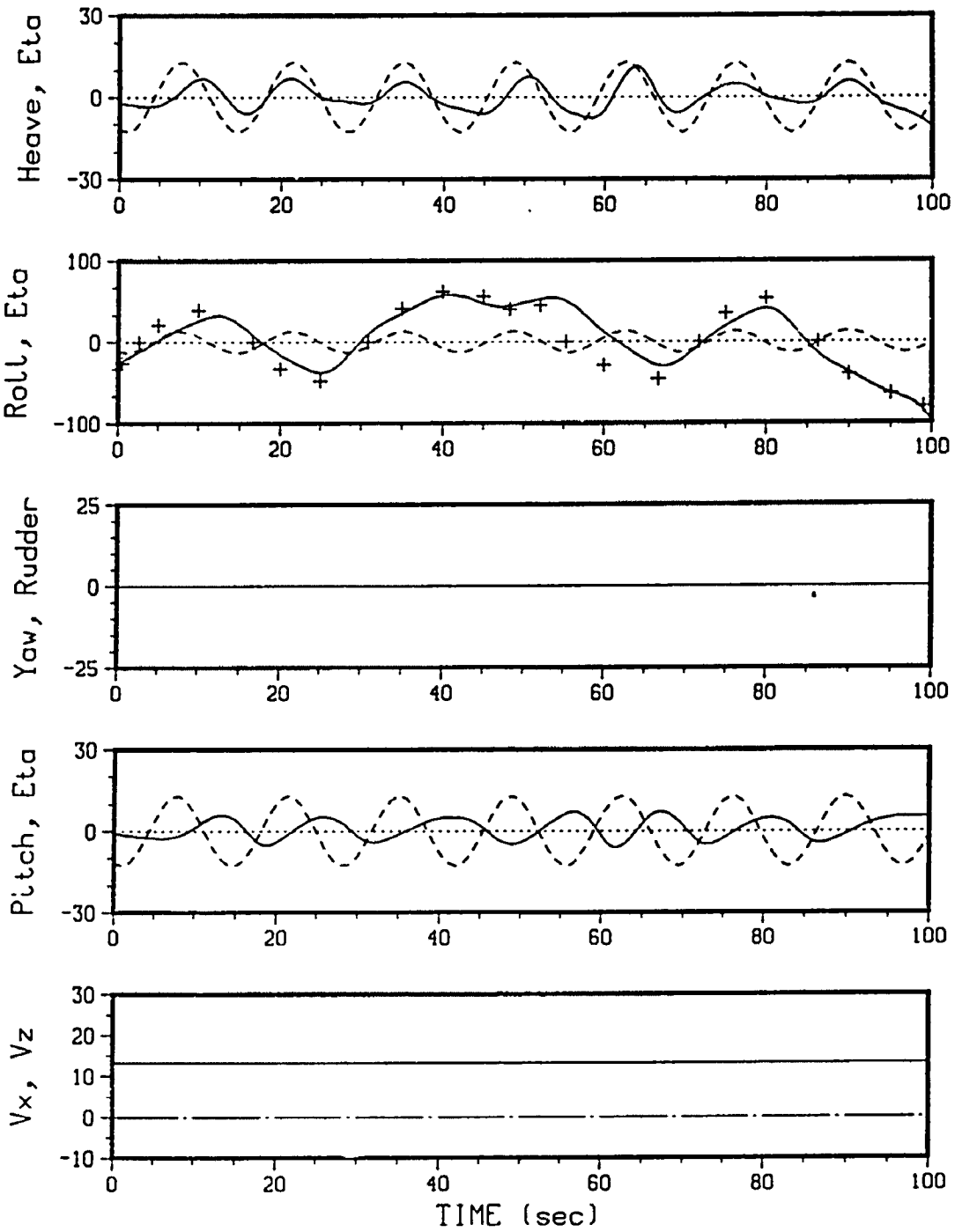

Figure 4.4. Capsize Simulation in Following Seas for Mariner Vessel. The + symbols refer to the digitized values of experimentally obtained roll angles, and the dashed lines refer to the wave elevation at the C.G. Displacements are in feet, angles in degrees, and velocities in ft/s.

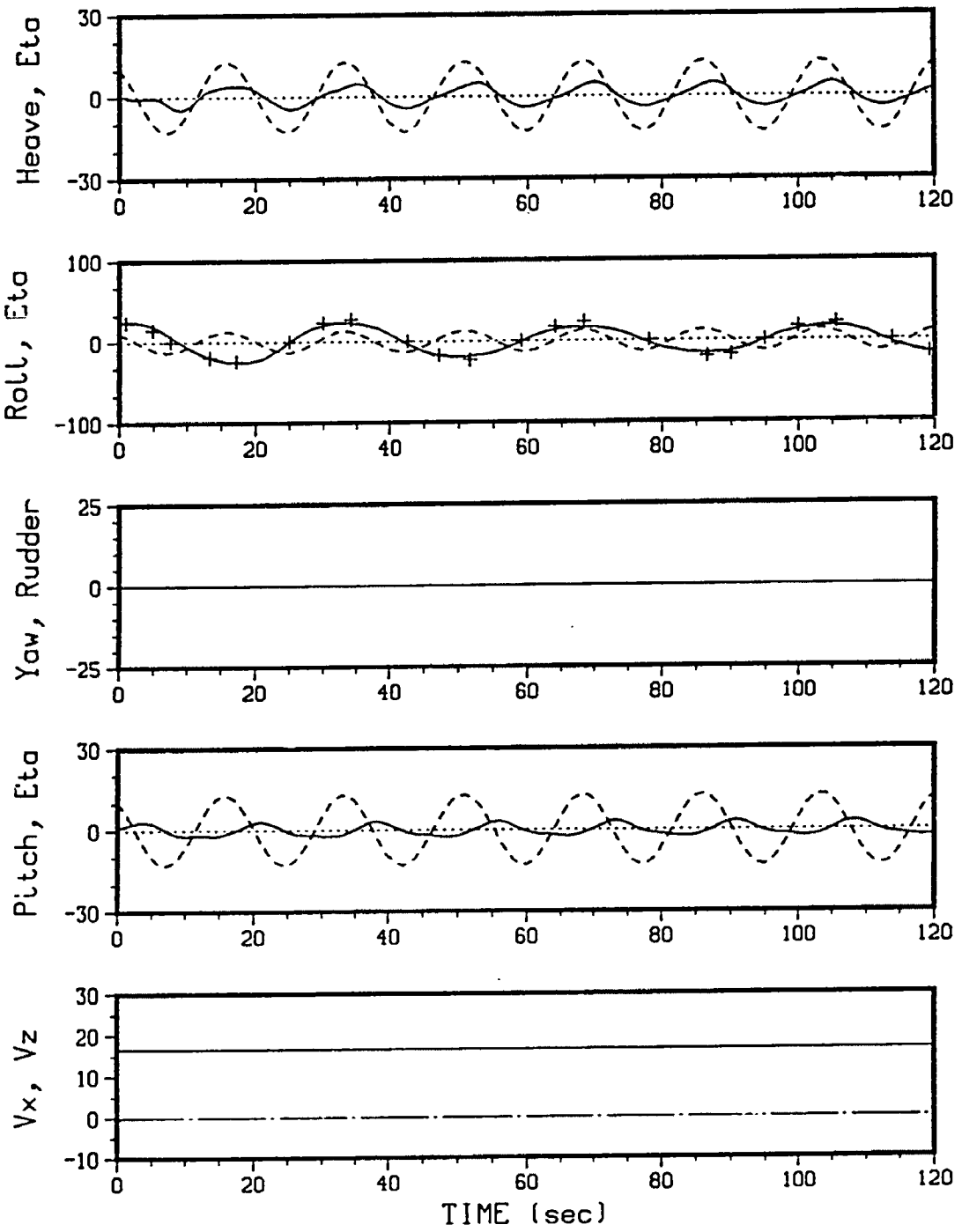

Figure 4.5. Motion Simulation in Following Seas for SL-7 Vessel. The + symbols refer to the digitized values of experimentally obtained roll angles, and the dashed lines refer to the wave elevation at the C.G. Displacements are in feet, angles in degrees, and velocities in ft/s.

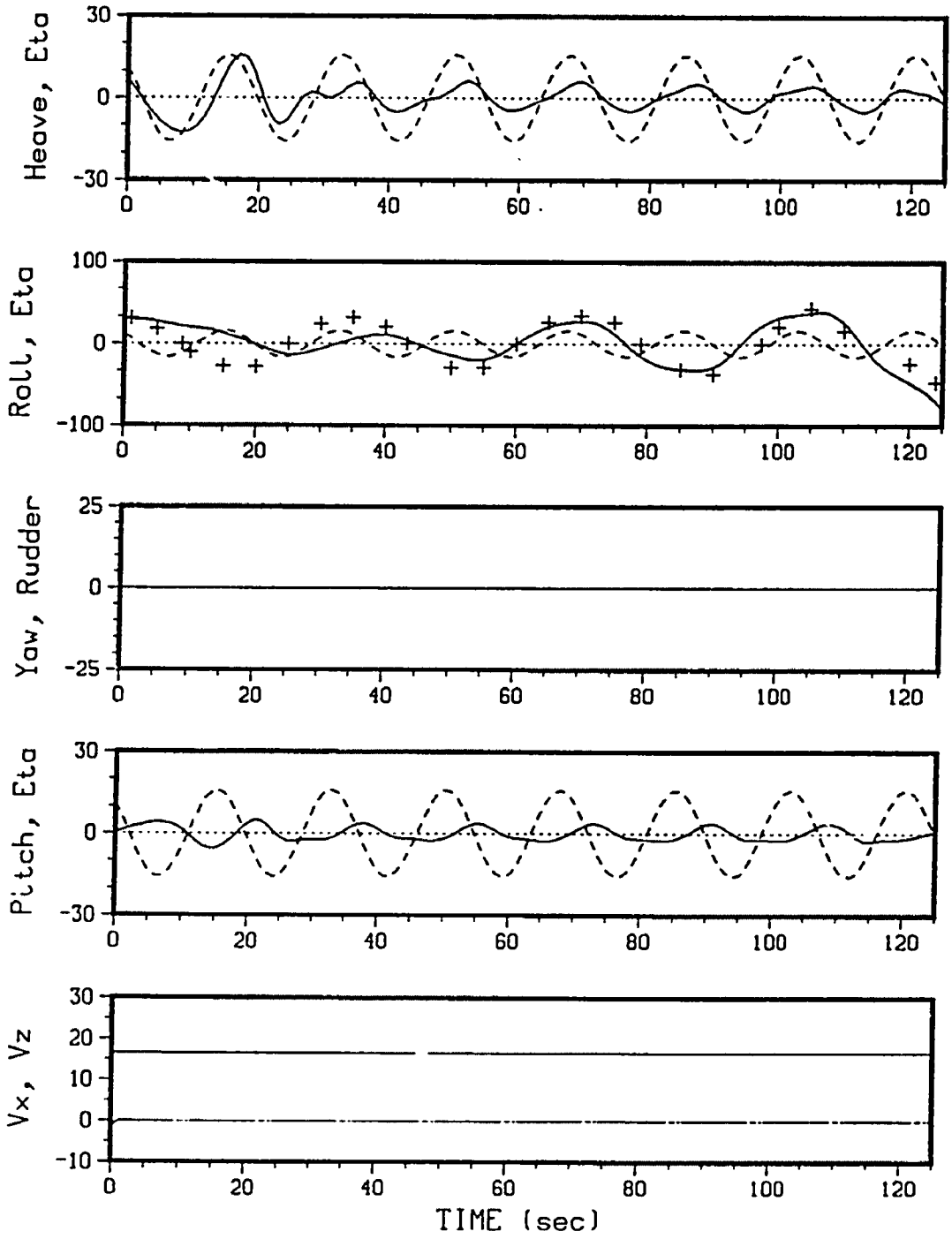

Figure 4.6. Capsize Simulation in Following Seas for SL-7 Vessel. The + symbols refer to the digitized values of experimentally obtained roll angles, and the dashed lines refer to the wave elevation at the C.G. Displacements are in feet, angles in degrees, and velocities in ft/s.

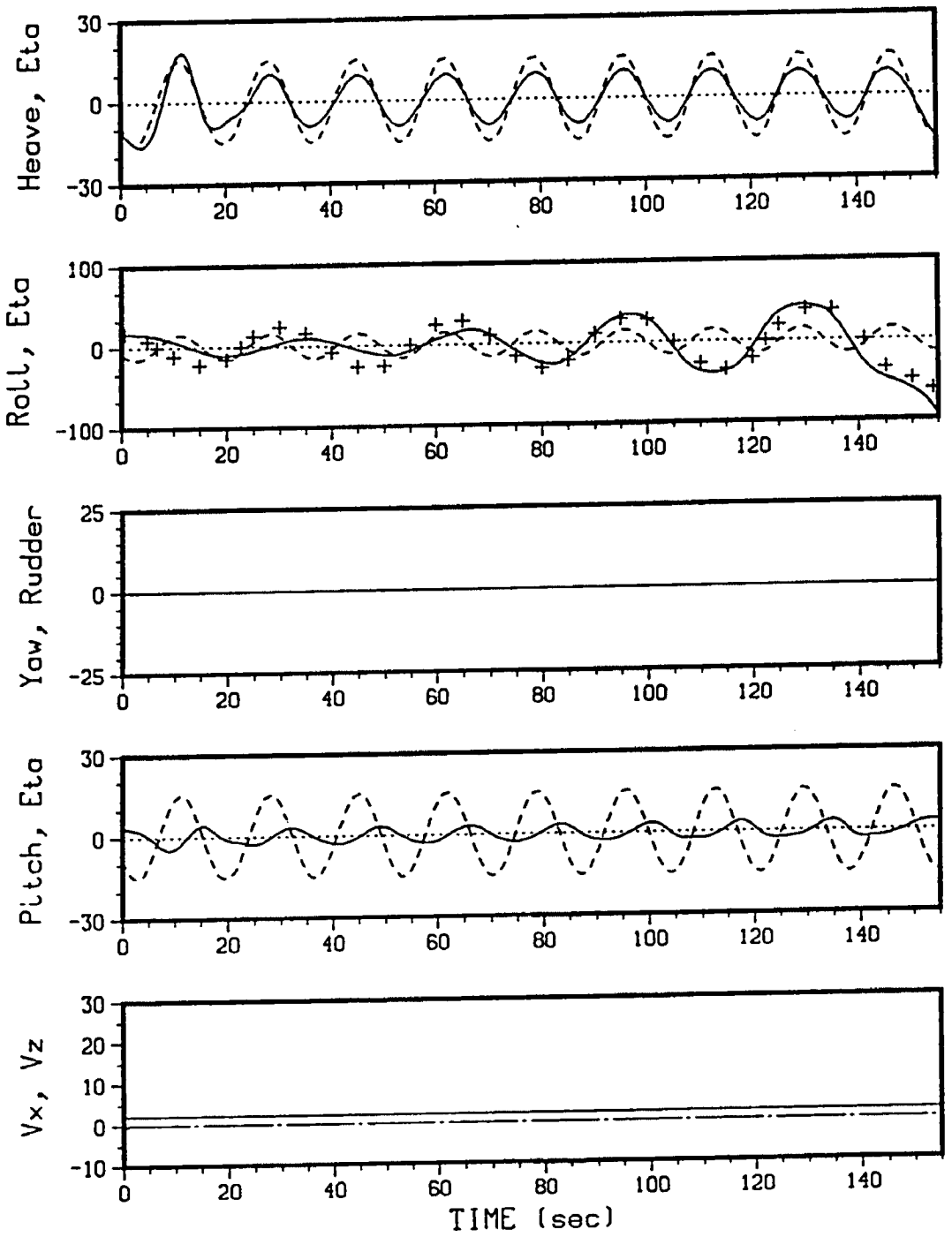

Figure 4.7. Capsize Simulation in Following Seas for SL-7 Vessel. The + symbols refer to the digitized values of experimentally obtained roll angles, and the dashed lines refer to the wave elevation at the C.G. Displacements are in feet, angles in degrees, and velocities in ft/s.

4.3.2. San Francisco Bay Experiments

Use is made of results from the San Francisco Bay experiments, reported by Haddara *et al.* (1972) and Chou *et al.* (1974), to compare some of the experimental results with numerical calculations for random seas. Most of the experiments were conducted in conditions that would correspond to different degrees of severe sea conditions for the models. The wave elevations were recorded in the vicinity of the model test location (at four stationary points), prior to and after the test runs with the models. Directional wave spectra have been presented by Chou *et al.* (1974), and as can be seen from an example shown in Figure 4.8, the spreading of the wave energy on that particular day was confined to quite a narrow region (which is typical of San Francisco Bay conditions). Interpolation was used to derive the wave spectrum associated with a given model test. During the seakeeping tests the following quantities pertaining to a model were measured: roll, yaw, pitch and rudder angle. For illustrational purposes, typical motion time series of a model run that ended with a capsize are shown in Figure 4.9. Extensive statistical analyses have been reported in the above references, and also by Kastner (1973), who has presented results in spectral form. The estimated motion spectra are given together with the wave spectra, which can be used as a basis for verification of simulations. It is noted that simulations in random seas do not provide a sound basis for verification, since a simulation gives only one particular realization of the wave and ship motion process, and no information is available with respect to the time histories of the incoming waves and resulting motions. Therefore, the simulations only indicate to a certain extent the possibility of predicting the motions in random seas correctly.

Similar to the preceding chapter, comparisons have been made between simulated and measured results for the American Challenger and SL-7 models for different wave heading angles, ship speeds and metacentric heights. Simulations were carried out for full scale conditions, necessitating scaling of the experimental results. The following scale factor was applicable for the American Challenger model (full scale length is 530 feet):

$$\frac{L_s}{L_m} = 30.189 \ ,$$

and for the SL-7 (full scale length 900 feet):

$$\frac{L_s}{L_m} = 55.01 \ .$$

The American Challenger had not been fitted with bilge keels, while the SL-7 had bilge keels during most of the model runs.

The usage of unidirectional seas in the simulations may be justified by the narrow spreading of the wave energy which was observed in most of the experiments. Simulations have been carried out for both capsize and non-capsize conditions. The loading condition of the American Challenger, considered in all verification simulations, was heavy (fully loaded); for the SL-7 both light and heavy conditions were considered. The waves were assumed to be unidirectional, the phases of the components were chosen randomly out of a uniform distribution, the wave energy was assumed to be distributed over equal intervals, and the frequencies were chosen randomly within each interval. The maximum number of wave components used in the simulations was N = 10, and the range of frequencies considered was taken as follows:

$$0.7\sigma_p \leq \sigma \leq 2.1\sigma_p \ ,$$

where σ_p is the peak frequency of the wave elevation spectrum.

(i) <u>American Challenger in Beam Seas.</u>

This case corresponds to Run 8.04 on 10 September 1971, which has been reported by Haddara *et al.* (1972) and Kastner (1973). The full scale initial metacentric height was GM = 1.77 ft (resulting in a natural roll frequency

of σ_θ = 0.28 rad/s), and the still water Froude number Fn = 0.17. No capsizing occurred during this experimental run, and the objective of this investigation was to compare the computed roll and pitch responses with the measured values, so as to obtain information on the predicted response in random waves.

Simulations were performed with N = 10 wave components for a duration of 300 seconds, using the full scale values for the observed wave heights and frequencies. The wave direction was assumed to be δ = 90° for all wave components. A summary of the simulation and experimental results is given below, where η_{RMS} denotes the root mean square value of the observed wave elevation.

σ_p	η_{RMS}	Roll (°)				Yaw (°)			
		Mean		RMS		Mean		RMS	
(rad/s)	(ft)	Exp.	N=10	Exp.	N=10	Exp.	N=10	Exp.	N=10
0.43	10.6	3.1	2.0	7.3	9.2	6.9	5.2	2.8	4.1

Pitch (°)			
Mean		RMS	
Exp.	N=10	Exp.	N=10
0.7	0.5	1.4	1.7

It is seen that the agreement between experimental and simulation results is reasonable for the mean and RMS values of the motions. The RMS roll amplitudes were overpredicted by approximately 25 %, which is possibly due to underprediction of the viscous roll damping coefficients.

(ii) American Challenger in Quartering Seas.

Simulations were carried out for the conditions corresponding to Run 8.03 on 10 September 1971, which has been reported by Haddara *et al.* (1971) and Kastner (1973). No capsizing occurred during this experimental run, and the objective of the simulation was to compare the predicted roll, yaw and pitch motions with experimental values. In the simulation 10 representative wave components were used, the wave direction was taken be $\delta = 35°$, the Froude number Fn = 0.17, and GM = 0.56 ft. The simulation was carried out for 300 seconds. The general results are summarized below for both the mean and RMS values.

σ_p	η_{RMS}	Roll (°)				Yaw (°)			
		Mean		RMS		Mean		RMS	
(rad/s)	(ft)	Exp.	N=10	Exp.	N=10	Exp.	N=10	Exp.	N=10
0.43	10.5	-1.4	-0.9	9.6	10.7	4.4	3.1	2.9	7.1

Pitch (°)			
Mean		RMS	
Exp.	N=10	Exp.	N=10
0.5	0.8	2.0	2.3

From the above summary it appears that the predicted roll, yaw and pitch responses are reasonably close to the measured values, except for the RMS yaw response. The vessel was predicted to yaw more severely than actually was the case in the experiments, which might be due to incorrect modelling of the maneuvering or rudder forces, for example. Roll amplitudes were slightly overpredicted, possibly because of underestimating the roll damping coefficients.

(iii) American Challenger in Following Seas.

Simulations were carried out for the conditions corresponding to Run 12.03 on 16 September 1971, which has been reported by Haddara *et al.* (1971) and Kastner (1973). This experimental run resulted in a capsize due to low cycle resonance, and is the one for which the motion records are shown in Figure 4.9. The initial metacentric height was GM = 0.56 ft, and the natural roll frequency was σ_θ = 0.17 rad/s. In the simulation three representative wave components were used to determine whether any kind of parametric excitation would occur, the wave direction was taken as $\delta = 0°$, the Froude number Fn = 0.22, and the vessel was given a small initial roll angle. A capsize was predicted to occur due to low cycle resonance after 275 seconds. The general results are summarized below, and the simulated motion records are presented in Figure 4.10. The roll moment components acting on the vessel up to the point of capsize are shown in Figure 4.11.

σ_p	η_{RMS}	RMS Roll (°)		RMS Pitch (°)	
(rad/s)	(ft)	Exper.	N=3	Exper.	N=3
0.47	8.4	13.21	15.04	2.36	2.42

From the above summary it appears that the RMS values of the roll and pitch responses are reasonably close to the measured values, and that the predicted motion behavior (see Figure 4.10) is similar to the experimentally observed behavior shown in Figure 4.9. Certain similarities between Figures 4.9 and 4.10 are quite clear, such as the roll amplitudes of the low cycle resonance being dependent on the passage of a wave group. From Figure 4.11 it is seen that the hydrostatic restoring moment is the dominant component, and that it varies with a frequency that is not equal to the encounter frequency. However, this behavior can be explained by the time dependence of the righting arm, or GZ, curve: the GM value for this vessel is low, so that in the crest of a wave, having a

length of the order of the ship length, the righting arm can become negative at small angles of heel. This can lead to parametric excitation at the resonance frequency. When the roll restoring moment record is compared with the roll motion record in Figure 4.10, it appears that as the vessel leans to starboard (positive roll angle), the righting moment is negative until the wave crest passes the midship area, at which point the righting arm is significantly reduced and becomes almost zero. The behavior is similar when the vessel leans to port and a wave crest moves by. From Figure 4.11 it appears that the hydrostatic moment can be represented by the summation of a slowly varying component, having a frequency equal to the natural roll frequency, and a fast varying component that has a frequency of approximately three times the roll frequency, which may result from parametric excitation and subharmonic resonance. More attention is paid to this behavior in Chapter 7. To illustrate the variation of the righting arm during the passage of a wave, the righting moment curves are shown in Figure 4.12 for the American Challenger and Mariner vessels used in the San Francisco Bay experiments. The curves are based on computations performed for following sea conditions, where the wave length is equal to the ship length, and have been taken from Fallon *et al.* (1980).

(iv) SL-7 in Quartering Seas.

Simulations were carried out for the conditions corresponding to Run 4.02 on 10 August 1973, which has been reported by Chou *et al.* (1974). No capsizing occurred during this experimental run, and the objective of the simulation was to compare the predicted roll, yaw and pitch motions with experimental values. In the simulation 10 representative wave components were used, the wave direction was taken be $\delta = 40°$, the Froude number Fn = 0.26, and GM = 2.54 ft for the lightly loaded condition. The simulation was carried out for 300 seconds. The general results are summarized below for both the mean and RMS values.

σ_p	η_{RMS}	Roll (°)				Yaw (°)			
		Mean		RMS		Mean		RMS	
(rad/s)	(ft)	Exp.	N=10	Exp.	N=10	Exp.	N=10	Exp.	N=10
0.34	15.0	5.3	0.5	11.8	16.0	14.7	3.5	7.9	5.9

Pitch (°)			
Mean		RMS	
Exp.	N=10	Exp.	N=10
0.7	0.0	1.5	2.3

From the above summary it is seen that the predicted mean roll and yaw angles are significantly smaller than the experimental values, and that the RMS roll angle is overpredicted by 25 %, while the RMS yaw angle is underpredicted by 25 %. The predicted pitch angles show the same tendency as the predicted roll angles, i.e., underpredicted mean and overpredicted RMS values.

(v) SL-7 in Head Seas.

Simulations were carried out for the conditions corresponding to Run 30.05 on 10 May 1974, which has been reported by Chou *et al.* (1974). No capsizing occurred during this experimental run, and the objective of the simulation was to compare the predicted roll, yaw and pitch motions, as well as forward speed, with experimental values. In the simulation 10 representative wave components were used, the wave direction was taken be $\delta = 175°$, the Froude number Fn = 0.27, and GM = 2.08 ft for the heavy condition. The simulation was carried out for 300 seconds. The general results are summarized below for both the mean and RMS values.

σ_p	η_{RMS}	Roll (°)				Yaw (°)			
		Mean		RMS		Mean		RMS	
(rad/s)	(ft)	Exp.	N=10	Exp.	N=10	Exp.	N=10	Exp.	N=10
0.40	13.2	3.8	0.0	2.0	3.6	-0.2	-1.6	3.0	0.9
		Speed (ft/s)				Pitch (°)			
		Mean		RMS		Mean		RMS	
		Exp.	N=10	Exp.	N=10	Exp.	N=10	Exp.	N=10
		37.5	26.6	3.0	6.9	1.4	0.3	2.2	2.5

From the above summary it is seen that the predicted mean roll and pitch angles are smaller than the experimental values, and that the RMS roll angle is overpredicted significantly (although still of the same order of magnitude as the experimental value), while the RMS yaw angle is underpredicted. It is noted that the measured mean value for roll (3.8°) seems too large for pure head sea conditions; it could have been caused by wind or waves from a significantly different direction (due to lack of data, such discrepancies cannot be solved by simulation). This was one of the few experiments where speed measurements were made, and the simulation shows that the predicted mean decrease in forward speed is significantly larger than was observed in the experiment. This suggests that, at least for severe head sea conditions, either the wave-induced resistance is overpredicted or the thrust increase (due to a speed decrease) underpredicted. As discussed in Chapter 2, integration of the Froude-Krylov forces over the instantaneous wetted surface may result in a time-independent drift force. The scattering of the incoming waves by the vessel, should also contribute to the mean resistance in a positive or negative sense, whereas the diffraction forces are based on pure linear theory in the present model. It can be argued that particularly in head sea conditions, with high frequencies of encounter, higher order diffraction effects should be accounted for, so that the present model may

not yield reliable results with respect to the forward speed behavior in severe head seas.

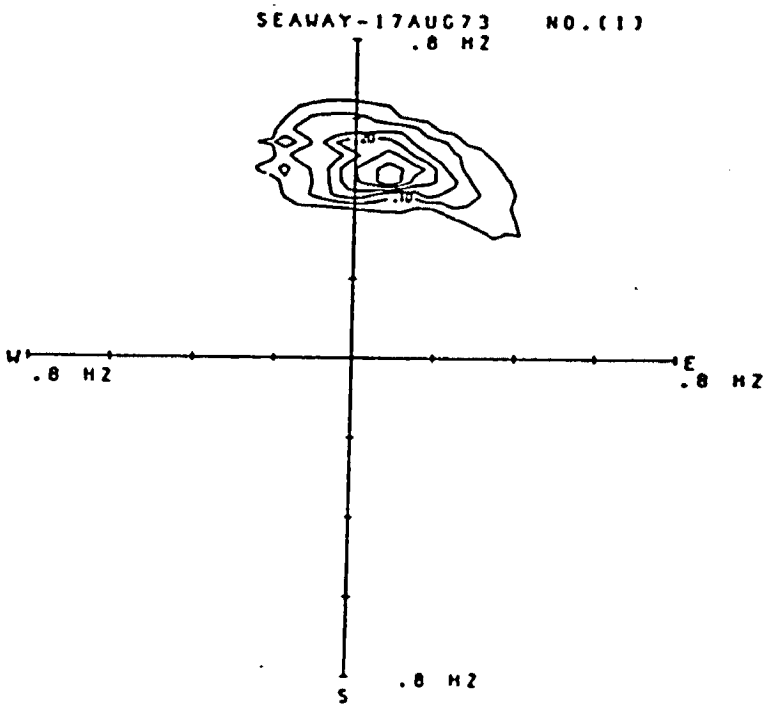

Figure 4.8. Typical Directional Wave Spectrum Obtained during San Francisco Bay Experiments, from Chou et al. (1972).

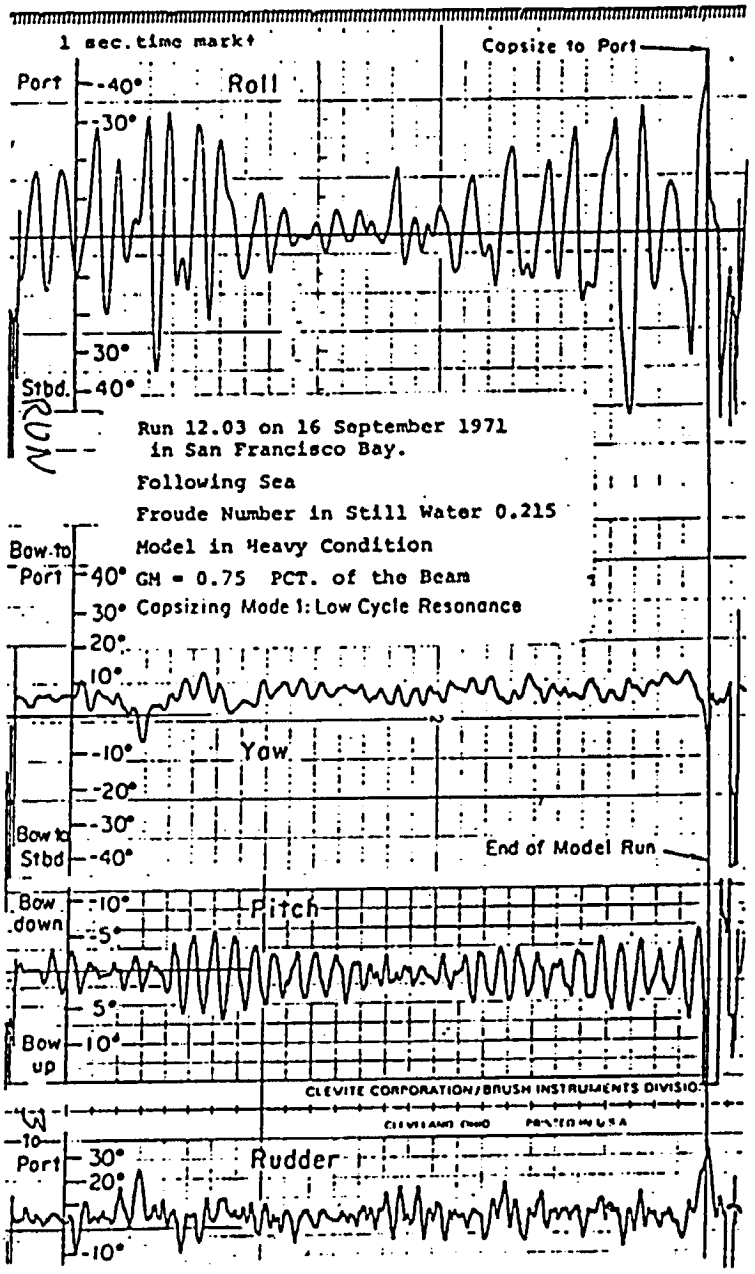

Figure 4.9. Typical Time Histories of Capsize Sequence of American Challenger Vessel Recorded on San Francisco Bay, from Haddara et al. (1972).

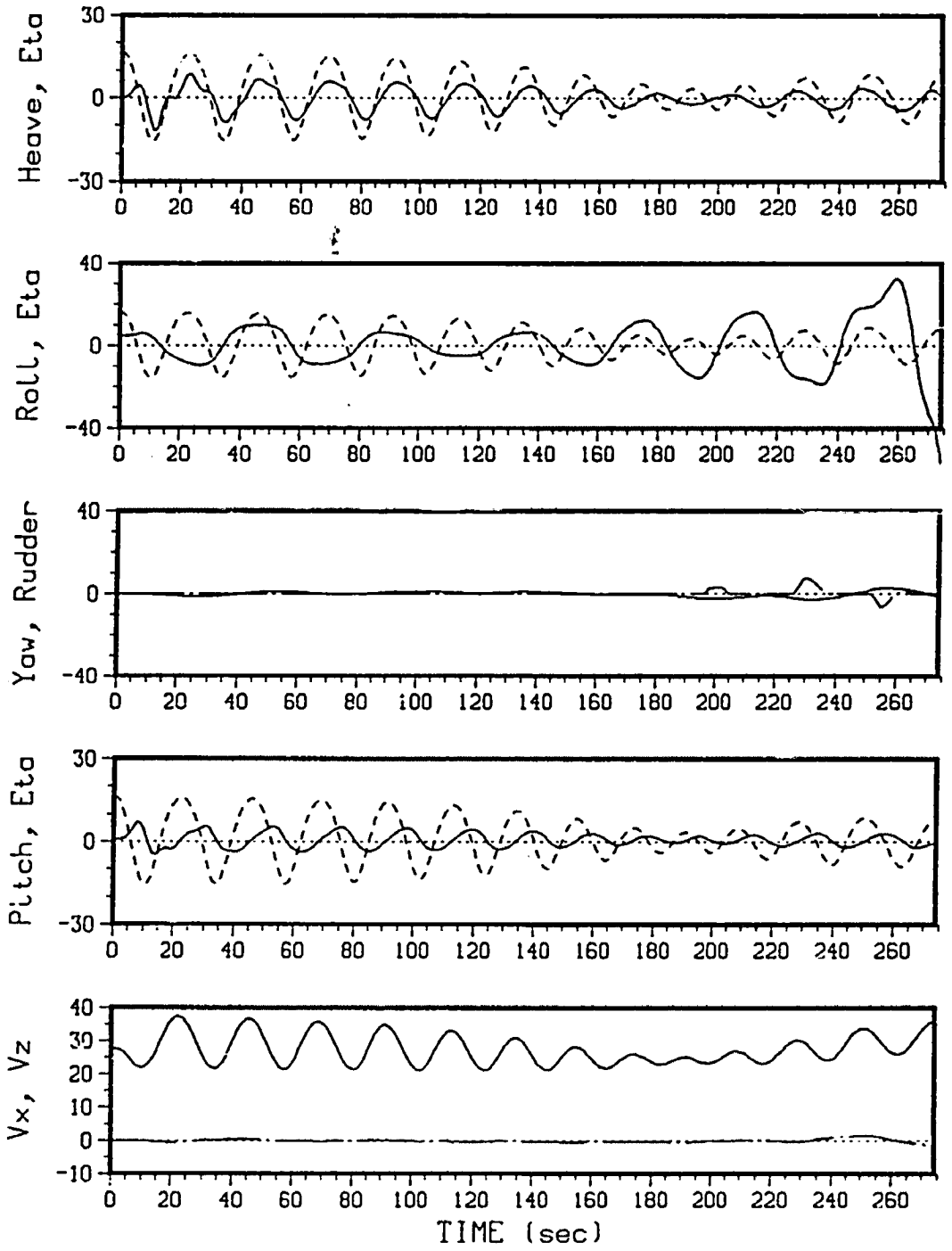

Figure 4.10. Capsize Simulation of American Challenger Vessel in Irregular, Following Seas for Comparison with Experimental Results (see Figure 4.9). The dashed lines refer to the wave elevation at the C.G. Displacements are in feet, angles in degrees, and velocities in ft/s.

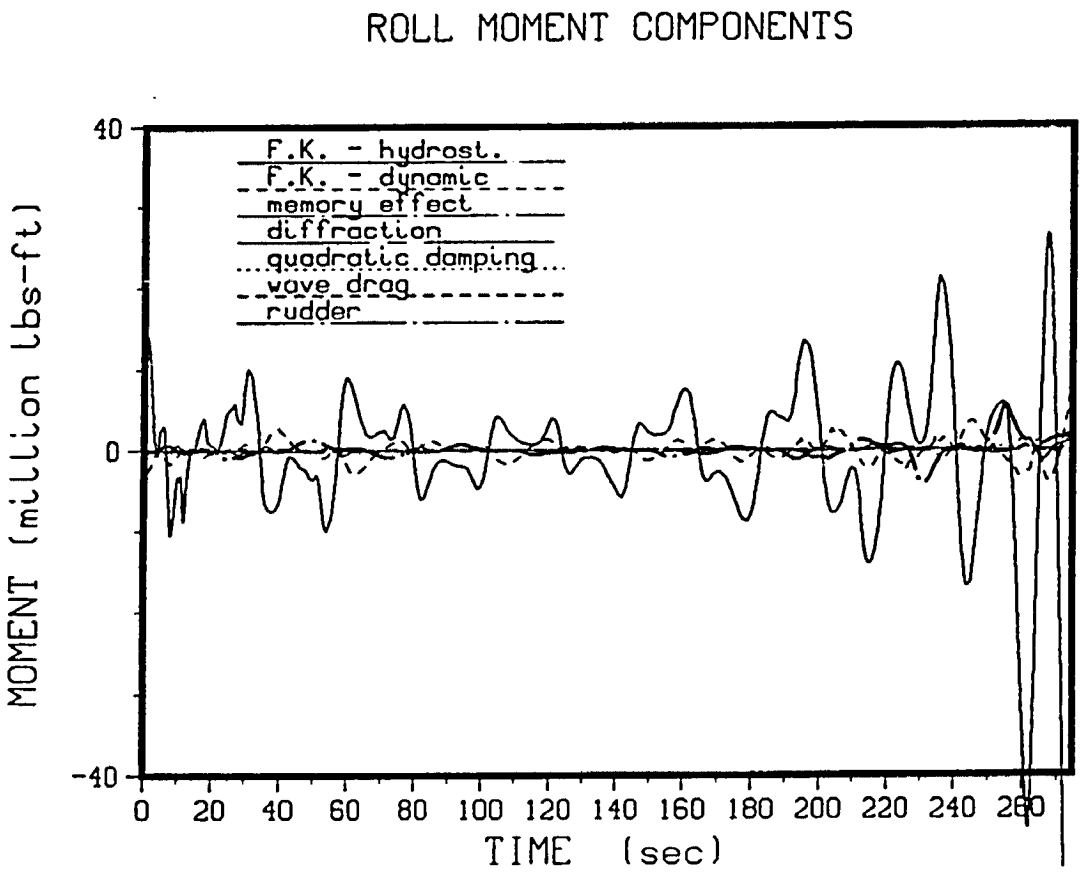

Figure 4.11. Roll Moment Components Associated with Capsize Simulation of American Challenger in Following Seas Shown in Figure 4.10.

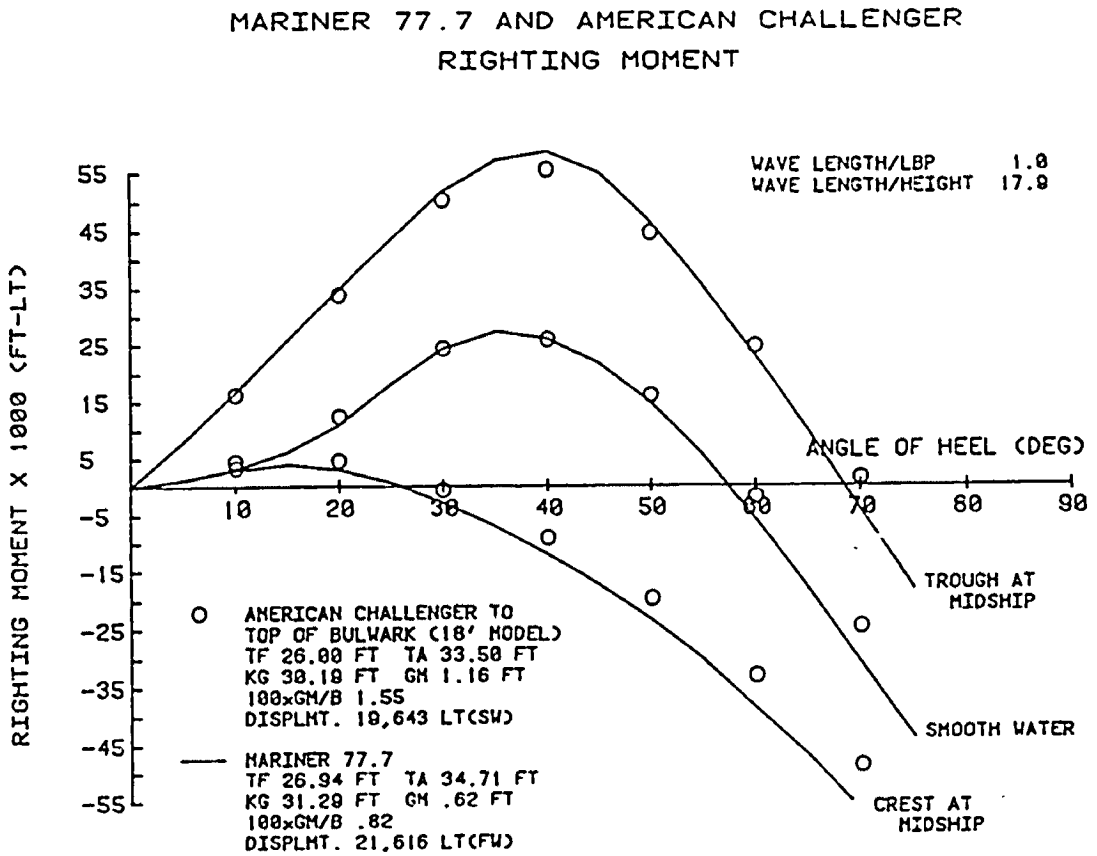

Figure 4.12. Typical Righting Moment Curves in a Longitudinal Wave for American Challenger and Mariner from Fallon et al. (1980).

CHAPTER 5

Response Sensitivity to Changes in Force Components

The theory described in Chapter 2 is an attempt to model the excitation and response of a floating structure in waves in a realistic manner. Obviously, quite a large number of simplifying assumptions were made to avoid certain theoretical complexities and to keep the CPU time of the mainframe computer within reasonable limits. Not knowing how closely the model represents the physical world, something that is hard to assess quantitatively even with the aid of experimental data, it is useful to determine the relative importance of the various theoretical components influencing the simulated motion behavior.

The question arises as to which theoretical components and which response modes should be investigated. In view of the overall objective of this work all six degrees of motion freedom must be modelled, and the most important aspect is the study of large amplitude motions. In normal operating conditions roll is often the most important response mode, and in survival conditions in which capsizing may occur, roll is of course the critical mode of motion. Thus, the aim is to determine the sensitivity of the roll response to changes in various components under identical conditions. The components that must be varied are those bearing a significant influence in the equations of motion, i.e., the components contributing to the total forces and moments. Each force component can be varied separately, and the influence of each individual change can be assessed. Obviously, the systematic variation of the force components can be done only within the framework of the present theory, and for a limited number of both wave and ship related conditions.

The sensitivity of the roll response is investigated quantitatively as follows. For a vessel of given configuration, i.e., fixed geometry and center of gravity, each of the force components is increased by a certain percentage throughout the time simulation process, while the other components remain unchanged. All force and moment components are multiplied with a coefficient that can be varied, so that the components of the total,

generalized force vector (on the right hand side of the equations of motion, as given in Chapter 3.1) are given by

$$f^i_{tot}(t) = \sum_{m=1}^{M} c_m . f^i_m(t) , \quad i = 1,...,6 \quad ,$$

where M is the total number of force components, and if, for example, the force components are varied by 10%, the coefficients c_m are defined as

$$\begin{aligned} c_m &= 1 \text{ for all m, except for } m = m_s \\ &= 1.10 \text{ for } m = m_s, \end{aligned}$$

where m_s refers to the component of which the sensitivity is being investigated. Let θ_0 be the roll amplitude that would be obtained for the normal case, where $c_m = 1$ for all m, and let θ be the roll amplitude due to a change in the force components. Then the response sensitivity, S_θ, is defined as the ratio of the proportional change in the roll angle to the change in the force component:

$$S_\theta = \frac{(\theta - \theta_0)/\theta_0}{c_{m_s} - 1} \quad .$$

Using this definition, the larger the absolute value of S_θ is for a given variation of a force component, the more sensitive the roll motion is to that force component. In the following the sensitivity is investigated of the roll response to changes in the force components for the American Challenger, SL-7 and Series 60 vessels. Although roll is the only degree of freedom considered in the sensitivity analysis, the change in the force components, c_m, applies to all six degrees of freedom simultaneously. The roll sensitivity has been determined for the case of three degrees of freedom to investigate the sensitivity in following seas, corresponding to some of the experiments carried out with the SL-7 model. One should keep in mind that the results are applicable only to the specific conditions considered, as it is very likely that the roll sensitivity, or the local slope of

the roll response with respect to the parameter varied, will not be the same for different wave heights, frequencies, loading conditions, etc.

In the subsequent sensitivity analyses wind loading has not been considered; the effects of wind on the capsizing behavior are investigated in Chapter 7. The sensitivity of roll is studied for moderate to severe sea conditions, where the wave height is of the order of 20 to 30 feet and roll amplitudes vary between 15 and 30 degrees. In general it was found that none of the parameters varied were consistently negligible, and that in resonant conditions ,especially, the sensitivity can be quite large to force changes. The hydrostatic (or static Froude-Krylov) forces were always predominant as regards roll sensitivity.

The following force components and coefficients were varied:

- $f_{FK,h}$: static Froude-Krylov force;
- $f_{FK,d}$: dynamic Froude-Krylov force;
- $f_{radiation}$: wave radiation forces consisting of memory effect integrals and added mass inertia terms;
- $B_{44,L}$: linear roll damping coefficient;
- $B_{44,Q}$: quadratic roll damping coefficient;
- $B_{43,Q}$: quadratic sway-into-roll coupling coefficient;
- f_{man}: viscous maneuvering forces;
- f_{rudder}: rudder lift and drag forces;
- $f_{drag,w}$: viscous wave-induced drag forces.

Roll Sensitivity in Beam Seas

The sensitivity of the roll response is first considered for severe, regular beam seas. Simulations were carried out for approximately 20 cycles after steady state conditions had been reached. The following general particulars were adhered to for the American Challenger vessel:

- L_{BP} = 530 ft, B = 75 ft, d = 29.75 ft
- C_B = 0.58

- no bilge keel
- GM = 0.0236xB
- Fn = 0.17;

and for the Series 60 vessel the particulars were as follows:

- L_{BP} = 400 ft, B = 57.14 ft, d = 22.86 ft
- C_B = 0.70
- with bilge keel (width = 0.004xL)
- GM = 0.05xB
- Fn = 0.10 .

The results are presented in nondimensional form in terms of the coefficient S_θ in Table 5.1, followed by a discussion.

Force Compon.	American Challenger		Series 60	
	$\sigma = \sigma_\theta$	$\sigma = 1.5\sigma_\theta$	$\sigma = \sigma_\theta$	$\sigma = 1.5\sigma_\theta$
$f_{FK,h}$	-5.526	4.785	1.726	1.532
$f_{FK,d}$	-0.828	-2.045	-1.343	--1.459
$f_{radiation}$	0.532	0.017	0.314	-0.744
$f_{diffraction}$	2.545	0.226	0.198	0.390
$B_{44,L}$	-0.176	-0.023	-0.020	0.047
$B_{44,Q}$	-3.420	-0.009	-0.403	-0.147
$B_{43,Q}$	0.224	-0.135	0.189	-0.230
f_{man}	-1.049	0.069	-0.145	0.785
f_{rudder}	0.909	0.181	-0.018	0.004
$f_{drag,w}$	-0.524	0.578	0.136	0.154

Table 5.1. Roll Sensitivity, S_θ in Beam Sea Conditions (6 d.o.f.)

From the table above several similarities pertaining to the roll sensitivity of the two ship types can be observed. For the beam sea conditions considered, both ships are sensitive to changes in the static and dynamic Froude-Krylov forces. The American Challenger was found to be most sensitive to the hydrostatic forces in resonant and nonresonant conditions, while for the Series 60 vessel the sensitivity to the static and dynamic Froude-Krylov forces was about the same. The dependence on these forces can be attributed to both the hydrostatic and dynamic Froude-Krylov roll moments being relatively large and of the same order of magnitude (in beam seas). For both vessels the sensitivity to the diffraction forces is quite significant, especially so for the American Challenger in resonant conditions. The radiation forces also can be significant; for the Series 60 the sensitivity to those forces is higher than to the diffraction forces. Obviously, the location of the center of gravity (KG) has an important bearing on the sensitivity behavior, however, this variable has not been included in the analysis.

The sensitivity to changes in the viscous damping coefficients indicates that changes in the quadratic damping coefficient affect the roll behavior more than is the case for the linear damping coefficients. This is most likely due to the severity of the sea state used in the computations, which resulted in relatively large roll amplitudes and velocities, and the eddy damping is assumed to be increasing as the square of the velocity. It is noted that for small wave amplitudes, and therefore small roll angles, the reverse seems to be the case: the sensitivity to linear damping predominates when the roll velocities are small. The American Challenger is more sensitive to quadratic roll damping than the Series 60 vessel, which may be related to the presence of the bilge keel for the Series 60, causing it to be more heavily damped, and hence not as sensitive. The Series 60 vessel was found to be more sensitive to the viscous maneuvering forces for nonresonant conditions than the American Challenger, while the opposite was observed for resonant conditions. Changes to the rudder forces had an important bearing on the roll behavior of the American Challenger, and had hardly any influence on the Series 60. The sensitivity to the wave-induced drag forces was significant for both vessels, particularly or the American Challenger.

Roll Sensitivity in Following Seas

The roll motion of a vessel travelling in following seas can be of importance when autoparametric resonance conditions occur. A sensitivity analysis has been carried out to highlight some of the differences in roll sensitivity with respect to beam sea conditions. The sensitivity of the roll response of the SL-7 vessel is shown in Table 5.2 for the three degree of freedom case, and in Table 5.3 for the six degree of freedom case for both the SL-7 and American Challenger vessels. A number of simulations were carried out for severe sea conditions for which autoparametric resonance would occur, i.e., where the encountered wave frequency is equal to approximately twice the natural roll frequency. The total duration of the simulations was 300 seconds and the sensitivity coefficients were based on the computed RMS values of the roll response. The following conditions were used for the SL-7:

- L_{BP} = 900 ft, B = 105.5 ft, d = 38.9 ft
- C_B = 0.56
- GM = 0.0167xB
- F_n = 0.072,

and for the American Challenger:

- L_{BP} = 530 ft, B = 75 ft, d = 29.75 ft
- C_B = 0.58
- with bilge keel
- GM = 0.0236xB
- F_n = 0.08 .

The results shown in Table 5.2 are based on the same conditions pertaining to the comparison in Chapter 4.3 with experimental results for the SL-7 model, as shown in Figure 4.5. In the simulations only heave, roll and pitch motions were allowed, and the ship speed was kept constant. Since in this case the roll motion is highly nonlinear, it was

deemed of interest to perform the sensitivity analysis for small and severe wave amplitude conditions, where the small amplitude was equal to 15% of the large amplitude.

Force Components	SL-7 $\sigma^e = 2\sigma_\theta$ (small ampl.)	SL-7 $\sigma^e = 2\sigma_\theta$ (large ampl.)
$f_{FK,h}$	-0.349	-1.848
$f_{FK,d}$	-0.003	0.075
$f_{radiation}$	0.081	0.075
$f_{diffraction}$	0.004	-0.003
$B_{44,L}$	-0.158	-0.051
$B_{44,Q}$	-0.358	-0.160
$B_{43,Q}$	-	-
f_{man}	-	-
f_{rudder}	-0.030	-0.004
$f_{drag,w}$	-	-

Table 5.2. Roll Sensitivity, S_θ in Following Sea Conditions (3 d.o.f.)

From Table 5.2 it is seen that the roll sensitivity of the SL-7 exhibits quite different behavior compared with the beam sea cases. For both the small and large amplitude case the roll motion is most sensitive to changes in the hydrostatic forces, where in the large amplitude case this sensitivity is very pronounced. If the roll response were linear, the sensitivity results would be the same for both the small and large wave amplitude case; here, the motion is clearly nonlinear. Since autoparametric resonance typically occurs in following sea conditions, the motion instability results from the time-varying hydrostatic restoring moment in crests and troughs, so that the roll motion can be expected to be sensitive to changes in the hydrostatic forces. For the small amplitude case the sensitivity to

the hydrostatic forces and quadratic damping moment is the same. It is interesting that the roll sensitivity to the viscous damping moments is larger (by a factor 2) for the small amplitude conditions. For both cases the sensitivity to the diffraction forces is very small, as would be expected for following sea conditions. The roll motion is sensitive to the wave radiation forces, but to a much smaller extent than is the case for the hydrostatic forces, which is possibly due to the low roll frequency at which there is little wave disturbance. This sensitivity is approximately the same for the small and large amplitude case. It is noted that the sensitivity to the radiation forces depends on how the memory effect moments are resolved: as has been mentioned in Chapter 2.1.2, the moments acting along the vessel's axes can be taken as the ones computed for the equilibrium system, or the equilibrium moments can be resolved along the ship axes taking into account the angles of rotation. Maybe neither of these options is the correct one, however, it was found that for most conditions the former approach yielded more reasonable results than the latter; the latter approach resulted in a much higher sensitivity to the radiation forces, and would also tend to cause ship steering problems because of high induced yaw moments.

Of interest also is that the roll motion is not sensitive to the dynamic Froude-Krylov forces. This is contrary to what one would expect it should be, as in following seas with low encounter frequencies the Froude-Krylov forces should predominate. It should be mentioned here that the heave and pitch motions were found to be quite sensitive to these forces (both S_{x2} and S_{ψ} were equal to approximately -0.2 due to changes in $f_{FK,d}$). If we examine the expressions for the dynamic Froude-Krylov forces, it is clear that in pure following seas the vertical force and roll moment are dependent only on the integration of the vertical dynamic pressure gradient, $\partial p_D/\partial y$, over the wetted volume. In beam seas the roll moment would depend on $\partial p_D/\partial x$ and $\partial p_D/\partial y$. From Appendix A it is seen that

$$p_D = \rho A g . e^{ky} . \cos(kx - \sigma t + \varepsilon) \ ,$$

so that

$$\frac{\partial p_D}{\partial y} = k.\rho Ag.e^{ky}.\cos(kx - \sigma t + \varepsilon) .$$

The above shows that the $\partial p_D/\partial y$ term is in phase with the wave elevation, i.e., in phase with the static restoring forces. Computations show that the magnitude of the dynamic Froude-Krylov moment is considerably smaller than the hydrostatic moment. In view of the foregoing it is not surprising that the roll motion is not very sensitive to the dynamic Froude-Krylov forces. Although the heave and pitch motions are sensitive to those forces, they do not apparently affect the roll behavior significantly. The hydrostatic heave force to which the sensitivity factors were applied, is in fact the change in hydrostatic force compared with the equilibrium condition (see Chapter 2.1.1.), so that its magnitude tends to be of the same order as the dynamic Froude-Krylov part. For this reason the sensitivity of the heave motion to changes in the static and dynamic Froude-Krylov forces is approximately the same.

In Table 5.3 the roll sensitivity is shown for the 6 degrees of freedom case, where the SL-7 vessel is steered by the autopilot. Two conditions were considered: autoparametric resonance and nonresonance conditions. Also sensitivity results are shown for the American Challenger vessel, which was subjected to a regular wave somewhat shorter than its length (but still resulting in parametric resonance). An additional force component was considered here: f_{surge}, which represents the total surge force, in order to determine the importance of modelling the forward motion.

Force Components	SL-7		American Ch.
	$\sigma^e = 1.7\sigma_\theta$	$\sigma^e = 2\sigma_\theta$	$\sigma^e = 1.9\sigma_\theta$
$f_{FK,h}$	0.154	-1.258	3.762
$f_{FK,d}$	0.047	0.038	-0.313
$f_{radiation}$	-0.018	0.002	-0.022
$f_{diffraction}$	0.002	0.006	0.0
$B_{44,L}$	-0.087	-0.026	-1.828
$B_{44,Q}$	-0.107	-0.136	-1.109
$B_{43,Q}$	-0.019	0.0	-0.021
$f_{maneuver}$	0.010	0.004	0.106
f_{rudder}	-0.037	0.032	-0.034
$f_{drag,w}$	0.0	0.0	0.018
f_{surge}	-0.026	0.004	0.340

Table 5.3 Roll Sensitivity, S_θ in Following Sea Conditions (6 d.o.f.)

From Tables 5.2 and 5.3 it is seen that there are many similarities between the 3 and 6 degrees of freedom cases that were considered for the SL-7. The main difference lies in the sensitivity to the radiation forces: for the 6 d.o.f. case this sensitivity is considerably less than for the 3 d.o.f. case. For the nonresonant case (where autoparametric excitation does not occur) the sensitivity to the hydrostatic forces is significant, but to a much smaller extent than for the resonant case; also the roll motion is more sensitive to the surge force in the nonresonant case.

For the American Challenger most trends are similar to those of the Sl-7 in parametric resonance conditions: sensitivity to the hydrostatic restoring forces is highest, followed by the viscous damping forces, while radiation and diffraction forces do not play an important role. It is seen that in this case almost all sensitivity levels are significantly higher than for the SL-7. The following differences with the SL-7 sensitivity behavior are observed: sensitivity to linear roll damping changes is larger than to

quadratic roll damping changes, and the sensitivity to the maneuvering forces is higher. Also it appears that the American Challenger is more sensitive to changes in the surge force, i.e., more sensitive to its position with respect to the wave than is the case for the SL-7. This may be due to the differences in length between the vessels, and wave conditions considered.

In conclusion, these sensitivity analyses suggest that the assumptions made in the theoretical model, presented in Chapter 2, are not very critical with respect to the roll behavior of the vessels considered. This applies to roll angles of moderate amplitude (±25°) in severe wave conditions. The critical features of the theory are those that are based solely on linear ship motion theory, which are the wave radiation and diffraction forces. In following seas these were found to be unimportant, while in beam seas they were significant, although not quite as significant as the Froude-Krylov forces. The sensitivity results suggest that the most critical features are modelled appropriately; here, we refer to one of the premises in this work, stating that the Froude-Krylov forces are important and should be evaluated in an exact fashion. Since those forces were found to be consistently significant, this assumption seems justified. Of course, this does not provide a conclusive argument that the present theory is adequate for analyzing large amplitude ship motions, but the results from Chapter 4 and 5 do suggest that the present theory models the wave-induced ship motions realistically.

If theoretical improvements were to be made, the sensitivity analysis results point to a number of areas. The results indicate that hydrostatic effects are always of importance (and this is corroborated by results from Chapter 7), so that better results may be obtained by modelling the exact free surface around the hull, whereby diffraction and wave radiation effects should be considered. Also various viscous force components can be of importance, depending on the conditions, which may warrant further effort into determining those forces more rationally.

CHAPTER 6

Numerical Simulations for Random Following Seas

The apparent behavior of a random seaway for following or quartering conditions has not received much attention, and is therefore considered next in some detail. Moreover, these conditions can be very critical with respect to large amplitude roll motions and capsizing. Wave characteristics observed in a stationary and moving reference frame, at a point and along the length of the vessel, are presented in Chapter 6.1. In Chapter 2.4.4 it was found that when an observer moves at an angle with random waves, the mean square value of the wave process as observed from the moving point can be different from the one at a stationary point. Simulations have been carried out to investigate the statistical behavior of the observed wave process for following sea conditions, results of which are shown also in Chapter 6.1. In Chapter 6.2 ship responses are investigated for irregular, following sea conditions. A procedure to simplify the random seaway by using a two-component wave system, has been outlined in Chapter 6.3

6.1. Wave Characteristics Encountered at Fixed and Moving Points

In the next two sections, attention is paid to the physical and statistical properties of waves observed from a moving reference point, and comparisons are made with observed behavior at a point fixed in space.

6.1.1. Wave Elevation Records

When an observer moves in the same direction as the waves in a random sea, there are a number of interesting features that do not appear in head sea conditions, for example. One aspect is that at certain speeds the observed waves seem to be purely sinusoidal for a prolonged period of time. This has been observed experimentally, and can also be shown by simulation. In the simulations the observed wave elevations were computed for different speeds of the observer: zero speed, i.e., fixed

location, and three speeds that are fractions of the mean group speed, $C_{g,p}$. The mean group speed is defined as in Chapter 2.4.3:

$$C_{g,p} = \frac{g}{2.\sigma_p} ,$$

where σ_p is the peak frequency associated with the sea spectrum (assuming, as usual, that the wave energy is concentrated around one frequency only). The observed wave elevation was determined using the superposition model discussed in Chapter 2.4:

$$\eta(t) = \sum_{i=1}^{N} A_i \cos\{(k_i U - \sigma_i)t + \varepsilon_i\} ,$$

where the individual wave amplitudes were obtained deterministically as a function of the spectral density and frequency interval (constant), and the phases ε_i were chosen randomly out of a uniform distribution. Also the frequencies were chosen randomly within each interval.

The spectral shape was assumed to be given by the Bretschneider formulation, and the following characteristics were used:

- H_s = significant wave height = 24 ft
- σ_p = (1) 0.50 rad/s and (2) 0.62 rad/s .

The peak frequency of 0.62 rad/s corresponds to a wave length equal to that of the American Challenger vessel (530 ft). For these sea states the mean group speeds are

(1) $C_{g,p}$ = 32.17 ft/s for σ_p = 0.50 rad/s, and
(2) $C_{g,p}$ = 25.94 ft/s for σ_p = 0.62 rad/s.

The number of frequencies used in the simulations was N = 1200, and the frequency range was determined by a lower and upper bound, σ^e_{min} =

$0.5x\sigma_p$, and $\sigma^e_{max} = 2.5x\sigma_p$, respectively. Simulations were carried out for a total (full scale time) period of 1000 s and a sampling interval of $\Delta t = 2$ s. In Figure 6.1 the observed wave elevations are shown for sea state (1). For the zero speed case the wave elevation looks random, and some wave groups can be discerned. The observed wave periods, as well as the length of wave groups, appear to become larger with increasing speed, i.e., the observed frequency range becomes narrower. Let us consider the case where the speed of the observer equals the mean group speed, and investigate the behavior of the observed sea surface. For example, the observer would be subjected to very small amplitude waves between t = 300 and t = 350 s, and to a wave group consisting of large amplitude, regular waves from t = 925 s to t = 975 s. It is tempting to argue that, under such conditions, the irregular sea can be replaced by a single sine wave yielding the same characteristics as those observed in Figure 6.1, for purposes of ship motion simulation. That is, one could chose a certain frequency, amplitude and duration, which would result in the same apparent behavior as observed from a *point* moving in a random, following sea. This procedure would simplify ship motion analyses considerably.

The observed wave behavior may appear to be regular to a moving point as a function of time only. However, at each time instant, the irregular sea surface would be always irregular in physical space, regardless of speed. Thus, for any forward speed and at any time, the wave elevation profile along the length of a ship would be irregular, although the basic characteristics would change slowly with time when the vessel moves with the random waves. This is of significance, because ship motions tend to be dominated to a large extent by hydrostatic effects (see e.g. Chapters 5 and 7), which are very dependent on the actual shape of the free surface. In order to illustrate these remarks, the imaginary wave profiles, as would be observed along the center line of a ship of 530 ft length when travelling at the mean group speed, have been plotted in Figure 6.2 and 6.3 for a number of consecutive time steps. The images shown in these figures, correspond to the case where the sea conditions are the same as in Figure 6.1, for which the observed wave elevation records would be those observed at the midship section of the vessel. The

profiles in Figure 6.2, from top to bottom, are associated with the time period from t = 935 s to t = 975 s (large, regular elevation changes amidships), with an interval of 4 s. The profiles in Figure 6.3 are associated with the time period from t = 310 s to t = 350 s (small elevation changes amidships), also with an interval of 4 s.

The following convention has been applied for the station numbers in the wave profile plots:

0 -- aft perpendicular
5 -- midships
10 -- forward perpendicular.

In Figure 6.2 the propagation of the dominant waves along the ship can be seen clearly. Obviously, a single sine wave would not be representative of the waves actually encountered by the vessel, although it might be possible to obtain a similar result by using only a few components. From Figure 6.3 it is seen that, for the time period considered, the observed behavior amidships (small wave elevations) is indeed representative of the the sea surface behavior all along the vessel.

Wave profile plots similar to the ones discussed above were obtained for case (2), where the length of the dominant waves is approximately equal to the ship length. The wave elevation records, observed from amidships at different speeds, are shown in Figure 6.4. It is seen that a series of apparently regular, large amplitude waves are encountered between t = 660 and t = 700 s. The corresponding wave profiles are shown in Figure 6.5, with intervals of 4 s. Small amplitude waves are encountered between t = 450 and t = 490 s, and the profiles are presented in Figure 6.6 at 4 s intervals. Comparison of Figure 6.4 with Figure 6.1, suggests that the encountered wave elevation appears to be more regular for case (2) than for case (1), when the observer travels at mean group speed. However, Figure 6.5 indicates that the actual wave profile along the vessel would look more irregular than was observed for case (1), shown in Figure 6.2. While for case (1) the small wave elevations were representative for the behavior along the vessel (Figure 6.3), it is clear from Figure 6.6 that the

behavior observed amidships is not indicative of what happens at other sections of the vessel.

We saw that in following sea conditions the wave elevation, observed amidships, appears to be regular over certain periods of time in spite of the randomness of the sea. In fact, *any* point of the vessel would be subjected to a regular excitation for some time, while the vessel as a whole does not necessarily respond as if it were excited by a single sine wave. It can be conjectured that the motion frequency of the ship is most likely dominated by the mean encounter frequency (which may stay approximately constant for an extended period of time in a wave group), and that the response amplitude depends on the actual composition of the sea surface. For certain time intervals, it may be possible to characterize the random wave process by the superposition of only two regular wave components, which would yield an equivalent wave system. A minimum of two components would be needed to represent wave group properties, such as group length, number of waves in the group, and average wave height. This would be advantageous for time domain simulation purposes, especially when many simulations must be performed to investigate capsizing. If one wants to predict the occurrence of a capsize correctly for following or quartering sea conditions, the conclusions should be evaluated carefully when they are based on results obtained using only a few harmonic wave components. A procedure for obtaining an equivalent wave system has been discussed in Chapter 6.3.

Summarizing, when a ship travels with the waves in a unidirectional, random sea, the wave elevation observed at any given point of the vessel will appear to be regular over certain periods of time. During those time periods the actual wave profile along the ship will be irregular, but may be represented by an equivalent wave system, consisting of only two wave components, for purposes of wave-induced motion simulation.

6.1.2. Wave Elevation Statistics and Cross-Coupling Effects

It has been shown in Chapter 2.4.4 that the mean square value of the wave elevation, observed at a point moving with random waves, can be different

from the value that would be obtained at any stationary point. The difference depends on the actual phasing between the wave components comprising the sea surface, and on the amplitudes of the components. This cross-coupling effect arises from the fact that the encounter frequencies with different wavc components can be the same. A number of simulations have been carried out to determine the variation in RMS values for a small and large number of wave components, N, where the phases of the individual wave components were varied randomly during each simulation.

A spectral shape with peak frequency $\sigma_p = 0.5$ rad/s was chosen, the wave direction used was $\delta = 0°$, and the sampling interval was $\Delta t = 2$ s. All different simulations were performed for a period of 2 hours (full scale) and two numbers of wave components: $N_1 = 50$ and $N_2 = 1000$. During each simulation the RMS values were computed for three speeds: $U_0 = 0$, $U_1 = C_{g,p}$, and $U_2 = 0.9C_{g,p}$. As above, the mean group speed is equal to $C_{g,p} = 32.17$ ft/s. The frequencies were chosen such that equal encounter frequencies were obtained for the mean group speed $U = U_1$, where the encountered frequencies in the three regions ***A***, ***B*** and ***C*** shown in Figure 2.4 are implied. The total number of simulations was 8, i.e., for $N = N_1$ and $N = N_2$ the phase components were varied randomly 8 times and different sequences were generated. The RMS values of the wave elevation for the zero speed cases were found to be largely independent of the phases and number of wave components, and equal to

$$\eta^0_{RMS} = 11.2\,\text{ft} .$$

The variation of the RMS values for the different speeds and runs is shown in Table 6.1.

Run #	N = 50		N = 1000	
	$U = U_2$	$U = U_1$	$U = U_2$	$U = U_1$
1	12.2	12.3	10.4	9.6
2	11.5	12.2	11.9	11.4
3	10.2	9.6	11.3	11.3
4	12.5	12.7	12.0	12.0
5	11.1	12.9	11.3	12.2
6	11.1	14.1	10.7	11.0
7	12.7	7.1	11.9	11.0
8	9.9	11.9	12.2	10.7

Table 6.1. Computed RMS Values (in Feet) of Wave Elevations Observed for Different Reference Speeds.

It is useful to determine the standard deviation (S.D., in feet) of the RMS values from the different runs, the results of which are summarized below:

	N = 50		N = 1000	
	$U = U_1$	$U = U_2$	$U = U_1$	$U = U_2$
S.D.	2.21 (19.7%)	1.03 (9.2%)	0.81 (7.2%)	0.65 (5.8%)

The value in brackets refers to the nondimensional standard deviation, expressed as a percentage in terms of the zero speed RMS value: S.D./11.2x100%.

Several observations can be made from Table 6.1, even though the number of samples is small. As one would expect, the variation in RMS values, i.e., their standard deviation, is larger for the case with fewer wave components, and has a mean of about 11.2 ft. The standard deviation will decrease as the number of wave components is increased, however, the actual decrease is difficult to predict statistically because the samples are

not identically and independently distributed. Also, it appears that the variation in RMS values is larger for the case where the observer's speed equals the mean group velocity ($U = U_1$), and for which the frequencies were chosen to yield equal encounter frequencies. This is obviously due to there being more cross-coupling terms that contribute to the total mean square value (in a positive or negative sense).

The folding of the frequencies into a more narrow band with forward speed, can be clearly illustrated by computing the encounter spectrum for certain speeds. Simulations were performed and time series generated, from which the wave spectra could be computed; an investigation was made to determine the effects of forward speed and choice of wave component frequencies on the spectra. The number of wave components used was N = 1200, $\sigma_p = 0.5$ rad/s, the frequency range varied from $0.5\sigma_p$ to $2.5\sigma_p$. Time histories were generated with 2048 samples at 2 s intervals, and for four speed cases: $U_0 = 0$, $U_1 = 0.5 \times C_{g,p}$, $U_2 = C_{g,p}$, and $U_3 = 1.5 \times C_{g,p}$. The spectra of the observed wave records were computed using the FFT technique and smoothing over a bandwidth of 0.0022 Hz was applied. Two sets of spectra were generated: (1) the frequency bandwidth was constant, but the actual frequencies were chosen randomly within each interval from a uniform distribution; (2) the frequencies were chosen so as to yield equal encounter frequencies at the mean group speed, $U_2 = C_{g,p}$. The same random phases were used for the two sets of time series. The encounter spectra corresponding to set (1) are shown in Figure 6.7, and the spectra from set (2) in Figure 6.8.

The general appearance of the spectra in Figures 6.7 and 6.8 is similar. As the speed of the observer increases until the mean group speed has been reached, the encountered spectrum will become progressively narrower and steeper, and the peak frequency will decrease. It is seen that for the case $U = C_{g,p}$, the spectrum is very narrow, and drops off abruptly for frequencies larger than the peak encounter frequency, which is approximately 0.25 rad/s. From Figure 6.8 it is seen that, choosing the wave frequencies so as to yield equal encounter frequencies at the mean group speed $U = C_{g,p}$, resulted in a distinctly larger spectral peak than was obtained using randomly chosen frequencies (Figure 6.7). The peak

frequency corresponds to the maximum encounter frequency that can be attained (see Chapter 2.4.4):

$$\sigma^{e}_{max} = \frac{g}{4.U} = 0.25 \text{ rad/s} \ .$$

The reason for the sharp drop-off, at the above frequency and observer speed, is seen by inspection of the shape and behavior of the encounter frequency curve, shown schematically in Figure 2.4. For encounter frequencies larger than the maximum encounter frequency, only one wave component will contribute to the spectral density (one-to-one mapping). For smaller frequencies there are three wave components that yield the same encounter frequency, and will contribute to the spectral density associated with a particular encounter frequency. Also, for each encounter frequency lying in the latter frequency range, there are pairs of wave components that contribute to the spectral density through the cross-coupling effects mentioned earlier. When the speed of the observer is equal or close to the mean group speed, most of the wave energy is concentrated around the maximum encounter frequency, so that a distinct peak will appear in the spectrum for that speed range.

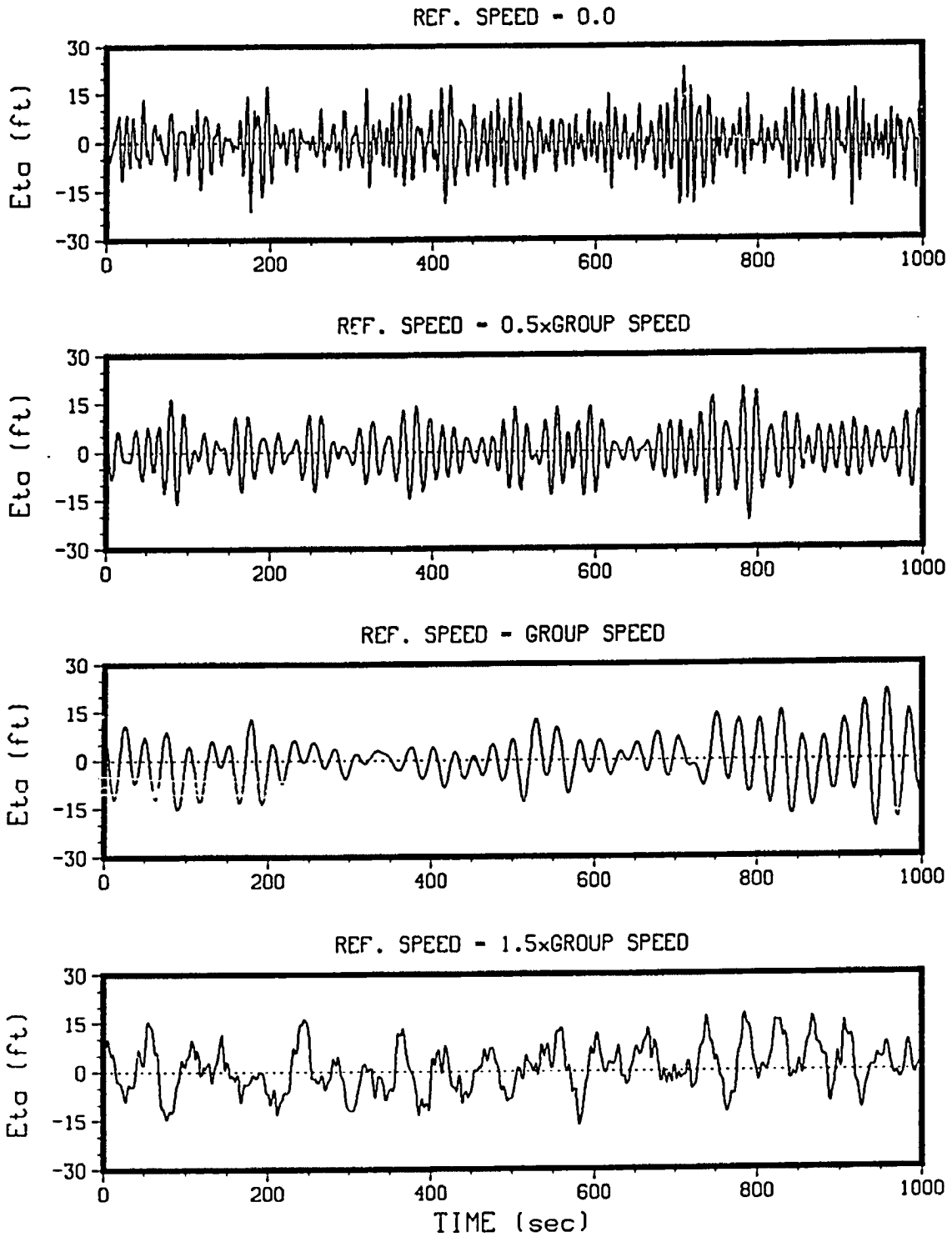

Figure 6.1. Simulation of Wave Elevations Observed at Stationary and Moving Reference Points in Random, Following Seas (σ_p = 0.5 rad/s, $C_{g,p}$ = 32.17 ft/s).

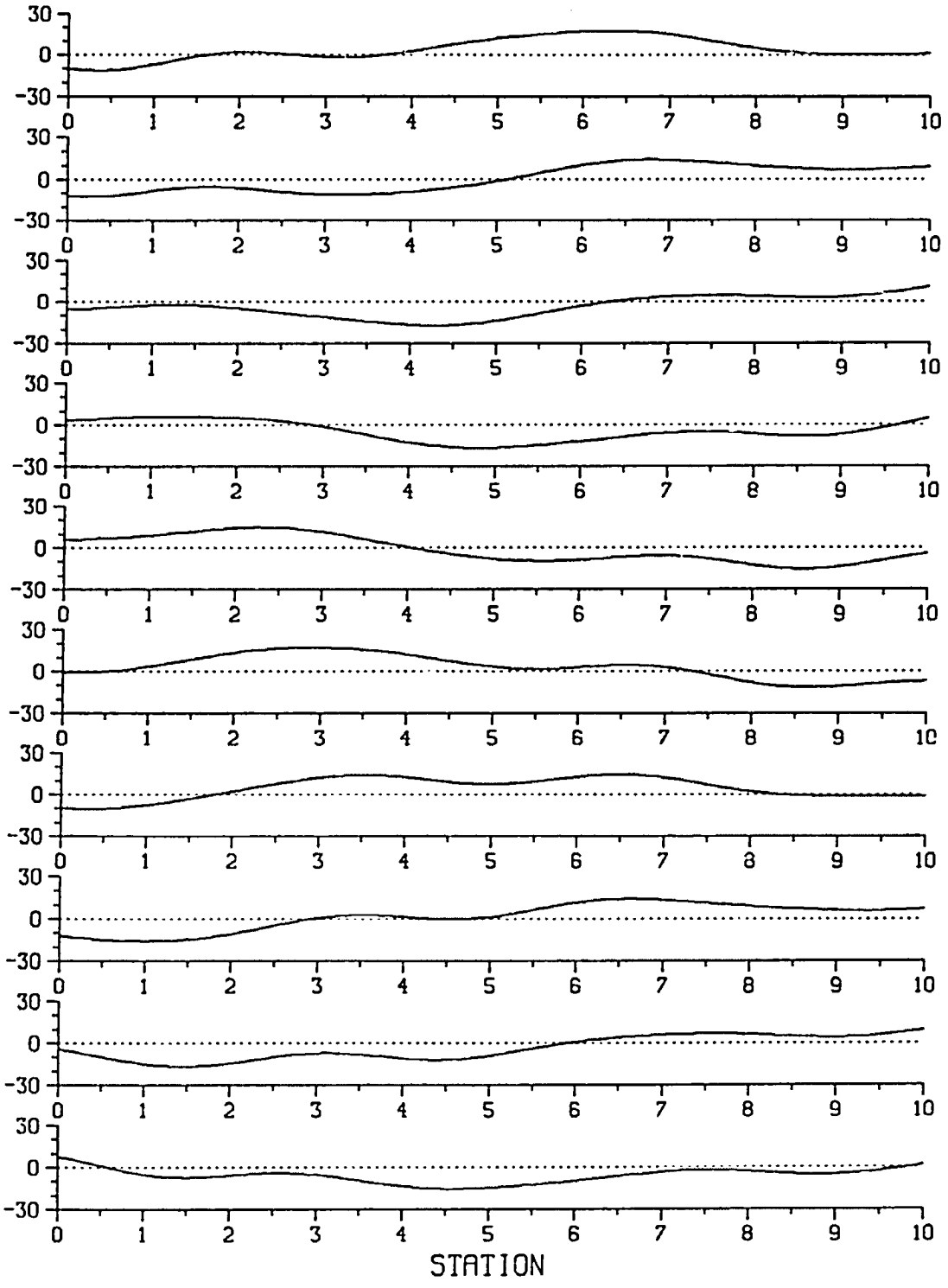

Figure 6.2. Simulation of Wave Profiles along the Length of a Vessel in Random, Following Seas for t = 935 to 975 s (see Figure 6.1). The time interval between profiles is 4 s, and U = $C_{g,p}$.

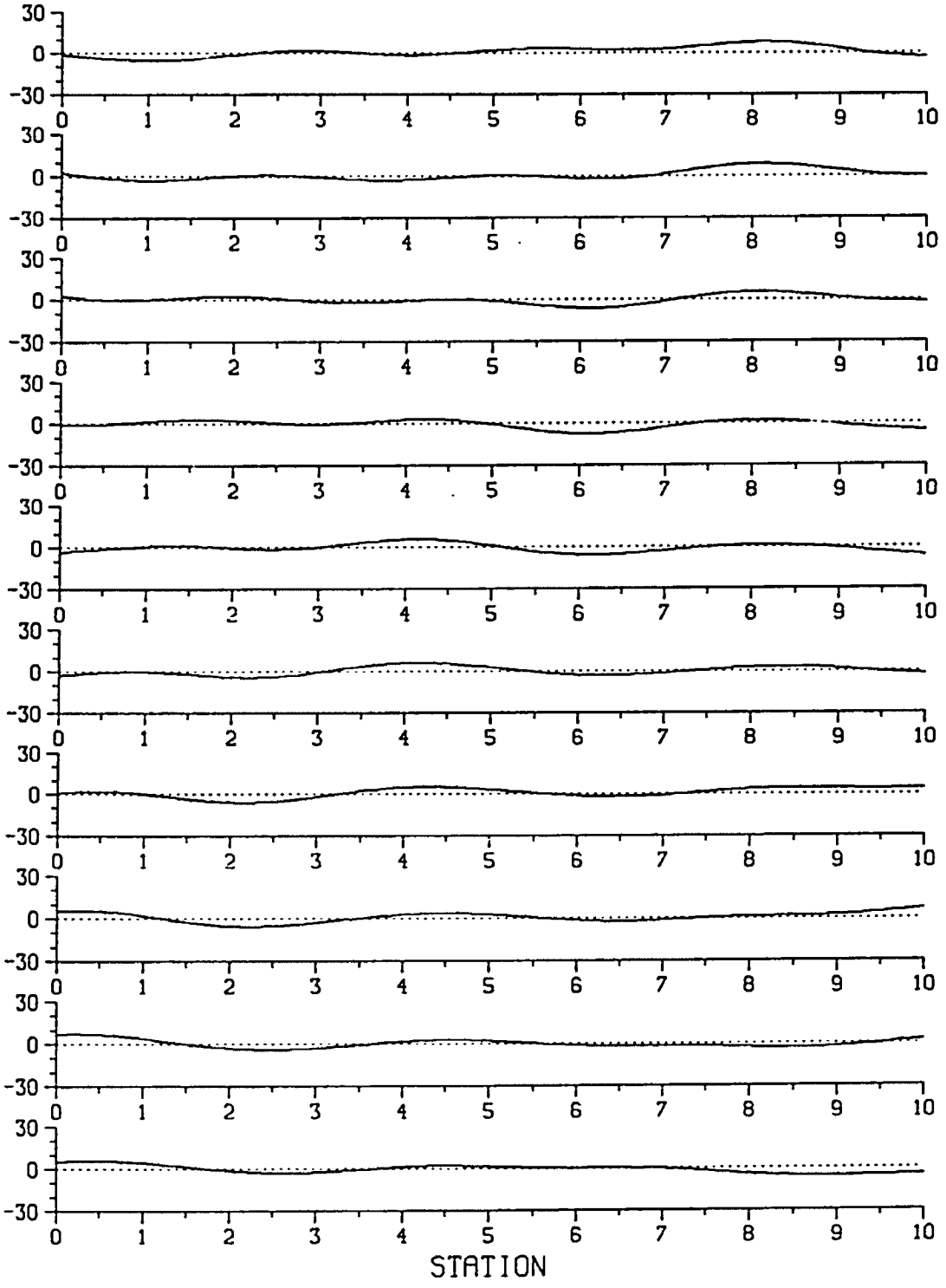

Figure 6.3. Simulation of Wave Profiles along the Length of a Vessel in Random, Following Seas for t = 310 to 350 s (see Figure 6.1). The time interval between profiles is 4 s, and U = $C_{g,p}$.

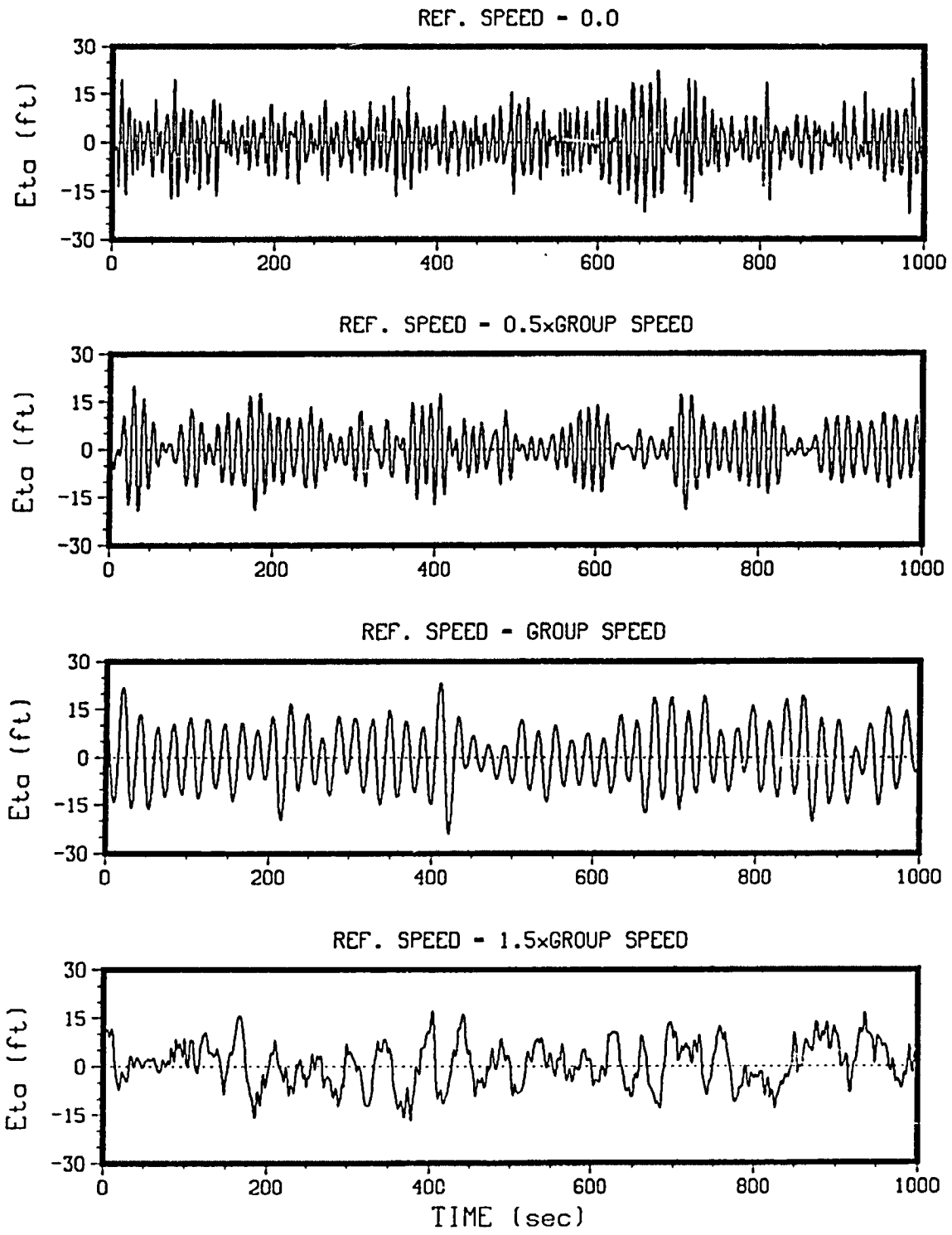

Figure 6.4. Simulation of Wave Elevations Observed at Stationary and Moving Reference Points in Random, Following Seas (σ_p = 0.62 rad/s, $C_{g,p}$ = 25.94 ft/s).

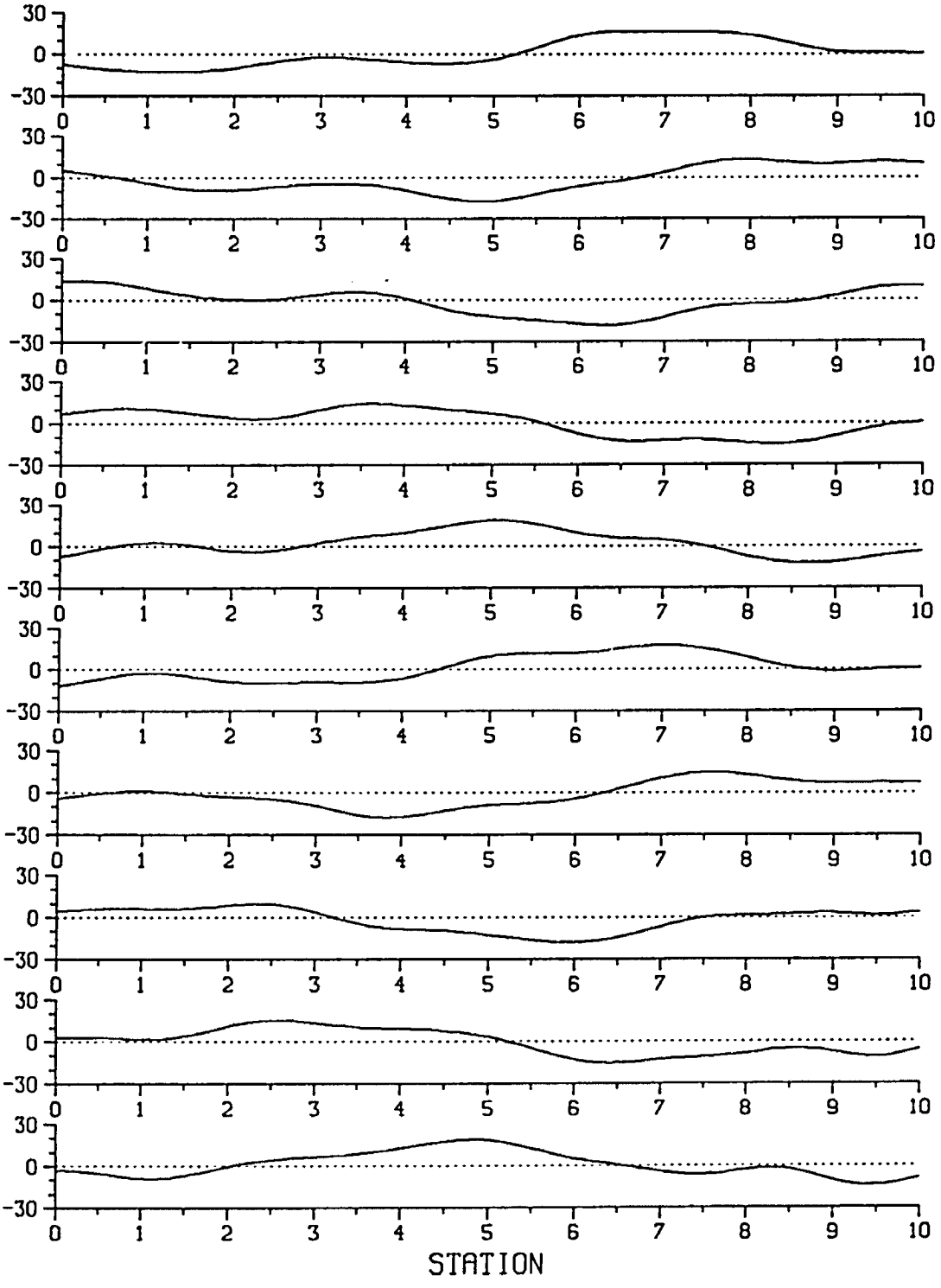

Figure 6.5. Simulation of Wave Profiles along the Length of a Vessel in Random, Following Seas for t = 660 to 700 s (see Figure 6.4). The time interval between profiles is 4 s, and U = $C_{g,p}$.

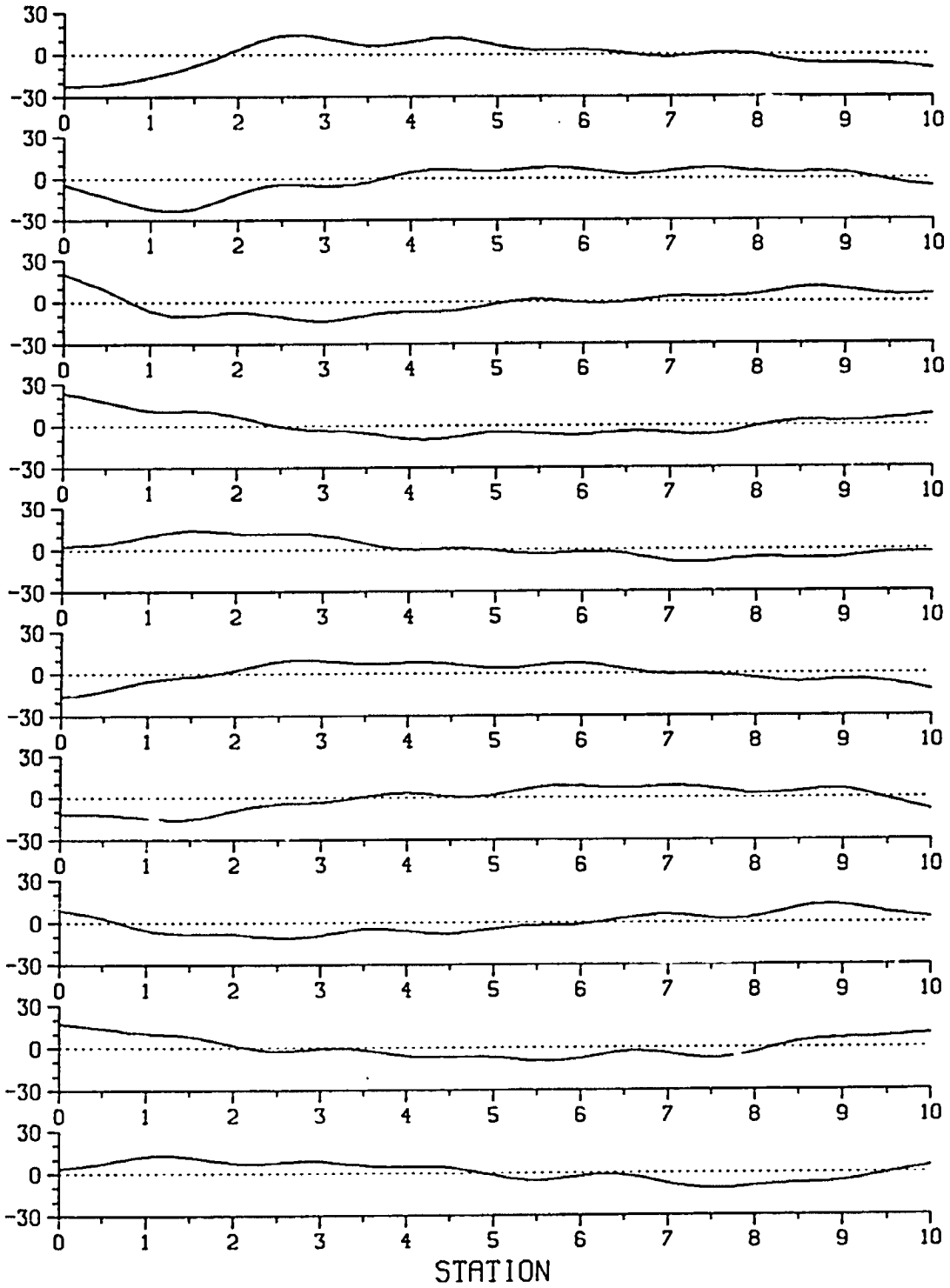

Figure 6.6. Simulation of Wave Profiles along the Length of a Vessel in Random, Following Seas for t = 80 to 120 s (see Figure 6.4). The time interval between profiles is 4 s, and U = $C_{g,p}$.

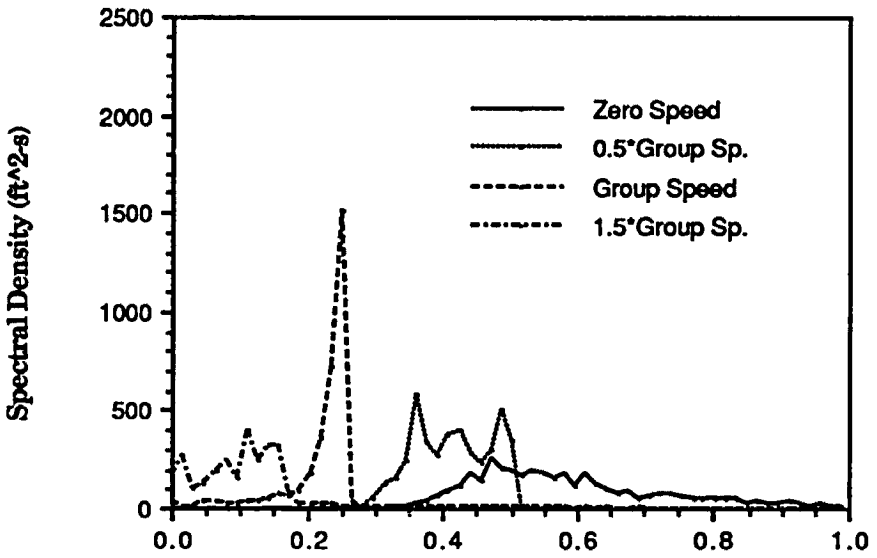

Figure 6.7. Estimated Wave Spectra for Different Speeds of Reference Frame in Random, Following Seas. The spacing between wave frequencies is random, and $C_{g,p}$ = *32.17 ft/s.*

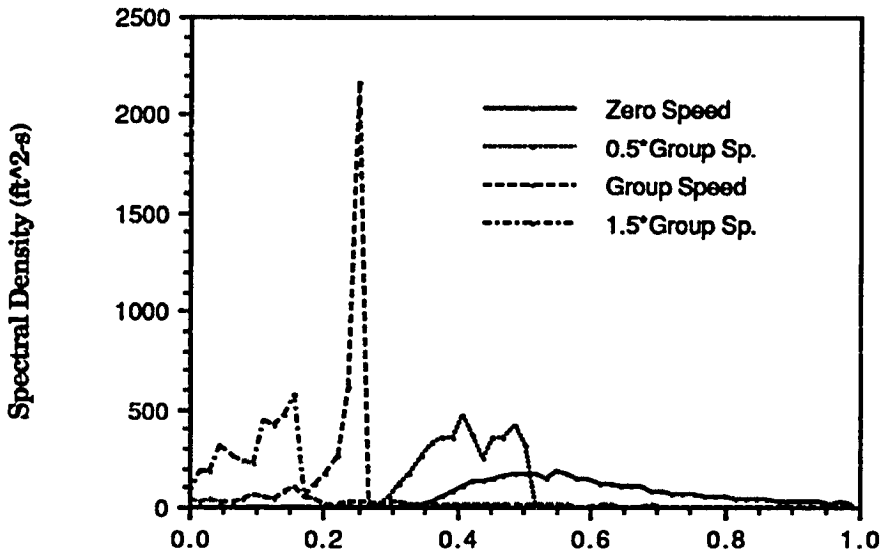

Figure 6.8. Estimated Wave Spectra for Different Speeds of Reference Frame in Random, Following Seas. The spacing between wave frequencies is such that equal encounter frequencies result for $U = C_{g,p} = 32.17$ *ft/s.*

6.2. Ship Motion Simulations

It appears from the theory in Chapter 2.4.4, and has been confirmed by simulations in the preceding section, that the mean square value of the observed wave process, for a point moving in following random seas, can be higher or less than the value observed at any stationary point. The difference depends on the phase angles of the individual wave components, on the spectral density, and on the frequency spacing and number of components. The implications of this phenomenon as regards predicted ship motions, are that over a large period of time, and for different choices of the wave component parameters, the mean square values of the observed wave process can differ between simulations. For relatively small numbers of wave components, especially, these differences could be quite large. This would result in different mean square values of ship response parameters, such as heave or roll. Also, different ways of selecting the wave frequencies and phasing of the components, will lead to different wave group properties, which may affect ship responses. For illustrational purposes, it is shown next by simulation that one formulation of wave conditions may lead to a capsize, while another formulation would not predict a capsize.

Random, following seas were considered, where

$\sigma_p = 0.62$ rad/s
$H_s = 24$ ft.

Simulations were carried out for the American Challenger vessel with the following characteristics:

GM = 0.56 ft
L = 530 ft
$U = C_{g,p} = 25.94$ ft/s
$\theta_0 = 3°$
with bilge keel.

The sea surface was modelled using N = 12 components, lying in the range $0.5x\sigma_p < \sigma < 1.5x\sigma_p$, and having randomly chosen phases. Two methods were used to determine the frequencies of the components:

(1) constant frequency intervals, and each frequency randomly chosen (out of a uniform distribution) within the intervals;

(2) frequencies chosen in such a way as to yield equal encounter frequencies with the ship travelling at mean group speed.

In the simulations the random phases of the components were equal for the two sets of different frequencies. The motion records obtained with method (1) are shown in Figure 6.9, and the times series associated with method (2) in Figure 6.10. The dashed lines refer to *Eta* (η), the wave elevation at the center of gravity of the vessel.

Figure 6.9 indicates that low cycle resonance conditions are reached during the simulation of 400 s without a capsize occurring, and that for the roll cycle between t = 80 s and t = 120 s the roll amplitude is largest. In contrast, from Figure 6.10 it is seen that with method (2) a capsize occurs at t = 100 s, after the cycle with large roll amplitudes starts at t = 80 s. The mean frequencies of encounter are approximately the same, and the wave amplitudes at the C.G. are equal, for both simulations until t = 80 s. The random wave frequencies (using method (1)) are such that the vessel has sufficient restoring energy to remain upright at t = 100 s, while this is not the case for method (2). The occurrence of the capsize using formulation (2) is not simply due to the difference in mean square values of the observed wave elevation process at the C.G., for the differences in amplitudes after t = 80 s are very small in the two simulations. It is more likely that the cause lies in differences between the predicted wave surfaces along the vessel, to which the hydrostatic roll moment is sensitive.

The sensitivity of the ship response to the wave conditions with equal encounter frequencies was high, as it would also capsize for even smaller initial roll angles ($\theta_0 = 2°$), while it would not capsize for $\theta_0 = 4°$ using the random frequency approach. These results indicate merely that care

must be taken when one wants to make predictions of capsizing in random, following seas using a finite number of wave components.

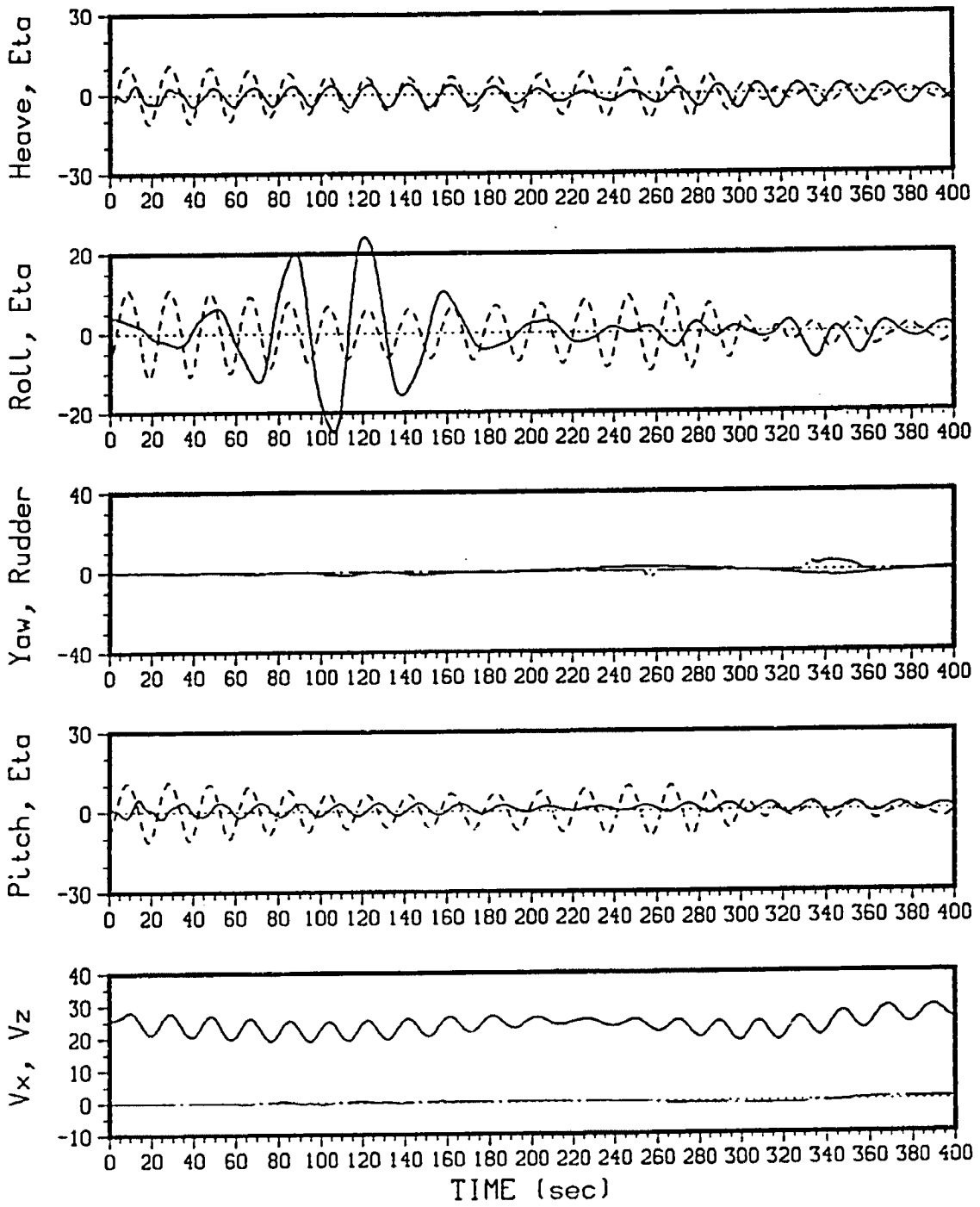

Figure 6.9. Simulation of American Challenger Travelling at $U = C_{g,p}$ in Random, Following Seas. The wave frequencies were chosen randomly. Displacements are in feet, angles in degrees, and velocities in ft/s.

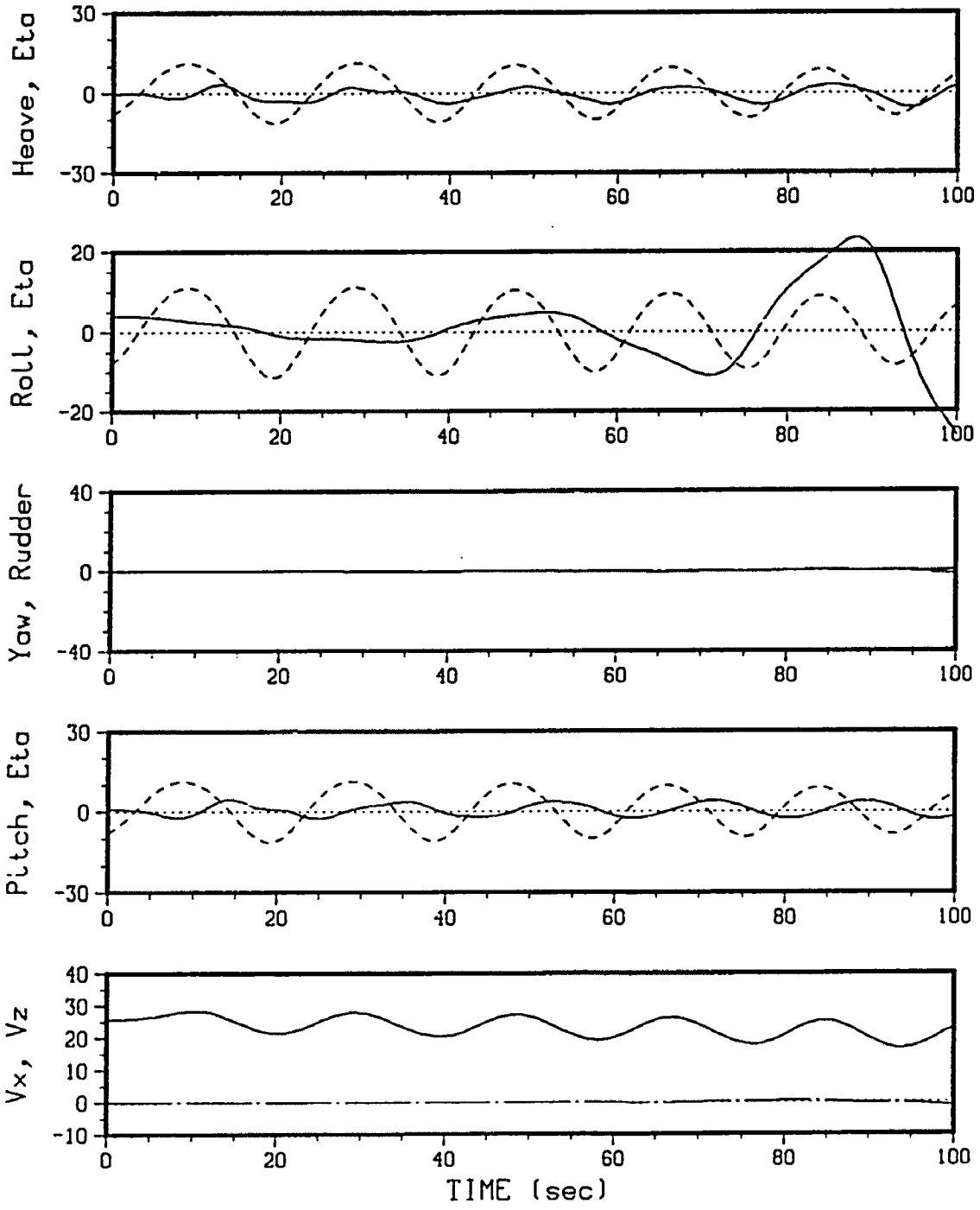

Figure 6.10. Simulation of American Challenger Travelling at Speed U = $C_{g,p}$ in Random, Following Seas. The wave frequencies were chosen so as to yield equal encounter frequencies.

6.3. Determination of Equivalent Wave System

When performing motion simulations for random, following sea conditions, it would be useful if one could replace the random wave system with a simple two-component system having equivalent characteristics with respect to the actual sea surface. In this chapter an attempt is made to provide a basic procedure by which to determine the amplitude and frequency parameters of the equivalent wave components. It was decided to consider a minimum of two components, because it is the minimum number needed to define group properties such as length, number of waves in the group, and average wave height.

Let us assume that we want to represent a random sea, having peak frequency σ_p, and spectral density $S_{\eta\eta}(\sigma)$, by an equivalent wave system with two components. The amplitudes and frequencies, $A_{i,eq}$ and $\sigma_{i,eq}$, of the components i =1,2 can be obtained from the following requirements.

(1) The group speed of the equivalent wave system must be equal to the mean group speed of the random sea, i.e.,

$$C_{g,eq} = C_{g,p} \Rightarrow \frac{\sigma_{2,eq} - \sigma_{1,eq}}{k_{2,eq} - k_{1,eq}} = \frac{g}{2.\sigma_p} .$$

(2) One of the frequencies should have a length that is of the same order as the ship length (O(L)), since the roll response is dominated by hydrostatic effects, which in turn depend significantly on waves having a length equal to the ship length. Obviously, this requirement would lead to unrealistic results if the ship length is significantly smaller than the characteristic wave length, λ_p, where

$$\lambda_p = \frac{2.\pi.g}{\sigma_p^2} .$$

Therefore, the equivalent wave length is determined as follows:

$$\begin{aligned} \lambda_{1,eq} &= L && \text{if } c_{min}.\lambda_p \le L \le c_{max}.\lambda_p \\ &= c_{min}.\lambda_p && \text{if } L < c_{min}.\lambda_p \\ &= c_{max}.\lambda_p && \text{if } L > c_{max}.\lambda_p \ , \end{aligned}$$

where $c_{min} = 0.7$ and $c_{max} = 1.3$, for example. Then the corresponding frequency is given by

$$\sigma_{1,eq} = \sqrt{\frac{2.\pi.g}{\lambda_{1,eq}}} \ .$$

The second frequency is given by requirement (1), stating that the group velocity should be equal to the mean group velocity, so that

$$\sigma_{2,eq} = \sigma_p - (\sigma_{1,eq} - \sigma_p) = 2\sigma_p - \sigma_{1,eq} \ .$$

(3) The mean square value of the equivalent wave system should be equal to the mean square value of the random sea. Assuming that the wave spectrum is characterized by a minimum and maximum cut-off frequency, σ_- and σ_+, respectively, this requirement leads to

$$\frac{1}{2}(A_{1,eq}^2 + A_{2,eq}^2) = \int_{\sigma_-}^{\sigma_+} S_{\eta\eta}(\sigma)\, d\sigma = \frac{1}{2}\sum_{i=1}^{N} A_i^2 \ ,$$

where A_i is the amplitude of the i^{th} individual wave component of the random sea surface.

(4) The ratio of the equivalent amplitudes is given by the ratio of their respective spectral densities, i.e.,

$$\frac{A_{1,eq}}{A_{2,eq}} = \sqrt{\frac{S_{\eta\eta}(\sigma_{1,eq})}{S_{\eta\eta}(\sigma_{2,eq})}} = \alpha \ .$$

Substitution of requirement (4) into (3) gives the following expressions for the two amplitudes of the equivalent wave system:

$$A_{2,eq} = \sqrt{\frac{\sum_{i=1}^{N} A_i^2}{1+\alpha}} \ ,$$

and

$$A_{1,eq} = \alpha . A_{2,eq} \ .$$

To illustrate the above approach, comparisons have been made between the observed wave profiles along a vessel of length L = 530 ft, travelling at a speed U = 26 ft/s in the same direction as the waves. Two sea states have been considered:

1. σ_p = 0.5 rad/s (λ_p = 810 ft)
   $C_{g,p}$ = 32.17 ft/s
   H_s = 24 ft,

and

2. σ_p = 0.62 rad/s (λ_p = 530 ft)
   $C_{g,p}$ = 25.94 ft/s
   H_s = 24 ft.

The Bretschneider spectrum was used to estimate the spectral density distribution. The total number of components for modelling the random

sea was N = 1200, and also the range of frequencies considered was the same as in Chapter 6.1:

$$0.5x\sigma_p < \sigma < 2.5x\sigma_p .$$

The following values for the equivalent wave system were found for sea states 1 and 2:

1. $\sigma_{1,eq} = 0.402$ rad/s, $A_{1,eq} = 6.68$ ft
   $\sigma_{2,eq} = 0.598$ rad/s, $A_{2,eq} = 8.12$ ft

2. $\sigma_{1,eq} = 0.596$ rad/s, $A_{1,eq} = 7.41$ft
   $\sigma_{2,eq} = 0.644$ rad/s, $A_{2,eq} = 7.42$ ft .

Comparisons of the profiles were made for the conditions during which the variation of the wave elevation at the midship section of the vessel was significant over a period of 40 s. At the first time step under consideration, the phases of the two equivalent wave components were adjusted until the equivalent wave profile was approximately similar to that of the actual sea state. These phase angles were used in subsequent time steps that have been plotted. The wave profiles for sea state 1 are shown in Figure 6.11, and those for sea state 2 in Figure 6.12. The actual wave profiles are represented by solid lines, and the equivalent profiles by dashed lines. The time interval between profiles is 4 s. From Figures 6.11 and 6.12 it appears that for both sea sea states the equivalent wave profiles have the same general characteristics as the actual wave profiles; the speed of the equivalent wave group is close to the speed of the main wave group, for the large crests and troughs of the equivalent system follow those of the random sea quite closely, disregarding the shorter waves that are present in the real wave system.

The objective is to determine whether such simple equivalent wave systems can be used in the prediction of capsizing in random seas. As an example, the capsizing of the American Challenger model is considered for random following seas, where the same conditions as on the San Francisco Bay are modelled (full scale). The loading condition of the

American Challenger and wave conditions are those corresponding to Run 15.04, which resulted in a capsize, reported in Haddara *et al.* (1972) and Kastner (1973). The full scale parameters of the American Challenger were the following for that experimental run:

$$GM = 0.86\,ft$$
$$\sigma_\theta = 0.21\,rad/s$$
$$U = 33.68\,ft/s\,(Fn = 0.26),$$

and the measured sea state parameters were

$$\sigma_p = 0.53\,rad/s$$
$$H_s = 28\,ft$$
$$\delta = 15°.$$

It is noted that the mean group speed for the above sea state is

$$C_{g,p} = 30.35\,ft/s.$$

For computational reasons it was decided to model the real sea surface by N = 20 components, having a frequency range of

$$0.7x\sigma_p < \sigma < 2.0x\sigma_p .$$

The interval associated with the frequencies was assumed fixed, and the frequencies were chosen randomly (out of a uniform distribution) within each interval. Also the phases were chosen randomly. Using the method described previously, the following values were found for the equivalent wave system:

$$\sigma_{1,eq} = 0.427\,rad/s,\ A_{1,eq} = 6.68\,ft$$
$$\sigma_{2,eq} = 0.633\,rad/s,\ A_{2,eq} = 8.12\,ft\ .$$

The phases of the two components were chosen so as to result in approximately the same starting conditions for the wave elevation at the C.G. (at t = 0) as for the random wave case. The capsize simulation of the

American Challenger in the (quasi) random sea is shown in Figure 6.13, and the motion records for the equivalent wave system have been plotted in Figure 6.14. As the motion records show, the simulation with the random waves results in a capsize after 190 s, and the vessel capsizes in the equivalent wave system after 250 s. The roll behavior in the two seaways is similar in that up to the point of capsizing the roll amplitude is approximately 10°, and in both cases the ship capsizes rather suddenly to starboard during the passage of the second wave group. Clearly, the vessel capsizes after a shorter duration in the second wave group of the random seaway than is the case for the equivalent wave system. Also the forward speed behavior is similar for both simulations. The RMS values for the roll motions and sway velocities compare quite well, while there are some differences for the other degrees of freedom, as can be seen from the following summary.

RMS	N = 20	N = 2
heave	3.38	4.30
roll	14.10	13.82
yaw	1.89	1.40
pitch	1.56	2.29
surge veloc.	4.53	5.42
sway veloc.	0.89	0.94

The last 40 seconds of the wave elevation profiles, as would be observed along the vessel before capsizing, have been plotted for the random and equivalent wave systems in Figures 6.15 and 6.16, respectively. The time interval between profiles is 4 s. Although in both cases the vessel capsizes after being poised on the crest of a wave for some time, it is clear that the actual profiles differ significantly for the two formulations. This is the reason that capsizing occurs at different points in time.

If it is possible at all, equivalent wave systems can be expected to be really equivalent for a relatively short time period only, such as during the passage of one wave group. Dispersion and phase effects will after a large time period cause appreciable differences between the two-component

wave system and the actual random wave surface. However, if a vessel capsizes in a particular wave group, it may be possible to fit an equivalent wave system to a certain period before capsizing occurs, and then determine whether capsizing also occurs in that wave system, provided all the initial conditions are the same as in the random case.

This approach has been applied to the capsize simulation results for the random wave (N = 20) case. The wave profiles of the random seaway were considered for the last 40 seconds before capsizing (from t = 152 to t = 190 s). The phases of the two equivalent wave components, observed from the vessel travelling at exactly the same speeds as in the simulation depicted in Figure 6.13, were adjusted until they closely represented the profiles of the random seaway. The profiles of the random and equivalent wave systems have been plotted in Figure 6.17, where the dashed lines refer to the equivalent wave profiles and the solid lines to the random wave profiles. The time interval between profiles is 4 s, and the first (top) profile corresponds to t = 152 s. It is seen that for that time period the equivalent wave profiles match those of the random seaway quite closely.

Next, a time simulation was performed with the equivalent wave system, starting at t = 152 s, and where the phases of the two wave components were those from which Figure 6.17 was obtained. Also, the vessel was given the initial same displacements, rotations and velocities as had been computed during the capsize simulation in the random seaway (see Figure 6.13) at t = 152 s. Using the equivalent wave approach, the vessel capsizes at t = 187 s in the same manner as for the random wave case, where capsizing occurred at t = 190 s, and the last 40 seconds of the motion simulation have been plotted in Figure 6.18. Figure 6.18 shows that the forward speed of the vessel, just before it capsizes, is higher for the equivalent wave system than was the case for the random seaway, while the roll behavior is the same for both representations. The results suggest that for these particular conditions the equivalent wave system is adequate for representing the general behavior in the random seaway.

Summarizing, it is obvious that the equivalent wave system results in certain discrepancies when comparing the motions with those computed

in random waves. However, it appears that the general characteristics of the random seaway can be approximated in a simple but fairly reasonable way. For certain periods of time the equivalent wave system may be useful for modelling the random sea in capsize simulations, as its feasibility has been shown for following sea conditions (provided that the correct initial conditions are chosen).

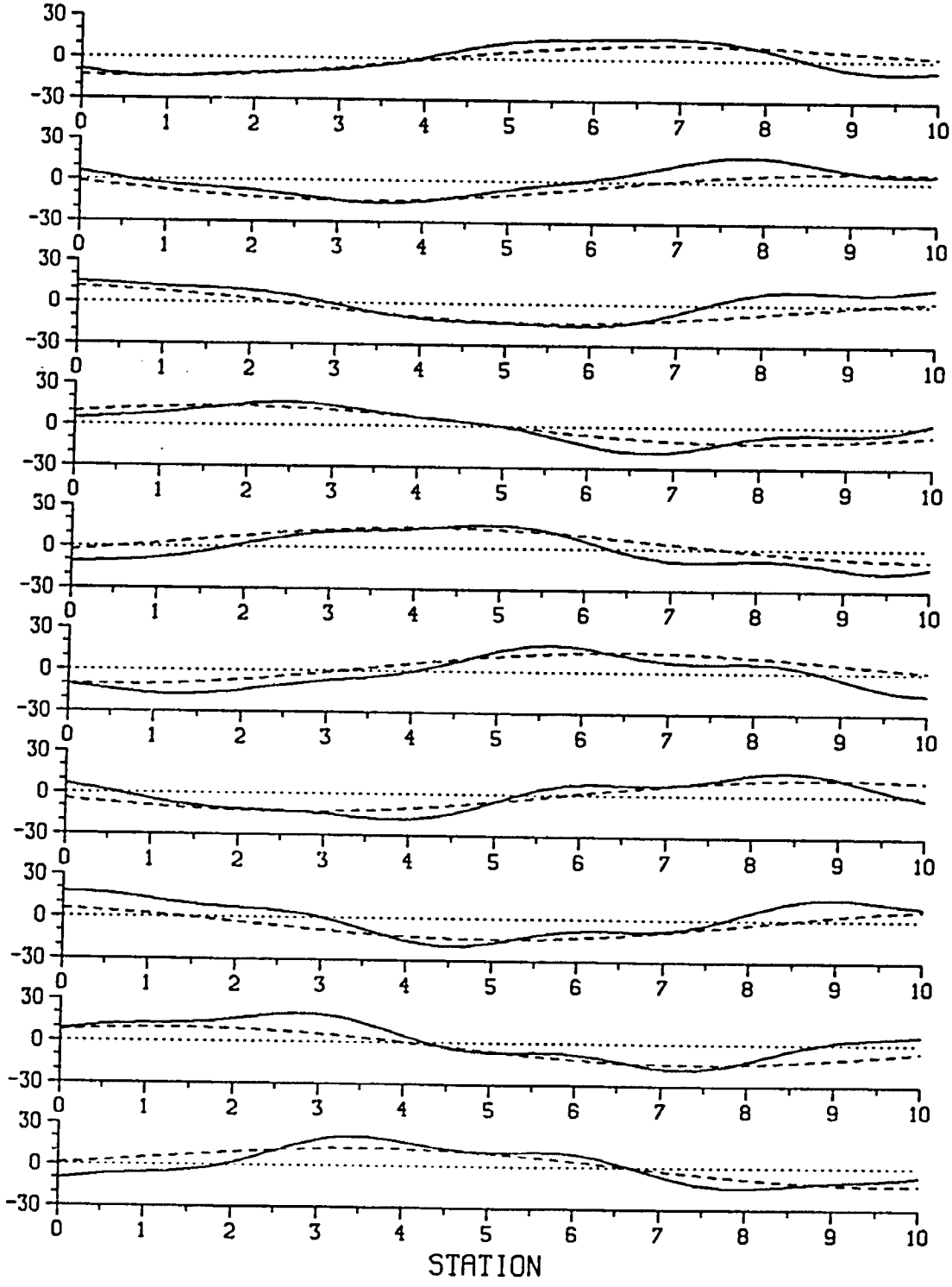

Figure 6.11. Simulation of Wave Profiles along the Length of a Vessel in Random, Following Seas. The dashed lines refer to the equivalent wave system. The time interval between profiles is 4 s, $\sigma_p = 0.5$, and $U = 26$ ft/s.

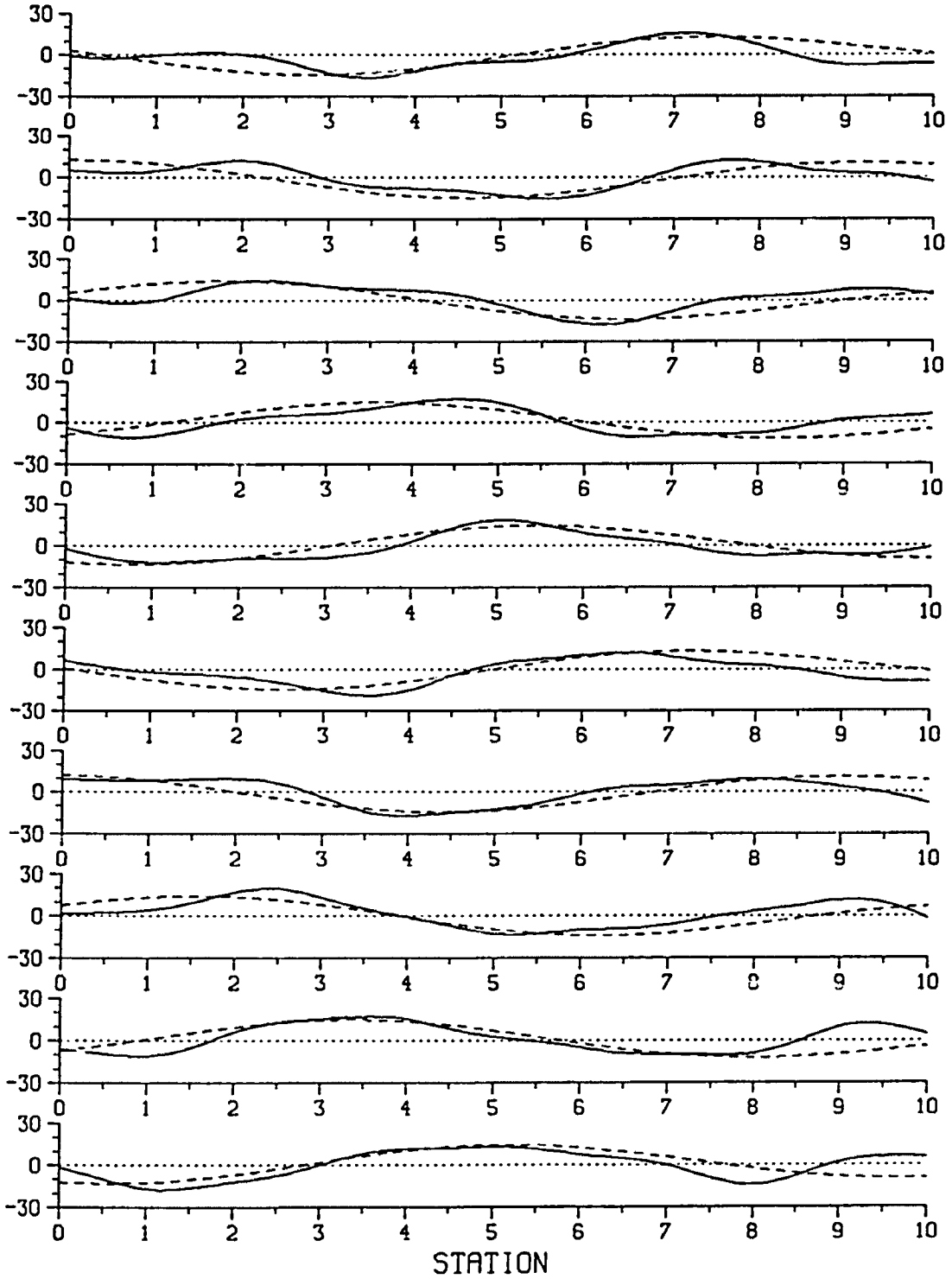

Figure 6.12. Simulation of Wave Profiles along the Length of a Vessel in Random, Following Seas. The dashed lines refer to the equivalent wave system. The time interval between profiles is 4 s, $\sigma_p = 0.62$, and $U = 26$ ft/s.

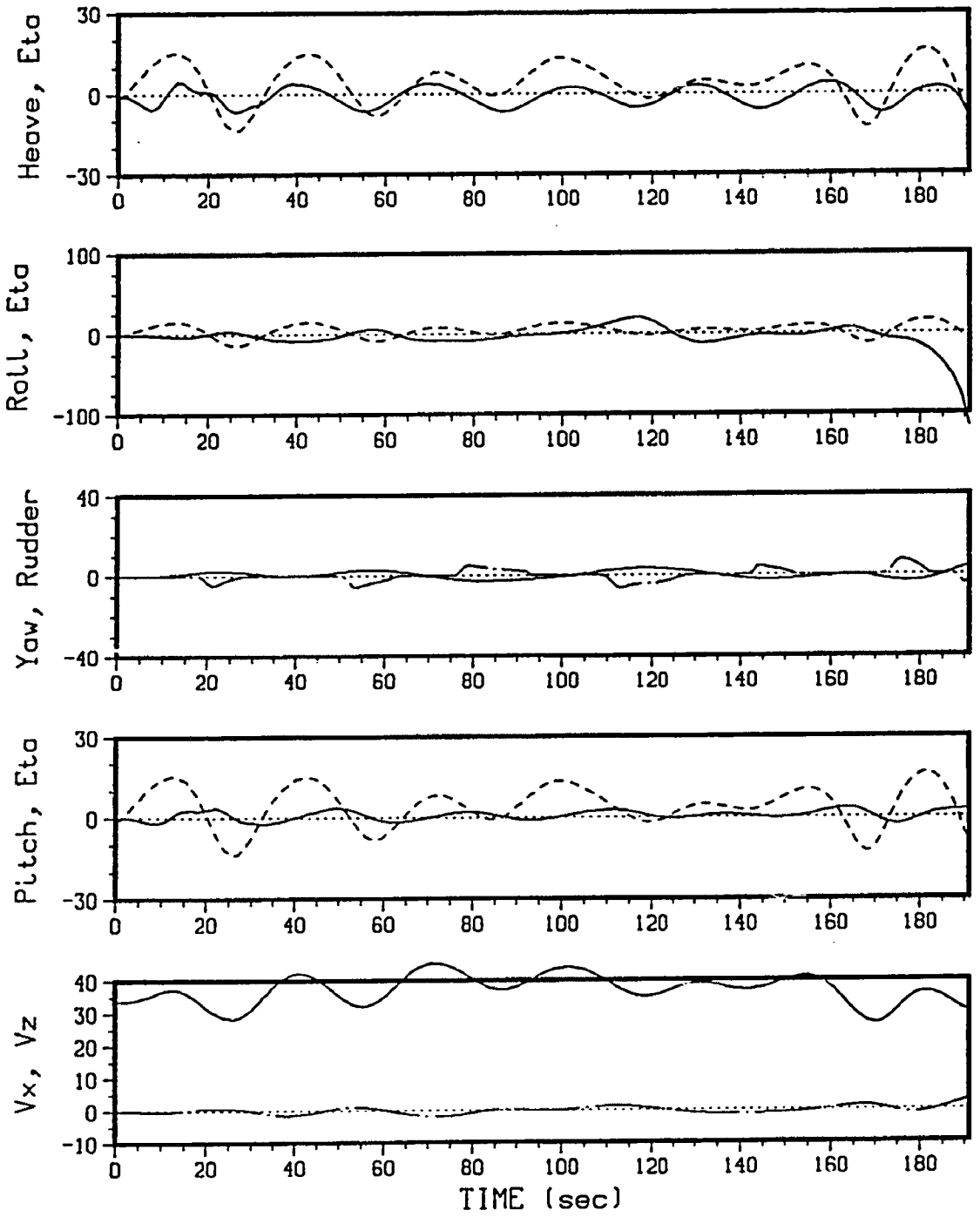

Figure 6.13. Simulation of American Challenger Travelling in Random, Following Seas. The dashed lines refer to the wave elevation at the C.G., $\sigma_p = 0.53\ rad/s$, $H_S = 28\ ft$.

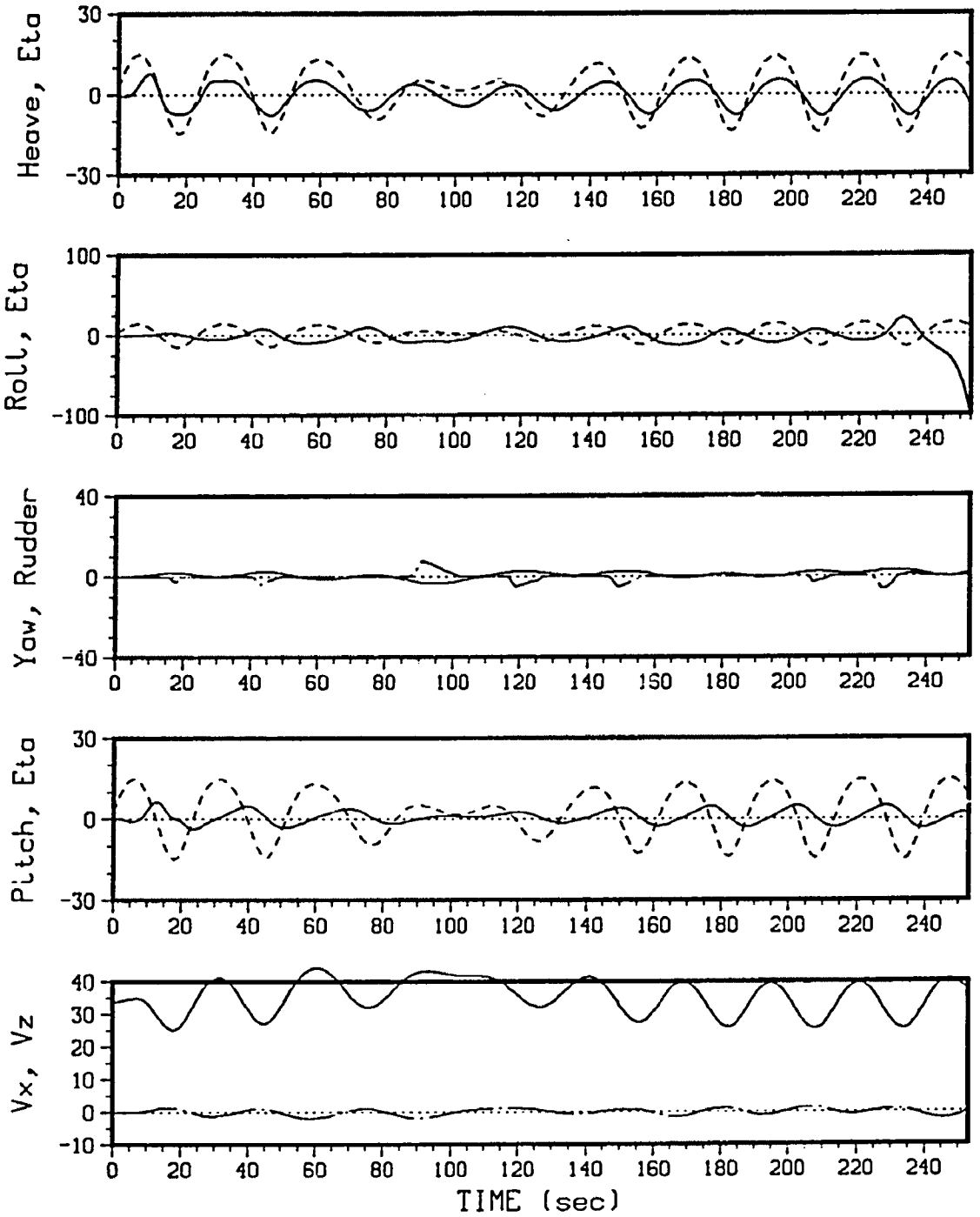

Figure 6.14. Capsize Simulation of American Challenger in a Two-Component, Following Sea. The parameters were chosen so as to yield a wave system equivalent (at t = 0) to the random sea from Figure 6.13.

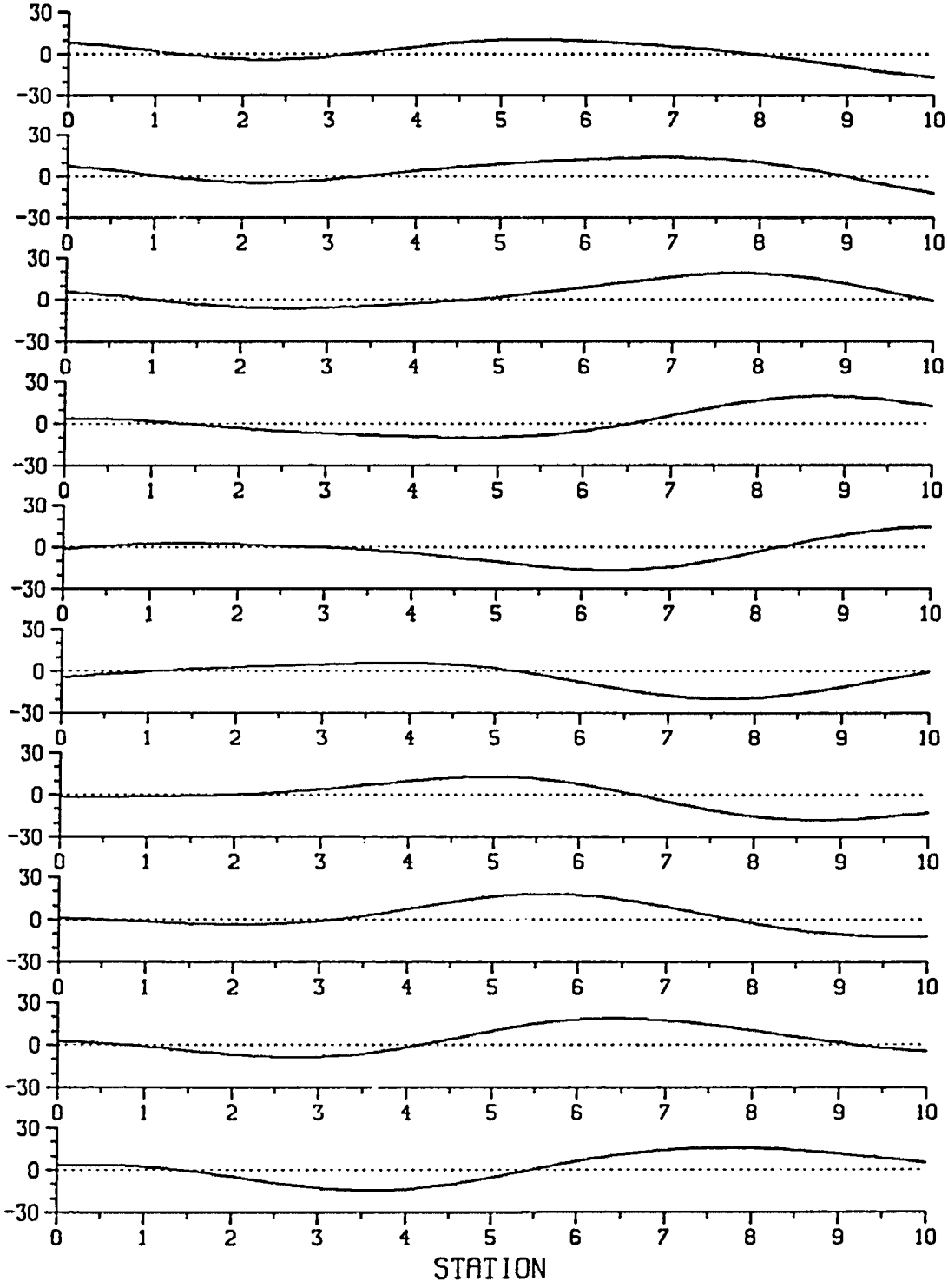

Figure 6.15. Wave Profiles along the Ship Length in Random, Following Seas (see Figure 6.13). The last 40 seconds before capsizing are shown. The time interval between profiles is 4 s.

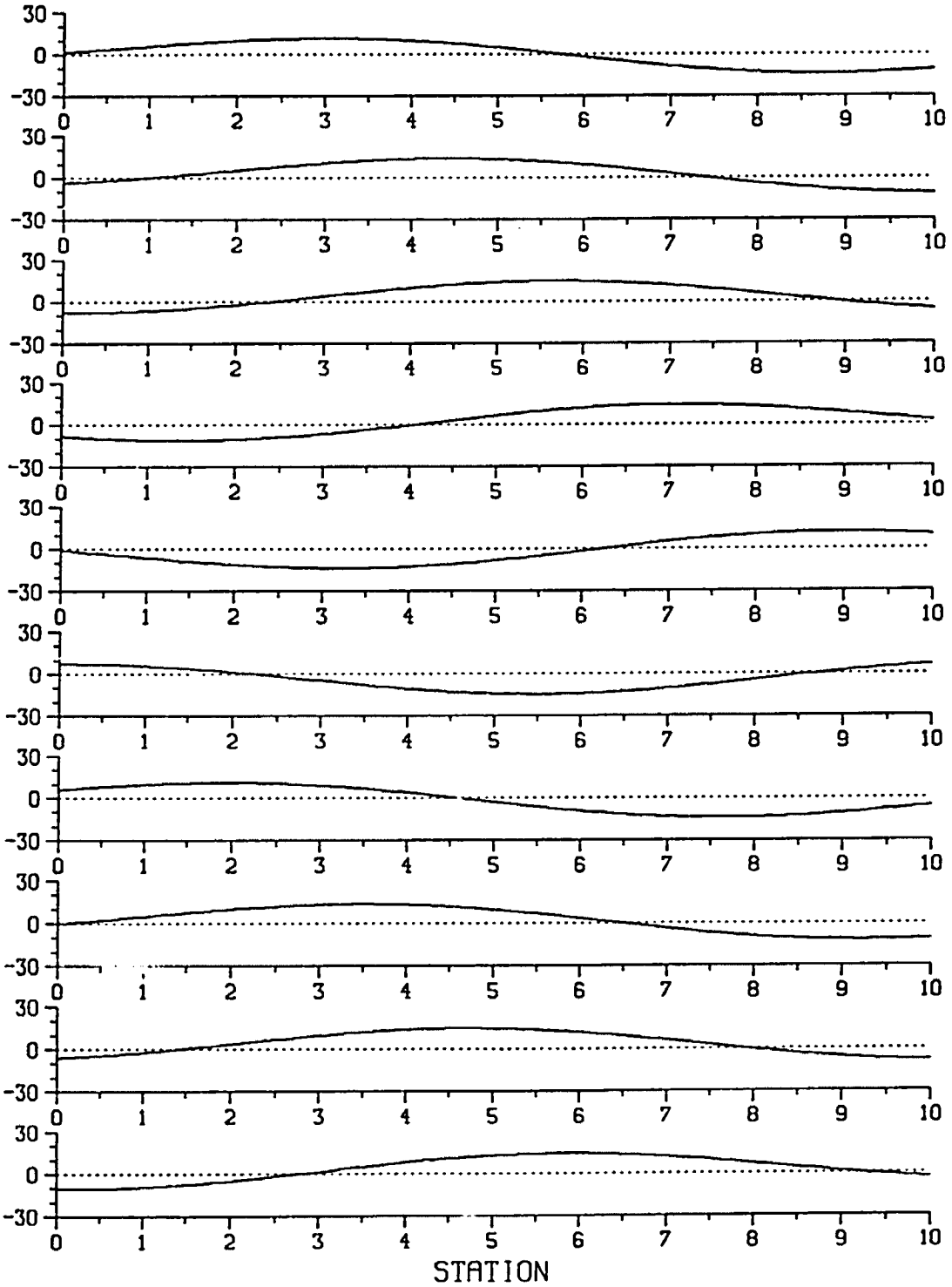

Figure 6.16. Wave Profiles along the Ship Length in Equivalent, Following Wave System (see Figure 6.14). The last 40 seconds before capsizing are shown. The time interval between profiles is 4 s.

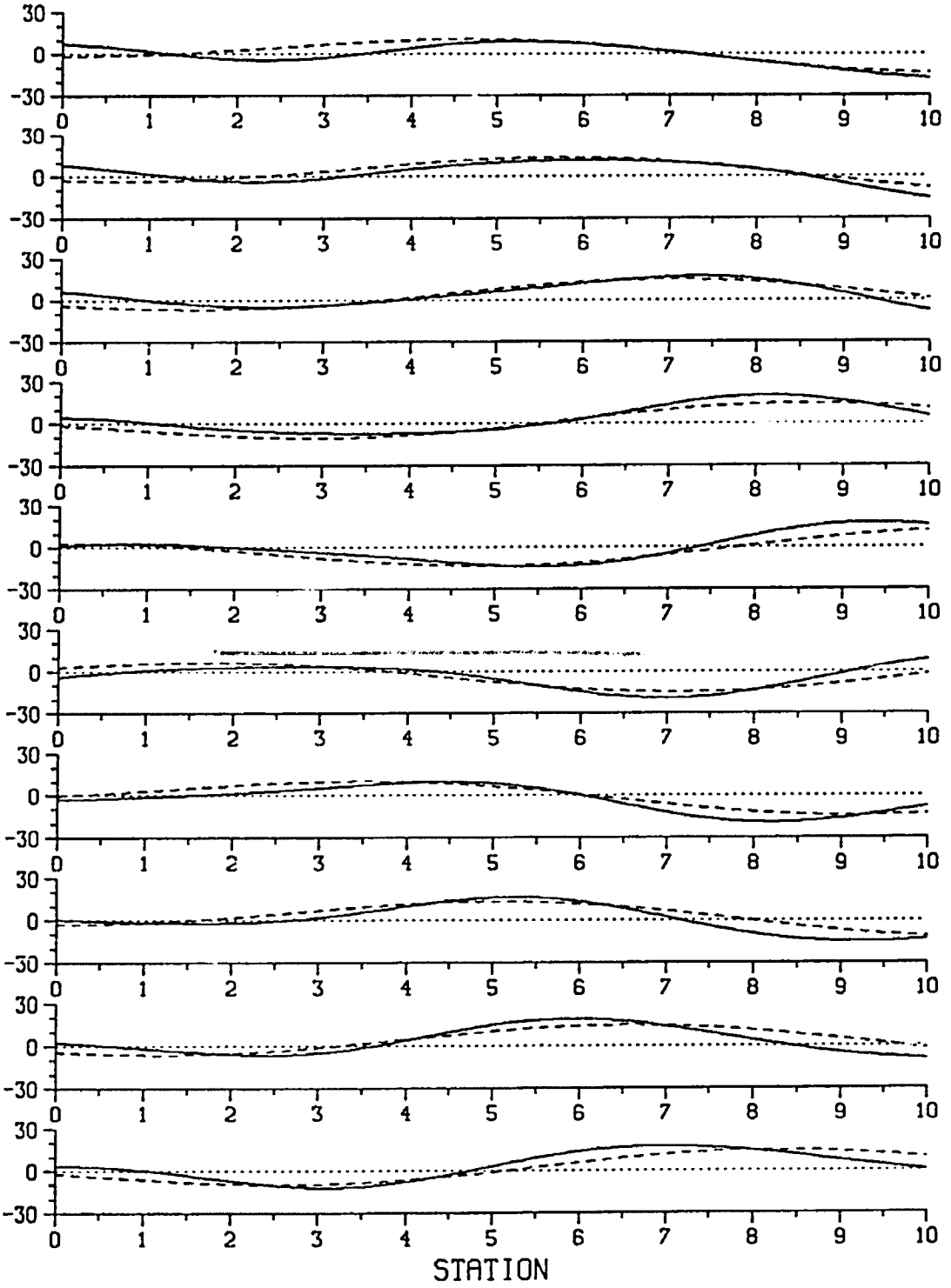

Figure 6.17. Wave Profiles along the Ship Length in Random, Following Seas (see Figure 6.13). The profiles start at t = 152 s. The dashed lines refer to the equivalent wave system. Time interval between profiles is 4 s.

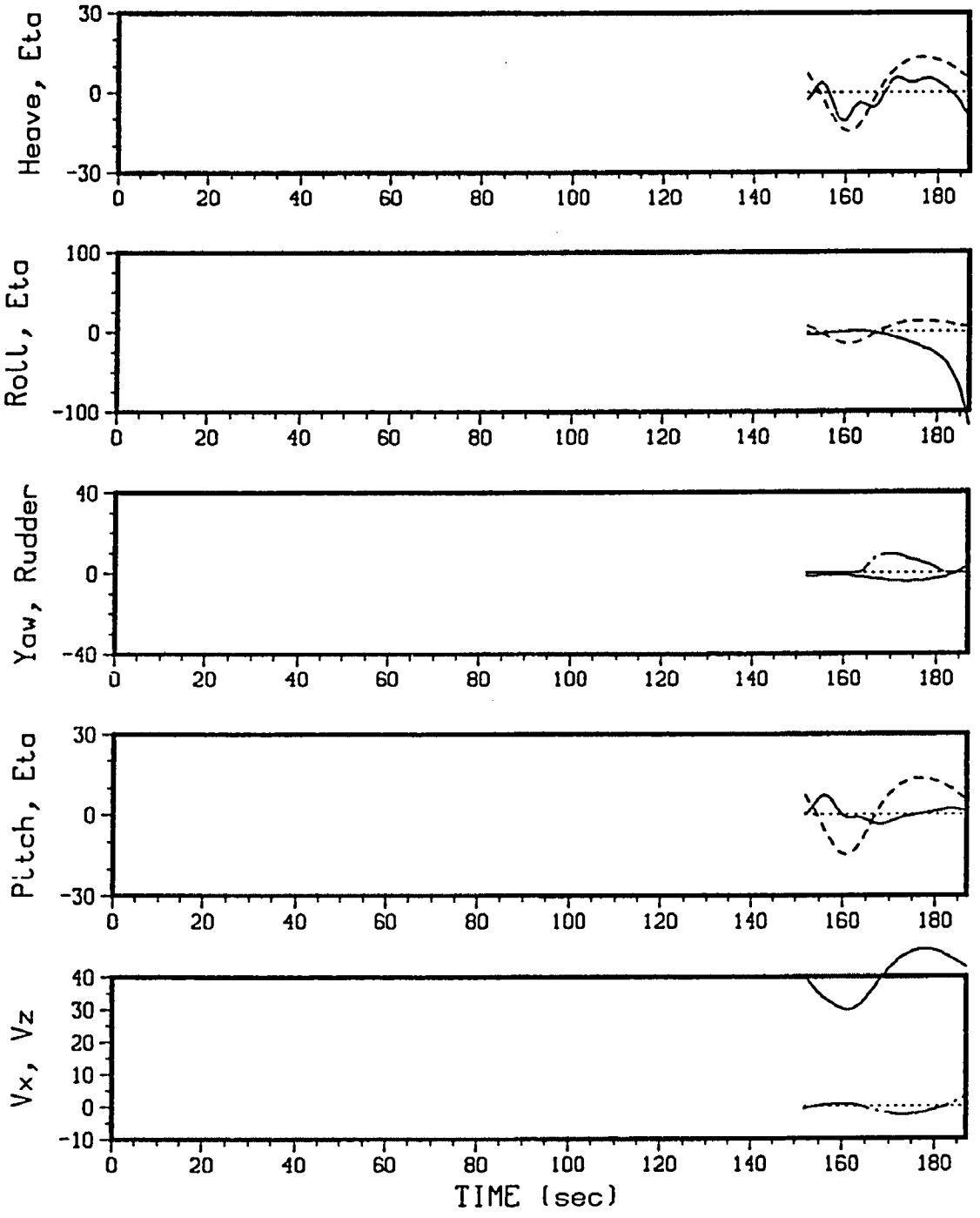

Figure 6.18. Capsize Simulation of American Challenger in Equivalent Wave System (Fitted to Model the Random Seaway from Figures 6.13 and 6.17). The last 40 seconds before capsizing are shown.

CHAPTER 7

Prediction of Motion Instabilities and Capsizing by Simulation

One of the major objectives of this work is the ability to identify by simulation the various modes of capsizing in waves that have been observed experimentally. If this is possible, the next step in the process would be to establish ranges of wave conditions for which it is likely that a capsize will occur (for given vessel geometry, loading condition, KG and speed). That is, it is of interest to predict for the different capsize modes *critical* wave frequencies, together with associated wave heights and direction, depending on the vessel characteristics. Wave-induced capsizing may be separated into the following dynamic modes, which have associated with them different physical phenomena:

(1) Low cycle resonance (following to quartering seas)
(2) Pure loss of transverse stability (following seas)
(3) Broaching (following to quartering seas)
(4) Resonant excitation in beam to quartering seas
(5) Loss of transverse stability in beam to quartering seas
(6) Impact excitation due to a steep beam wave.

The first three modes of capsizing were observed in the San Francisco Bay experiments, as was mentioned in Chapter 1. The above capsize modes can be characterized briefly as follows. Low cycle resonance (1) can be recognized by the frequency of the roll motion, which will lie close to the natural roll frequency, being different from the wave excitation frequency (typically, the encounter frequency equals twice the natural frequency). The wave amplitude need not be high to result in large roll angles under the appropriate conditions. Pure loss of transverse stability (2) is what the name implies: the righting arm is decreased so much that there is not sufficient restoring energy present in the vessel to upright itself. Typically, the vessel heels to one side for a prolonged period of time, and may then roll to the other side, before capsizing. This may happen in large amplitude, following seas, especially when the vessel travels at a relatively high speed. Broaching (3) implies the loss of directional control,

i.e., the vessel veers off course, broadside to the waves, regardless of rudder action. Due to the forward momentum of the vessel and change in heading angle, the exciting roll moment can become large. A vessel may broach in two ways: (i) when its speed is close to the phase speed of the wave, it will be forced to move along with the wave, so that it can become directionally very unstable and a broach may occur in a relatively short time span; (ii) when the vessel is hit from astern by sufficiently steep waves in a successive manner, it can be yawed to such an extent that rudder action cannot rectify the situation before the next wave yaws the vessel even further. The latter type of broach will occupy a longer time span than the former. Resonant excitation (4) refers to the condition where the vessel is excited at its natural roll frequency, which may result in very large roll angles if the wave amplitude is sufficiently large. Capsize mode (5) refers to the same phenomenon as mode (2), however, mode (5) is introduced to separate loss of static stability in beam or quartering seas from following sea conditions. For mode (2) there is a significant speed dependence, while mode (5) may occur at any speed. Impact excitation (6) due to a steep, possibly breaking, wave from abeam can be such that the vessel is heeled over to a large angle, in which position it is vulnerable to the action of consecutive waves (if it has not already capsized).

It is certainly possible for two different modes to occur in a combined fashion: for example, broaching may be followed by pure loss of transverse stability, or resonant excitation may be followed by loss of transverse stability. Also, in many cases water-on-deck effects can play an important role in the capsizing behavior (extra weight, free surface effect, sloshing), especially so for small vessels. These effects, together with capsizing due to steep, breaking waves (mode (6)), are not considered in the present work because of theoretical limitations.

The first two capsize modes have been treated in some detail by Haddara *et al.* (1972), Chou *et al.* (1974), and Oakley, Paulling and Wood (1974). Capsizing due to broaching has been observed during the San Francisco Bay experiments and has been reported in the previous three references; the loss of directional control in waves has been treated by Davidson (1948),

Du Cane and Goodrich (1962), Conolly (1972), Nicholson (1974), Renilson (1982), Motora, Fujino and Fuwa (1982), and Grim (1983), among others. It is noted that a broach implies the loss of rudder control and large deviations from the intended course, but not necessarily a capsize. There has been very little research concerning broaching *and* capsizing. The capsizing of small vessels in beam and quartering seas has been investigated experimentally by Kawashima et al. (1978), who also considered the effect of shifting cargo and shipping of green water, and by Takaishi (1982) and Yamakoshi *et al.* (1982). Capsizing due to steep breaking waves from abeam has been investigated experimentally by Dahle and Kjærland (1979), and Morrall (1979). Blume and Hattendorf (1984) have reported an extensive series of experiments, aimed at determining the safety against capsizing of medium size cargo ships in following to quartering seas.

The various capsize modes have been obtained by numerical simulation for the American Challenger vessel, the results of which are given in the first section. Also, attention is paid to the behavior of the force components acting on the hull. Critical conditions are established for the different modes of capsizing in the second section. Because of time limitations, it was deemed impractical to attempt the determination of a complete set of critical wave conditions for different vessels at different loading conditions. Instead, an investigation was made concerning speed and heading changes, which would be necessary to avoid a given capsize situation.

7.1. Numerical Identification of Capsize Modes

The first five capsize modes listed above have been simulated numerically and are presented in graphical form below, each followed by a short discussion pertaining to the capsize behavior and individual force components. All capsize simulations were performed for the American Challenger vessel subjected to regular waves, except for mode 4 for which two components were used. Three values of the metacentric height were considered (with corresponding natural roll frequencies):

GM (ft)	σ_θ (rad/s)	T_θ (s)
0.56	0.17	37
0.86	0.21	30
1.77	0.28	22

The various motion and force records corresponding to the simulated modes (1) through (5) are shown in Figures 7.1 to 7.11. The corresponding time series of the roll moment components are shown for each mode. Since mode (3), which represents capsizing induced by broaching, is largely yaw dominated, Figure 7.7 represents the record with the associated yaw moment components. An overview of the simulation conditions is given in Table 7.1.

Mode #	GM (ft)	U (ft/s)	σ (rad/s)	A (ft)	δ (°)
1	0.56	22.7	0.61	9.8	0
2	1.77	25.8	0.80	13.8	0
3	0.56	12.7	0.68	16.0	40
4	0.86	33.7	0.43/0.63	6.7/8.1	25
5	1.77	21.8	0.65	20.1	90

Table 7.1. Conditions for Simulations of Capsize Modes for American Challenger.

In the above table σ refers to the wave frequency, A to the wave amplitude, and δ to the wave direction with respect to the x-axis. In the figures with the moment components, the legends need some clarification. The moments are taken about the axes fixed in the vessel, and the following moment components have been plotted:

- static Froude-Krylov moment, $f_{FK,s}$;

- dynamic Froude-Krylov moment, $f_{FK,d}$;

- memory effect moment, which is the summation of all of the memory effect integrals, and for roll would be given by

$$\sum_{j=1}^{6} \int_{0}^{t} L_{4j}(\tau).\dot{x}_j(t-\tau)\, d\tau \ ;$$

- diffraction moment, f_D ;

- quadratic damping, which here represents the sum of the actual viscous quadratic damping moment (based on the relative roll motion) and the roll moment due to viscous sway-into-roll coupling;

- wave drag moment, $f_{drag,w}$;

- rudder moment, f_{rud} .

The time records of the motions and corresponding moment components have several interesting features, which are discussed next for the various modes of capsizing.

Figure 7.1 shows a typical case of low cycle resonance before capsizing occurs, which represents mode (1). The roll period is approximately equal to the natural roll period, and the encounter period is half the period of roll. The wave length is approximately equal to the ship length:

$$\frac{L}{\lambda} = 0.975 \ .$$

Examination of the roll moments in Figure 7.2 reveals that the static Froude-Krylov moment, i.e., the hydrostatic restoring moment, is the dominant component. The dynamic Froude-Krylov moment is small and its frequency equals the encounter frequency. From inspection of the time record, it is seen that the hydrostatic moment consists of two superposed frequencies: a slowly varying component having a frequency equal to the roll frequency, and a fast varying frequency component whose frequency is equal to *three* times the roll frequency (or $1^1/_2$ times the encounter

frequency). The existence of the slowly varying component is obvious: it represents the actual restoring moment, and its sign is opposite to the roll motion, i.e., positive roll angle results in negative restoring moment. When the roll motion is such that its frequency is half the encounter frequency, and the maximum roll angle is in phase with the maximum (or minimum) wave elevation, the slow restoring moment is altered during the passage of a wave as follows. As the vessel heels to starboard (positive roll angle), the restoring moment is negative. This coinciding with the wave crest passing the center of gravity (i.e., amidships), results in the restoring moment being significantly reduced, in this particular case to approximately zero. After the crest has passed amidships, and the vessel still being heeled to starboard, the restoring moment becomes negative again until the vessel starts to roll to port (it reaches its equilibrium position of zero roll angle as the wave trough passes amidships). While being heeled to port and a wave wave crest passing by, the positive restoring moment is reduced to zero, after which it becomes positive again, etc. In this manner the restoring moment is reduced three times during two periods of encounter, and thereby has a frequency of three times the roll frequency. From Figure 7.2 it is seen that each time after the restoring moment has been reduced in the wave crest, the magnitude of the restoring moment and the roll amplitude are increased to a larger extent than during the previous cycle, up to the point where capsizing occurs.

Thus, in this case there seems to be excitation both at the natural roll frequency and at three times that frequency. This may be explained by the Mathieu equation, which is a classical model in vibration theory for parametric excitation. In the Mathieu model, the parametric excitation results from the time-dependent restoring coefficient, and in the case of a ship in a seaway the restoring coefficient will vary at the encounter frequency. If the encounter frequency is equal to twice the natural frequency, the restoring coefficient will vary at a frequency of twice the natural frequency. Then, if the vessel rolls at its natural frequency, σ_θ, the total restoring force in the Mathieu equation consists of the following time-dependent product (multiplied with a constant):

$$\cos(2\sigma_\theta.t) \,.\, \cos(\sigma_\theta.t) \quad .$$

Now it is easy to prove the following:

$$2 \,.\, \cos(2\sigma_\theta.t) \,.\, \cos(\sigma_\theta.t) = \cos(\sigma_\theta.t) + \cos(3\sigma_\theta.t) \quad .$$

The above suggests that the observed summation of the two different frequencies comprising the static Froude-Krylov roll moment, at the natural roll frequency and at three times that frequency, can indeed be modelled by the Mathieu equation. Therefore, low cycle resonance can be considered to be caused by parametric excitation.

A somewhat similar behavior of roll response and force components was observed in one of the simulations presented in Chapter 4, shown in Figures 4.10 and 4.11. That simulation was also carried out for the American Challenger vessel having a low GM value, and low cycle resonance was produced in a composite wave system by the hydrostatic restoring moment, which consisted of a slowly varying component equal to the frequency of roll, and a fast varying component having a frequency approximately three times the roll period.

The motion records for mode (2), loss of transverse stability in following seas, are shown in Figure 7.3, and the corresponding roll moment components in Figure 7.4. This capsize mode is characterized by the vessel being heeled over to one side for a prolonged period of time due to lack of sufficient restoring energy in the system, and where the period of roll is not equal to the natural roll period. Typical conditions of mode (2) are steep, large amplitude waves, and a large enough ship speed so that the vessel stays in the wave crest for a relatively long period, during which static stability is reduced. In this case the wave height was 28 ft, and the ship to wave length ratio:

$$\frac{L}{\lambda} = 1.678 \quad .$$

For this mode of capsizing there is a certain critical amplitude, say A_{cr}. If $A < A_{cr}$, it was found that the roll motion (for a given initial roll angle) will decay to zero with increasing time, while for the case where $A > A_{cr}$, the vessel will lean over to either side for a significant amount of time before capsizing. The latter behavior has been observed during the San Francisco Bay experiments. Figure 7.4 shows that the roll motion consists of a slowly varying component, having a period equal to twice the encounter period (≈ 45 s), and a fast varying component of which the period is approximately equal to one-third of the slow roll period, namely 15 s. Examination of the moment components reveals that the hydrostatic moment is most dominant, followed by the Froude-Krylov moment. The latter moment has a frequency equal to the slow roll period, and the hydrostatic moment has a frequency of three times the slowly varying roll frequency, i.e., the period of this roll moment component is 15 s. The behavior of the hydrostatic roll moment is similar to the one observed in the first capsize mode, except that now during the passage of a wave crest the restoring arm is reduced considerably beyond the zero value. The slowly varying component of the restoring moment has almost completely disappeared because of these large reductions in the wave crests, so that the fast varying part dominates its behavior. The fluctuations in the hydrostatic component become increasingly large with increasing time, until the roll angle becomes becomes so large as to cause total loss of restoring moment.

Figure 7.5 represents mode (3) of capsizing, which is capsizing preceded by broaching; it is predicted to occur in steep, quartering seas of 30 ft height and a length of about 80 per cent of the ship length. The motion records show that up to about t = 75 s, a steady yaw angle of $\varphi = -12°$ is reached. Subsequently, during the passage of four wave crests, the yaw angle monotonically increases to -35° (despite the rudder being hard over), thereby putting the vessel in a position broadside to the waves, at an angle of 15° off the wave crest parallels. This part constitutes the broach. During the initial stage of the broach, the roll angle was quite large (40°), and once the vessel reached the broadside position to the waves, the angle of roll increased rapidly, and the vessel capsizes on the crest of a wave. The roll moment components are shown in Figure 7.6, and the sudden

rise in the hydrostatic restoring moment during the capsize, having the *same* sign as the roll angle, may be due to the loss of righting arm in the crest of the wave. Before capsizing, the amplitudes of the static and dynamic Froude-Krylov forces are of the same magnitude. The yaw moment components have been plotted in Figure 7.7, which shows that up to t = 80 s the dynamic Froude-Krylov moment is dominant and has a negative mean (resulting in a mean negative yaw angle). The yaw moment exerted by the rudder has a positive mean, and periodically reaches almost zero when a wave trough is amidships, i.e., when a wave crest is approximately at the stern.

Capsizing due to resonant excitation, mode (4), is shown in Figure 7.8 for quartering sea conditions. It is seen that the vessel rolls at the encounter period (≈ 30 s), which is approximately equal to the natural roll period. The roll motion is 180° out of phase with the wave motion and has a negative mean; the roll angles are negative in the crests and positive in the troughs. There is no tendency for capsizing during the passage of the first wave group, while in the second wave group the roll amplitude is seen to increase after t = 200 s until the vessel capsizes on the crest of a wave at t = 265 s. The roll moments are shown in Figure 7.9, from which it is seen that the static and dynamic Froude-Krylov moments have approximately the same amplitudes, and the dynamic Froude-Krylov moment appears to be more regular than the hydrostatic moment component. The moments associated with quadratic roll damping and wave drag are also of significance.

The loss of transverse stability, mode (5), is shown in Figure 7.10 for steep beam sea conditions. Although the vessel rolls 180° out of phase with the waves, it is seen that after t = 20 s, the mean of the roll angle becomes progressively negative until capsizing occurs. From the roll moments plotted in Figure 7.11, it appears that the static and dynamic Froude-Krylov components are dominant. The hydrostatic restoring moment has a positive mean until the point of capsizing. Once the vessel has reached a roll angle of approximately -55°, there is not sufficient restoring energy left after the last wave crest has passed, and the ship rolls further towards port.

The Influence of Wind in Beam Sea Conditions

Wind effects may be of significant influence when the wind direction is at right angles with the beam. Under some conditions, a different angle of attack (e.g. 30° with respect to the ship's longitudinal axis) will lead to the largest wind-induced moment due to hull lift effects. Let us consider exactly the same conditions as for capsize mode (5), and assume that the wind comes from the sane direction as the waves. Without wind, we saw that capsizing occurred after t = 68 s, as is shown in Figure 7.10. It was found that the time span before capsizing was quite sensitive to additional wind forces: for a wind speed of V = 40 ft/s capsizing (toward port) was predicted to occur after t = 53 s, and for V = 50 ft/s capsizing occurred after t = 45 s. The motion records corresponding to the case V = 50 ft/s are shown in Figure 7.12. These results may not be accurate, since the wind velocity and drag coefficient are assumed to be time independent. However, they do suggest that wind should not be omitted from the analysis, when reliable capsize predictions are to be made by simulation for beam seas, and possibly quartering sea conditions.

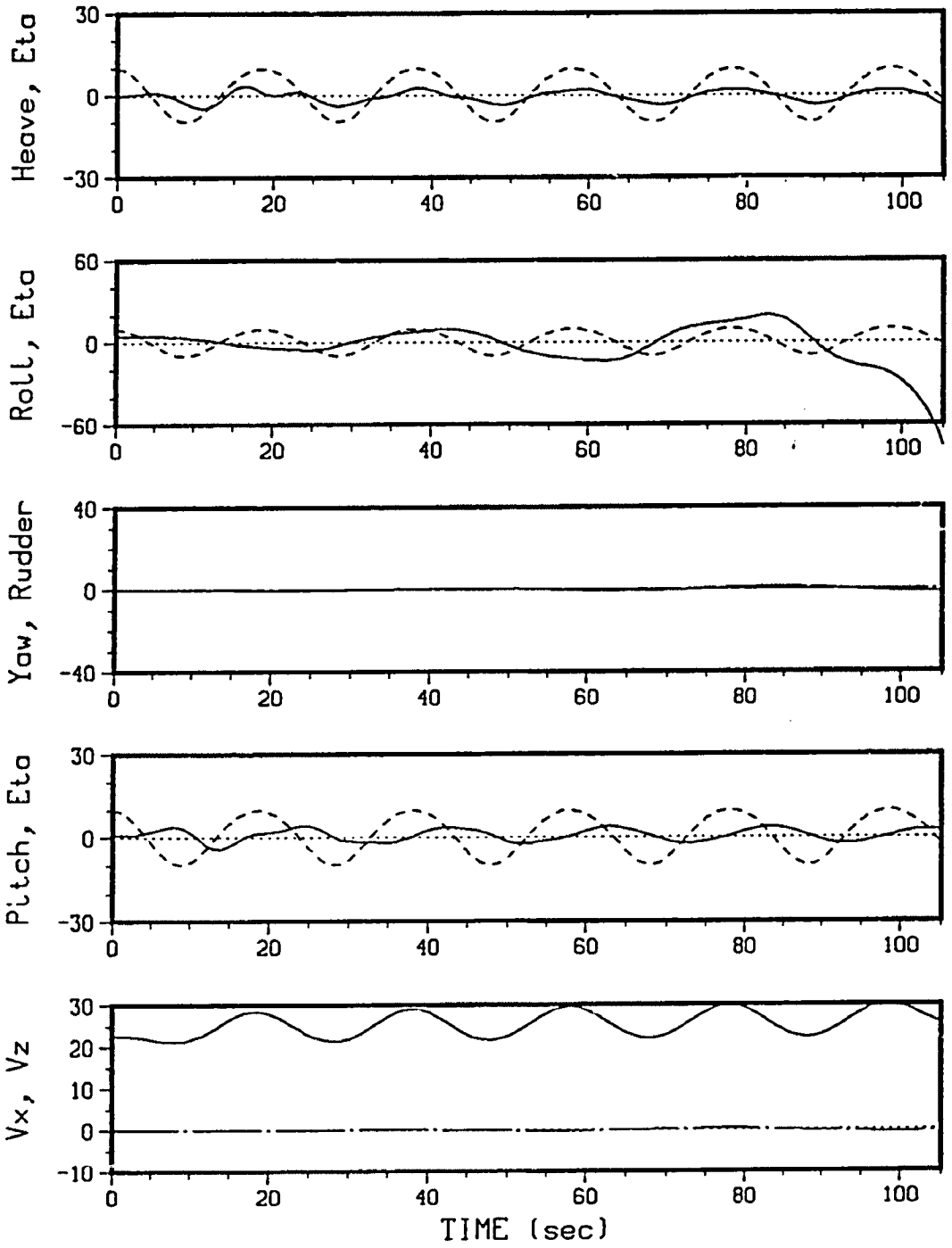

Figure 7.1. Simulation of Capsize Mode (1): Low Cycle Resonance in Following Seas. The dashed lines refer to the wave elevation at the C.G. Displacements are in feet, angles in degrees, and velocities in ft/s.

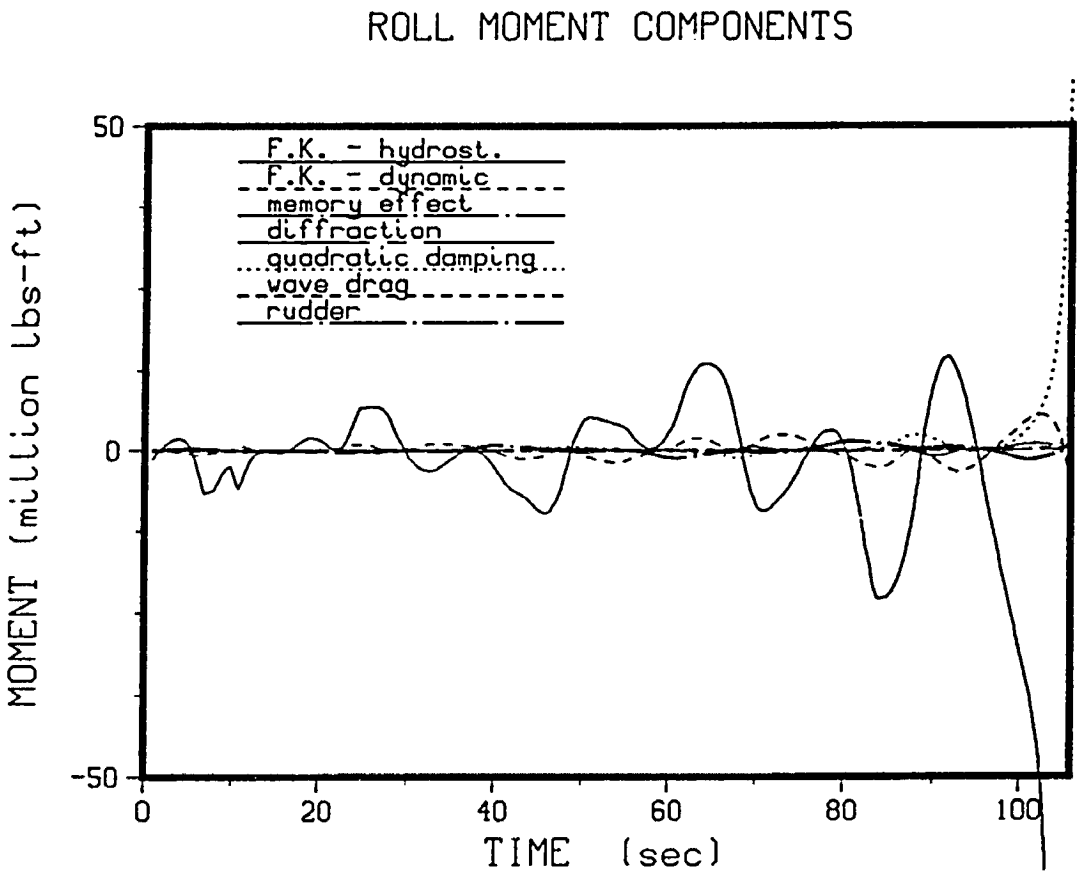

Figure 7.2. Roll Moment Components Associated with Simulation of Capsize Mode (1): Low Cycle Resonance in Following Seas.

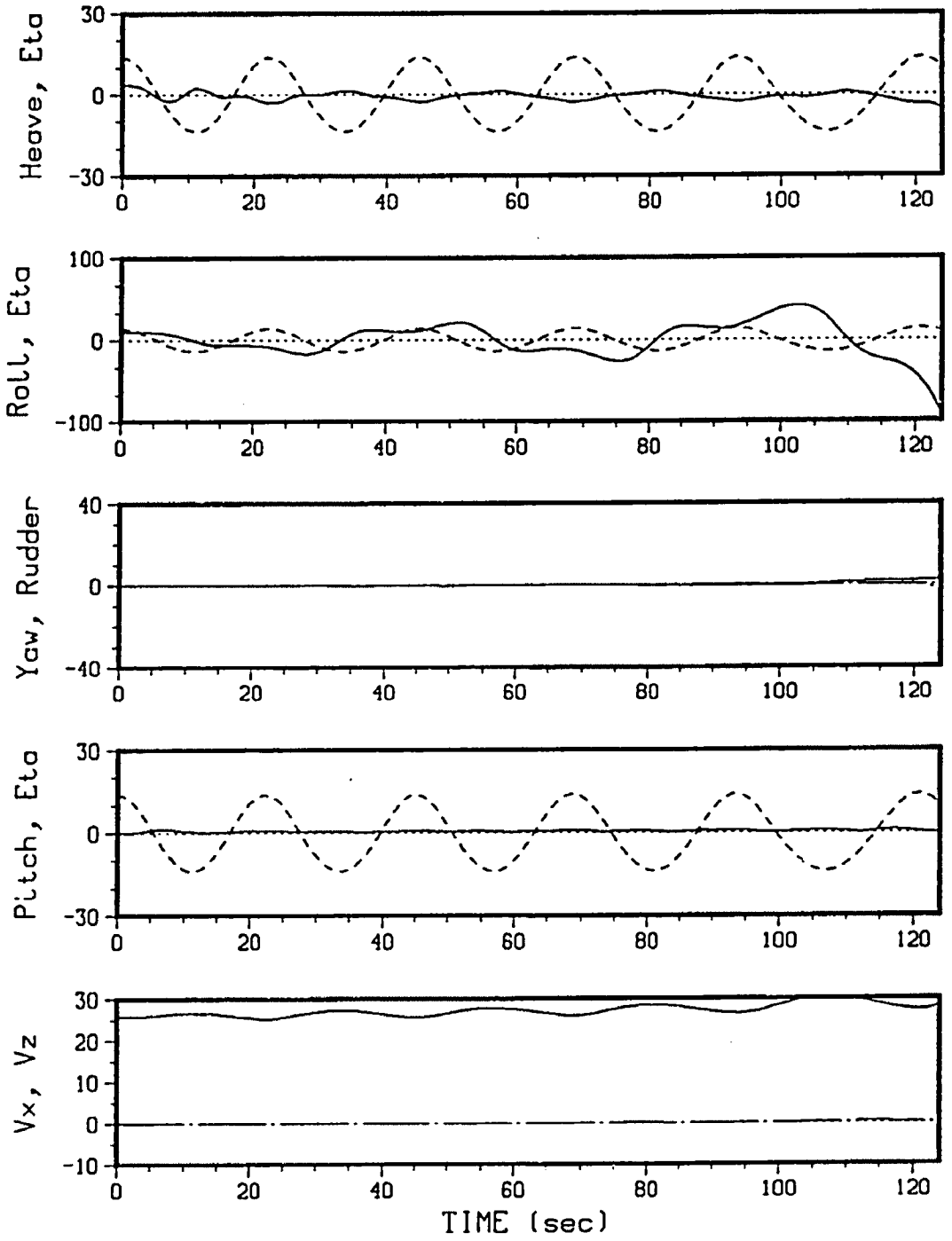

Figure 7.3. Simulation of Capsize Mode (2): Loss of Transverse Stability in Following Seas. The dashed lines refer to the wave elevation at the C.G. Displacements are in feet, angles in degrees, and velocities in ft/s.

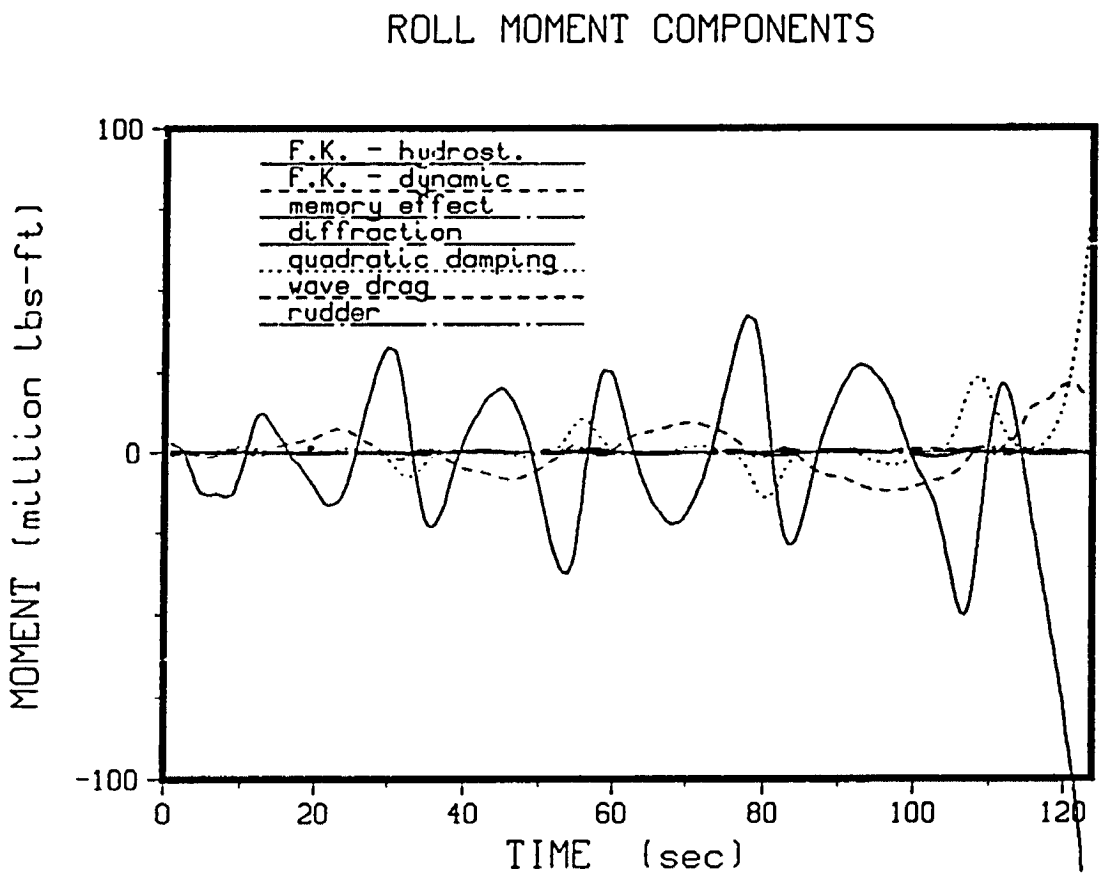

Figure 7.4. Roll Moment Components Associated with Simulation of Capsize Mode (2): Loss of Transverse Stability in Following Seas.

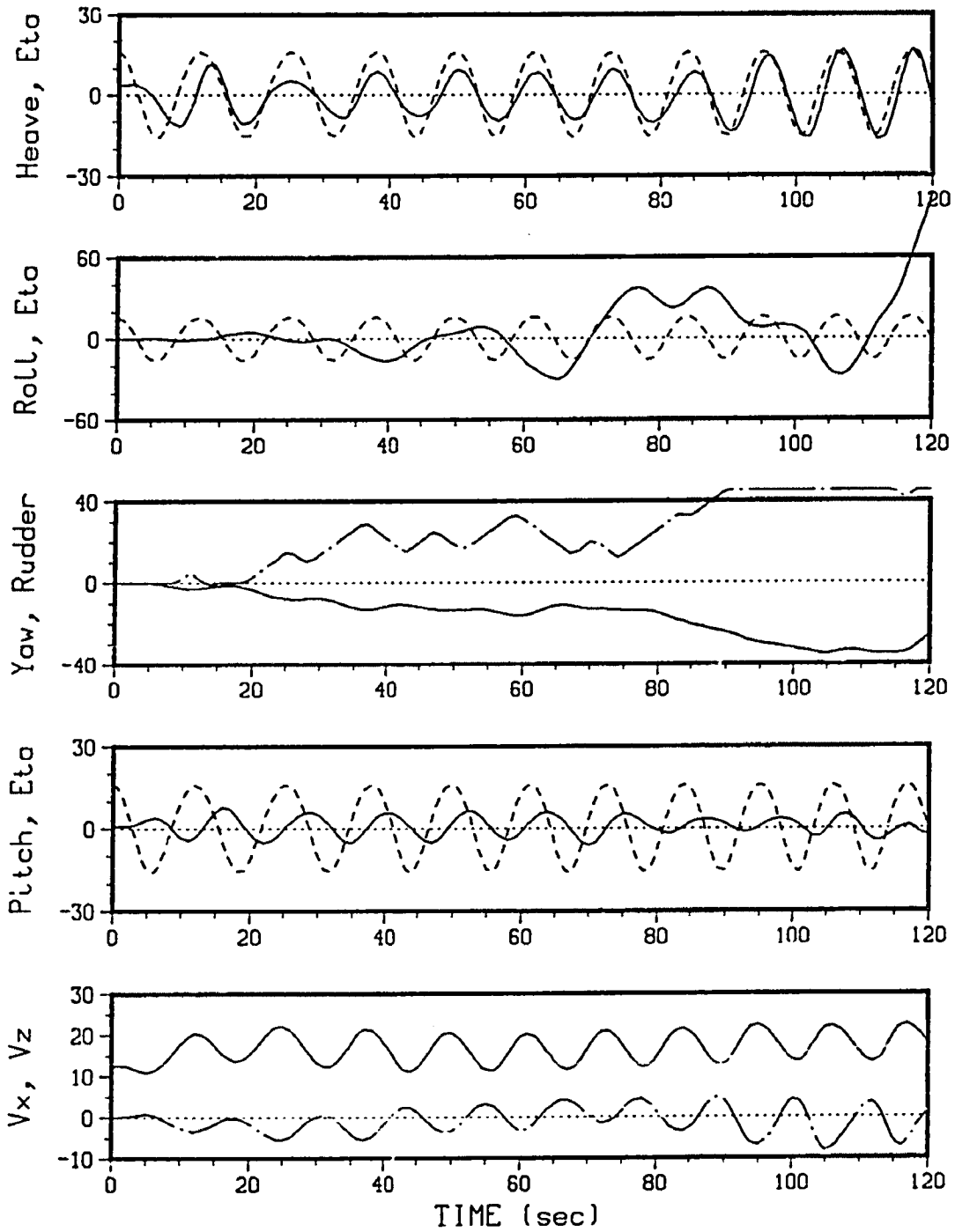

Figure 7.5. Simulation of Capsize Mode (3): Broaching in Successive Quartering Waves. The dashed lines refer to the wave elevation at the C.G. Displacements are in feet, angles in degrees, and velocities in ft/s.

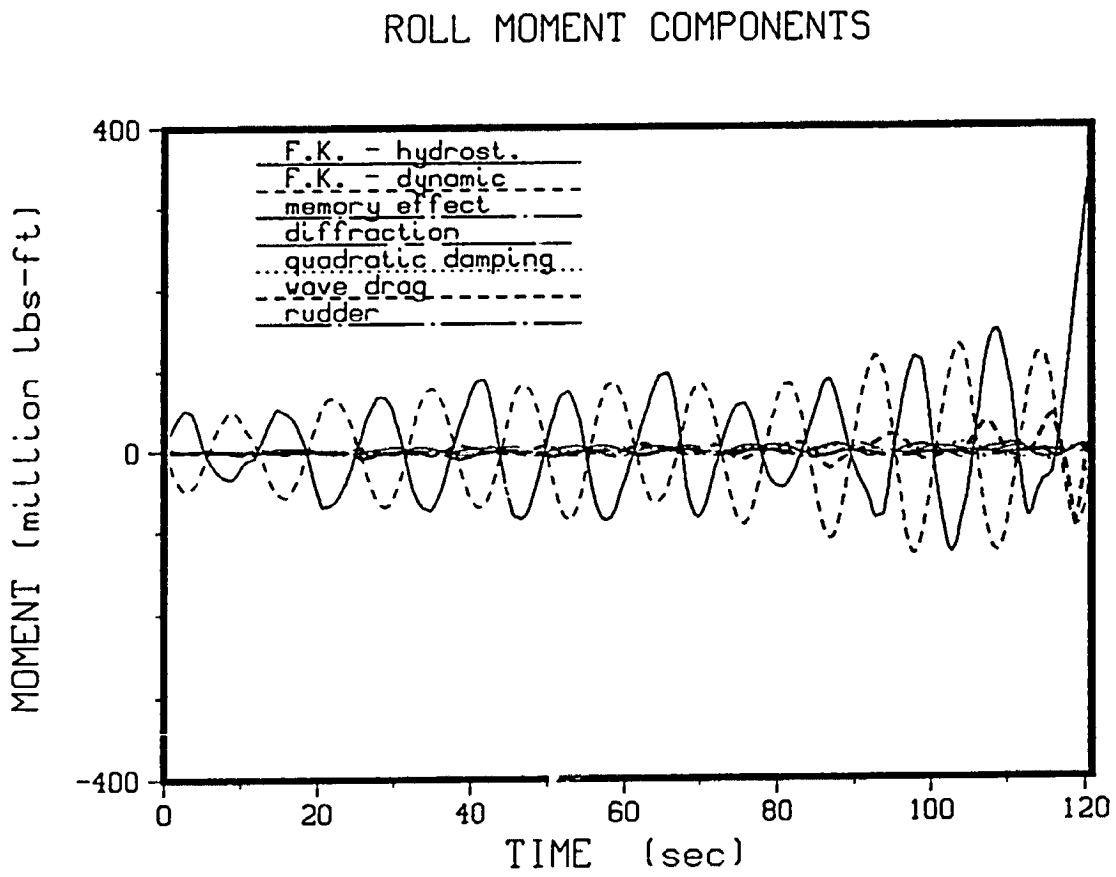

Figure 7.6. Roll Moment Components Associated with Simulation of Capsize Mode (3): Broaching in Successive Quartering Waves.

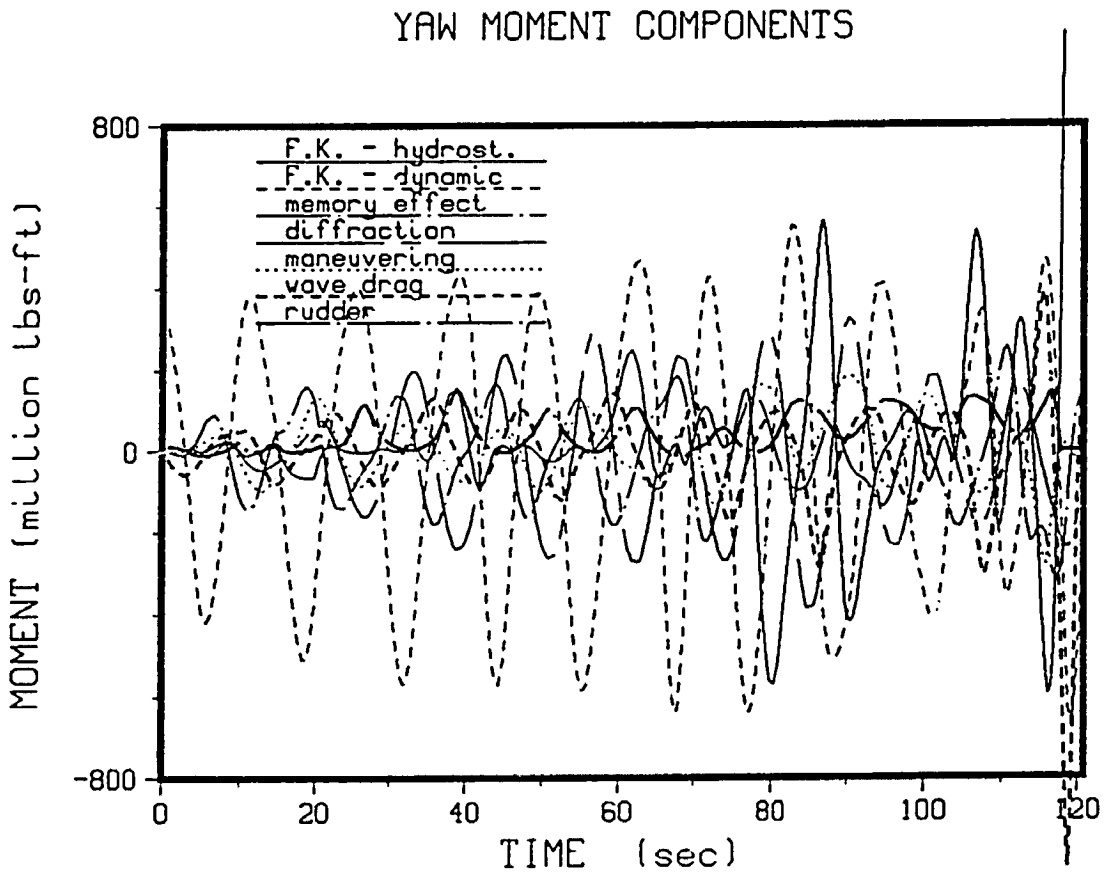

Figure 7.7. Yaw Moment Components Associated with Simulation of Capsize Mode (3): Broaching in Successive Quartering Waves.

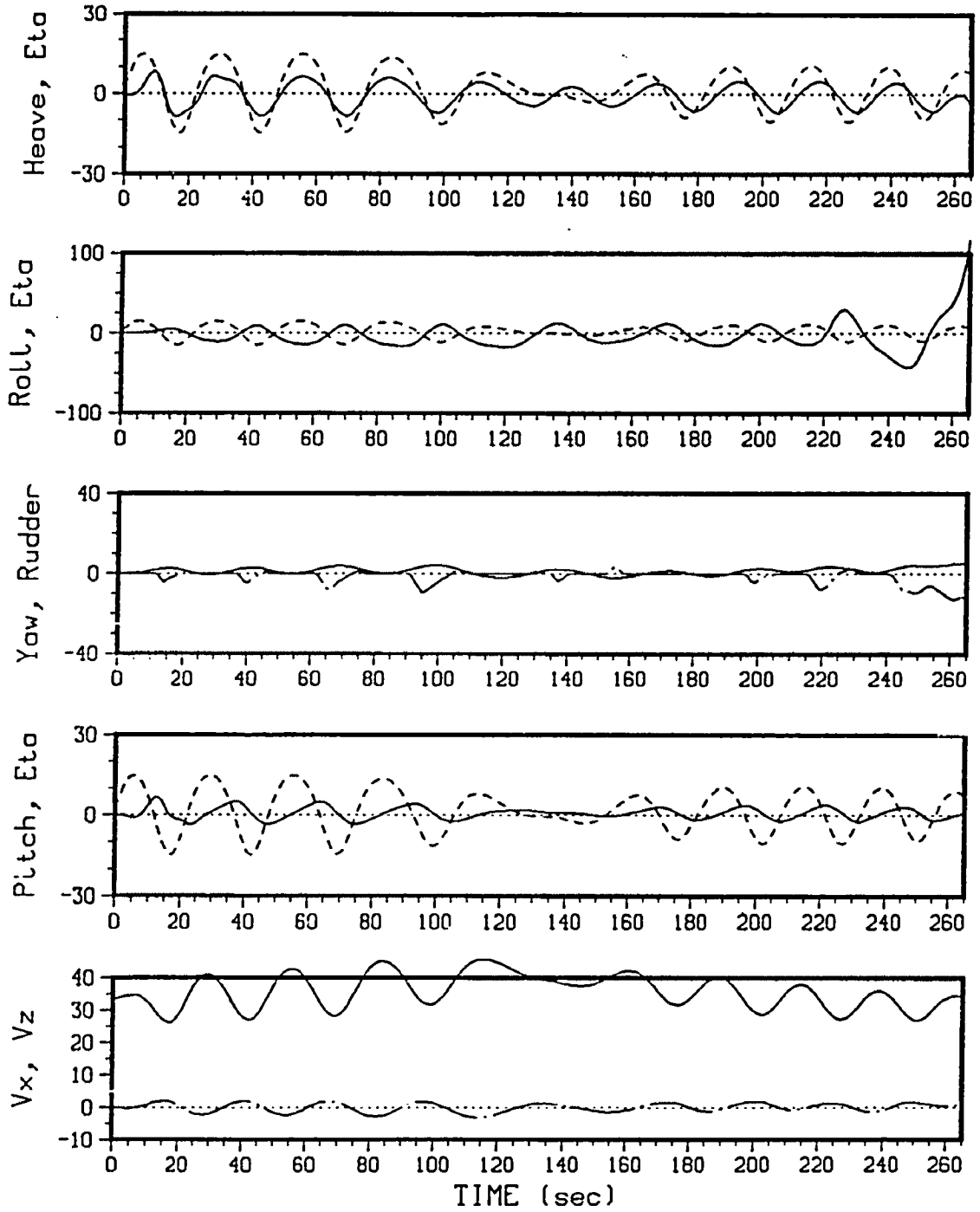

Figure 7.8. Simulation of Capsize Mode (4): Resonant Excitation in Quartering Seas. The dashed lines refer to the wave elevation at the C.G. Displacements are in feet, angles in degrees, and velocities in ft/s.

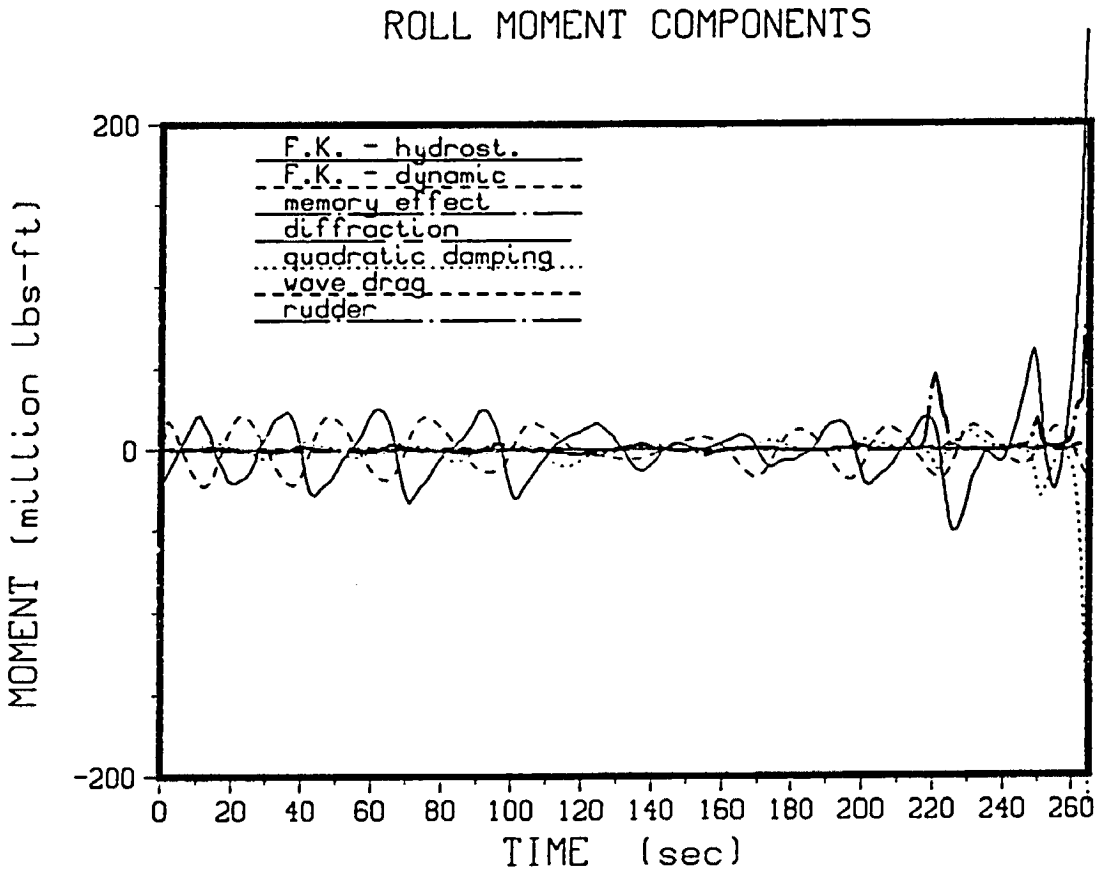

Figure 7.9. Roll Moment Components Associated with Simulation of Capsize Mode (4): Resonant Excitation in Quartering Seas.

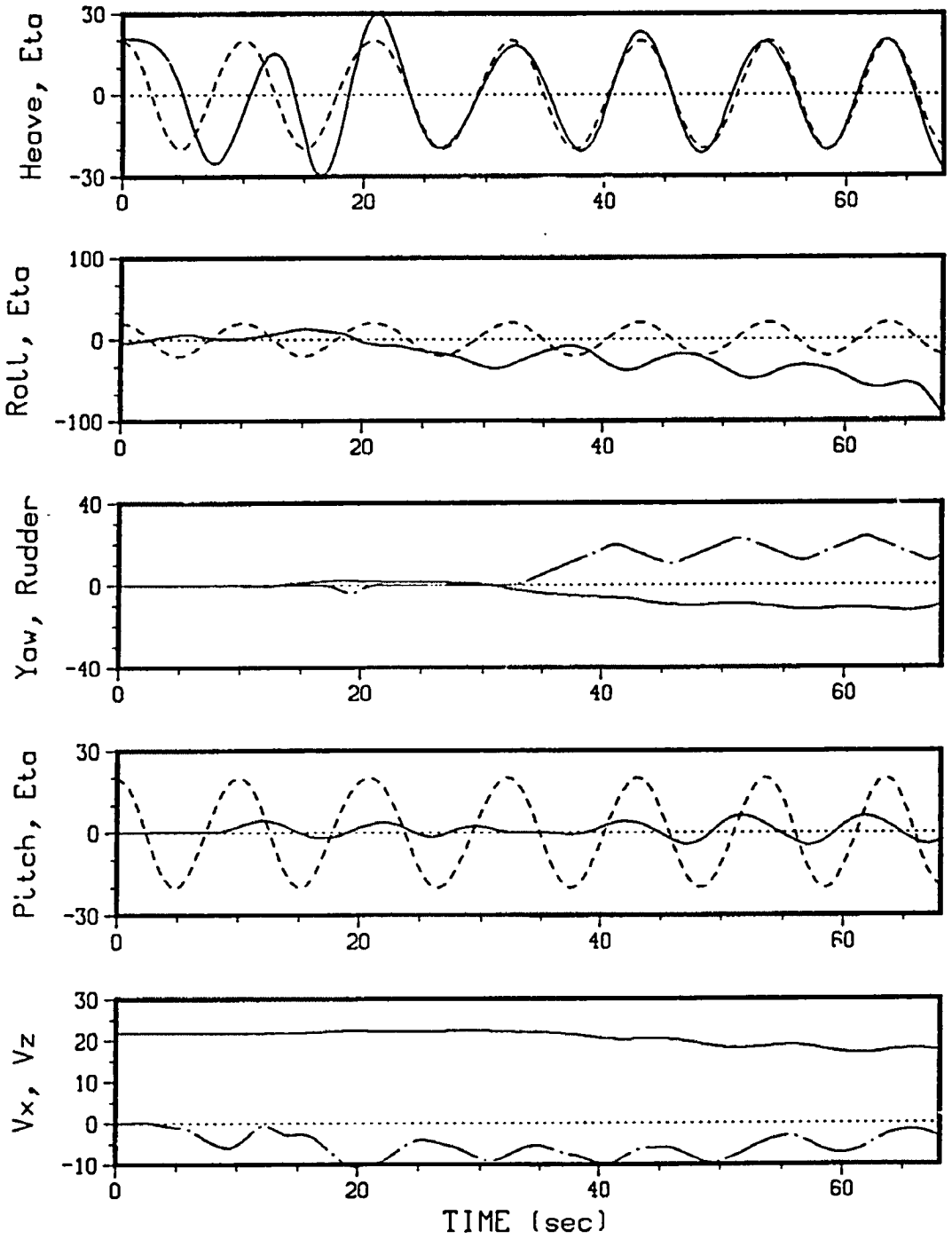

Figure 7.10. Simulation of Capsize Mode (5): Loss of Transverse Stability in Beam Seas. The dashed lines refer to the wave elevation at the C.G. Displacements are in feet, angles in degrees, and velocities in ft/s.

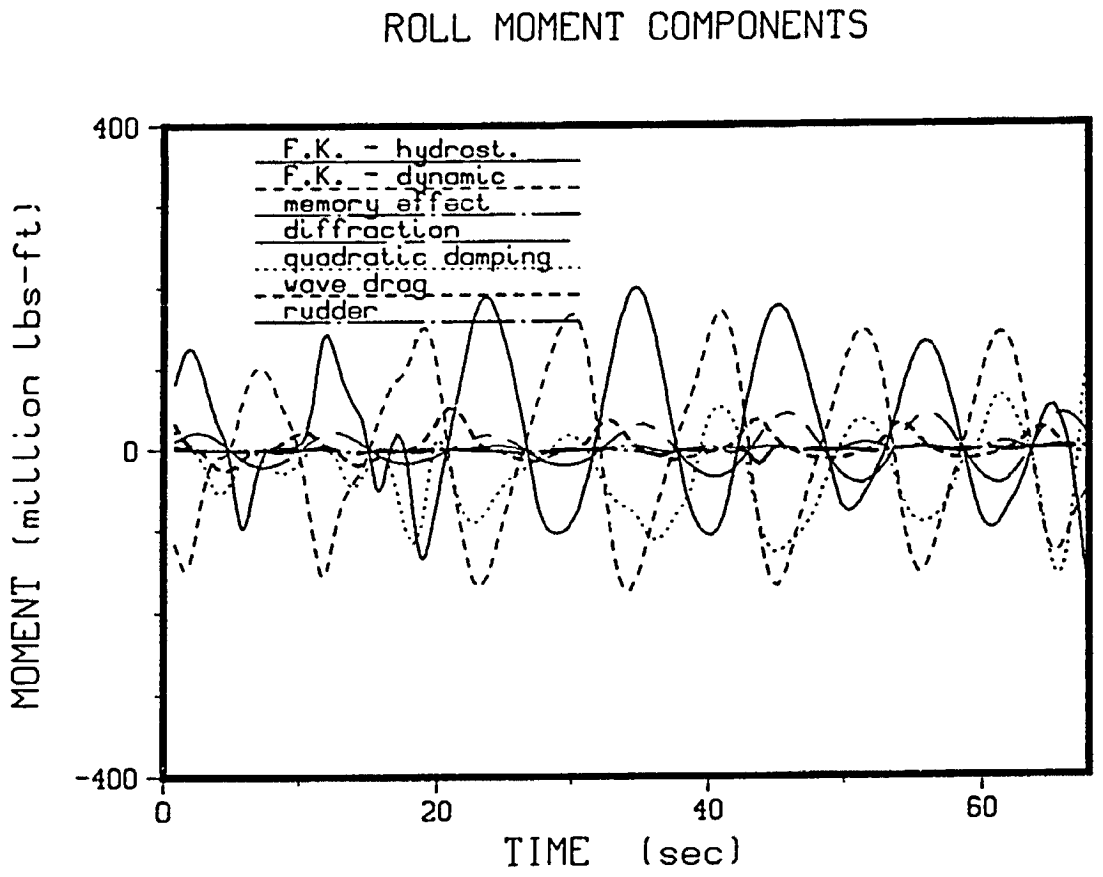

Figure 7.11. Roll Moment Components Associated with Simulation of Capsize Mode (5): Loss of Transverse Stability in Beam Seas.

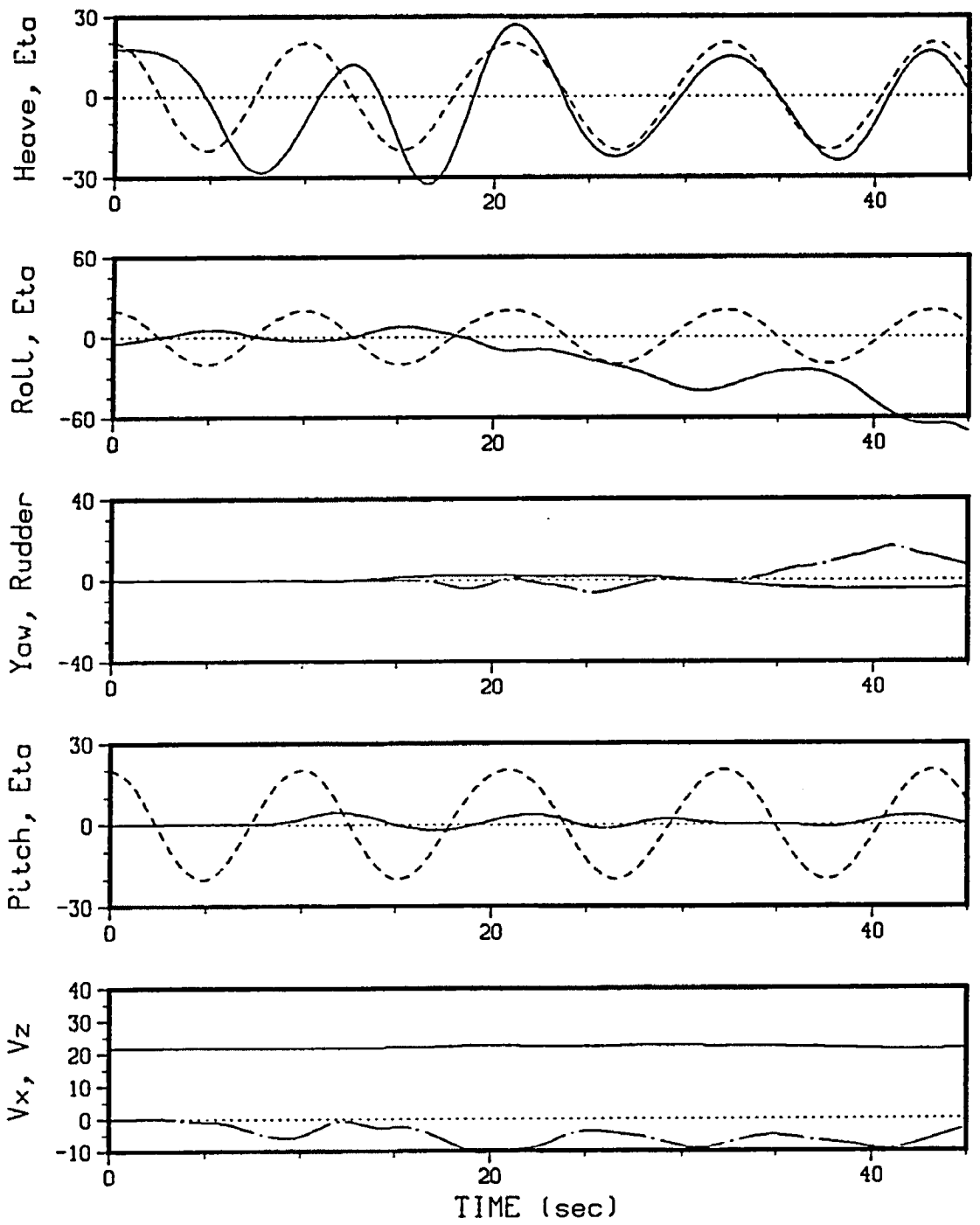

Figure 7.12. Simulation of Capsize Mode (5): Loss of Transverse Stability in Beam Seas with Wind. The wind speed is 40 ft/s, and the same wave conditions are used as in Figure 7.10.

7.2. Critical Conditions for Capsizing

With the aid of the present theory and numerical model, in principle one would be able to develop design charts for a given vessel, indicating ranges of wave, speed, heading and loading conditions that would most probably lead to capsizing. One could do this for a variety of vessel types and sizes, and produce some kind of nondimensional region where capsizing can be expected to occur. Quite a large number of simulations would be needed to produce any data useful for design purposes. It is not the aim of the present author to do so, but instead to consider a certain vessel under conditions for which it is known to capsize in. Next an investigation is made concerning the changes in capsize behavior due to changes in forward speed and heading angle, while the wave conditions are kept the same.

The vessel under consideration is the American Challenger moving along the x-axis in a two-component wave system, representing random sea conditions. The same conditions are used as in the simulation shown in Figure 6.14. The full scale parameters of the American Challenger are the following:

$$\begin{aligned} GM &= 0.86 \text{ ft} \\ \sigma_\theta &= 0.21 \text{ rad/s} \\ U &= 33.68 \text{ ft/s (Fn = 0.26)}, \end{aligned}$$

and the sea state parameters are

$$\begin{aligned} \sigma_p &= 0.53 \text{ rad/s} \\ H_s &= 28 \text{ ft} \\ \delta &= 15°, \end{aligned}$$

where use is made of the equivalent wave system described in Chapter 6.3. An overview of the behavior of the American Challenger is shown in Table 7.1. Capsize occurrences are denoted by crosses (×), with a subscript denoting the mode of capsizing, where

L.R. = low cycle resonance
S.S. = loss of static stability
R.E. = resonant excitation .

U (ft/s)	5	10	15	20	32	33.68	35	40
δ(°)								
5						✓		
10						✓		
15	✓	×L.R.	×L.R.	✓	✓	×S.S.	✓	✓
20						✓		
25						×R.E.		
30						×R.E.		
40						✓		

Table 7.1. Capsize Occurrences of American Challenger

From Table 7.1 it is seen that the vessel will avoid capsizing by a speed increase, while too much of a speed decrease will lead to low cycle resonance followed by capsizing. It is also interesting that increasing the heading angle to between 25 and 30 degrees with respect to the waves will also lead to capsizing. A few more remarks are made below about low cycle resonance.

Autoparametric excitation leads to low cycle (or subharmonic) resonance, which typically ends in a capsize, if the oscillations continue to grow and not enough damping is available in the system to limit the amplitudes to an acceptable level. For small amplitudes of roll, subharmonic resonance will occur when the encounter frequency is twice the natural roll frequency, provided the wave length is sufficiently long, i.e., on the order of the ship length. This behavior can be explained by means of the Mathieu equation, in which one of the coefficients describing the restoring force is time dependent. This kind of excitation is referred to as parametric excitation, which was originally investigated in relation to ships by Grim (1952). The Mathieu equation is a special case of the Hill

equation, which is the following general differential equation (see e.g. Stoker (1950)) for a single degree of freedom system having a time-dependent restoring force term:

$$\frac{d^2\theta}{dt^2} + k(t)\,\theta = 0,$$

where k(t) is periodic in t. If k(t) is sinusoidal, the Mathieu equation with respect to the roll motion θ can be written as

$$\frac{d^2\theta}{dt^2} + (\delta + \varepsilon.\cos\theta)\,\theta = 0 \ .$$

For a vessel rolling in waves the hydrostatic restoring moment can be considered as having a time-dependent coefficient, because the righting arm depends on both the position of the wave with respect to the vessel and on the angle of heel of the vessel itself. For small values of ε (i.e., small roll motions), instabilities are predicted to occur when the solutions are unbounded; for $\varepsilon = 0$, it has been shown (see e.g. Grim (1952), Paulling and Rosenberg (1959), or Nayfeh (1981)) that instabilities occur at the points where the stable and unstable regions meet, that is, at the following discrete values of δ:

$$\frac{\sigma_\theta^2}{(\sigma^e)^2} = \frac{n^2}{4} = \delta, \qquad n = 0, 1, 2, \ldots$$

where σ^e is the encounter frequency and σ_θ is the natural roll frequency. In ship roll problems the case n = 1 is usually of most concern. As is apparent from the regions where Mathieu instabilities occur, autoparametric resonance will occur for a larger range of encounter frequencies when the roll amplitudes are larger. Thus, the regions exhibiting stable motion behavior become smaller as the roll amplitude increases. Paulling and Rosenberg (1959) also showed that parametric

excitation can result from coupling between roll and pitch motions, for example. Lindemann and Skomedal (1983) describe low cycle resonance with the Mathieu equation, and it is argued that the relative heave motion may result in a significant transfer of energy into the roll mode of motion.

In order to determine the range of conditions for which parametric resonance may occur, it is useful to examine the behavior of the encounter frequency curve, which is shown for following sea conditions in Figure 7.12. From Figure 7.12 it is seen that reducing speed or increasing the heading slightly will in theory always result in the possibility of parametric excitation. The speed can be increased to a certain speed beyond which no such excitation should occur; this speed is such that the following should be satisfied: $\sigma^e_{max} < \sigma^*$, where (see Chapter 2.4.4)

$$\sigma^* = 2\sigma_\theta \text{, and}$$

$$\sigma^e_{max} = \frac{g}{4U.\cos\beta} .$$

Thus, to avoid parametric excitation for the case n = 1, the speed should be as follows:

$$U > \frac{g}{8.\sigma_\theta.\cos\beta} .$$

The range of frequencies possibly leading to low cycle resonance and capsizing is shown schematically in Figure 7.13.

Some of the characteristics of autoparametric resonance are the following. This type of resonance occurs typically for ships of fine shape and relatively small block coefficient, i.e., ships that exhibit large changes in waterplane area with small changes in draft, such as container and Ro-Ro ships. The wave conditions during which it can be expected to occur are following to quartering seas, where the length of the wave must be of the order of the ship length. In regular waves, the wave amplitude

does not have to be very large for low cycle resonance to start, although this depends on the hull shape. The response behavior is dominated by hydrostatic forces and viscous damping. In theory, a ship may experience low cycle resonance also in other conditions, such as head seas (which has been observed experimentally for small boats); it is questionable whether it is of relevance with respect to capsizing because of the high frequency of encounter relative to the roll frequency. It should be noted also that there have been no documented cases of capsizing that were clearly attributable to low cycle resonance.

In order to determine which conditions will actually lead to low cycle resonance and capsizing, the following procedure could be used. For a given vessel configuration, speed and heading, one can calculate the frequency (or range of frequencies) for which parametric excitation is likely to occur. By means of simulation it would then be possible to determine the corresponding wave amplitude range, where unacceptable motions could be expected. It would be of interest also to investigate random sea conditions that may cause low cycle resonance.

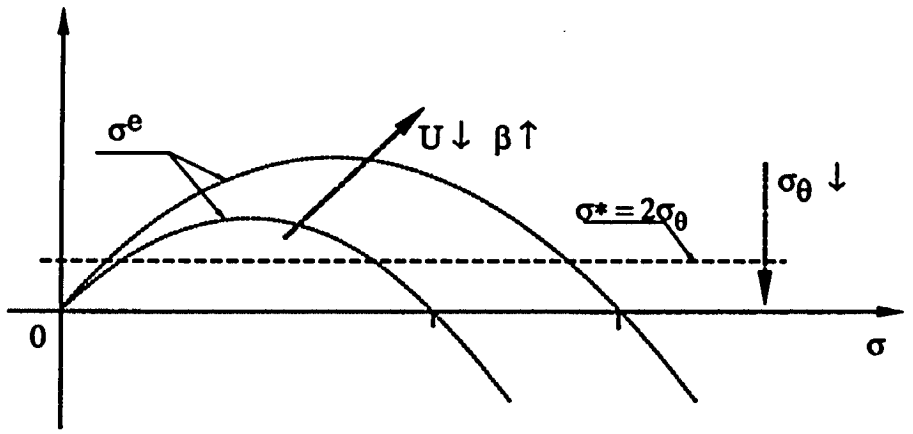

Figure 7.12. Schematic Behavior of Encounter Frequency Curve as a Function of Varying Speed, Wave Heading, and Natural Roll Frequency. E.g. the positive root of the parabola increases as the ship speed decreases.

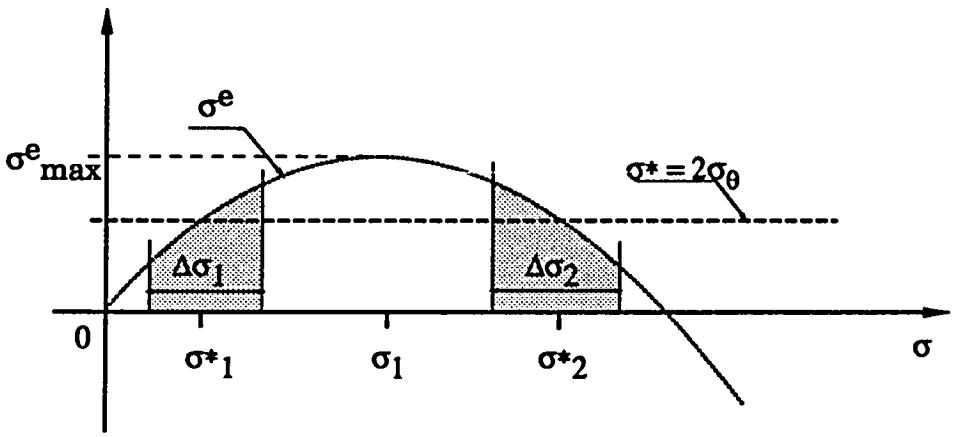

Figure 7.13. Schematic Representation of Range of Wave Frequencies for Which Parametric Excitation May Occur.

CHAPTER 8

Conclusions

In this work a numerical model has been developed to determine the large amplitude motions of a steered vessel subjected to severe wave conditions, including those that may lead to capsizing. With this model it was possible to study several mechanisms of capsizing, together with the conditions that would cause such catastrophic behavior. Different modes of capsizing observed experimentally were obtained by simulation.

The theory is based on a combination of potential and viscous flow approaches in the time domain. The potential theory for determining the wave-induced motions is essentially linear, but extended so as to take into account the time-dependent free surface as well as memory effects. Nonlinear viscous effects are modelled in an empirical fashion, where attention is paid to roll damping in waves, drag forces due to waves, maneuvering forces, and coupling between sway and roll. The following physical factors have been neglected in this work: cargo shifting, water on deck, wave breaking and slamming. The present model could be greatly enhanced by including these additional features.

Reasonable agreement was found between predicted motion results and experimental results, both for small and large wave amplitudes. Comparisons were made with respect to the heave, roll and pitch motions of typical cargo vessels, such as containerships. A number of capsizes observed in the towing tank, for following sea conditions, were simulated quite successfully using the present theory. Also, it was possible to predict capsizing in severe random seas, as observed by experiment.

Since little was previously known about the relative importance of the various force contributions as regards the ship motion problem in waves, an investigation has been carried out to determine the sensitivity of the roll response to changes in the force components. It was found that the Froude-Krylov forces are always of importance, irrespective of the wave conditions. This suggests that one of the main assumptions in this work

is correct, namely, that the Froude-Krylov forces are the most critical and need to be evaluated accurately when predicting motions in severe seas. For following sea conditions, the hydrostatic forces and roll damping forces are dominant, while in beam seas the relative importance of the various components depends very much on the ship and wave conditions. None of the force components considered in the theoretical model were consistently insignificant. Only a little attention has been paid to wind effects, although simulations and experience suggest that wind may play an important role when considering motions in beam sea conditions.

In the course of this work some new light was shed on wave statistics observed in simulated random following seas, where the number of superposed wave components is finite. Contrary to common procedures, it was found that the mean square value of the wave elevation observed at a fixed point, and from a reference point moving at an angle with the waves, can be different, even as time approaches infinity. The differences will depend on the phases of the individual wave components and on the distribution of the wave energy (spectral shape). For a large number of wave components, the variance of the observed mean square values is less than for a small number of components. When an observer travels with the waves at mean group speed, the variance of the encountered mean square wave elevation will be highest.

The observed wave elevation at any point on the hull may appear to be regular when the vessel moves with a random wave system, as has been shown by simulations. Under those conditions, the spectrum of the observed waves may become very narrow and peaked. However, simulations in this work have shown that one cannot arbitrarily replace the random wave system with a regular wave, because such an approach neglects the spatial randomness of the sea surface. Simulations indicated that the wave profile along the ship is not reflected by the behavior observed at only one fixed point on the vessel. The roll motion behavior is quite sensitive to the spatial characteristics of the sea surface, and care should be taken in the choice of the seaway representation when conducting simulations in random waves.

For capsize simulations in following sea conditions, it has been shown that the random sea may be replaced by an equivalent wave system, consisting of only two components. Such an equivalent wave system would greatly reduce the required computation time when studying capsizing in random following seas, provided that the correct initial conditions are used in the simulations. More work is needed to fully assess the usefulness of this approach.

Several modes of capsizing in following to beam seas have been identified by simulation: parametric excitation, loss of transverse stability, broaching and resonant excitation. These modes have been previously identified by experiment. An analysis has been made of the behavior of the roll moment components associated with the various capsize modes. For a given mode of capsizing, the necessary changes in speed and heading to avoid a capsize situation were determined by simulation.

CHAPTER 9

Nomenclature

$\mathbf{a}$	acceleration vector
A_i	amplitude of i^{th} wave component in seaway
$A_w(\sigma)$	wave amplitude associated with frequency σ
A_S	cross-sectional area at a station
$\mathbf{A}$	generalized added mass matrix (6x6)
$A_{ij}(\sigma)$	three-dimensional added mass coefficient (i,j = 1,...,6), component of $\mathbf{A}$
$\mathbf{B}$	angular velocity transformation matrix (3×3)
B	beam of the vessel
$B_{44,L}$	linear roll damping coefficient
$B_{44,Q}$	quadratic roll damping coefficient
$B_{34,Q}$	quadratic roll-sway damping coefficient
$B_{43,Q}$	quadratic sway-roll damping coefficient
$B_{ij}(\sigma)$	three-dimensional damping coefficient (i,j = 1,...,6)
C_D	drag coefficient
C.G.	center of gravity of the vessel
C_g	wave group velocity
$C_{g,p}$	mean wave group velocity associated with peak frequency σ_p
C_L	lift coefficient
C_p	wave phase velocity
d	draft of the vessel
$\mathbf{f}(t)$	generalized force vector (6×1)
$\mathbf{f}_D(t)$	time-dependent diffraction force vector
$\mathbf{F}_D(\sigma)$	frequency-dependent diffraction force amplitude vector
$\mathbf{f}_{FK}(t)$	time-dependent Froude-Krylov force vector
$\mathbf{f}_{FK,s}(t)$	static Froude-Krylov force vector
$\mathbf{f}_{FK,d}(t)$	dynamic Froude-Krylov force vector
$f_i(t)$	force vector component (i = 1,...,6)
$f_{drag,w}(t)$	wave-induced viscous drag force (i = 3,4,5)
$f_{m,i}(t)$	maneuvering force vector component (i = 3,5)
$f_{res}(t)$	ship resistance force
$f_{rud}(t)$	rudder force

g	gravitational acceleration coefficient
GM	transverse metacentric height
$H(\sigma)$	frequency domain transfer function
H_s	significant wave height (average of 1/3 of the highest waves)
$\mathbf{I}$	moments of inertia matrix (3 ×3)
J	propeller advance ratio
k	wave number
k_x, k_z	wave number components in x and z directions
K_T	thrust coefficient
KG	vertical position of center of gravity of vessel
L	length of the vessel
$L_{ij}(\tau)$	first order kernel function (i,j = 1,...,6)
m	structural mass of vessel
$\mathbf{M}$	generalized structural mass matrix (6 ×6)
M_{ij}	component of $\mathbf{M}$ (i,j = 1,...,6)
$\mathbf{n}$	unit normal vector (outward is positive)
N	total number of wave components in random seaway
$Oxyz$	earth-fixed reference system
$O^ex^ey^ez^e$	reference system translating with the vessel at its mean speed in the Oxz plane
$O^*x^*y^*z^*$	local coordinate system, fixed in the structure (O* located at C.G.)
p	pressure
$P(.)$	probability of occurrence of a certain event
S	instantaneous (time-dependent) wetted surface
S_0	wetted surface in calm water equilibrium condition
$S_{\eta\eta}(\sigma)$	one-sided spectral density of the waves
S_θ	response sensitivity coefficient
t	time
$\mathbf{T}$	direction cosine transformation matrix (3 ×3)
U	forward speed of vessel in calm water
$u_i(t)$	wave particle displacement component (i = 1,2,3)
$\dot{u}_i(t)$	wave particle velocity component (i = 1,2,3)
$\mathbf{v}$	translational velocity vector of structural center of gravity
V	total displaced volume of vessel

$\mathbf{x}$	displacement vector in Oxyz system of structural center of gravity
$\dot{\mathbf{x}}(t)$	velocity vector of C.G. in Oxyz system
$\ddot{\mathbf{x}}(t)$	acceleration vector of C.G. in Oxyz system
$x_i(t)$	displacement component of C.G. in Oxyz system (i = 1,2,3)
x_A	x*-coordinate of most aft point on wetted hull
x_F	x*-coordinate of most forward point on wetted hull
α	wave slope parameter
β	relative heading angle between ship heading and wave direction (0 degrees is following seas)
δ	wave direction w.r.t. x-axis (0 degrees is along the positive x-axis)
$\delta(.)$	Dirac delta function
ε	wave phase angle (0 degrees is wave crest at C.G.)
ζ_0	(linear) critical damping coefficient
$\eta(t)$	time-dependent wave elevation
$\eta_{M.S.}$	mean square value of wave elevation process
λ	wave length
ρ	sea water density
ρ_{xx}	roll radius of gyration
ρ_{yy}	yaw radius of gyration
ρ_{zz}	pitch radius of gyration
σ	circular frequency (rad/s)
σ^e	encounter frequency
σ_p	peak frequency in random sea spectrum
τ	time lag
ω	angular velocity vector (components about O*x*y*z* axes)
$\dot{\omega}$	angular acceleration vector
ϕ, ψ, θ	Euler angles (yaw, pitch and roll, respectively)
$\Phi(t)$	time-dependent velocity potential
φ	time-independent velocity potential
Φ_D	time-dependent diffraction potential
Φ_I	time-dependent potential of undisturbed incoming wave system
Φ_R	time-dependent potential due to radiated waves
Φ_U	time-independent potential due to steady forward speed

χ	vector containing Euler angles (3 x 1)
∇	gradient operator

CHAPTER 10

Bibliography

Adachi, H., and Ohmatsu, S. (1980), "On the Time Dependent Potential and Its Application to Wave Problems", *13th Symp. Naval Hydrodyn.*, Tokyo, pp. 281-302

Allievi, A.G., Calisal, S.M., and Rohling, G.F. (1986), "Motions and Stability of a Fishing Vessel in Transverse and Longitudinal Seaways", *Proc. 11th STAR Symposium*, Portland, May, pp. 13- 31

Ankudinov, V. (1983), "Simulation Analysis of Ship Motion in Waves", *Int. Workshop on Ship and Platform Motions*, Berkeley, Oct. 26-28, pp. 384-403

Barr, R.A., and Ankudinov, V. (1977), "Ship Rolling, Its Prediction and Reduction Using Roll Stabilization", *Marine Technology*, Vol. 14, No. 1, Jan., pp. 19-41

Barrie, D.A. (1986), "The Influence of Diffraction on the Stability Assessment of Ships", *The Naval Architect*, Jan.

Beck, R.F., and Liapis, S. (1987), "Transient Motion of Floating Bodies at Zero Forward Speed", *J. Ship Research*, Vol. 31, No. 3, Sept., pp. 164-177

Bedel, J.W., and Lee, C.M. (1971), "Numerical Calculation of the Added Mass and Damping of Cylinders Oscillating In or Below a Free Surface", *NSRDC Report* , No. 3551, March

Bishop, R.E.D., Burcher, R.K., and Price, W.G. (1973), "The Uses of Functional Analysis in Ship Dynamics", *Proceedings Roy. Soc. London*, Vol. 332, pp. 23-35

Blagoveshchensky, S.N. (1962), *Theory of Ship Motions*, 2 Volumes, Dover Publications

Blocki, W. (1980), "Ship Safety in Connection with Parametric Resonance of the Roll", *Int. Shipb. Progress*, Vol. 27, No. 306, Feb., pp. 36-53

Blume, P. (1987), "Uber ein Konzept zur Beurteilung der Sicherheit gegen Kentern", *Schiffstechnik*, Vol.34, No. 1, May, pp. 21-27

Blume, P., and Hattendorf, H.G. (1984), "Ergebnisse von systematischen Modellversuchen zur Kentersicherheit", *Jahrbuch der Schiffbautechnischen Gesellschaft*, Vol. 78, pp. 219-243

Brillinger, D.R. (1981), *Time Series: Data Analysis and Theory*, Holden-Day, Inc.

Brook, A.K. (1986), "The Role of Simulation in Determining the Roll Response of a Vessel in an Irregular Seaway", *RINA Int. Conf. on the Safeship Project: Ship Stability and Safety*, London, June

Børresen, R., and Hambro, L. (1978), "Heave Motion of Floating Bodies with Nonlinear Restoring Force", *Det norske Veritas Report*, No. 78-620, Oct.

Børresen, R. and Tellsgård, F. (1979), "Nonlinear Response of Vertical Motions and Loads in Regular, Head Waves", *Det norske Veritas Report*, No. 79-1097, Part I and II, Dec.

Chakrabarti, S.K. (1971), Discussion on "Dynamics of Single Point Mooring in Deep Water", *J. of Waterways, Harbor and Coastal Engg.*, Vol. 97, WW3, pp. 588-590

Chapman, R.B. (1979), "Large-Amplitude Motion of Two-Dimensional Floating Bodies", *J. Ship Research*, Vol. 23, No. 1, March, pp. 20-31

Chapman, R.B. (1980), "Time-Domain Method for Computing Forces and Moments Acting on Three Dimensional Surface-Piercing Ship Hulls with Forward Speed", *Science Applications Report*, No. SAI-462-80-560-LJ, Sept.

Chou, S.-J. (1977), "Selection of Optimum Wave Conditions for Time Domain Simulations of Nonlinear Phenomena", *Ph.D. Dissertation*, Dept. of Naval Arch. and Offshore Eng., Univ. of California, Berkeley, Aug.

Chou, S.J, Oakley, O.H., Paulling, J.R., Van Slyke, R., Wood, P.D., and Zink, P.F. (1974), "Ship Motions and Capsizing in Astern Seas", Final Report for Period August 1970 - December 1974, Dept. of Naval Arch. and Offshore Eng., University of California, Berkeley, Dec.

Comstock, J.P., Ed. (1967), *Principles of Naval Architecture*, Soc. of Nav. Arch. and Mar. Eng.

Conolly, J.E. (1972), "Stability and Control in Waves: A Survey of the Problem", Proc. Int. Symp. on Directional Stability and Control of Bodies Moving in Water, *J. Mech. Engg. Science*, Vol. 14, No. 7, Supplem. Issue, pp. 186-193

Cummins, W.E. (1962), "The Impulse Response Function and Ship Motions", *Schiffstechnik*, Vol. 9, No. 47, June, pp. 101-109

Dahle, A.E., and Kjærland, O. (1980), "The Capsizing of M/S Helland-Hansen", *The Naval Architect*, pp. 51-70

Dahle, L.A. (1984), "Mobile Platform Stability Project Synthesis", *MOPS* Report No. 21, Norwegian Hydrodynamic Laboratories, Dec.

Davidson, K.S.M. (1948), "The Steering of Ships in Following Seas", *Proc. VIIth Int. Congress for Appl. Mech.*, Vol. 2, London, Sept., pp. 554-568

Dillingham, J. (1981), "Motion Studies of a Vessel with Water on Deck", *Marine Technology*, Vol. 18, No. 1, pp. 38-50

Dillingham ,J. (1986), "A Numerical Method for Simulating Three-Dimensional Sloshing", *Proc. 11th STAR Symposium*, Portland, May, pp. 75-85

Downie, M.J., Bearman, P.W., and Graham, J.M.R. (1988), "Effect of Vortex Shedding on the Coupled Roll Response of Bodies in Waves", *J. Fluid Mech.*, Vol. 189, pp. 243-264

Du Cane, P., and Goodrich, G.J. (1962), "The Following Sea, Broaching and Surging", *Quarterly Trans. Roy. Inst. Nav. Arch.*, Vol. 104, No. 2, April, pp. 109-140

Eda, H. (1972a), "Yaw Control in Waves", Int. Symp. on Directional Stability and Control of Bodies Moving in Waves, *Inst. of Mech. Eng.*, London, April, pp. 180-184

Eda, H. (1972b), "Directional Stability and Control of Ships in Waves", *J. Ship Research*, Sept., pp. 205-218

Elgar, S., Guza, R.T., and Seymour, R.J. (1985), "Wave Group Statistics from Numerical Simulations of a Random Sea", *Applied Ocean Research*, Vol. 7, No. 2, pp. 93-96

Elsimillawy, N., and Miller, N.S. (1986), "Time Simulation of Ship Motions: A Guide to the Factors Degrading Dynamic Stability", *Trans. Soc. Nav. Arch. and Mar. Eng.*, Vol. 94, pp. 215-240

Fallon, W., Hwang, Y.-L., Liguori, J.S., Paulling, J.R., Visineau, G., and Wood, P. (1980), "Model Tests and Numerical Simulation of Ship Capsizing in Following Seas", Report, Dept. of Nav. Arch. and Offsh. Eng., Univ. of California, Berkeley, Jan.

Faltinsen, O.M., and Sortland, B. (1987), "Slow Drift Eddy Making Damping of a Ship", *Applied Ocean Research*, Vol. 9, No. 1, pp. 37-46

Frank, W. (1967), "Oscillation of Cylinders In or Below the Free Surface of Deep Fluids", *NSRDC Report*, No. 2375, Oct.

Frank, T., Loeser, D.J., Scragg, C.A., Sibul, O.J., Webster, W.C., and Wehausen, J.V. (1976), "Transient-Maneuver Testing and the Equations of Maneuvering", *Proc. 11th Symp. Naval Hydrodynamics*, London

Froude, W. (1872), "On the Rolling of Ships", *Trans. Inst. Nav. Arch.*, pp. 180-229

Fujino, M., and Yoon, B.S. (1986), "A Practical Method of Estimating Ship Motions and Wave Loads in Large Amplitude Waves", *Int. Shipb. Progress*, Vol. 33, No. 385, Sept., pp. 159-172

Gerritsma, J. (1960), "Ship Motions in Longitudinal Waves", *Int. Shipb. Progress*, Vol. 7, No. 66, February, pp. 49-71

Golovato, P. (1959), "A Study of Transient Pitching Oscillations of a Ship", *J. Ship Research*, March, pp. 22-30

Graham, J.M.R. (1980), "The Forces on Sharp-Edged Cylinders in Oscillatory Flow at Low Keulegan-Carpenter Numbers, *J. Fluid Mech.*, Vol 97, Part 1, pp. 331-346

Greenhow, M. (1986), "High- and Low-Frequency Asymptotic Consequences of the Kramers-Kronig Relations", *J. Engg. Math.*, Vol. 20, pp. 293-306

Greenhow, M., Vinje, T., Brevig, P., and Taylor, J. (1982), "A Theoretical and Experimental Study of the Capsize of Salter's Duck in Extreme Waves", *J. Fluid Mech.*, Vol. 118, pp. 221-239

Grim, O. (1951), "Das Schiff in von achtern auflaufender See", *Jahrbuch der Schiffbautechnischen Gesellschaft*, Vol. 45, pp. 264-287

Grim, O. (1952), "Rollschwingungen, Stabilität und Sicherheit im Seegang", *Schiffstechnik*, Vol. 1, No. 1, pp. 10-21

Grim ,O. (1963), "Surging Motion and Broaching Tendencies in a Severe Irregular Sea", *Deutsche Hydrographische Zeitschrift*, Vol. 16, No. 5, pp. 201-231

Grim ,O. (1983), "Das Schiff in von achtern kommendem Seegang", *Schiffstechnik*, Vol. 30, No. 2, Sept., pp. 84-94

Gudmestad, O.T., and Conner, J.J. (1986), "Engineering Approximations to Nonlinear Deepwater Waves", *Applied Ocean Research*, Vol. 8, No. 2, pp.76-88

Guo, C.-L. (1978), "Nonlinear Theory of Ship Maneuvering", *Ph.D. Dissertation*, Dept. of Naval Arch. and Offshore Engg., Univ. of California, Berkeley, July

Haddara, M.R. (1970), "Stability of Ship Motion in Oblique Seas", Report, Dept. of Naval Arch. and Offshore Eng., Univ. of California, Berkeley, March

Haddara, M.R., Kastner, S., Magel, L.F., Paulling, J.R., Pérez y Pérez, L., and Wood, P.D. (1972), "Capsizing Experiments with a Model of a Fast Cargo Liner in San Francisco Bay", Final Report for Period August 1970 - December 1971, Dept. of Naval Arch. and Offshore Eng., University of California, Berkeley, Jan.

Haskind, M.D. (1946), "Oscillation of a Ship on a Calm Sea", Translation of which is given in *SNAME Technical and Research Bulletin*, No. 1-12, April 1953, pp. 45-60

Himeno, Y. (1981), "Prediction of Ship Roll Damping - State of the Art", Dept. of Naval Arch. and Marine Eng., Univ. of Michigan, Report No. 239, Sept.

Hooft, J.P. (1986), "Computer Simulations of the Behavior of Maritime Structures", *Marine Technology*, April, pp. 139-157

Hooft, J.P. (1988), "The Extreme Motions of a Frigate in High Seas", Paper Presented at the *Bicentennial Maritime Symposium*, Sydney, Jan.

Huang, X., Hoff, J.R., and Næss, A. (1982), "Loads and Motions Measured on a Semisubmersible Having a Large Permanent List Angle", *Norwegian Maritime Research*, No. 2, pp. 24-33

Ikeda, Y., Ishikawa, M., and Tanaka, N. (1980), "Viscous Effect on Damping Forces of Ship in Sway and Roll Coupled Motion", *Jap. Soc. of Naval Arch. Kansai*, No. 176, pp. 44-53

Inoue, S., Hirano, M., and Kijima, K. (1981), "Hydrodynamic Derivatives on Ship Manoeuvring", *Int. Shipb. Progress*, Vol.28, No. 321, May, pp. 112-125

Inoue, S., Hirano, M., Kijima, K., and Takashina, J. (1981), "A Practical Calculation Method of Ship Maneuvering Motion", *Int. Shipb. Progress*, Vol. 28, No. 325, Sept., pp. 207-222

Jefferys, E.R. (1987), "Directional Seas Should Be Ergodic", *Applied Ocean Research*, Vol. 9, No. 4, pp. 186-191

Kastner, S. (1973), "Analysis and Evaluation of Capsize Experiments in the San Francisco Bay", Report, Dept. of Naval Arch. and Offshore Eng., Univ. of California, Berkeley, March

Kawashima, R., Takaishi ,Y., Morimura, S., Yoshino, T., and Sasaki, H. (1978), "Model Experiments on Capsize and its Prevention for a Small

Fishing Boat in Waves", *Jap. Soc. Naval Arch. Japan*, Vol. 143, June, pp. 69-90

Kerwin, J.E. (1955), "Notes on Rolling in Longitudinal Waves", *Int. Shipb. Progress*, Vol. 2, No. 16, pp. 597-614

Kröger, H.P. (1986), "Rollsimulation von Schiffen im Seegang", *Schiffstechnik*, Vol. 33, No. 4, Nov., pp. 187-216

Liapis, S., and Beck, R.F. (1985), "Seakeeping Computation Using Time-Domain Analysis", *Proc. 4th Symp. on Numerical Ship Hydrodynamics*, Washington D.C., Sept.

Lin, W.-M., Newman, J.N., and Yue, D.K. (1984), "Nonlinear Forced Motions of Floating Bodies", *Proc. 13th Symp. Naval Hydrodyn.*, Hamburg

Lindemann, K., and Skomedal, N. (1983), "Modern Hull Forms and Parametric Excitation of the Roll Motion", *Norwegian Maritime Research Report*, No.2

Longuet-Higgins, M.S. (1984), "Statistical Properties of Wave Groups in a Random Sea State", *Phil. Trans. Roy. Soc. London*, Vol. A 312, pp. 219-250

Matsuura, M., Ikegami, K., and Seto, H. (1987), "Dynamic Response Analysis of Semisubmersibles Under Extreme Conditions", Mitshubishi Heavy Ind., Ltd., Technical Review, Vol. 24, No. 1, Feb., pp. 23-29

McCreight, W.R. (1986), "Ship Maneuvering in Waves", *Proc. 16th Symp. on Naval Hydrodyn.*, Berkeley, July

Morrall, A. (1979), "Capsizing of Small Trawlers", *The Naval Architect*, pp. 71-101

Motora, S., Fujino, M., Fuwa, T. (1982), "On the Mechanism of the Broaching-to Phenomenon", *Proc. 2nd Int. Conf. on Stability of Ships and Ocean Vehicles*, Tokyo, Oct., pp. 1-15

Nayfeh, A.H. (1981), *Introduction to Perturbation Techniques*, Wiley-Interscience, New York

Newman, J.N. (1966), "Some Hydrodynamic Aspects of Ship Maneuverability", *Proc. 6th Symp. on Naval Hydrodyn.*, Washington D.C., Oct., pp. 203-237

Newman, J.N. (1977), *Marine Hydrodynamics*, MIT Press

Nicholson, K. (1974), "Some Parametric Model Experiments to Investigate Broaching-to", Paper 17 of *The Dynamics of Marine Vehicles and Structures in Waves*, R.E.D. Bishop and W.G. Price (Ed.), London, April, pp. 160-166

Næss, A., and Hoff, J.R. (1984), "Time Simulation of the Dynamic Response of Heavily Listed Platforms in Waves", *Norwegian Maritime Research*, No. 1, pp. 2-14

Oakley, O.H., Paulling, J.R., and Wood, P. (1974), "Ship Motions and Capsizing in Astern Seas", *Proc. 10th Symp. on Naval Hydrodyn.*, Cambridge, June, pp. 297-350

Odabasi, A.Y. (1981), "Hydrodynamic Reaction to Large Amplitude Rolling Motion", *Int. Shipb. Progress*, Vol. 28, No. 320, April, pp. 74-82

Ohkusu, M. (1986), "Prediction of Wave Forces on a Ship Running in Following Waves with Very Low Encounter Frequency", *J. Soc. Nav. Arch. Japan*, Vol. 159, pp. 129-138

Ogilvie, T.F. (1964), "Recent Progress Toward the Understanding and Prediction of Ship Motions", *Proc. 5th Symp. on Naval Hydrodyn.*, Bergen

Papanikolaou, A. (1984), "On Calculations of Nonlinear Hydrodynamic Effects in Ship Motion", *Schiffstechnik*, Vol. 31, No. 3, pp.91-129

Papanikolaou, A., and Zaraphonitis, G. (1987), "Computer-Aided Simulations of Large Amplitude Roll Motions of Ships in Waves and of Dynamic Stability", *Int. Shipb. Progress*, Vol. 34, No. 399, Nov., pp. 198-206

Paulling, J.R. (1961), "The Transverse Stability of a Ship in a Longitudinal Seaway", *J. Ship Research*, March, pp. 37-49

Paulling, J.R. (1977), "Time Domain Simulation of Semisubmersible Platform Motion with Application to the Tension-Leg Platform", *Proc. STAR Symposium*, San Francisco, pp. 303-314

Paulling, J.R., and Rosenberg, R.M. (1959), "On Unstable Ship Motions Resulting From Nonlinear Coupling", *J. Ship Research*, June, pp. 36-46

Paulling, J.R., Kastner, S., and Schaffran, S. (1972), "Experimental Studies of Capsizing of Intact Ships in Heavy Seas", Technical Report, Dept. of Naval Arch. and Offshore Eng., University of California, Berkeley, Nov.

Pérez y Pérez, L. (1974), "A Time-Domain Solution to the Motions of a Steered Ship in Waves", *J. Ship Research*, Vol. 18, No. 1, March, pp. 32-45

Pinkster, J.A. (1980), "Low Frequency Second Order Wave Exciting Forces on Floating Structures", Publication No. 650, Netherlands Ship Model Basin, Wageningen

Rawson, K.J., and Tupper, E.C. (1984), *Basic Ship Theory*, Vol. 2, Longman

Renilson, M.R. (1982), "An Investigation into the Factors Affecting the Likelihood of Broaching-To in Following Seas", *Proc. 2nd Int. Conf. on Stability of Ships and Ocean Vehicles*, Tokyo, Oct., pp.17-28

Renilson, M.R., and Driscoll, A. (1982), "An Investigation into the Loss of Directional Control in Severe Following Seas", *Trans. Roy. Inst. Nav. Arch.*, pp. 253-273

Robinson, R.W., and Stoddart, A.W. (1987), "An Engineering Assessment of the Role of Non-linearities in Transportation Barge Roll Response", *The Naval Architect*, July/August, pp. 65-79

Rutgersson, O., and Ottosson, P. (1987), "Model Tests and Computer Simulations - An Effective Combination for Investigation of Broaching Phenomena", Paper Presented at the *Annual SNAME Meeting*, New York, Nov.

Rydill, L.J. (1959), "A Linear Theory for the Steered Motions of Ships in Waves", *Trans. Inst. Naval Arch.*, Vol. 101, pp. 81-112

Salvesen, N. (1978), "Ship Motions in Large Waves", *Symp. on Appl. Math. dedicated to the late Prof. Dr. R. Timman*, Delft, Jan., pp. 215-226

Salvesen, N., Tuck ,E.O., and Faltinsen ,O. (1970), "Ship Motions and Sea Loads", *Trans. Soc. Nav. Arch. and Mar. Eng.*, Vol. 78, pp. 250-287

Schmitke, R.T. (1978), "Ship Sway, Roll, and Yaw Motions in Oblique Seas", *Trans. Soc. Nav. Arch. and Mar. Eng.*, Vol. 86, pp. 26-46

Sjöholm, U., and Kjellberg, A. (1984), "RoRo Ship Hull Form: Stability and Seakeeping Properties", Paper Presented at the *Ro-Ro 84 Conference*, Nice; see also *The Naval Architect*, Jan. 1985, pp. E12-E14

Sobey, R.J., Goodwin, P., Thieke, R.J., and Westberg, R.J. (1987), "Application of Stokes, Cnoidal, and Fourier Wave Theories", *J. of Waterway, Port, Coastal and Ocean Engg.*, Vol. 113, No. 6, Nov., pp. 565-587

Söding, H. (1987), "Ermittlung der Kentergefahr aus Bewegungssimulationen", *Schiffstechnik*, Vol.34, No.1, May, pp. 28-39

Stoker, J.J. (1950), *Nonlinear Vibrations*, Wiley (Interscience), New York

Su, M.-Y. (1986), "Large, Steep Waves, Wave Grouping and Breaking", *Proc. 16th Symp. on Naval Hydrodyn.*, Berkeley, July, pp. 78-97

Takaishi, Y. (1982), "Consideration on the Dangerous Situations Leading to Capsize of Ships in Waves", *Proc. 2nd Int. Conf. on Stability of Ships and Ocean Vehicles*, Tokyo, Oct., pp. 161-169

Tanaka, N. (1979), "Experimental Study on Hydrodynamic Viscous Force Acting on Oscillatory Bluff Body", *J. Soc. Naval Arch. Japan*, Vol. 179, p. 35

Tucker, M.J., Challenor, P.G., and Carter, D.J.T. (1984), "Numerical Simulation of a Random Sea and its Effect upon Wave Group Statistics", *Applied Ocean Research*, Vol. 6, No. 2, pp. 118-122

Van Oortmerssen, G. (1976), "The Motions of a Moored Ship in Waves", Publication No. 510, Netherlands Ship Model Basin, Wageningen

Vinje, T., and Brevig, P. (1981), "Nonlinear Ship Motions", *Proc. 3rd Int. Conf. on Num. Ship Hydrodyn.*, Paris, June, pp. 257-268

Vinje, T., Maogang, X., and Brevig, P. (1983), "A Numerical Approach to Nonlinear Ship Motion", *Proc. 14th Symp. Naval Hydrodyn.*, Michigan, pp. 245-278

Virgin, L.N. (1987), "The Nonlinear Rolling Response of a Vessel Including Chaotic Motions Leading to Capsize in Regular Seas", *Applied Ocean Research*, Vol. 9, No. 2, pp. 89-95

Visineau, G. (1979)," Relative Roll Motion of a Ship in Beam Seas", *Paper Presented to North. Calif. Section of Soc. Nav. Arch. and Mar. Eng.*, San Francisco, March

Vossers, G., Swaan, W.A., and Rijken, H. (1960), "Experiments with Series 60 Models in Waves", *Trans. Soc. of Nav. Arch. and Mar. Eng.*, Vol. 68, pp. 364-435

Vugts, J.H. (1968), "The Hydrodynamic Coefficients for Swaying, Heaving and Rolling Cylinders in a Free Surface", *Int. Shipb. Progress*, Vol. 15, No. 167, July, pp. 251-276

Wahab, R., and Swaan, W.A. (1964), "Coursekeeping and Broaching of Ships in Following Seas", *J. Ship Research*, Vol. 7, No. 4, April, pp. 1-15

Webster, W.C., and Trudell, R.W. (1981), "Statistics of Local Motions on a Ship", *Proc. Conference on Directional Wave Spectra Applications*, Berkeley, Sept., pp. 461-482

Wehausen, J.V. (1967), "Initial-Value Problem for the Motion in an Undulating Sea of a Body with Fixed Equilibrium Position", *J. Engg. Math.*, Vol. 1, No.1, pp. 1-17

Wehausen, J.V. (1971), "The Motion of Floating Bodies", *Annual Review of Fluid Mech.*, Vol. 3, pp. 237-268

Wehausen, J.V. (1978), "Some Aspects of Mancuverability Theory", *Symp. on Appl. Math. dedicated to the late Prof. Dr. R. Timman*, Delft, Jan., pp. 203-214

Wiegel, R.L. (1964), *Oceanographical Engineering*, Prentice Hall

Wright, J.H.G., and Marshfield, W.B. (1980), "Ship Roll Response and Capsize Behaviour in Beam Seas", *The Naval Architect*, May, pp. 129-150

Wu, X.-J. (1985), "A Hybrid 3D-Strip Method for Evaluating Surging Coefficients of Full-Shaped Ships", *Proc. 7th Int. Conf. on Boundary Element Method in Engg.*, Como, Sept.

Yamakoshi, Y., Takaishi, Y., Kan, M., Yoshino, T., and Tsuchiya, T. (1982), "Model Experiments on Capsize of Fishing Boats in Waves", *Proc. 2nd Int. Conf. on Stability of Ships and Ocean Vehicles*, Tokyo, Oct., pp. 123-136

Yamamoto, Y., Fukasawa, T., Arai, M. and Kajita, E. (1982), "Nonlinear Effects for Ship Motion in Head Seas", *Int. Shipb. Progress*, No. 333, May, pp. 118-124

Yeung, R.W. (1982), "The Transient Heaving Motion of Floating Cylinders", *J. Engg. Math.*, Vol. 16, pp. 97-119

Yeung, R.W., and Kim, S.-H. (1981), "Radiation Forces on Ships with Forward Speed", *Proc. 3rd Int. Conf. on Num. Ship Hydrodyn.*, Paris, pp. 499-515

APPENDICES

Appendix A

A.1. Coordinate Systems and Transformations

The nature of the computations necessitates the use of a number of coordinate systems. Both earth fixed and structure fixed systems are needed and it must be possible to alternate between the various systems. The following right-handed coordinate systems are considered. The first is the reference system Oxyz fixed on earth, with the y-axis extending vertically upwards. The second is the local coordinate system $O^*x^*y^*z^*$, which is fixed in the structure. The third is the system $O^ex^ey^ez^e$ translating with the structure at its mean forward speed, U, along the x-direction in the horizontal plane Oxz. The coordinate systems are shown in Figure A.1 below.

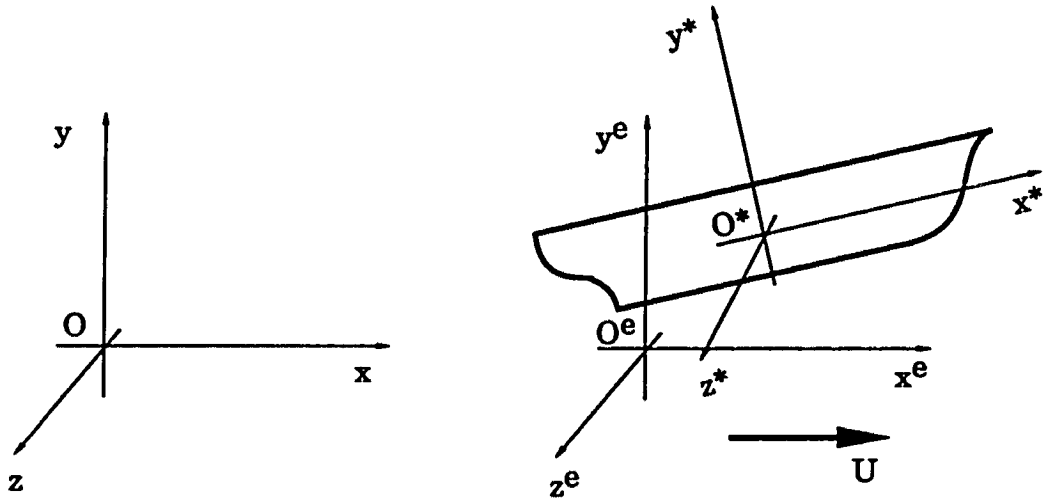

Figure A.1. Coordinate System Representation

Since the local O*x*y*z* system may undergo rotations as well as translations, a special convention is needed to express vectors in the O*x*y*z* system in terms of the Oxyz system. Throughout this work a sequential order of rotation using Euler angles is adhered to: yaw, pitch, roll (in that order), or in terms of the angles, ϕ, ψ, and θ, respectively. Each Euler angle has associated with it a transformation matrix to express a vector in the local coordinate system, $\mathbf{x}^*$, in terms of the global system Oxyz:

$$\mathbf{x} = \mathbf{T}\,\mathbf{x}^* \ .$$

For yaw the transformation matrix is given by:

$$\mathbf{T}_{\phi} = \begin{bmatrix} \cos\phi & 0 & \sin\phi \\ 0 & 1 & 0 \\ -\sin\phi & 0 & \cos\phi \end{bmatrix},$$

for pitch:

$$\mathbf{T}_{\psi} = \begin{bmatrix} \cos\psi & -\sin\psi & 0 \\ \sin\psi & \cos\psi & 0 \\ 0 & 0 & 1 \end{bmatrix},$$

and for roll :

$$\mathbf{T}_{\theta} = \begin{bmatrix} 1 & 0 & 0 \\ 0 & \cos\theta & -\sin\theta \\ 0 & \sin\theta & \cos\theta \end{bmatrix}.$$

It is assumed that the position of the origin of $O^*x^*y^*z^*$ is located at the center of gravity of the vessel, and that if the vessel has forward speed, its location is given in terms of the translating system $O^e x^e y^e z^e$ as follows:

$$x^e_{C.G.} = \begin{bmatrix} x^e_1 \\ y^e_1 \\ z^e_1 \end{bmatrix} .$$

The transformation matrix T for a yawed, pitched and rolled ship coordinate system, can be represented by the vectorial relationship

$$\begin{bmatrix} x - x^e_1 \\ y - y^e_1 \\ z - z^e_1 \end{bmatrix} = T \cdot \begin{bmatrix} x^* \\ y^* \\ z^* \end{bmatrix} ,$$

where T is given by the product of the individual transformation matrices in the sequence of the Euler angles:

$$T = T_\phi \cdot T_\psi \cdot T_\theta$$

$$= \begin{bmatrix} \cos\phi\cos\psi & -\cos\phi\sin\psi\cos\theta+\sin\phi\sin\theta & \cos\phi\sin\psi\sin\theta+\sin\phi\cos\theta \\ \sin\psi & \cos\psi\cos\theta & -\cos\phi\sin\theta \\ -\sin\phi\cos\psi & \sin\phi\sin\psi\cos\theta+\cos\phi\sin\theta & -\sin\phi\sin\psi\sin\theta+\cos\phi\cos\theta \end{bmatrix}$$

This matrix allows one to express a vector in the $O^*x^*y^*z^*$ system in terms of the (possibly translating) reference system $O^e x^e y^e z^e$. The inverse of the rotation matrix T is given by its transpose, since T is orthogonal:

$$\mathbf{T}^{-1} = \mathbf{T}^{T} .$$

If only yaw and pitch of the local reference system are considered, the coordinate transformation matrix **R** is given by the product $\mathbf{T}_\phi \cdot \mathbf{T}_\psi$, which is the following:

$$\mathbf{R} = \begin{bmatrix} \cos\phi\cos\psi & -\cos\phi\sin\psi & \sin\phi \\ \sin\psi & \cos\psi & 0 \\ -\sin\phi\cos\psi & \sin\phi\sin\psi & \cos\phi \end{bmatrix} = \begin{bmatrix} r_{11} & r_{12} & r_{13} \\ r_{21} & r_{22} & r_{23} \\ r_{31} & r_{32} & r_{33} \end{bmatrix} .$$

The inverse coordinate transformation matrix $\mathbf{S} = \mathbf{R}^{-1}$ is also given by the transpose:

$$\mathbf{S} = \mathbf{R}^{T} .$$

If the structure is moving in the x-direction, the position of the center of $O^e x^e y^e z^e$ is given by the vector

$$\mathbf{x}_{O^e} = \begin{bmatrix} x_{O^e} \\ 0 \\ 0 \end{bmatrix} ,$$

where the y and z coordinates of O^e are zero, and for a system moving steadily at speed U, x_{O^e} would be equal to

$$x_{O^e} = U.t \quad .$$

The following relationship applies between the fixed and moving reference systems :

$$\begin{bmatrix} x \\ y \\ z \end{bmatrix} = \begin{bmatrix} x_{O^e} + x^e \\ y^e \\ z^e \end{bmatrix} .$$

Then, for a yawed and pitched O*x*y*z* coordinate system, a vector in the local coordinate system can be expressed in terms of the earth-fixed reference system as follows :

$$\begin{bmatrix} x \\ y \\ z \end{bmatrix} = \begin{bmatrix} x_1 + r_{11}x^* + r_{12}y^* + r_{13}z^* \\ y_1^e + r_{21}x^* + r_{22}y^* \\ z_1^e + r_{31}x^* + r_{32}y^* + r_{33}z^* \end{bmatrix} = \begin{bmatrix} x_1 + s_{11}x^* + s_{21}y^* + s_{31}z^* \\ y_1^e + s_{12}x^* + s_{22}y^* \\ z_1^e + s_{13}x^* + s_{23}y^* + s_{33}z^* \end{bmatrix} .$$

Here the individual subscript 1 denotes the position of the center of gravity, which in the earth-fixed system Oxyz is given by:

$$\begin{aligned} x_1 &= x_{O^e} + x_1^e \\ y_1 &= y_1^e \\ z_1 &= z_1^e . \end{aligned}$$

For convenience from the computational point of view, the approach followed in the numerical model is to consider the vessel undergoing roll, yaw and pitch rotations. However, at each time step, the forces are first expressed in terms of a local coordinate system O*x*y*z* that has undergone only yaw and pitch by the same amount as that of the actual rotations. After all force components have been determined and summed, the final exciting forces are expressed in the structure fixed coordinate system by taking the roll angle into account.

Rotational Velocities

If the Euler angles ϕ, ψ and θ are represented by the vector

$$\chi = \begin{bmatrix} \theta \\ \phi \\ \psi \end{bmatrix},$$

the time derivatives are given by

$$\frac{d\chi}{dt} = \dot{\chi} = \begin{bmatrix} \dot{\theta} \\ \dot{\phi} \\ \dot{\psi} \end{bmatrix}.$$

These rotational velocities are defined in the earth-fixed coordinate system Oxyz . The angular velocities about the ship coordinate axes x*, y*, and z* are represented by the vector

$$\omega = \begin{bmatrix} \omega_1 \\ \omega_2 \\ \omega_3 \end{bmatrix}.$$

This vector can be related to the Eulerian velocity vector $\dot{\chi}$ as follows:

$$\omega = B\,\dot{\chi} \quad .$$

The above transformation matrix **B** can be obtained by a series of transformations, reflecting the order of rotation of the Euler angles, which is yaw, pitch and roll :

$$\begin{bmatrix} \omega_1 \\ \omega_2 \\ \omega_3 \end{bmatrix} = T_\theta^{-1} \cdot T_\psi^{-1} \cdot \begin{bmatrix} 0 \\ \dot{\phi} \\ 0 \end{bmatrix} + T_\theta^{-1} \cdot \begin{bmatrix} 0 \\ 0 \\ \dot{\psi} \end{bmatrix} + \begin{bmatrix} \dot{\theta} \\ 0 \\ 0 \end{bmatrix},$$

so that **B** can be expressed as

$$\mathbf{B} = \begin{bmatrix} 1 & \sin\psi & 0 \\ 0 & \cos\theta\cos\psi & \sin\theta \\ 0 & -\sin\theta\cos\psi & \cos\psi \end{bmatrix}.$$

It is noted that the inverse of **B** is not equal to its transpose, but is given by

$$\mathbf{B}^{-1} = \begin{bmatrix} 1 & -\cos\theta\tan\psi & \sin\theta\tan\psi \\ 0 & \cos\theta/\cos\psi & -\sin\theta/\cos\psi \\ 0 & \sin\theta & \cos\theta \end{bmatrix}.$$

A.2. Definition of Relative Heading Angle in Waves

The absolute ship heading at any time instant is determined with respect to the x-axis of the system Oxyz by the yaw angle ϕ, which is the same as the angle of the vessel with respect to the x^e-axis of the reference system moving with the ship. The direction of wave travel is defined in similar terms by the angle δ. i.e.. δ is positive according to the right-handed rule. Thus the relative heading is given by

$$\beta = \delta - \phi.$$

The various angles are shown schematically in Figure A.2.

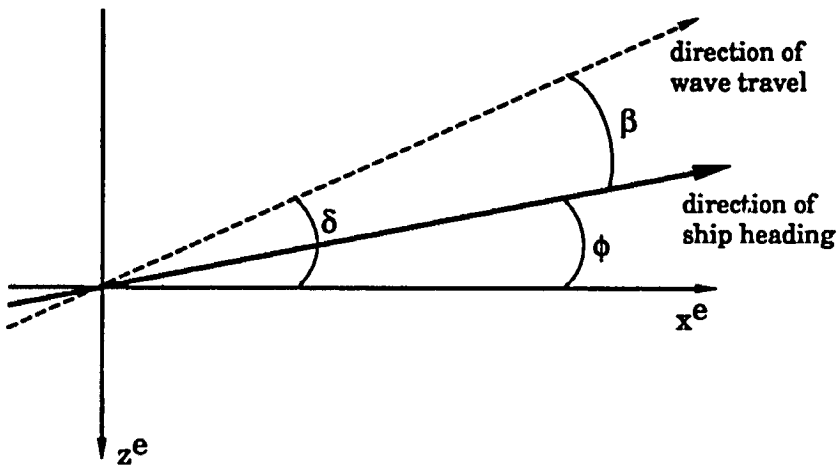

Figure A.2. Definition of Relative Heading Angle β of Ship

Appendix B

Froude-Krylov Forces

In the first section expressions for the Froude-Krylov forces are obtained, and these forces are separated into a "static" and "dynamic" part (it is noted that both components are time dependent). Next a brief discussion is given concerning steady drift forces arising from integrating the wave pressure over the instantaneous wetted surface of the vessel.

B.1. Static and Dynamic Components

In this section expressions for the Froude-Krylov forces are obtained in terms of a yawed and pitched coordinate system located in the structure, where the structure itself may have undergone roll rotation as well. All derivations are based on conventional, linear potential theory which is extended to above the mean water level. The forces are evaluated for large angles, and the computations are performed over the instantaneous wetted surface of the structure. The total Froude-Krylov force is split up into a static and dynamic component.

Assuming the origin of the structure-fixed coordinate system to be located at the center of gravity of the structure, the generalized 6x1 Froude-Krylov force vector, comprising forces and moments, is given by integration of the pressure in the undisturbed wave system:

$$\mathbf{f}(t) = \iint_S p\,\mathbf{n}\,ds = \iint_S (p_S + p_D)\,\mathbf{n}\,ds \ ,$$

where S is the instantaneous wetted surface (and therefore time dependent), and $\mathbf{n}$ is the generalized normal vector. The first three components of $\mathbf{n}$ ($\mathbf{n}_{1,2,3}$) are the conventional components of the unit normal directed out of the fluid, and the last three components ($\mathbf{n}_{4,5,6}$) are cross products: $\mathbf{n}_{4,5,6} = \mathbf{r}^* \times \mathbf{n}_{1,2,3}$. Here $\mathbf{r}^*$ represents the vector of a point

on the hull to the center of gravity. The pressures p_S and p_D are the static and dynamic wave pressures, respectively, given by

$$p_S = -\rho g y \ , \ -\infty < y < \eta$$

$$p_D = -\rho \frac{\partial \Phi_I}{\partial t} \ .$$

It is assumed that the velocity potential Φ_I can be evaluated up to the instantaneous free surface, given by $y = \eta(x,z;t)$; this was discussed in Chapter 2.4. The velocity potential of the incoming wave train is the following (for a one-component wave system):

$$\Phi_I(x,y,z;t) = \frac{A.g}{\sigma} e^{ky}.\sin(k_x x + k_z z - \sigma t + \varepsilon) \ ,$$

and

$$\eta(x,z;t) = A.\cos(k_x x + k_z z - \sigma t + \varepsilon) \ .$$

As discussed in Chapter 2.4, the total pressure in a random seaway would be obtained in terms of the overall velocity potential of the incoming wave system, consisting of the superposition of the potentials of the individual wave components.

The components of the generalized Froude-Krylov force can be expressed conveniently in terms of volume integrals using Gauss' Theorem. The volume integrals can be evaluated per section, and then integrated over the length of the vessel to yield the total force or moment. Expressions must be derived in terms of the yawed and pitched coordinate system located in the structure; the local coordinates in this system are taken to be x^*, y^* and z^*. For the actual forces (i = 1,2,3) Gauss' Theorem gives

$$f_i(t) = -\iiint_V \frac{\partial p}{\partial x_i} dV$$

$$= -\int_L \left\{ \iint_S \frac{\partial p}{\partial x_i} ds \right\} dx , \quad i = 1,2,3 ,$$

and for the moments about the center of gravity:

$$f_i(t) = -\iiint_V r^* \times \nabla p \, dV , \quad i = 4,5,6 .$$

The force components expressed in a yawed and pitched coordinate system O*x*y*z* would be given by

$$f_i(t) = -\iiint_V \frac{\partial p}{\partial x^*_i} dV$$

$$= -\int_L \left\{ \iint_S \frac{\partial p}{\partial x^*_i} ds \right\} dx^* , \quad i = 1,2,3 ,$$

S is the instantaneous cross-sectional area (bounded by the imaginary free surface of the waves, as if the hull were not there), V is the displaced volume, and L is the length of the vessel. The individual moment components are then given by

$$f_4(t) = \int_L \left\{ \iint_S (z^*.p_{y^*} - y^*.p_{z^*}) dy^* \, dz^* \right\} dx^* ,$$

$$f_5(t) = \int_L \left\{ \iint_S (x^*.p_{z^*} - z^*.p_{x^*}) dy^* \, dz^* \right\} dx^* ,$$

$$f_6(t) = \int_L \left\{ \iint_S (y^*.p_{x^*} - x^*.p_{y^*}) dy^* \, dz^* \right\} dx^* .$$

Static Froude-Krylov Forces

The static pressure is given by

$$p_S = -\rho g y \ ,$$

and y can be expressed in terms of a yawed and pitched coordinate system with its origin located at the center of gravity, as has been illustrated in Appendix A:

$$y = y_1^e + s_{12}x^* + s_{22}y^* \ .$$

In the above expression y* is the local y-coordinate of a section point of the vessel, which may have undergone rotation as well, so that in terms of the yawed and pitched coordinate system the section may have a nonsymmetrical shape when the roll angle is not equal to zero. The pressure derivatives are the following:

$$\frac{\partial p_S}{\partial x^*} = -s_{12}\rho g$$
$$\frac{\partial p_S}{\partial y^*} = -s_{22}\rho g$$
$$\frac{\partial p_S}{\partial z^*} = 0 \ .$$

The sectional hydrostatic forces, i.e., the first three compcnents of the generalized force vector, are given by

$$f_{FK,s}^{(1)}(x^*;t) = -\rho g s_{12}\iint_S dy^*dz^* = -\rho g s_{12}\int(\eta_1 - y_b^*)\Big|_{z^*} dz^* \ ,$$

$$f_{FK,s}^{(2)}(x^*;t) = -\rho g s_{22}\iint_S dy^*dz^* = -\rho g s_{22}\int(\eta_1 - y_b^*)\Big|_{z^*} dz^* \ ,$$

$$f^{(3)}_{FK,s}(x^*;t) = 0 \ ,$$

where η_1 is the wave elevation above a section point, and y_b^* is the y*-coordinate of the section point, so that their difference constitutes the hydrostatic head above the section point. The static Froude-Krylov moments for a section at x* are given by

$$f^{(4)}_{FK,s}(x^*;t) = \iint_S z^* p_{S_{y^*}} dy^* dz^* = -\rho g s_{22} \int (\eta_1 - y_b^*)\Big|_{z^*} z^* \, dz^* \ ,$$

$$f^{(5)}_{FK,s}(x^*;t) = -\iint_S z^* p_{S_{x^*}} dy^* dz^* = \rho g s_{12} \int (\eta_1 - y_b^*)\Big|_{z^*} z^* \, dz^* \ ,$$

$$f^{(6)}_{FK,s}(x^*;t) = \iint_S (p_{S_{x^*}} y^* - x^* p_{S_{y^*}}) dy^* dz^*$$

$$= \rho g \left\{ -s_{12} \iint_S y^* \, dy^* dz^* + s_{22} x^* \iint_S dy^* dz^* \right\} \ .$$

The above sectional forces and moments are assumed constant over each ship section, so that the total forces and moments can be obtained through simple addition of the sectional components.

Dynamic Froude-Krylov Forces

In order to obtain the dynamic forces in terms of a yawed and pitched coordinate system, it is necessary to express the dynamic pressure in terms of the local coordinates. The dynamic pressure is based on expressions for the velocity potential defined previously, and the expressions are derived for a single harmonic wave train.

The dynamic pressure is given by

$$p_D = -\rho \frac{\partial \Phi_I}{\partial t} = \rho A g e^{ky} \cos(k_x x + k_z z - \sigma t + \varepsilon) \ ,$$

where all the parameters are defined as in Chapter 2.4. The dynamic pressure can be expressed in terms of the yawed and pitched coordinate system by making use of the previously obtained coordinate relationships:

$$p_D(x^*,y^*,z^*;t) = \rho A g e^{k(y_1^e + s_{12}x^* + s_{22}y^*)} . \cos\{k_x(x_1 + s_{11}x^* + s_{21}y^* + s_{31}z^*) + k_z(z_1^e + s_{13}x^* + s_{23}y^* + s_{33}z^*) - \sigma t + \varepsilon)\} \ ,$$

where

$$x_1 = x_{O^e} + x_1^e \ .$$

By defining

$$\xi = x_1 + s_{11}x^* + s_{21}y^* + s_{31}z^* \ ,$$
$$\zeta = z_1^e + s_{13}x^* + s_{23}y^* + s_{33}z^* \ ,$$

the derivatives of the dynamic pressure can be written as

$$\frac{\partial p_D}{\partial x^*} = \rho A g e^{ky_1^e} . \{ k s_{12} e^{k(s_{12}x^* + s_{22}y^*)} . \cos(k_x\xi + k_z\zeta - \sigma t + \varepsilon) - e^{k(s_{12}x^* + s_{22}y^*)} . (k_x s_{11} + k_z s_{13}) . \sin(k_x\xi + k_z\zeta - \sigma t + \varepsilon)\} \ ,$$

$$\frac{\partial p_D}{\partial y^*} = \rho A g e^{ky_1^e} . \{ k s_{22} e^{k(s_{12}x^* + s_{22}y^*)} . \cos(k_x\xi + k_z\zeta - \sigma t + \varepsilon) - e^{k(s_{12}x^* + s_{22}y^*)} . (k_x s_{21} + k_z s_{23}) . \sin(k_x\xi + k_z\zeta - \sigma t + \varepsilon)\} \ ,$$

$$\frac{\partial p_D}{\partial z^*} = -\rho A g e^{ky_1^e} . e^{k(s_{12}x^* + s_{22}y^*)} . (k_x s_{31} + k_z s_{33}) . \sin(k_x\xi + k_z\zeta - \sigma t + \varepsilon) \ .$$

In order to integrate over the displaced volume, it is convenient to separate the x* terms from the y* and z* terms, and evaluate the sectional integrals first, as was done above for the static force components. Let us define

$$k_x' = k_x s_{11} + k_z s_{13} ,$$
$$k_y' = k_x s_{21} + k_z s_{23} ,$$
$$k_z' = k_x s_{31} + k_z s_{33} ,$$

and also

$$B_1 = k_x' x^* + k_x x_1 + k_z z_1^e - \sigma t + \varepsilon ,$$
$$B_2 = k_y' y^* + k_z' z^* .$$

Then

$$\cos\{k_x(x_1+s_{11}x^*+s_{21}y^*+s_{31}z^*) + k_z(z_1^e+s_{13}x^*+s_{23}y^*+s_{33}z^*) - \sigma t + \varepsilon\}$$
$$= \cos\{B_1 + B_2\}$$
$$= \cos B_1 \cos B_2 - \sin B_1 \sin B_2 ,$$

and likewise,

$$\sin(k_x\xi + k_z\zeta - \sigma t + \varepsilon) = \sin(B_1 + B_2)$$
$$= \sin B_1 \cos B_2 + \cos B_1 \sin B_2 .$$

Using the above notation, the pressure derivatives can be written as

$$\frac{\partial p_D}{\partial x^*} = \rho A g e^{ky_1^e}.\{ks_{12}e^{ks_{12}x^*}.e^{ks_{22}y^*}.(\cos B_1\cos B_2-\sin B_1\sin B_2)$$
$$-e^{ks_{12}x^*}.k_x'.e^{ks_{22}y^*}.(\sin B_1\cos B_2+\cos B_1\sin B_2)\} ,$$

$$\frac{\partial p_D}{\partial y^*} = \rho A g e^{ky_1^e}.\{ks_{22}e^{ks_{12}x^*}.e^{ks_{22}y^*}.(\cos B_1\cos B_2-\sin B_1\sin B_2)$$
$$-e^{ks_{12}x^*}.k_y'.e^{ks_{22}y^*}.(\sin B_1\cos B_2+\cos B_1\sin B_2)\} ,$$

$$\frac{\partial p_D}{\partial z^*} = -\rho A g e^{ky_1^e}.e^{ks_{12}x^*}.k_z'.e^{ks_{22}y^*}.(\sin B_1\cos B_2+\cos B_1\sin B_2) .$$

The following sectional integrals are defined:

$$ZC0(x^*) = \iint_S e^{ks_{22}y^*}.\cos B_2\, dy^*dz^* ,$$

$$ZS0(x^*) = \iint_S e^{ks_{22}y^*}.\sin B_2\, dy^*dz^* ,$$

$$ZCY(x^*) = \iint_S y^*.e^{ks_{22}y^*}.\cos B_2\, dy^*dz^* ,$$

$$ZSY(x^*) = \iint_S y^*.e^{ks_{22}y^*}.\sin B_2\, dy^*dz^* ,$$

$$ZCZ(x^*) = \iint_S z^*.e^{ks_{22}y^*}.\cos B_2\, dy^*dz^* ,$$

$$ZSZ(x^*) = \iint_S z^*.e^{ks_{22}y^*}.\sin B_2\, dy^*dz^* .$$

These sectional integrals can be solved analytically with respect to y^*, and then integrated with respect to z^* using Filon's method (see Appendix C). Defining

$$E = A.e^{k(y_1^c + s_{12}x^*)} ,$$

the following expressions for the dynamic Froude-Krylov forces and moments are obtained:

$$f_{FK}^{(1)}(t) = \rho g\{\int_L E.(k_x'.ZS0 - ks_{12}.ZC0).cosB_1\, dx^* + \int_L E.(k_x'.ZC0 + ks_{12}.ZS0).sinB_1\, dx^*\} ,$$

$$f_{FK}^{(2)}(t) = \rho g\{\int_L E.(k_y'.ZS0 - ks_{22}.ZC0).cosB_1\, dx^* + \int_L E.(k_y'.ZC0 + ks_{22}.ZS0).sinB_1\, dx^*\} ,$$

$$f_{FK}^{(3)}(t) = \rho g.\{\int_L E.k_z'.ZS0.cosB_1\, dx^* + \int_L E.k_z'.ZC0.sinB_1\, dx^*\} ,$$

$$f_{FK}^{(4)}(t) = \rho g.\{\int_L E.(-k_y'.ZSZ+k_z'.ZSY+ks_{22}.ZCZ).cosB_1\, dx^* + \int_L E.(-k_y'.ZCZ+k_z'.ZCY-ks_{22}.ZSZ).sinB_1\, dx^*\} ,$$

$$f_{FK}^{(5)}(t) = \rho g.\{\int_L E.(-x^*k_z'.ZS0+k_x'.ZSZ-ks_{12}.ZCZ).cosB_1\, dx^* + \int_L E.(-x^*k_z'.ZC0+k_x'.ZCZ+ks_{12}.ZSZ).sinB_1\, dx^*\} ,$$

$$f_{FK}^{(6)}(t) = \rho g.\{\int_L E.(x^*k_y'.ZS0-k_x'.ZSY-x^*ks_{22}.ZC0+ks_{12}.ZCY).cosB_1\, dx^* + \int_L E.(x^*k_y'.ZC0-k_x'.ZCY+x^*ks_{22}.ZS0-ks_{12}.ZSY).sinB_1\, dx^*\} .$$

The integration with respect to x*, i.e., along the length of the ship, is performed from the aftmost submerged section to the most forward submerged section.

Determination of Instantaneous Free Surface

In the integration over the wetted surface at each time step it is necessary to find the wave elevation, η^*, above each offset point (in the rotated coordinate system). Examination of the coordinate expressions of the wave elevation shows that η^* occurs recursively, so that it is not possible to find an explicit expression for the unknown η^* in terms of the other known parameters. To avoid this problem the same procedure is used as reported by Fallon *et al.* (1980). The assumption is made that the product involving the wave slope, kA, and pitch angle, ψ, is small. Defining the quantity $\gamma = kA.\sin\psi$, the following applies:

$$|\gamma| << 1 \Rightarrow \sin\gamma \approx \gamma \text{ and } \cos\gamma \approx 1 .$$

For the type of vessel under consideration it is reasonable to assume that the pitch angle is small. Also, the wave slope is usually quite small, and this is consistent with the wave theory used here. Therefore, the product of the two quantities is always small, and the above procedure is expected to yield accurate results for typical large ships, in realistic situations.

B.2. Froude-Krylov Drift Forces

In this section an investigation is made as regards the occurrence of steady drift forces, resulting from integrating the Froude-Krylov forces over the wetted surface of a thin cylinder in regular waves. The integration is performed over the exact wetted surface, that is, up to the instantaneous water level due to the undisturbed, incoming wave. Regular wave conditions are considered. Two cases have been investigated:

(1) Fixed, vertical cylinder in monochromatic wave;
(2) Vertical cylinder oscillating (heaving) at the wave frequency.

It was found that for the fixed cylinder the steady (Froude-Krylov) drift force is zero. For the heaving cylinder, however, the steady drift force was found to depend on the phase angle between the heave motion and the wave oscillation. The drift force due to the incoming wave pressure field is only one of the components comprising the total drift force. This has been shown by Pinkster (1980), who derived expressions for the various forces up to second order acting on a moored structure; the pressures were integrated over the wetted surface, and evaluated up to the mean water level rather than the actual free surface, in accordance with the perturbation theory approach.

1. Fixed Vertical Cylinder in Monochromatic Wave.

We wish to calculate the horizontal (surge) force on a fixed cylinder in a regular wave. The cylinder is assumed thin, i.e., its length is small compared with the wave length, has a rectangular cross-section, extends to a depth $y = -d$ below the mean water level, and extends to an indefinite height above the MWL.

The elevation of the incoming wave, assumed to be travelling along the x-axis with zero phase angle, is given by

$$\eta(t) = A\cos(kx-\sigma t)$$

and the corresponding velocity potential is

$$\Phi_1(t) = \frac{A.g}{\sigma} e^{ky} \sin(kx-\sigma t) \ .$$

The Froude-Krylov component of the surge force is obtained by integrating the pressure over the wetted surface:

$$F_1(t) = \iint_S p\, n\, ds = -\iiint_V \frac{\partial p}{\partial x} dV = -\int \{ \iint \frac{\partial p}{\partial x} dydz \} dx \ .$$

The cylinder is considered to have a unit width in the z-direction, and the length is taken to be dx_0, where $dx_0 << \lambda_w$. Then the time-dependent Froude-Krylov force is

$$F_1(t) = -\int_{-d}^{\eta} \frac{\partial p}{\partial x} dy \; dx_0 \; .$$

In subsequent expressions for the pressure, the static pressure component has been omitted, since it does not contribute to forces in the surge direction. The dynamic pressure is given by the linearized Euler's Integral:

$$p(x;t) = -\rho \frac{\partial \Phi}{\partial t} = \rho \, g \, A \, e^{ky} \cos(kx-\sigma t) \; .$$

Then

$$\frac{\partial p}{\partial x} = -\rho \, g \, A \, k \, e^{ky} \sin(kx-\sigma t) \; ,$$

and the surge force is given by (assuming $dx_0 = 1$):

$$F_1(t) = -\int_{-d}^{\eta} \rho \, g \, A \, k \; e^{ky} \sin(kx-\sigma t) \, dy$$

$$= -\rho \, g \, A \sin(kx-\sigma t) \, . \, \{e^{k\eta(t)} - e^{-kd}\} \; .$$

To compute the steady drift force, F_{DC}, it suffices to find the average of $F_1(t)$ over one wave period ($T = 2\pi/\sigma$):

$$F_{DC} = \frac{1}{T}\int_0^T F_1(t)\,dt = \rho g A \int_0^T \sin(kx-\sigma t)\,.\,\{e^{-kd} - e^{k\eta(t)}\}\,dt\ .$$

The drift force can be evaluated for any position, x, of the cylinder. If the cylinder is located at x = 0, the forces can be evaluated for x = 0 also, as the cylinder is assumed to be thin. The integrals are determined as follows:

$$\text{(a)}\ \int_0^T e^{-kd}\sin(kx-\sigma t)\,dt = 0.$$

$$\text{(b)}\ \int_0^T e^{kA\cos(kx-\sigma t)}\sin(kx-\sigma t)\,dt = \frac{1}{kA\sigma}\{e^{k\eta(T)} - e^{k\eta(0)}\} = 0.$$

From the above it is seen that the steady drift force due to the Froude-Krylov force is zero. Also the instantaneous force $F_1(t)$ becomes zero when the wave crest or trough passes by.

2. Heaving Cylinder in Monochromatic Wave.

The heave motion of the cylinder is assumed to have the same frequency as the wave, while having a certain phase angle, ε, with respect to the wave. The heave motion about the mean water level y = 0 is given by

$$y_c = H\cos(\sigma t+\varepsilon)\ .$$

The instantaneous Froude-Krylov surge force is then obtained by integrating the pressure gradient over the wetted surface in the fixed coordinate system:

$$F_1(t) = -\int_{-d+y_c}^{\eta} \frac{\partial p}{\partial x}\, dy$$

$$= \int_{-d+H\cos(\sigma t+\varepsilon)}^{A\cos(kx-\sigma t)} \rho\, g\, A\, e^{ky} \sin(kx-\sigma t)\, dy \ .$$

$$\Rightarrow F_1(t) = \rho\, g\, A \sin(kx-\sigma t) \,.\, \{e^{kA\cos(kx-\sigma t)} - e^{-kd+kH\cos(\sigma t+\varepsilon)}\} \ .$$

In this case the steady drift force in the surge direction is given by

$$F_{DC} = \frac{1}{T}\int_0^T F_1(t)\, dt = \rho\, g\, A \,.\, \{ \int_0^T e^{kA\cos(kx-\sigma t)} \sin(kx-\sigma t)\, dt$$

$$- \int_0^T e^{-kd+kH\cos(\sigma t+\varepsilon)} \sin(kx-\sigma t)\, dt \} \ ,$$

where $T = 2\pi/\sigma$.

Again two different integrals have to be solved (where the cylinder can be considered to be located at x = 0):

$$\text{(a)} \int_0^T e^{kA\cos(kx-\sigma t)} \sin(kx-\sigma t)\, dt = 0 \ ,$$

and

$$(b)\ \int_0^T e^{-kd + kH\cos(\sigma t+\varepsilon)} \sin(kx-\sigma t)\, dt$$

$$= \int_0^T e^{-kd+kH\{\cos(\sigma t)\cos\varepsilon - \sin(\sigma t)\sin\varepsilon\}} \sin(kx-\sigma t)\, dt$$

$$= \int_0^T e^{-kd+kH\cos(\sigma t)\cos\varepsilon} \cdot e^{-kH\sin(\sigma t)\sin\varepsilon} \cdot \sin(kx-\sigma t)\, dt$$

$$= e^{-kd} \int_0^T e^{kH\cos\sigma t\cos\varepsilon} \cdot e^{-kH\sin\sigma t\sin\varepsilon} \cdot \sin(kx-\sigma t)\, dt\ .$$

The above integral can be evaluated qualitatively by means of inspection of the integrand. The following three functions are considered:

$$\text{Curve (1): } z_1 = e^{kH\cos(\sigma t)\cos\varepsilon}$$

$$\text{Curve (2): } z_2 = e^{-kH\sin(\sigma t)\sin\varepsilon}$$

$$\text{Curve (3): } z_3 = \sin(kx-\sigma t)\ .$$

It is seen that the combined function $z_1 \cdot z_2 \cdot z_3$ is even when the heave motion is out of phase with the wave, so that integration of that function over one wave period would then result in a non-zero steady force. The integral has a maximum for a phase angle of 90 degrees. The drift force is zero when the heave motion of the cylinder is in phase, or 180 degrees out of phase, with the wave :

$$F_{DC} = 0 \text{ for } \varepsilon = 0, \pm\pi, \pm 2\pi, \ldots$$

Hence, a vessel advancing in for example head or following seas, will experience a mean drift force, i.e., resistance, due to the Froude-Krylov force contribution. The drift force will increase with increasing wave amplitude, and the sign of the mean force will depend on the relative

heading between the vessel and waves. This drift force is only part of the total added resistance in waves, since radiation and diffraction effects contribute also to the mean resistance. These efects are not considered in this this work.

Appendix C

Numerical Integration Procedures

C.1. Filon's Method

An integral which occurs frequently in the computation of the wave forces on objects is one in which the integrand consists of a function, say M(x), multiplied by a sine or cosine function of x. If one must consider high frequencies in the sine or cosine function, a very fine mesh is required when evaluating the integral by the usual numerical approximation such as Simpson's Rule. Filon has suggested a procedure for avoiding this inconvenience in cases where the function M(x) varies smoothly with x. By Filon's procedure, it is assumed that the function M(x) is linear between integration points, which is a reasonable assumption for small enough intervals dx. To illustrate this method, we consider the following integral:

$$I(k) = \int_{x_1}^{x_N} M(x) \cos kx \, dx \approx \sum_{i=2}^{N} \int_{x_{i-1}}^{x_i} (a_i + b_i x) \cos kx \, dx = \sum_{i=2}^{N} I_i \, .$$

The coefficients are given by

$$a_i = \frac{M(x_{i-1})x_i - M(x_i)x_{i-1}}{x_i - x_{i-1}} \, ,$$

$$b_i = \frac{M(x_i) - M(x_{i-1})}{x_i - x_{i-1}} \, ,$$

and the incremental value of the integral is found analytically to be the following:

$$I_i = a_i\left[\frac{\sin kx_i - \sin kx_{i-1}}{k}\right] + b_i\left[\frac{\cos kx_i - \cos kx_{i-1}}{k^2}\right]$$

$$+ b_i\left[\frac{x_i \sin kx_i - x_{i-1}\sin kx_{i-1}}{k}\right].$$

Now consider the following integral :

$$I^* = I_{i-1} + I_i + I_{i+1}$$

$$\Rightarrow I^* = \frac{M(x_{i-2})x_{i-1} - M(x_{i-1})x_{i-2}}{x_{i-1} - x_{i-2}} \cdot \left[\frac{\sin kx_{i-1} - \sin kx_{i-2}}{k}\right]$$

$$+ \frac{M(x_{i-1}) - M(x_{i-2})}{x_{i-1} - x_{i-2}} \cdot \left[\frac{\cos kx_{i-1} - \cos kx_{i-2}}{k^2} + \frac{x_{i-1}\sin kx_{i-1} - x_{i-2}\sin kx_{i-2}}{k}\right]$$

$$+ \frac{M(x_{i-1})x_i - M(x_i)x_{i-1}}{x_i - x_{i-1}} \cdot \left[\frac{\sin kx_i - \sin kx_{i-1}}{k}\right]$$

$$+ \frac{M(x_i) - M(x_{i-1})}{x_i - x_{i-1}} \cdot \left[\frac{\cos kx_i - \cos kx_{i-1}}{k^2} + \frac{x_i \sin kx_i - x_{i-1}\sin kx_{i-1}}{k}\right]$$

$$+ \frac{M(x_i)x_{i+1} - M(x_{i+1})x_i}{x_{i+1} - x_i} \cdot \left[\frac{\sin kx_{i+1} - \sin kx_i}{k}\right]$$

$$+\frac{M(x_{i+1}) - M(x_i)}{x_{i+1} - x_i} \cdot \left[\frac{\cos kx_{i+1} - \cos kx_i}{k^2} + \frac{x_{i+1}\sin kx_{i+1} - x_i \sin kx_i}{k} \right] .$$

Combining terms for $M(x_{i-2})$, $M(x_{i-1})$, etc. results in similar expressions for each of these quantities, facilitating the numerical integration. For example, the terms associated with $M(x_i)$ are the following :

$$M(x_i) \cdot \left\{ \frac{1}{x_i - x_{i-1}} \cdot \left(-x_{i-1} \cdot \frac{\sin kx_i - \sin kx_{i-1}}{k} \right.\right.$$

$$\left. + \frac{\cos kx_i - \cos kx_{i-1}}{k^2} + \frac{x_i \sin kx_i - x_{i-1}\sin kx_{i-1}}{k} \right)$$

$$+ \frac{1}{x_{i+1} - x_i} \cdot \left(x_{i+1} \cdot \frac{\sin kx_{i+1} - \sin kx_i}{k} \right.$$

$$\left.\left. - \frac{\cos kx_{i+1} - \cos kx_i}{k^2} - \frac{x_{i+1}\sin kx_{i+1} - x_i \sin kx_i}{k} \right) \right\} .$$

Similarly, terms associated with $M(x_{i-1})$, for example, are the same as above but with x_{i-1} substituted for x_i, and x_{i-2} substituted for x_{i-1} in the above expression. Also, integrals involving moments and a harmonic function can be solved in a manner analogous to the above, as would be applicable to the following integral, for example:

$$I(k) = \int M(x).x.\cos kx \, dx \quad .$$

C.2. Euler's Integration Method

The Euler method is a simple method for numerically integrating first order differential equations in the form of an initial value problem. Consider the following set of first order equations:

$$\begin{aligned}
\dot{x}_1 &= f_1(t;x_1,x_2,\ldots,x_n) \\
\dot{x}_2 &= f_2(t;x_1,x_2,\ldots,x_n) \\
&\vdots \\
\dot{x}_n &= f_n(t;x_1,x_2,\ldots,x_n) \ ,
\end{aligned}$$

where

$$\dot{x}_n = \frac{dx_n}{dt} \ ,$$

and the corresponding initial values are

$$\begin{aligned}
x_1(t_0) &= x_1^{(0)} \\
x_2(t_0) &= x_2^{(0)} \\
&\vdots \\
x_n(t_0) &= x_n^{(0)} \ .
\end{aligned}$$

The variable t is taken as the independent variable, and x_i (i=1,2,...,n) are the dependent variables. In vector notation the above set of equations can be written as :

$$\dot{\mathbf{x}} = \mathbf{f}(t;\mathbf{x}), \text{ and } \mathbf{x}(t_0) = \mathbf{x}^{(0)} \ .$$

The following quantities are introduced:

$t_k = t_0 + kh$;
h = time step interval;
$\mathbf{x}_i = \mathbf{x}(t_i)$ is the exact solution to the set of differential equations;
$\mathbf{u}_i$ is the numerical approximation to $\mathbf{x}_i$.

Then the numerical solution to the problem can be estimated by a first order time stepping procedure, where the solution for the present time, t_i, is used to estimate the solution vector $\mathbf{u}_{i+1}$ for the next time step, viz.:

$$\mathbf{u}_{i+1} = \mathbf{u}_i + h\, \mathbf{f}(t_i, \mathbf{u}_i)\,;\ \mathbf{u}_0 = \mathbf{x}_0\ .$$

The local truncation error associated with Euler's method is of the order h^2, i.e.,

$$E_T(t_{i+1}) = O(h^2)\ .$$

Appendix D

Flowcharts of Program *KAPSIZE*

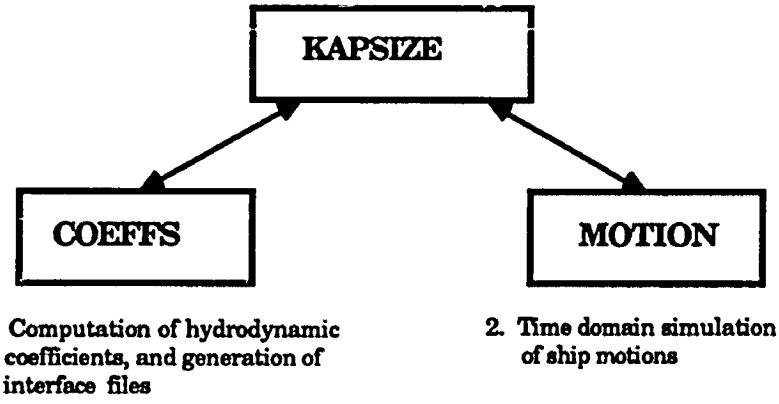

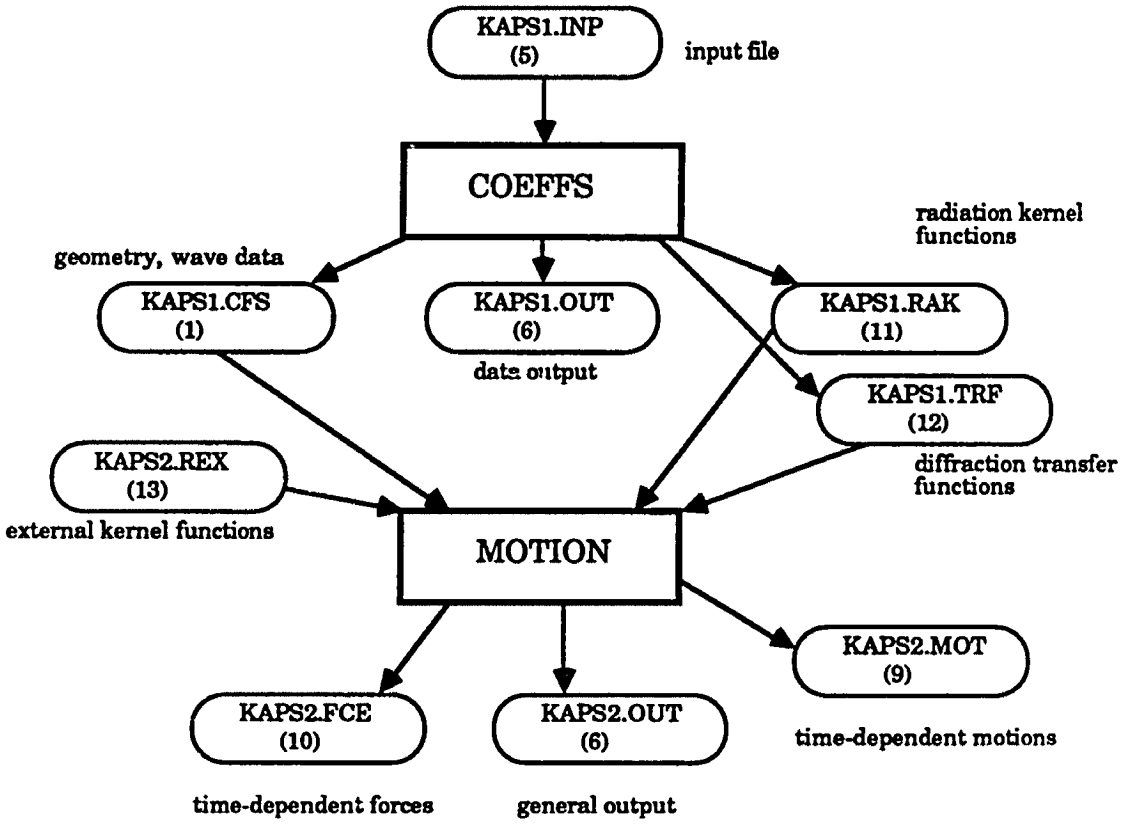

Figure D.1. Block diagram showing principal segments and file handling of program KAPSIZE

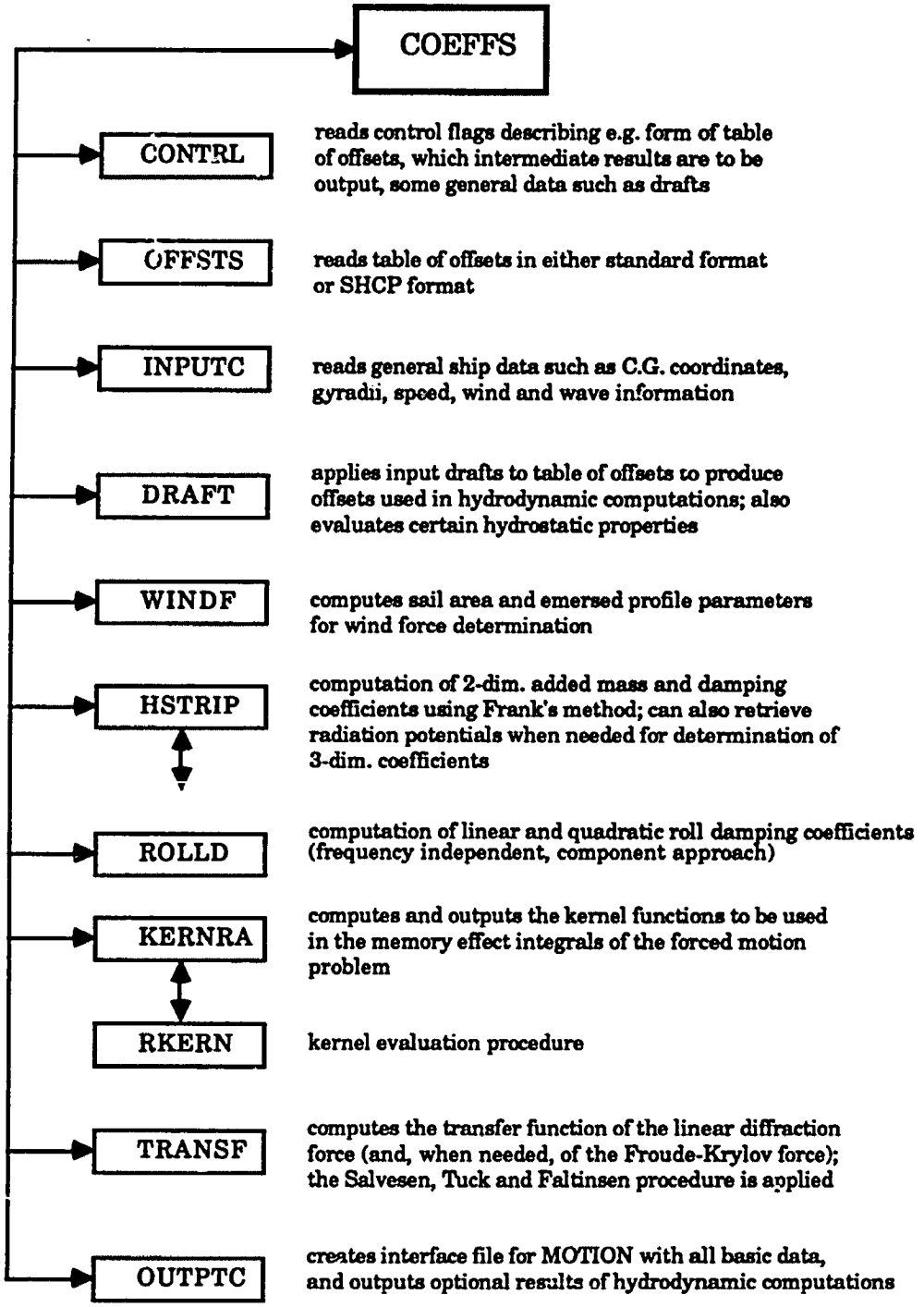

Figure D.2. Block diagram showing subroutines accessed by sub-program COEFFS

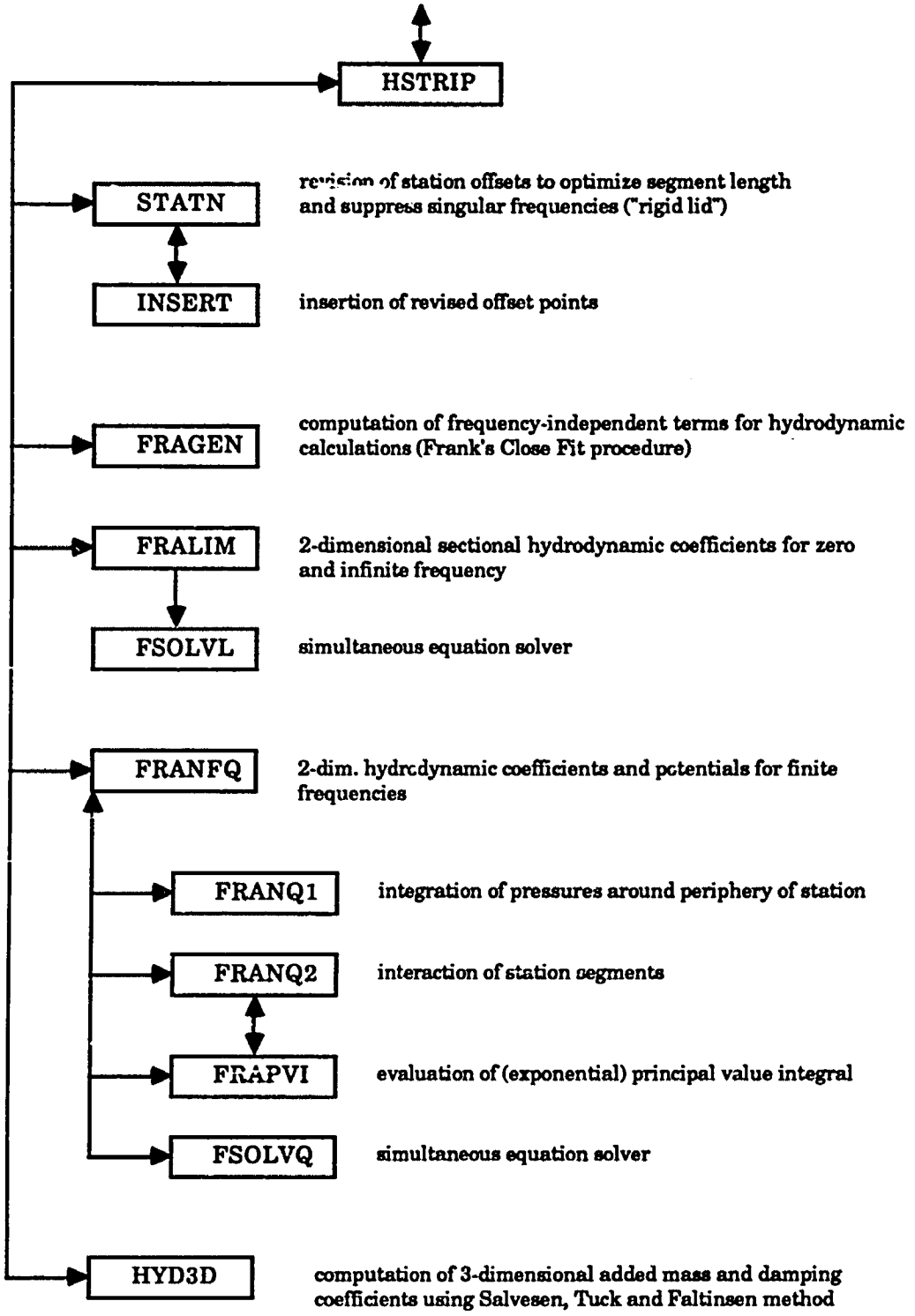

Figure D.3. Block diagram of subroutines accessed by subroutine HSTRIP

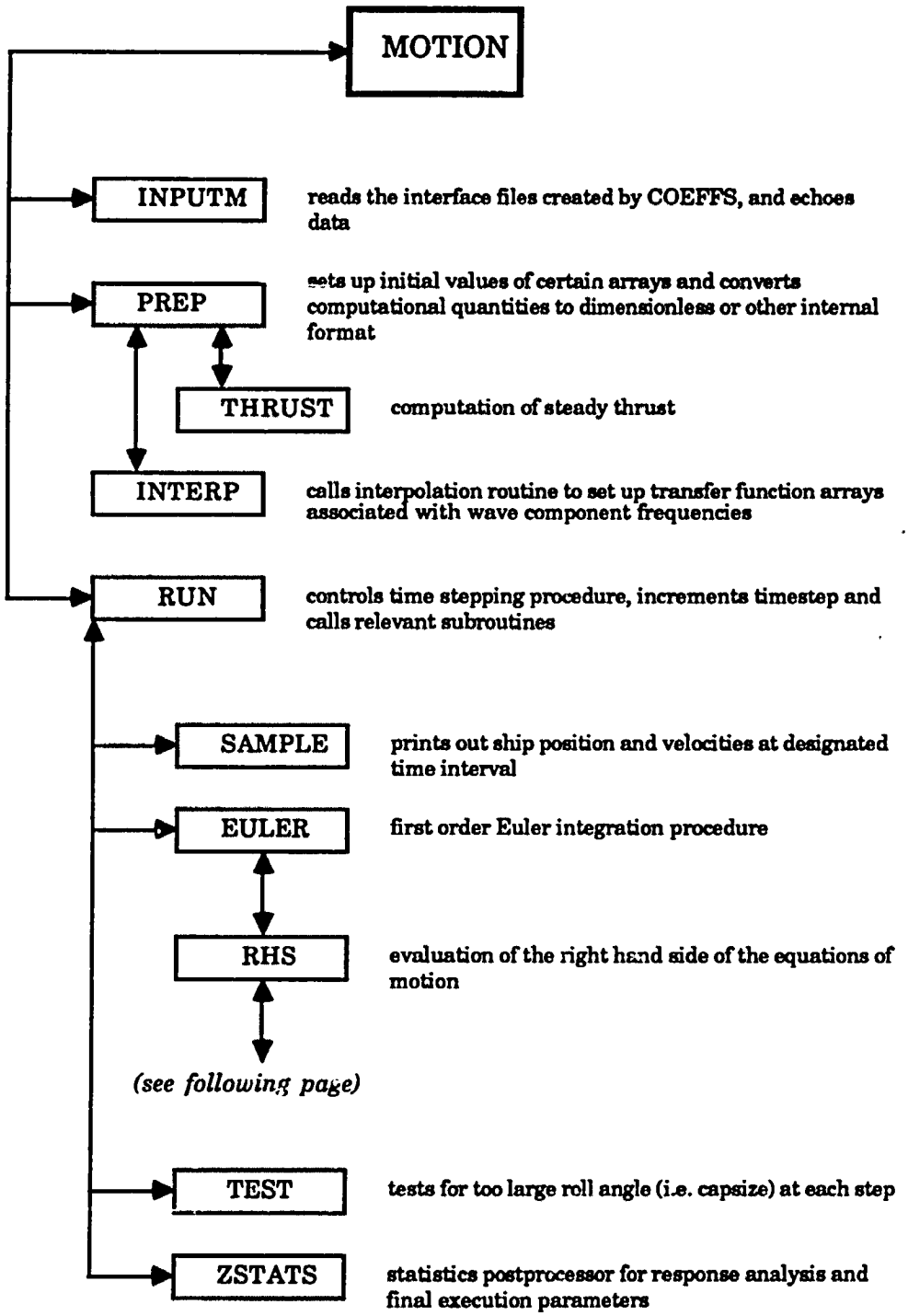

Figure D.4. Block diagram of principal segments of subprogram MOTION

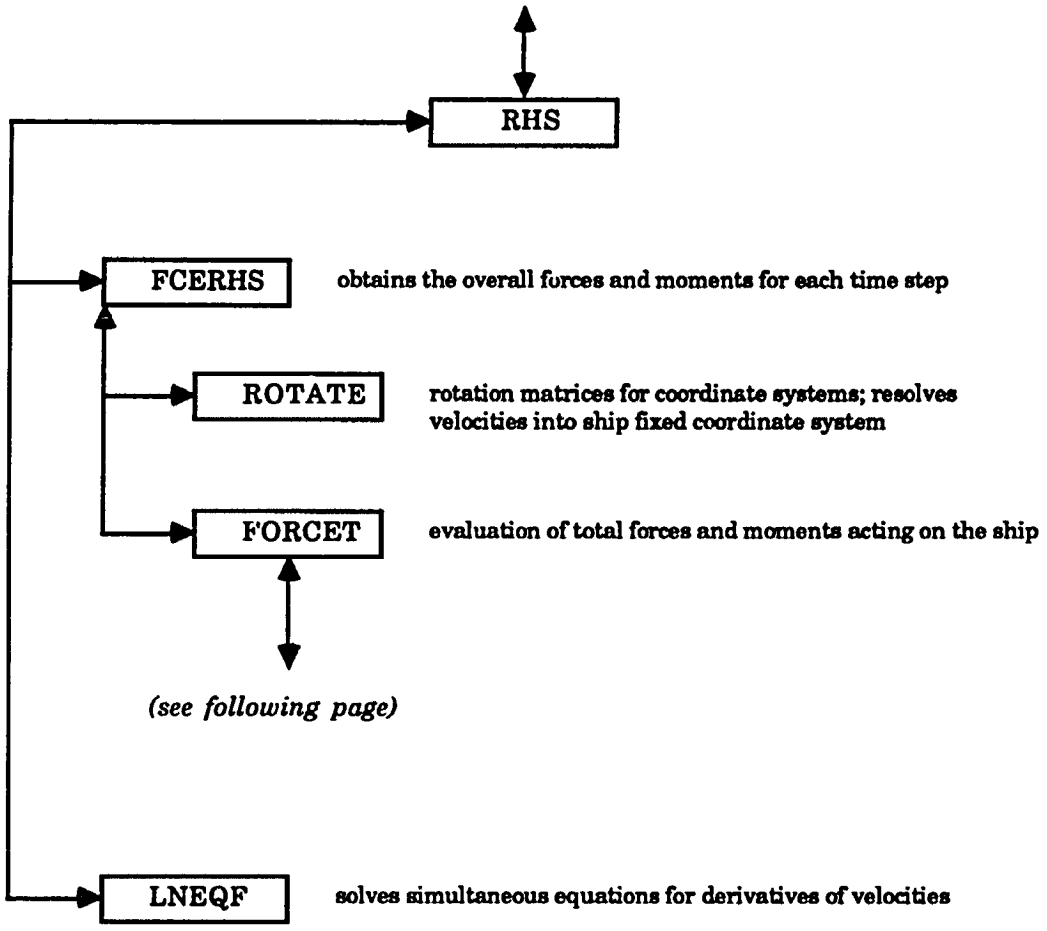

Figure D.5. Block diagram showing subroutines accessed by subroutine RHS

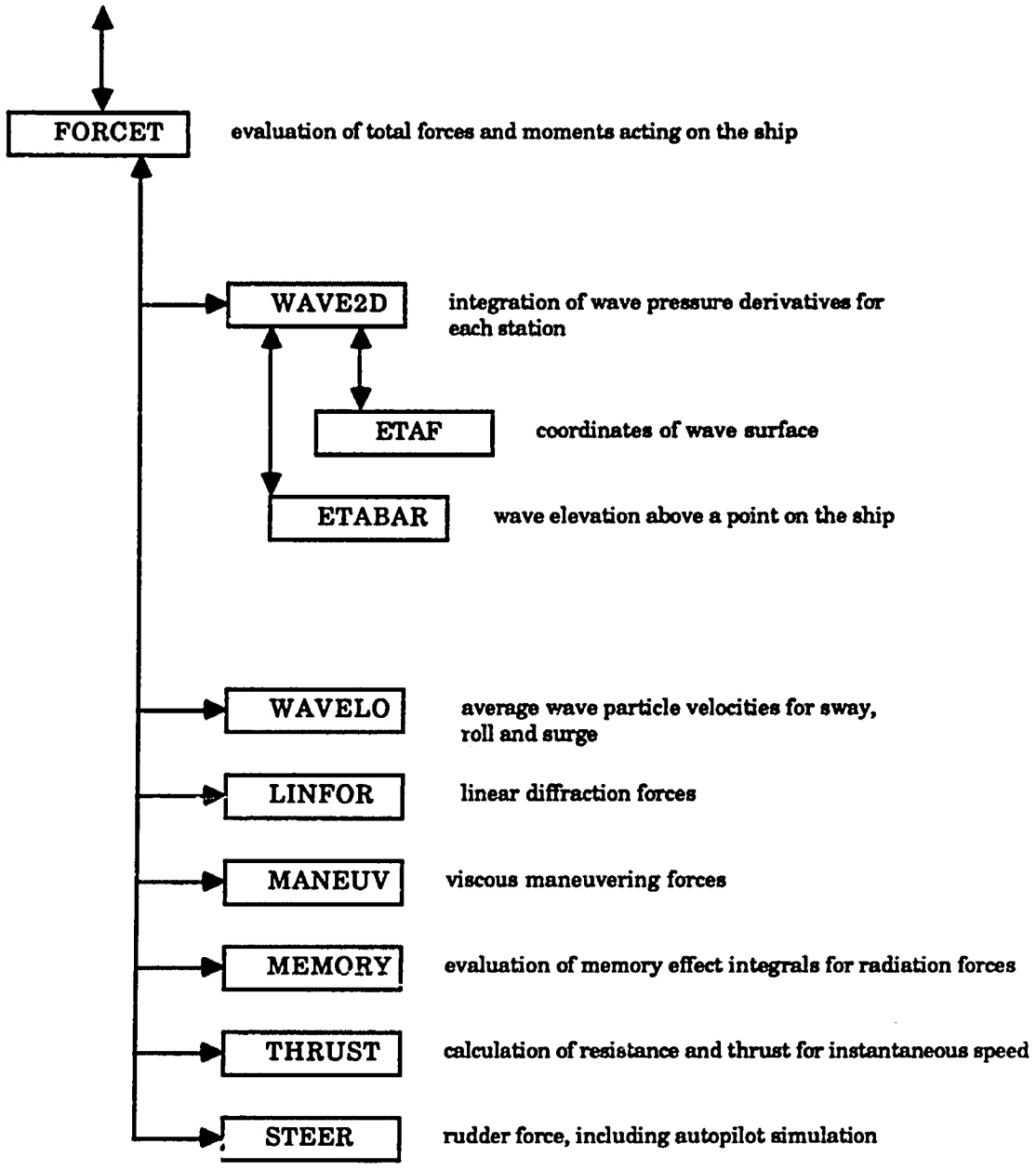

Figure D.6 Block diagram showing subroutines accessed by subroutine FORCET